Title
Extending the Strange Metal Phenomenology of High-Tc Superconductors With High Magnetic Fields

Author
Hayes, Ian Matthew

Publication Date
2018

Peer reviewed|Thesis/dissertation

Extending the Strange Metal Phenomenology of High$-T_c$ Superconductors With High Magnetic Fields

by

Ian Matthew Hayes

A dissertation submitted in partial satisfaction of the

requirements for the degree of

Doctor of Philosophy

in

Physics

in the

Graduate Division

of the

University of California, Berkeley

Committee in charge:

Professor James G. Analytis, Chair
Professor Joseph Orenstein
Professor Sayeef Salahuddin

Fall 2018

Extending the Strange Metal Phenomenology of High$-T_c$ Superconductors With High Magnetic Fields

Abstract

Extending the Strange Metal Phenomenology of High$-T_c$ Superconductors With High Magnetic Fields

by

Ian Matthew Hayes

Doctor of Philosophy in Physics

University of California, Berkeley

Professor James G. Analytis, Chair

Probably the most significant challenge facing condensed matter physics today is to understand metallic behavior that falls outside the independent electron approximation. The number of metallic systems for which this approximation fails is small but these systems are of exceptional interest because they often display exciting phenomena like high$-T_c$ superconductivity. Additionally, these systems exhibit a common pattern of anomalies, giving us hope that there is a universal physical picture by which we can understand them. Two of these anomalies are in the charge transport sector: a $T-$linear resistivity and a strongly $T-$dependent Hall effect. This dissertation seeks to extend this pattern by studying the charge transport properties of the iron-pnicited superconductor $BaFe_2(As_{1-x}P_x)_2$ at very high magnetic fields. The data obtained in these experiments reveal significant magnetic analogues of both the aforementioned anomalous temperature dependencies, and confirm that the dynamics in this system conform to two of the predictions of quantum critical theory: scale invariance and the existence of a uniform fan-like region around the quantum anti-ferromagnetic quantum phase transition. These findings support the hypothesis that quantum criticality is at the root of these particular anomalies, while simultaneously challenging the naïve version of the theory and creating new opportunities for investigating the microscopic nature of the strongly correlated state.

Contents

List of Figures

List of Tables

Acknowledgments

Physics is hard. Without help, it's impossible. There are many people who helped me get to this point, both during graduate school and before, and it is a pleasure to be able to thank them here. I doubt there is anyone who has enjoyed more consistent support and encouragement from his parents than I have. Thanks to them I have never suffered from imposter syndrome, despite being a Ph.D. student at UC Berkeley. Thank you, mom and dad, for teaching me to never give up, to never be intimidated, and to never compromise on clarity in my thinking. And thank you, Eric, for keeping me grounded and for making me feel like less of a nerd than I am.

I was extremely fortunate to be searching for an advisor at the same time that Professor Analytis was starting his laboratory. Thanks to him I finally found a deeply fascinating research area, and got to experience the joys and challenges of building a laboratory from scratch. When I first came to his office I probably seemed a little like a lost soul. I'm grateful for the chance that he gave me, as well as for all of the hours of stimulating discussion and considered advice he has offered me since then. Of course, advising is a shared enterprise. My laboratory chops were largely developed under the guidance of two wonderful post-docs, Nick Breznay and Toni Helm. Their patient instruction and unflagging enthusiasm for science made a huge difference in my growth as a physicist. To my own advisee, Zeyu Hao, I say thank for keeping me on my toes in the lab and for helping me with the trickier aspects of contacting crystals. Most of the data in this dissertation could not have been obtained without the technical expertise of the staff of the National High Magnetic Field Laboratory's Pulsed Field Facility in Los Alamos. My friends Ross McDonald, Brad Ramshaw, Mun Chan, and Jon Betts made the laboratory a fun and exciting place to visit, and were willing to go considerably beyond the call of duty to make my experiments succeed. My fellow graduate students in the Analytis laboratory also deserve a big thanks for making it a positive and productive place to work, for teaching me the ins and outs of so many different experimental techniques, and for the fun times on ski trips and at trivia nights.

Completing a Ph.D. is an emotionally as well as intellectually challenging task. I'm fortunate to have had the support and encouragement of my friends outside of the university. My furry friends, Juno and Artemis, were especially helpful during the long days of dissertation writing. And finally, to Katy, my partner-in-love and partner-in-life, I say thank you for keeping my sails full and my keel even. I'm deeply grateful to have had you with me from the beginning of this project to the end.

Chapter 1

Introduction, Background, and Literature Review

> *"...the lesson which we have received from the whole growth of the physical sciences is that the germ of fruitful development often lies just in the proper choice of definitions. "*
>
> — Niels Bohr, *Atomic Physics and Human Knowledge*[15]

Depending on one's taste, condensed matter is either the most or least satisfying branch of physics. Decades of research have yielded little in the realm of quantitative, first-principles predictions about materials, and certainly nothing that rivals the twelve-decimal-place agreement between calculation and experiment in the electron $g-2$ measurement.[85] On the other hand, condensed matter physics has given us several powerful frameworks for understanding collective behavior that, almost miraculously, allow one to predict the general shape of physical response functions without any need to calculate the detailed behavior of a system's microscopic constituents. Perhaps the best example of this is the Landau theory of phase transitions.[70, 103] This theory was essentially an innovation in mathematical language. Landau noticed that a phase transition almost always involves the appearance of some sort of order: the regular array of atoms in a crystal, or the common orientation of the electron spins in a ferromagnet, for example. Each phase can therefore be described by identifying a particular average of local observables, called the order parameter, whose average value is nonzero only in the ordered phase. Once we see that this is the case, we can write down the free energy of the system as a function of this order parameter. Near the phase transition, where the order parameter goes from zero to nonzero, we can compute basic properties of the system by keeping track of only the lowest-order terms allowed by symmetry. Everything important about the thermodynamics of the system has been encoded in the order parameter, and we do not have to worry about the microscopic degrees of freedom.

Our modern theory of metals is of a very similar form. Solving for the detailed behavior of $\sim 10^{23}$ interacting electrons is not feasible. However, almost nothing about the details of those interactions turns out to be important for determining the gross features of the electronic spectrum. The excitations of the system are well approximated by the excitations of a non-interacting collection of electrons. This was not a mathematical insight; it came

first from the experimental observations that the thermodynamic properties of metals were of the same form as those expected for the noninteracting gas of electrons.[11] However, there was a key mathematical insight contributed, once again, by Landau. This is that small interactions in a dense collection of Fermions do not necessarily lead to large scattering of the electrons by other electrons, so that a single-electron excitation can be very nearly an eigenstate of an interacting system.[69] Once again, the key step is to guess the right language for describing the system. This language then gives you most of the basic results about your system, without your needing to know almost any materials-specific details.

One of the most difficult and significant challenges in modern condensed matter physics is understanding metals that are not well described by this Fermi liquid theory (FLT). These systems are generally referred to as strongly-correlated electron systems because the weakly correlated description—one in which electrons are treated as being nearly independent—is exactly the theory of a Fermi liquid. As we will see, any theory which uses the weak-coupling starting point inherits some rather severe restrictions on the kinds of behavior that it can capture, especially in the limit of low temperature. Although FLT describes the majority of metallic systems quite well, there are also a number of systems that violate these restrictions imposed by an independent-electron picture. The conceptual challenge posed by these non-Fermi liquid (NFL) systems is deep: it is very hard to imagine any tractable description of 10^{23} particles that does not make the simplifying assumption that electrons can be slotted into independent states and that this gives you a full description of the material. What's needed, clearly, is a new picture of the relevant physics.

Judging solely by their number, these non-Fermi liquid metals would seem to be of little significance. They usually exist only at isolated points in phase diagrams, surrounded by great seas of Fermi liquids. However, they are often associated with phenomena of great intrinsic interest, such as high$-T_c$ superconductivity. More importantly, they offer a possibility of finding fundamentally different kinds of metallic behavior, and may hold the key to understanding why the Fermi liquid phase is so stable. The goal of this project is to contribute to the ongoing effort of finding a new language for NFL metals by looking for clear patterns in their response functions that can serve as a basis for building this new language. This path has been successfully followed in the past. Before Landau put the quasiparticle picture of metals on a sound theoretical footing, the field was motivated to consider an independent electron picture by broad patterns in the behavior of metals. Today, certain patterns in the behavior of strongly-correlated metals suggest a similar path forward.[110] Once again, we see broadly similar behavior in basic thermodynamic and transport quantities, and the pattern is reminiscent of a certain language that we already have at hand: that of the scale-invariant thermodynamics that emerges near continuous, classical phase transition. The theory constructed by Landau in the 1950s was based on a classical free energy and so only covered thermodynamics observables, i.e. those that are derivatives of the free energy. In particular this leaves out electrical transport coefficients, which depend on dynamics as well as thermodynamics. If, however, one considers a quantum free energy, derived from a Hamiltonian operator, the states that are counted in the partition function are constrained by the dynamics encoded in the Hamiltonian. This is an immediate con-

sequence of the uncertainty principle. As a result, one naturally expects a diverging time scale near a quantum critical point, in addition to a diverging length scale (see chapter 2 for details). This strongly suggests that dynamic quantities like the electrical resistivity should follow strict power laws down to very low temperatures, similar to what one in fact sees in the canonical NFL metals.

The rest of this chapter will review the literature on each of these subjects. First the experimental status of NFL metals will be presented, including an evaluation of the significance of $T-$linear resistivity, which will be a major focus of this dissertation. A more detailed look at the theory of quantum critical metals and its pitfalls will be delayed to chapter 2. Next, the key facts about the cuprate high$-T_c$ superconductors, which have been responsible for much of the interest in NFL physics, will be summarized. Section 1.3 will look in detail at the literature on the central subject of this study, the iron-based high$-T_c$ superconductor $BaFe_2(As_{1-x}P_x)_2$, and the chapter will conclude with a presentation of the particular goals for this project and a summary of results.

1.1 Experimental aspects of quantum criticality and NFL physics

Landau's theory of the Fermi liquid makes a number of strong predictions for the temperature dependencies of metallic response functions in the limit of zero temperature.[69] These include that the electrical resistivity will go as the temperature squared, the heat capacity will be linear in temperature, and the spin susceptibility will be independent of temperature. Here I will only cover the derivation of the T^2 resistivity, since that is the most pertinent the experimental substance of this dissertation, and because discussions of all of them are widely available.[92, 11]

At low temperatures in a Fermi liquid, excitations are confined to a region of phase space near the Fermi surface of width $\sim T/E_F$. This follows simply form the Fermi-Dirac statistics of independent fermions. Assuming that the interactions between electrons are short-ranged, we can count the number opportunities that an electron has to scatter off another electron. The number of electrons that are available to be scattered is proportional to T. This pair of electrons must then decay into two new state. With combined energy of $\sim 2T$, the first electron has final state options proportional to T, whereupon the final state of the second electron is determined by energy and momentum conservation. This means that the number of scattering processes available will scale as T^2, and the total scattering rate derived from electron-electron processes will grow quadratically with temperature.

This phase space restriction on the scattering is essential for our ability to treat electrons as quasi-independent particles in a metal. It is because the scattering rate decreases more quickly as a function of temperature than the average excitation energy that there is guaranteed to be a region near zero temperature where the excited states of the system are nearly free electron states (this is discussed further in chapter 2).[69, 11] It is not obvious, however,

that electron-electron scattering is relevant to the resistivity. Momentum is conserved in these collisions, and since the current is just proportional to the total electronic momentum, the total electrical current will be conserved as well. However, two-electron scattering can also involve the static ionic lattice, which will reduce the joint electronic momentum by an amount equal to $\hbar k_R$, where k_R is a crystal reciprocal lattice vector. At low temperatures, phonons will have frozen out, so this process is the only one available to relax momentum, and it will not contribute a temperature-dependent term to the scattering rate. Therefore, in the limit of zero temperature, the resistivity is limited by the phase-space restrictions for electron-electron scattering described above.

One thing to note about this argument is how few assumptions are required for it to hold. Any system in which the excitations are approximately described as independent fermions will meet this phase-space constraint at low enough temperatures. For a long time it was assumed that this would be the low-temperature fate of all metals. However, late in the twentieth century apparent counterexamples started to appear.[110] Achieving confidence that one has a NFL metal is a challenge. Since the robust predictions of FLT occur in the zero temperature limit, one could always argue that an experiment simply has not reached low enough temperatures to see the expected behavior. However, the deviations of real metals from perfect quasiparticle behavior are typically ascribed to the interactions of the electrons with other degrees of freedom in the system, which are always bosons. The excited states of bosonic degrees of freedom always depopulate more quickly than those of fermions in the zero temperature limit. What's more, they depopulate according to a known functional form, so that it is often possible to say that they should be largely irrelevant below some temperature. If one continues to see violations of the FLT predictions below this temperature, then he can be confident that the system is not well described by FLT. Furthermore, some of the NFL anomalies seem to actually get stronger at lower temperature. A good example is the $C_p/T \sim log(T)$ behavior seen in many NFL systems.[110] In a Fermi liquid, C_p/T should be approaching a constant at low temperatures, while a logarithm shows a stronger temperature dependence the closer the system gets to absolute zero. All of these considerations have lead to the conclusion that there really are NFL metals in nature, even if they are comparatively rare.

For this project, the most relevant example of NFL behavior is the $T-$linear resistivity. As will be discussed below, NFL metals are essentially a set of measure zero in the space of all possible metals. Nonetheless, there are many individual examples and it would not be worth it to take a close look at all of these here. Instead, I will look in detail at two well-studied examples to illustrate the way that $T-$linear resistivity usually manifests. These examples will provide context for the data that I have gathered on $BaFe_2(As_{1-x}P_x)_2$. The first of these examples will be ytterbium-rhodium-silicide-122: $YbRh_2Si_2$.[33, 42] This compound comes from a large class of materials known as heavy fermion systems.[110] Compounds of this type have a valence band that is made out of hybridized $d-$ and $f-$orbitals, which makes it very flat. Consequently, the band mass of the electrons is very large, which gives these compounds their name. Early debates on the origin of NFL behavior focused on whether this flat band was essential. We now know that it is not, as we shall see below.

In zero magnetic field, $YbRh_2Si_2$ shows $T-$linear resistivity down to about one hundred millikelvin, but below that the system undergoes a phase transition to an antiferromagnetic state and the resistivity drops abruptly before leveling out into a $\sim T^2$ form. In order to reach a NFL regime, one has to suppress this magnetic order. This can be done by alloying on either the ytterbium site or the silicon site, or by applying a modest magnetic field.[42, 32, 40] The minimum amount of germanium that has to be substituted onto the silicon site to suppress the magnetism is about five percent. The resulting alloy shows a linear resistivity down to the lowest temperatures measured. Further alloying, however, produces a system with a $\sim T^2$ resistivity at low temperatures.

This is the first important fact about $T-$linear resistivity in NFL systems: it almost always appears at an isolated point in the phase diagram. This point is either at or very near the zero temperature endpoint of second order phase transition. This naturally leads to the hypothesis that NFL systems are metals with a critical ground state. Indeed, some simple arguments about so-called quantum critical systems suggest that $T-$linear resistivity, even in the zero kelvin limit might be natural in these systems.[100] I will look at this specific argument in chapter 2. For now, I just wish to note that it is a remarkable experimental fact that $T-$linear resistivity is often associated with the presence of a quantum critical point.

It is also useful, however, to look at the pattern of behavior in the resistivity as a function of temperature in the region around this special point, as this pattern also turns out to be common to many of these materials. Figure 1.1 shows a color plot of the local exponent of the resistivity versus temperature of $YbRh_2Si_2$ as a function of temperature and magnetic field. This figure is reproduced from reference [33]. The local exponent in temperature is evaluated by taking the logarithmic derivative, $dlog(\rho)/dlog(T)$, of the inelastic part of the resistivity. If the resistivity were given by a pure power law, this quantity would just be its exponent, so it is a reasonable numeric way of capturing local power law behavior. As can be readily seen in Figure 1.1, this quantity is one down to zero temperature at just one point in the phase diagram. This is the point where antiferromagnetism is completely suppressed. As one moves away from this point, the local exponent is still one above some crossover temperature, which gets higher the farther away one is from the critical point. This leads to a fan-like region in the $T - B$ plane in which the system exhibits $T-$linear resistivity. This is the second important general feature of how $T-$linear resistivity manifests in metals. Once again, general arguments suggest that this behavior is natural near a quantum critical point (see section 2.4).[100]

These patterns are borne out again and again in heavy fermion materials.[110] They are not, however, exclusive to this set of materials. A good example of a system that shows this same set of NFL properties but has no $f-$electron weight near the Fermi level is strontium-ruthenate-327: $Sr_3Ru_2O_7$.[18, 16, 98, 91, 75] This material is part of a Ruddleson-Popper series of ruthenates that has attracted considerable attention as structural analogues to the high$-T_c$ cuprate superconductors. They have several intriguing properties of their own, including possible $p-$wave superconductivity in Sr_2RuO_4.[54] The critical phase transition of $Sr_3Ru_2O_7$ is a meta-magnetic one, in which there is a singular increase in the magnetization at a certain strength of applied magnetic field. This transition is sharp at zero temperature

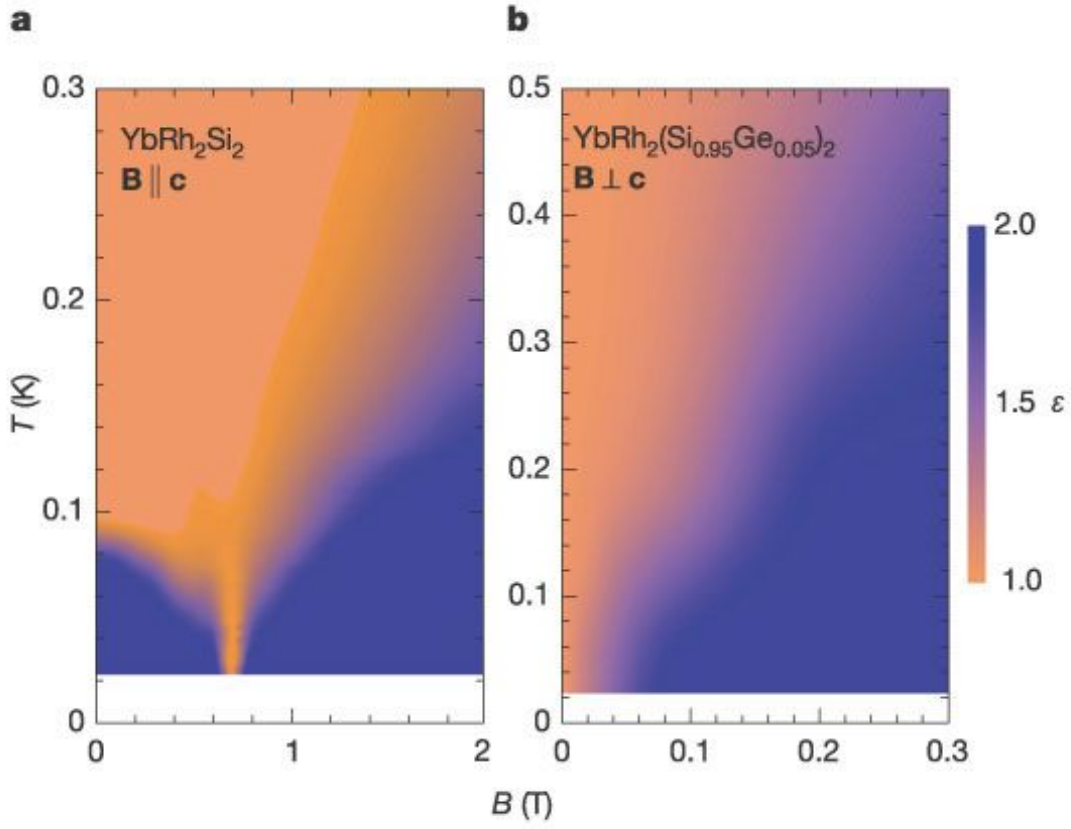

Figure 1.1: $T-$**linear resistivity down to zero temperature in** $YbRh_2Si_2$**.** The local power law of the resistivity, "ϵ", is plotted as a function of temperature and field. The $T-$linear resistivity continues down to the lowest measure temperatures at a single field value, identified with a quantum critical point. The $T-$linear resistivity is also present throughout a fan-like region emanating from the critical point. This figure is taken from reference [33]. Reproduced with permission from Springer Nature.

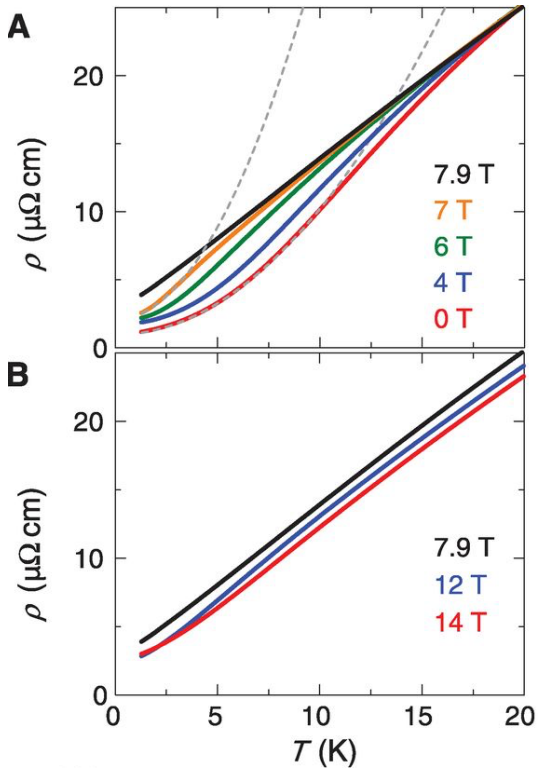

Figure 1.2: $T-$**linear resistivity down to low temperatures in** $Sr_3Ru_2O_7$ At the single field value $H = 7.9$ tesla, the resistivity remains $T-$linear down to the lowest temperatures. The $\sim T^2$ behavior on either side of this critical value is similar to that displayed by both $YbRh_2Si_2$ and the cuprate superconductors (see references [42, 8]). This figure is taken from reference [18]. Reproduced with permission from AAAS.

but not at higher temperatures. Naturally, therefore, the critical point is accessed by applying a magnetic field. Figure 1.2, reproduced from reference [18], shows resistance versus temperature curves for several values of the magnetic field. Once again, the $T-$linear resistivity continue to very low temperatures right at the critical field of 7.9 tesla. At higher or lower fields, the resistivity crosses over to a $\sim T^2$ form at low temperatures. The crossover from $T-$squared to $T-$linear resistivity moves to higher temperatures as one moves away from the critical point, creating a fan-like region of $T-$linear resistivity that is qualitatively very similar to what one sees in $YbRh_2Si_2$. Strontium ruthenate also shows the $Tlog(T)$ heat capacity at low temperatures, confirming that this state is indeed very similar to the NFL state in heavy fermion compounds.[98] The existence of $Sr_3Ru_2O_7$ demonstrates that this NFL behavior does not require the presence of $f-$electrons.

Thus, there is a clear pattern of NFL behavior in the resistivity that is associated with quantum critical points.[110, 71] The difference in the microscopics of these systems (d versus

f electron systems, antiferromagnetic versus meta-magnetic order) strongly suggests that we should be able to understand this pattern in some simple, effective description that is not sensitive to details of the systems' microscopics. This would be a significant problem in its own right, but it is made even more important by the fact that this behavior reappears in the high temperature superconductors as well.

1.2 Non-Fermi liquid behavior in high$-T_c$ superconductors: the strange metal phase

Around the same time that the NFL physics of heavy fermion metals was taking off, most of the condensed matter community was engaged in studying the recently discovered, high-temperature, cuprate superconductors.[14] In addition to their shockingly high superconducting transition temperatures, these materials displayed a wealth of properties that are unexpected for ordinary metals. Many of these are bound up with the "pseudogap" regime at low doping, where a gap appears to open on some parts of the Fermi surface at low temperatures, but not on others.[120, 95, 36, 60] This partial gap creates the unacceptable situation of a Fermi surface that does not enclose a definite volume. In the charge transport sector, there were two anomalous observations: the Hall coefficient showed a very strong temperature dependence, which should not exist in a metal with only one relaxation rate, and the resistivity shows a linear temperature dependence that is most pronounced near optimal doping.[22, 112] This second observation, in particular, drew a lot of attention, as it indicated that a significant departure from Fermi liquid theory and the basic concept of a quasiparticle might be necessary.

It was already suggested in 1989 that this $T-$linear resistivity, as well as other essential aspects of the physics of the cuprates, arose from critical fluctuations.[115] However, this was only one of a number of competing views.[5, 62, 13, 78, 102] Many reviews have been dedicated to this topic in the intervening thirty years.[60, 10, 36] I will not try to do justice to the full range of views that exist about the overall phenomenology of the cuprates, as doing so would take all of the remaining space in this thesis. Instead, I will discuss the charge transport properties in some detail, with a focus on how it compares to the phenomenology displayed by the quantum critical systems. This will provide context for my claims about the implications of the results on $BaFe_2(As_{1-x}P_x)_2$ for high$-T_c$ superconductivity in general. In passing, I will mention a few other striking observations that seem to fit the quantum critical scenario.

In the case of the high$-T_c$ superconductors, one faces a major obstacle in determining whether $T-$linear resistivity continues down to very low temperatures: the charge transport data are not available below T_c. Although many of the heavy fermion materials that are thought to have a quantum critical point also superconduct, their critical temperatures are low enough that $T-$linear resistivity right above the transition is still strange, since it is still below the temperature at which phonons should have frozen out. However, the cuprates have

superconducting transition temperatures of up to one hundred kelvin, well into the region in which lattice vibrations are thermally activated. The case for the existence of NFL behavior in these materials must therefore be based, at least with regards to their charge transport properties, on a broader analysis of the resistivity as a function of temperature across their phase diagrams.

The cuprates come in dozens of families,[60, 10] but they show an almost universal pattern of behavior in the charge transport domain.[49, 8, 52] The parent compound is an insulator, with an increasing resistivity as a function of decreasing temperature. Superconductivity is induced by doping the material, either with electrons or holes. The insulating state persists up to roughly the edge of the superconducting dome, but the underdoped superconducting samples have a metallic resistivity that is roughly $T-$squared at low temperatures, crossing over to $T-$linear behavior at higher temperatures. This crossover temperature decreases as the compound is doped further, and near optimal doping (that is, where the superconducting transition temperature reaches its maximum value) the resistivity is very nearly linear in temperature from T_c up to extremely high temperatures.[112, 52] Beyond optimal doping the low temperature resistivity once again shows a $T-$squared to $T-$linear crossover as a function of increasing temperature, and this crossover temperature increases as the system is doped further.[49] The net effect is to create a fan-like region wherein the local exponent of the resistivity in temperature is approximately one, mirroring the fan-like regions of $T-$linear resistivity seen in quantum critical metals. Furthermore, on the underdoped side of the phase diagram the resistivity as a function of temperature shows an S-like shape, while on the overdoped side the derivative of the resistivity in temperature is monotonically increasing. This is qualitatively very similar to what is seen in both $Sr_3Ru_2O_7$ and $YbRh_2(Si_{1-x}Ge_x)_2$ (see Figure 1.2).

At this point a few caveats should be given. The first is that there is no clearly visible phase transition in the cuprates that extrapolates to zero kelvin near optimal doping. Therefore, one of the key ingredients for a quantum critical metal seems to be missing. Depending on the property from which one is extracting it, the temperature at which the pseudogap opens more or less extrapolates to zero temperature at optimal doping, but most experiments do not show any singular behavior that would indicate a phase transition.[49, 8] There have been a few experiments over the years that suggest there is some sort of symmetry breaking that happens at the pseudogap temperature, and these measurements do seem to indicate that the transition would extrapolate to zero temperature near optimal doping.[39, 104, 123, 89] This may be the missing piece of the puzzle. However, this issue is not considered settled. Even if there does turn out to be some order that defines the pseudogap, the fact that no singular behavior is seen in the resistivity (or even the heat capacity) may lead one to doubt the relevance of this order to the broad features of the charge transport behavior. The second important caveat is that the $T-$squared resistivity seen in these materials appears at a temperature far too high for it to be considered evidence of a Fermi liquid state. While in materials like $Sr_3Ru_2O_7$ and $YbRh_2(Si_{1-x}Ge_x)_2$, the $T-$squared resistivity is seen at temperatures below where we expect phonons to have frozen out, in the cuprates the visible $T-$squared regime is one in which the lattice is definitely thermally active. This complicates

the naïve mapping of the two phase diagrams onto each other. Finally, this pattern is not exhibited by the electron-doped materials. In those materials, the resistivity shows curvature in its temperature dependence at all temperatures across the phase diagram, except at very low temperatures on the overdoped side.[56] Certainly there is no extended $T-$linear regime near optimal doping. Furthermore, given that the $T-$linear resistivity that is seen at very low temperatures on the overdoped side is present for a range of dopings, it is doubtful that it relates directly to quantum criticality as currently understood. However, even on this point there is some dispute.[50]

These facts should be kept in mind as the possible role of quantum criticality is evaluated. However, since there is no well developed theory of a quantum critical metal, the author takes the attitude that the current task for experimenters is to map the significant features of the phenomenology. It is a striking fact that the same broad pattern is seen in the temperature dependence of the resistivity in all of these materials, and the phenomenon is clearly of fundamental interest when the $T-$linear resistivity can be tracked to zero temperature. Furthermore, the relevance of $T-$linear resistivity to the problem of high$-T_c$ superconductivity is based on more that just an analogy to the superconductivity observed in some of the heavy fermion materials. Several studies have found correlations between the presence of a $T-$linear scattering rate and the superconducting transition temperature, in cuprates and other superconductors.

Some of these studies proceed by simply fitting the the resistance versus temperature curves above T_c to a simple sum of a $T-$linear and $T-$squared term, or to a single term with an exponent, n ($\rho \sim T^n$), that is allowed to vary continuously from one to two.[37, 52] This approach has the shortcoming that neither of these forms is well motivated theoretically. Although $T-$squared resistivity is often treated as the default behavior of a Fermi liquid, it is not the behavior expected for a real metal in the temperature range being studied, as noted above. It is not at all clear that the resistivity should cross over to a $T-$squared form at fifty or one hundred kelvin just because an NFL state disappears. Others have approached the problem by trying to look directly at the $T \to 0$ behavior by applying a large magnetic field to suppress superconductivity.[31, 56] These studies do indeed see $T-$linear behavior that vanishes at the edge of the superconducting dome, for both the hole- and electron-doped systems, but the interpretation is complicated by the fact there is now a large magnetic energy scale present in the system. A final approach was taken by Abdel-Jawad and Hussey who looked at the angle dependence of the magnetoresistance.[1] The form of the angle dependence that is observed suggests an anisotropic quasiparticle scattering rate. If one fits the scattering rate to two terms, one an anomalous $\sim cos(2\theta)$ term and one a more natural isotropic term, it is possible to show that the anisotropic term alone is $T-$linear, and that the strength of this term does correlate with T_c.

There are a number of other experiments on the cuprates that confirm the generic predictions for a quantum critical metal. Prominent among these is the observation of an effective mass enhancement near optimal doping. This can be seen both in quantum oscillation data and in the heat capacity.[96] Most significant for the present work is the observation of ω/T scaling in the optical conductivity of $Bi_{2.23}Sr_{1.9}Ca_{0.96}Cu_2O_{8+\delta}$.[76] The next chapter will

outline this in more detail, but in quantum critical systems, the scaling behavior that exists in thermodynamic quantities near a phase transition extends to dynamic quantities like the optical conductivity or the resistivity. This essentially arises from the fact that dynamics and thermodynamics are mixed by the uncertainty principle in quantum mechanics. The observation of scaling in the magnetoresistance will play a central role in this thesis, and the fact that it connects to a significant observation in the cuprates strengthens the case that the charge dynamics in all these materials may fit into a single theoretical picture.

Finally, before leaving the subject of high$-T_c$ superconductivity in the cuprates, I should say a few words on the the history of magnetoresistance measurements in these systems. Since the cuprates exhibit a wide variety of anomalous behaviors, the magnetoresistance has also been scoured for anomalies for many years. Some systems, such as $YBa_2Cu_3O_{7-\delta}$ and $La_{2-x}Sr_xCuO_4$ have been shown to violate Kohler scaling as a function of temperature.[44] This scaling relationship says $\Delta\rho/\rho_0$ should be a single function of H/ρ_0.[93] This is expected to hold in a metallic system with only one relaxation time where the magnetoresistance is due just to the reduction in the current carriers' average velocity as they are deflected by the Lorentz force. In this case the degree of the reduction in the conductivity is determined simply by how far the carriers travel before they are scattered, i.e. by the scattering rate (see section 5.3 for more details). However, any deviation from a single scattering rate per unit time, such as nonuniform phonon occupation numbers (which leads to a frequency-dependent scattering rate) should lead to such violations. As a result, Kohler scaling often fails in simple metals as a function of temperature (although it usually holds as a function of disorder.) Thus it is not clear that this is an indication of anything seriously anomalous. Additionally, recent measurements have found Kohler scaling to hold in other cuprate systems, such as $HgBa_2CuO_{4+\delta}$.[21]

Thus, at the time of writing the strange metal behavior in the cuprates' charge transport properties is restricted to the fan-like pattern in the resistivity and the strongly $T-$dependent Hall effect (see section 7.6 for a discussion of the Hall effect in the cuprates). These observations were made very soon after the cuprates were discovered, and they haven't been significantly extended since then. They have been sufficient to indicate that something like the NFL behavior common to heavy fermion metals and other quantum critical systems is relevant to the cuprates, but it has not been enough to find a satisfying conceptual framework for understanding these materials.

1.3 An introduction to $BaFe_2(As_{1-x}P_x)_2$ and its virtues

This is some of the most well-trodden territory in condensed matter physics. Any proposal for a new experiment, especially on a frequently measured property like a transport coefficient, must explain why it will add fundamentally new information to this vast field. In this section I will cover the basic features $BaFe_2(As_{1-x}P_x)_2$ that will allow the reader to understand the significance of the results in this dissertation, and to understand why high field magnetoresistance measurements on $BaFe_2(As_{1-x}P_x)_2$ were chosen as an avenue for

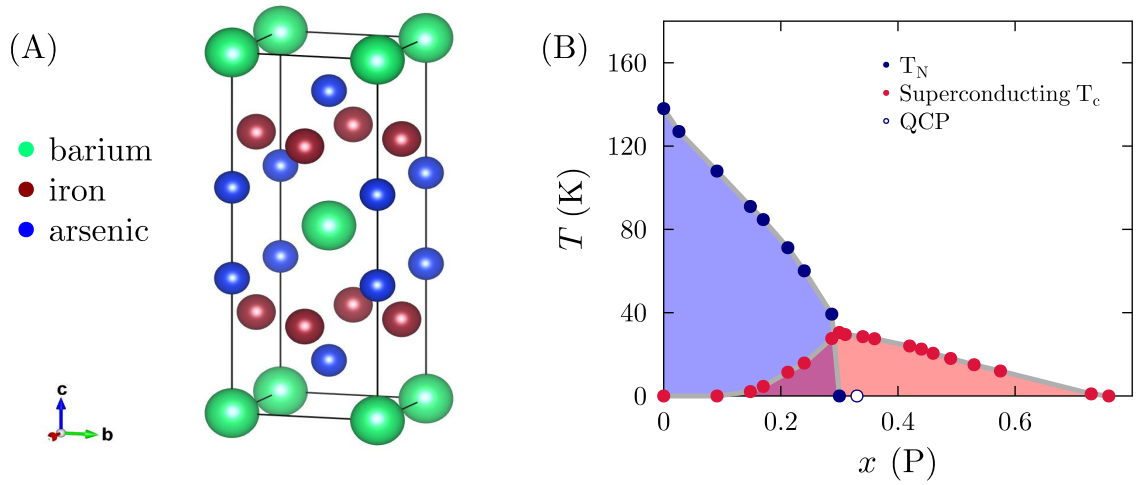

Figure 1.3: **The temperature-doping phase diagram of** $BaFe_2(As_{1-x}P_x)_2$**.** (A) The crystal structure of $BaFe_2(As_{1-x}P_x)_2$. The basic structural constituents are the iron-arsenide planes, where the iron forms a square lattice and the arsenic sits at the center of those squares, alternately above and below the plane. (B) The phase diagram of $BaFe_2(As_{1-x}P_x)_2$ as a function of doping and temperature, showing both the antiferromagnetic/orthorhombic transition at low dopings, and the superconducting dome. The zero kelvin endpoint of the antiferromagnetic/structural transition is labeled with a white circle. This phase diagram shows strong similarities to both the cuprate and heavy-fermion superconductors.

extending our understanding the NFL behavior of high$-T_c$ superconductors.

Many good reviews of the iron-based superconductors exist, and I will draw heavily on two of them for this section.[111, 88] Like the cuprates, the iron-based superconductors come in several classes, generally denoted by the ratio of elements in their formula units: there are the 1111 compounds, the 122 compounds, the 11 compounds and the 122* compounds, along with a few more niche examples like the 21311 or skutterudite compounds. However, the basic constituent of all of these compounds is a layer of iron atoms bonded to either pnictogen atoms (most often arsenic) or chalcogen atoms (usually selenium). The iron atoms sit on a square lattice with the pnictogen/chalcogen atoms at the center of the iron squares, alternately raised and lowered above the plane defined by the iron atoms. In the 11 compounds, no other elements are present, so in some sense these are the simplest of the iron-based superconductors. However, their phase diagrams do not contain magnetism, except under pressure, so their relevance for the study of the nexus of $T-$linear resistivity and quantum criticality is limited. In the 1111 compounds the iron-pnictogen planes alternate with an oxy-lanthanoid layer (the other two "1"s in the name). There are versions of this compound that utilize most of the lanthanoid elements. Superconductivity in these compounds is usually induced by substituting fluorine for oxygen. This suppresses the antiferromagnetism

of the parent compound and leads to a superconducting ground state. However, chemistry limits the amount of fluorine that can be introduced into the compound and typically one cannot dope these compounds all the way to a nonmagnetic, non-superconducting state.

The 122 compounds contain a single alkaline element between the iron-pnictide planes. Several elements can be used for the "1" position, including barium, calcium, and strontium. Each of these compounds is an antiferromagnetic metal, and becomes a nonmagnetic superconductor upon alloying which can be done on any chemical site. Hole doping on the alkaline site, electron doping on the iron site (with either cobalt or nickel) and isovalent substitution on the pnictogen site all suppress magnetism and induce superconductivity. All of these alloying procedures allow one to dope the system back to the non-superconducting state, and therefore to explore the full phase diagram. This phase diagram is qualitatively similar to the cuprates and heavy fermion superconductors in many regards. The antiferromagnetic phase transition of the parent compound is suppressed with phosphorous substitution. There is a superconducting dome that reaches its maximal T_c right around this apparent quantum critical point (see Figure 1.3).[111] Weirdly enough, alternative schemes (such as hole doping on the iron site) have not been shown to induce superconductivity. This gives us a wide menu of options from which we have chosen the isovalently substituted compound $BaFe_2(As_{1-x}P_x)_2$. This compound is distinctive for being one of the cleanest in the wide world of iron-based superconductors. It is the only one of the doped compounds to exhibit magnetic quantum oscillations,[106, 3] and has clearly the highest residual resistivity ratios as well.[58] This is likely for two reasons. First, isovalent substitution does not introduce irregular space charges into the lattice; since phosphorous and arsenic are both pnictogens, they have the same preferred oxidation states. Second, the orbital content at the Fermi level is believed to be about 95% iron $d-$orbitals, based on density functional theory calculations and angle-resolved photoemission measurements.[63, 108] This means that quasiparticles near the Fermi surface will only see a small change to their local electronic environment when phosphorous is substituted for arsenic, even when those substitutions reach the order of 50%.

The fact that $BaFe_2(As_{1-x}P_x)_2$ is an exceptionally clean material has one very important consequence for charge transport measurements: of all the iron-based superconductors, $BaFe_2(As_{1-x}P_x)_2$ has the most pronounced $T-$linear resistivity. All of the other materials in this class have notably low residual resistivity ratios ($\rho(300K)/\rho(0K)$) across their respective phase diagrams, making the $T-$linear part of the resistivity (if it is observable at all) a smaller part of the signal, especially at low temperatures.[113, 23, 38] Some compounds show signs of resistivity saturation at temperatures as low as three hundred kelvin.[12] By contrast, in $BaFe_2(As_{1-x}P_x)_2$ the $T-$linear resistivity continues up to four hundred kelvin with no signs of deviation from linearity (see Figure 1.4). This extended region of $T-$linear resistivity allows us to define the gradient of the linear-in-T scattering rate unambiguously and to clearly identify where the resistivity deviates from linear-in-T behavior. This makes $BaFe_2(As_{1-x}P_x)_2$ especially well suited for transport studies of the strange metal state.

Of course, as with the cuprates, we cannot trace the $T-$linear resistivity down to zero kelvin. The connection to the the cuprates and to quantum critical metals is therefore based,

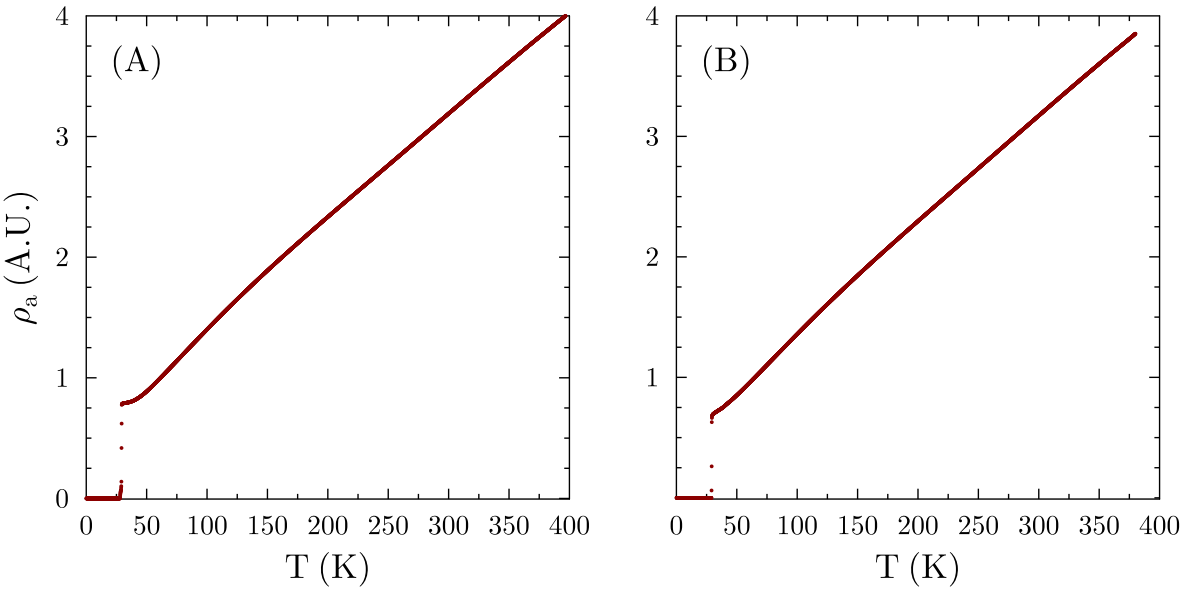

Figure 1.4: **Linear-in-temperature resistivity up to high temperatures in optimally-doped $BaFe_2(As_{1-x}P_x)_2$.** Panels (A) and (B) show resistance versus temperature curves for two samples of $BaFe_2(As_{1-x}P_x)_2$ with thirty percent phosphorous substitution, AG186s10 and s19. This substitution level is the lowest necessary to completely suppress antiferromagnetic order, which means these samples should be very close to being quantum critical. The $T-$linear resistivity continues up to the highest measured temperature of four hundred kelvin.

to a large extent, on the overall behavior of the resistance as a function of temperature across the doping phase diagram and not just on the existence of $T-$linearity over a narrow region. As can be seen in Figure 1.5, $BaFe_2(As_{1-x}P_x)_2$ has an S-shaped resistivity in the underdoped regime, and even slightly into the optimally doped regime, where an approximately quadratic resistivity crosses over to a region of negative curvature and eventually a $T-$linear region at higher temperatures. Slightly beyond optimal doping, there is narrow region of $T-$linear behavior extending over the entire temperature range, and beyond that there is a region of exclusively positive curvature that continues to the far overdoped side. This is the characteristic pattern in the dependence of resistivity on temperature that is seen in the cuprates and in several classical quantum critical systems like $Sr_3Ru_2O_7$ (compare with Figure 1.2).[8, 18] Whatever is responsible for this characteristic pattern is likely to be the same in all of these contexts, especially in the cuprates and pnictides, where high-T_c superconductivity is also present.

However, the low temperature limit is still of intrinsic interest. Part of the motivation for studying these materials in high magnetic fields is that one can gain access to the low

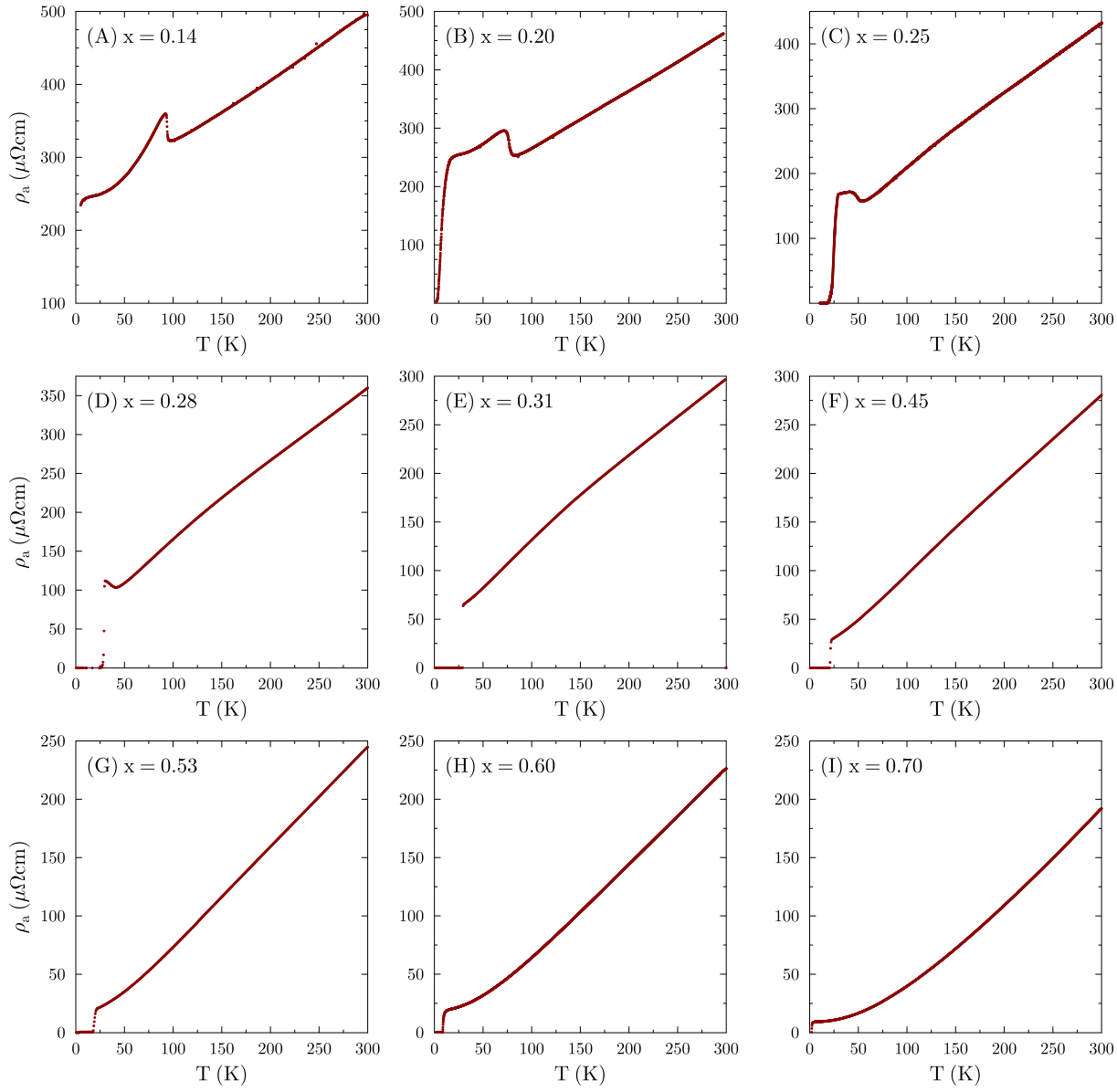

Figure 1.5: **Resistivity versus temperature across the phase diagram in $BaFe_2$-$(As_{1-x}P_x)_2$.** The overall trends are strikingly similar to what is seen in both the cuprates and quantum critical metals, with $T-$linear resistivity over a wide temperature range confined to a narrow region around optimal doping, with $T-$squared resistivity gradually appearing at low temperatures on the overdoped side.

temperature normal state in a superconductor. Even if the magnetic field perturbs the system significantly, the resulting system is still in a condition where thermal fluctuations are minimized. In this regard, $BaFe_2(As_{1-x}P_x)_2$ sits at a happy medium: it is recognizably a high-T_c superconductor, but the upper critical field at optimal doping is around forty-five tesla, which is low enough that we can access its normal state at fields that are available in contemporary high field laboratories. This allows us to look directly at low-temperature behavior in the zero temperature limit near the critical point. In the cuprates, the critical fields at optimal doping are well above one hundred tesla, rendering the actual quantum critical point inaccessible to charge transport experiments.

In addition to being a nice system from the perspective of doing charge transport measurements, $BaFe_2(As_{1-x}P_x)_2$ shows the greatest evidence for the relevance of quantum critical physics of all the iron-pnictide superconductors, and perhaps of all the high$-T_c$s overall.[105, 2, 35] Beyond the presence of $T-$linear resistivity, this evidence comes mainly in the form of observations of a strongly enhanced or even diverging effective mass near the zero kelvin endpoint of the antiferromagnetic and orthorhombic phase boundary. Critical fluctuations are expected to modify the effective mass of quasiparticles as the critical point is approached, leading to a diverging effective mass at the critical point itself.[71] An actual divergence is unlikely in real systems, but a strong enhancement of the effective mass, localized around one point, suggests the influence of a critical point. There is also supporting evidence that comes from direct measurements of time scales in the systems via nuclear magnetic resonance. The next few paragraphs will discuss this evidence in more detail.

Unfortunately, as far as measuring the effective mass is concerned, the very low temperature measurements that would normally provide the most convincing evidence for criticality are once again not available because of the high superconducting transition temperature. The thermodynamic effective mass would usually be inferred from measurements of the linear-in-T component of the heat capacity in the zero temperature limit. As a result, other methods have had to be employed. One is to measure the size of the heat capacity jump at the critical temperature. In the standard weak-coupling scenario the size of this jump depends directly on the effective mass. Holding everything else constant, ΔC_p can therefore be used to measure the change in effective mass across the phase diagram. This method shows a strong growth in $m_{effective}$ on approach to $x = 0.3$, from both the under- and overdoped side.[119]

Robust measurements of the effective mass can also be made from magnetic quantum oscillation data. These measurements are robust in the sense that the theory of these oscillations is very well developed, and the fit by which the mass term is extracted from the data is therefore highly reliable.[107] If one sees magnetic quantum oscillations, then their temperature dependence is determined exclusively by the quasiparticle effective mass. As mentioned above, $BaFe_2(As_{1-x}P_x)_2$ is the only doped iron-pnictide to show magnetic quantum oscillations.[106, 20] They only appear in the magnetization and only for doping levels greater than thirty-eight percent, but they show a clear enhancement in the effective mass of around a factor of two on approach to optimal doping. Furthermore, a reasonable fit to a logarithmic divergence gives a critical point of $\sim 31\%$ phosphorous substitution, which is in

good agreement with the actual phase diagram.[106] It is also in good agreement with the effective masses derived from the heat capacity jump at T_c.[119]

Effective mass values have also been extracted from the penetration depth in the superconducting phase. These measurements also show a very sharp peak in the penetration depth near optimal doping.[45] Penetration depth is another indirect measurement of the effective mass: a lighter mass generally leads to better screening near the surface and therefore a smaller penetration depth. Thus, the enhanced screening length near optimal doping implies an increase in the effective mass. The location and size of this enhancement is in broad agreement with divergences reported from heat capacity and quantum oscillations.[105]

Finally, there are more or less direct measurements of the length and time scales of the spin correlations. Nuclear magnetic resonance (NMR) measurements probe the local magnetic field at the nucleus. The shift in the effective field seen by the nucleus is a measurement of the uniform ($q = 0$) magnetic susceptibility. With a radio wave polarization measurement, one can observe the decay rate of the nuclear spins, which is in turn a measure of the correlation time for the local magnetic environment. For a normal Fermi liquid, this is predicted to vary inversely with the temperature, such that $(Tt_{relaxation})^{-1} \propto constant$.[65] This follows from the independence of the electrons (and therefore of their spins) and the phase space restrictions of a degenerate Fermi gas.

Measurements of nuclear spin-relaxation times in $BaFe_2(As_{1-x}P_x)_2$ show a growth in the the magnetic correlation time as the temperature is lowered, in excess of what is predicted for a Fermi liquid.[81] This behavior is natural for a system with magnetic correlations. In a system with a magnetic phase transition, the correlation time is expected to diverge at a magnetic transition. Indeed this is what one sees at the antiferromagnetic transition in underdoped samples of $BaFe_2(As_{1-x}P_x)_2$. The key finding in the NMR data is that if one fits the temperature dependence for this correlation time to the standard form, then samples with phosphorous levels near thirty percent show a divergence temperature of zero kelvin. This wouldn't have to happen. Recall that criticality occurs near a second order phase transition. It is possible that the zero temperature magnetic transition in $BaFe_2$-$(As_{1-x}P_x)_2$ is first order. In this case, the divergence temperature should jump precipitously from positive to negative and skip over zero. The fact that it does not–at least based on extrapolations from above T_c–is good evidence that the transition is second order and critical.

There is one outstanding tension in the experimental picture of quantum criticality in iron-pnictide superconductors. The most direct probe of the length scale of magnetic fluctuations, neutron scattering, does not see evidence for a magnetic critical point in these materials. In the cuprates, it is also the case that the antiferromagnetic correlation length is short.[79] However, given the contours of their phase diagrams, it was always unlikely that magnetism is responsible for the anomalous properties near optimal doping. Those who argue for the relevance of quantum criticality have proposed that the pseudogap temperature, which reaches zero kelvin around optimal doping, in fact represents a true thermodynamic phase transition, and that fluctuations of this phase lead to critical dynamics. In the Iron-based superconductors, the clear candidate phase is magnetism, since the magnetic transition temperature extrapolated to zero temperature at the doping levels that display the most pro-

nounce $T-$linear resistivity. Therefore, the absence of such features in the neutron data is more problematic.

The most comprehensive neutron work on optimally-doped, single crystals of $BaFe_2(As_{1-x}P_x)_2$ was done by Hu et al.[48] They found that the antiferromagnetic/structural transition temperature jumps abruptly from about thirty kelvin at $x = 0.29$ to zero at $x = 0.30$. Similar results have been found in other doped, 122-series compounds.[74, 94, 72, 73] This makes it look as though the zero temperature transition is not second order, but first-order, at least weakly. On the other hand, there is at least one doping series, copper-for-iron substituted $BaFe_2As_2$, that shows a correlation length that seems to be diverging towards zero temperature, although this compound does not show superconductivity.[61]

These observations seem to be in tension with the NMR experiments, which suggest that the correlation time is in fact diverging. It is possible that this is just a reflection of the fact that correlations in time can grow independently of correlations in space. Although both length and time scales are expected to diverge near a quantum critical point, they will in general do so with different exponents.[109] Some approaches to quantum criticality even have the length scale diverging only logarithmically.[116] On the other hand, it may be the case that the criticality in $BaFe_2(As_{1-x}P_x)_2$ is not driven by magnetism at all, but by symmetry breaking in the electronic orbitals. This phenomenon goes by the name of nematicity on analogy with the rotational symmetry breaking in liquid crystals. A number of studies have found evidence for nematic critical behavior, and it seems that nematic criticality may also be present in the cuprates.[24, 68]

Alternatively, this may just be an indication that metallic criticality does not manifest in exactly the same ways as its insulating counterpart. Perhaps the coupling to gapless excitations always keeps the correlation length short while the dynamics becomes singular, leading to anomalies like $T-$linear resistivity. Because the theory of metallic quantum criticality is not well developed, it is impossible to say that this represents a definite contradiction with a certain theoretical proposal. Rather, it may be a clue that points towards the correct description of quantum critical metals.

1.4 Goals for High-Field Measurements on $BaFe_2(As_{1-x}P_x)_2$ and Summary of Results

In the previous sections I have tried to summarize the experimental situations that define two of the most significant problems in strongly correlated electron physics and condensed matter physics as a whole. Unlike other contemporary research projects they are characterized by the absence of any well established theory. Other major contemporary research topics in condensed matter physics, like topological states of matter or spin liquids, enjoy major theoretical as well as experimental progress. The first has at its disposal the very successful band theory of crystals and the latter can claim several well-defined and solvable models. The fields of quantum critical metals and high$-T_c$ superconductivity, on the other

hand, are in something like the state that the study of metals was in prior to landmark achievements of Landau. Various patterns in the data suggest that a universal physics is present, but we find ourselves unable to construct a reasonable theoretical framework that captures it.

The theory of quantum critical metals, in particular, is in a very rough state. The key challenge is the existence of a robust Fermi surface and the attendant large number of gapless excitations. If one tries to write down a free energy functional for the fluctuations of the order parameter that includes any coupling to the electrons, he quickly finds that the theory becomes uncontrolled. The essence of the problem is that scattering rate of the electrons does not damp fast enough on approach to zero temperature for there to be a regime in which quasiparticles are well defined. This fact is more or less obvious from the observation of $T-$linear resistivity: the characteristic energy of excitations is the temperature, and if the resistivity (and therefore the scattering rate) continues to be linear in temperature down to zero kelvin, then there is no regime in which the scattering of the electrons is a small correction to their energies. That is, free electrons are not "almost" eigenstates of the system. Recall that it was the $\sim T^2$ behavior of the electron-electron scattering that allowed Landau to define quasiparticles in the zero temperature limit. Without quasiparticles to define the excitations of a system, physicists are left searching for a whole new language to explain the behavior of these anomalous metals. Chapter 2 will take a look at the theory of quantum critical metals in more depth.

In the field of high$-T_c$ superconductivity, the picture is inverted. There are, if anything, too many theories purporting to describe these materials, and none of them commands a very wide following. The relevance of critical physics for this problem is still hotly debated, though today it enjoys a wider following than any other particular approach to the high$-T_c$ superconductors. This is thanks largely to the data described in sections 1.2 and 1.3. Not all of the leading theorists are impressed, however.[7] Of course, even it one could conclude positively that quantum criticality were central to the problem, it would only substitute one mystery for another, as the physics of quantum criticality in metals is poorly understood. What is not in doubt is that there is a certain pattern in their physical response functions that holds across most of the high$-T_c$ compounds, and that this includes the existence of $T-$linear resistivity at a special point in the phase diagram.

Despite all of the attention these issues have received, a satisfactory theory for either of these two major problems remains elusive. This may well be because in thirty years the basic experimental picture has not been expanded upon. The goal of this project is to change that. Measuring the charge transport properties in high magnetic fields provides a significant opportunity to expand our understanding of the physics responsible for the $T-$linear resistivity. As mentioned above, high magnetic fields make it possible to measure resistive properties at low temperatures, even in high$-T_c$ materials. But more than this, the fact that magnetic fields have a known coupling to free electrons gives us another chance to test how well the theory of free electrons describes these materials and, if it fails, in what way it fails. If there were well developed theories of quantum critical metals it would be important to check their predictions with these data. However, as emphasized above, theories

in this area tend to be uncontrolled and our confidence in their predictions is low. Therefore we take it as our goal to search for behavior in the field dependence of the resistivity that is clearly related to its anomalous temperature dependence, and that could perhaps inspire future theory development.

In this, nature was unusually kind to the author. Several striking patterns were found in the magnetotransport of $BaFe_2(As_{1-x}P_x)_2$, some of which have already inspired model builders.[90] The first of these was the observation of a linear-in-field resistivity that only exists at low temperatures near the hypothesized critical point in $BaFe_2(As_{1-x}P_x)_2$. This offers a tantalizing parallel with the $T-$linear resistivity observed at this same doping level and offers some support to a certain framework for thinking about transport in a quantum critical metal (discussed in chapter 2). Furthermore, all of the magnetoresistance data near optimal doping conforms to a scaling form in H/T, similar to what one sees for thermodynamic quantities near a classical phase transition.[103] This also supports a certain theoretical perspective (if not a fully developed theory) on quantum critical metals.[109] Having identified a concrete phenomenon in the magnetoresistance of $BaFe_2(As_{1-x}P_x)_2$ near its putative critical point, we ask whether this phenomenon is special to certain orientations of the field and the current. Once again, a simple pattern presented itself: the scaling obtains for any orientation of the current as long as the field is oriented along the crystallographic $c-$axis, i.e. perpendicular to the iron-arsenic planes. For small deviations from field along c, the scaling pattern still obtains if one uses only the $c-$axis component of the field. These observations cannot be explained by the dynamics of nearly free electrons and therefore require the introduction of significant correlation effects in any future model of the electronic dynamics in $BaFe_2(As_{1-x}P_x)_2$. They also require that the physics responsible for the $T-$linear resistivity to have a strongly anisotropic coupling to magnetic fields, but to still influence the scattering rate equally for currents in all directions. This provides a significantly more precise goal for theories of $T-$linear resistivity.

In addition to the extensive data set on the the high field magnetoresistivity of $BaFe_2(As_{1-x}P_x)_2$, this thesis will present the measurements of the Hall effect in $BaFe_2(As_{1-x}P_x)_2$ up to very high fields for a wide variety of dopings. Once again, the known consequences of a magnetic field for the physics of free electrons offers us an opportunity to make the strange metal phenomenology of the high$-T_c$ superconductors more precise. The Hall coefficient of $BaFe_2(As_{1-x}P_x)_2$ is found to decrease in field over most of the phase diagram, contrary to what would be expected if the independent electron approximation were valid. This decreasing Hall coefficient allows us to map the precise range of the anomalous regime that is also characterized by $T-$linear resistivity. Two important facts are thereby revealed. The anomalous behavior conforms to a fan-like pattern temperature and doping that is expected on general grounds for quantum critical systems (and that is in fact seen in many quantum critical systems, see Figure 1.1), and the appearance of superconductivity in this material is perfectly correlated with the presence of anomalous behavior in the ground state. This establishes a powerful direct link between high$-T_c$ superconductivity and anomalous charge transport behavior. Finally, this anomalous behavior in the Hall coefficient turns out to be remarkably sensitive to the size of the sample, even at the nearly macroscopic scale of

$\sim 1 - 4\mu m$. This explicitly confirms that it is not a band structure effect and must arise from some very long wavelength phenomenon in the material. Since length and time scales are expected to diverge near criticality, it also provides further support to the idea that criticality is driving the electronic dynamics in this system.

In different ways these data all seem to support something like a quantum critical scenario for $BaFe_2(As_{1-x}P_x)_2$. As emphasized above, this is not really a claim that the physics of high$-T_c$ superconductivity is given by the theory of quantum critical metals. Even to the extent that one can be confident in our predictions from these theories, there is significant tension between several of these findings (for example, the fact that the clearly critical-fan like pattern in R_H is observed in a separate term that adds in series) and what is predicted of the theory of quantum critical metals. Rather, it is a statement that this physical system (and perhaps others like it) are most likely described by a language whose basic terms are the familiar ingredients of quantum critical theory. These data should provide the guidance that theory requires for what to focus on; in any case they provide hope that there is a solution in this direction.

The rest of this dissertation is organized as follows. The next chapter will present the theory, such as it is, of quantum critical metals and $T-$linear resistivity. Chapters 3 and 4 will be dedicated to the experimental techniques employed, the first in the realm of materials synthesis and characterization and the second on charge transport measurements in pulsed magnetic fields. Each of the next four chapters will cover one segment of the high field data and interpret it. Finally, chapter 9 will conclude with an overview of the contributions of these data to the broad challenges facing strongly-correlated electron physics and suggestions for further research.

Chapter 2

Theory of Quantum Critical Metals and $T-$linear Resistivity

2.1 Introduction

This chapter will outline the theory that exists on quantum critical metals, with the goal of providing a context for the claims made in later chapters. This short summary should make it clear that the primary goal of experiments in this field cannot be to test detailed predictions of specific theories, as such predictions cannot be made with confidence for models of realistic systems. Rather, experiments in this field are most useful when they can identify clear patterns in the data that can provide new starting points for theories. The principle reason for the messy state of theory in this field is that the most elemental constituent of the ordinary theory of metals, the quasiparticle, seems likely to be unusable in this case. This chapter will start by presenting the physics of classical critical systems, which are very well understood, and the necessary extensions required for describing quantum phase transitions, i.e. those that happen at zero temperature as a function of some non-thermal parameter. Quantum phase transitions are well understood when the system is an insulator (and so does not have gapless excitations).[29] This will make clear the challenges of capturing the physics of metallic critical systems (which will have gapless excitations) from a theoretical perspective. The final section will look in detail at the phenomenon of $T-$linear resistivity and the problem that it creates for any theory based on quasiparticles. Throughout I will be following several useful reviews, and one especially useful APS march meeting tutorial.[109, 100, 27]

2.2 Classical critical theory and the $D+1$ mapping

Although phase transitions are some of the most familiar of all physical processes, an adequate framework for describing them did not exist until Lev Landau made the conceptual breakthrough of introducing the "order parameter."[70] This quantity is meant to capture

quantitatively the idea that phases of matter are distinct when one of them observes some sort of regular order among their constituent elements over time. For example, an ice cube in a cup of water is distinct from the liquid that surrounds it because the water molecules that constitute it remain, on average, the same distance apart from each other. In the liquid, molecules travel throughout the medium and do not remain in any fixed relationship to another molecule. This means that the quantity

$$\sum_i e^{-iG_i r}\rho \tag{2.1}$$

where ρ is the density and the vectors G_i are the reciprocal lattice vectors of the solid, would maintain a nonzero value within the solid phase but would be zero in the liquid.[6] This is the essential property of an order parameter that allows us to characterize a phase transition: its value is zero while the system remains in the disordered phase, but it takes on a nonzero value in the ordered phase. From statistical mechanics we know that a system in equilibrium will adopt the state with the lowest value of the relevant thermodynamic potential. Thus, we can write down an abstract version of the thermodynamic potential as a function of the order parameter. To allow us to capture a phase transition, the function needs to contain a temperature dependence such that the minimum value of the potential occurs at $\phi = 0$ for temperatures above the critical temperature and at some nonzero value of ϕ for temperatures below it. The simplest example would be

$$F(T, \phi) = F_0 + A(T - T_c)\phi^2 + \phi^4 \tag{2.2}$$

As the sign of the ϕ^2 term goes from positive to negative, the minimum value of the function moves away from zero. As long as we are principally interested in the behavior of the system in the immediate vicinity of the phase transition, it is sufficient to include the lowest order terms in ϕ. If we assume that the "directions" ϕ and $-\phi$ are energetically equivalent, then second and fourth ordered terms included above are the lowest order terms available, and are sufficient to describe a phase transition.

From this simple and abstract formula one can make rigorous and quantitative predictions for how various quantities should change near the critical point. For example, the heat capacity, which is given by $C_v = -T\frac{\delta F}{\delta T}$, can be shown to diverge (because of the cusp-like change in the minimum value of F), and this divergence has a characteristic exponent of $1/2$. This model might seem like it is too simple to be a good description of any interesting physical system, but in fact a wide variety of real systems display exactly this kind of divergence in their heat capacity, along with singularities in other thermodynamic variables all of which follow from this simple free energy function.[103]

This seems like a minor miracle to most people the first time they encounter it, but a few moments reflection can help relieve one of this disbelief. Recall that if we assume that our system has the $\phi \to -\phi$ symmetry these are the lowest order terms that could possibly describe the change in the free energy. Therefore, any system with an order parameter that obeys this symmetry (and no others) will *have* to obey the form of equation 2.2 sufficiently

close to its critical point because as $\phi \to 0$ only the lowest order terms are relevant. Critical points that have the same symmetries and dimension thus fall into what is called a universality class (in this case the ϕ-to-the-fourth universality class, after the free energy function given above), and will generically exhibit the same pattern of physical responses near their critical points, despite their wildly varying microscopic constituents.

The key advance in developing this theory was not solving any especially complicated mathematics, or finding any surprising new feature of the system that appears near a critical point, but simply identifying the correct quantity to examine. Once one has recognized the existence of the order parameter, it is easy to analyze its essential behavior. Recognizing that there is such a quantity to be examined is the difficult step. This is, in the author's opinion, the kind of insight necessary for extending our understanding of metals into the non-Fermi liquid regime. Historically, it was the fact that so many microscopically distinct systems showed the same critical exponents that made scientists believe in the existence of simple, universal theory of phase transitions.[103] They were right at the time, the same attitude may well be appropriate today.

In principle, this approach to studying phase transitions is appropriate for a classical system. The extension to quantum systems is just the usual one of deriving the free energy from the eigenstates of the Hamiltonian operator:

$$F(T, \hat{H}) = k_B T log(\sum_i exp(\frac{-\epsilon_i}{k_B T})) = k_B T log(Tr(exp(\frac{-\hat{H}}{k_B T}))) \tag{2.3}$$

where the sum is over all eigenstates of the system, resulting in the trace on the far right-hand side. In many ways, the statistical mechanics of quantum systems is formally identical to that of classical systems. However, the presence of the Hamiltonian operator in the exponent has some interesting consequences. In classical mechanics the energy is a number and not an operator, so the free energy splits into two terms, one which contains all of the momentum variables, and one which contains exclusively position variables. In quantum mechanics this is no longer true. Because of the uncertainty principle, the allowed states are defined by particular combinations of momentum and position. As a result, the dynamics ends up being encoded in the thermodynamics.[109]

However, the presence of the trace operation in the formula for F (eq. 2.3) relieves us, to some extent, from the need to actually solve for the eigenstates of the complicated, many-body system. The trace is, after all, independent of the basis in which the operator is written, so that as a long as one has a complete set of states, and a definition for their interactions, one can compute the free energy without diagonalizing the Hamiltonian. The trick is to exploit the formal analogy between $exp(\frac{-\hat{H}}{k_B T})$ and the time evolution operator. If we were to make the substitution $1/k_B T \to it/\hbar$, this operator would exactly be the time evolution operator for the system over a time $t = \beta/\hbar$. We can then evaluate each element in the trace as a time evolution from one of the basis elements back on to itself. This time evolution can, in turn, be evaluated by introducing a resolution of the identity every fixed unit of time. The system is therefore transformed into another lattice model, whose free energy is evaluated by including another dimension, albeit one of a finite length $L = \hbar\beta$.

We can see then, that if we wish to describe a singularity in F at zero temperature (where $\beta \to \infty$), the free energy is formally identical to that of an analogous classical system in one higher dimension. This it might make it seem that there is nothing new to discover in quantum critical systems, but this mapping between classical and quantum models conceals two important facts. The first is that this extra dimension is connected rather directly to the time-evolution of the system. Since the free energy uses an operator that is formally the time evolution operator in imaginary time, one can, in principle, derive correlation functions across finite time from the free energy by analytically continuing the expression to real time. In practice, performing this continuation is often analytically impossible and numerically treacherous. Nonetheless, it leads us to expect that the long-range correlations that develop at the critical point will appear in the real-time correlation functions as well, and therefore in dynamics quantities. There is no guarantee that the power-laws will be the same, but the singularity, which is responsible for the scale-invariant behavior that is captured in the power law divergences near a critical point, should also dominate real time correlation functions, and therefore lead to scale-invariant dynamics. The first half of this thesis will be devoted to searching for signs of this scale-invariant dynamics in the prototypical dynamic quantity: the momentum relaxation time, as represented in the electrical resistivity of the system.

The second fact which this formal analogy between quantum and classical critical systems conceals is the possibility of a Fermi surface. Classical dynamics has no analogue of the "degeneracy pressure" felt by fermions in their degenerate state, and therefore no analogue of the macroscopically large number of momentum carrying states that exist in a Fermi liquid. Because momentum and positional degrees of freedom cannot be disentangled, the long-range correlations that necessarily develop near a critical point can transform the whole set of degrees of freedom that the model is supposed to describe. The next section will describe how this creates problems for the theory of quantum critical metals.

2.3 Problems with the weak coupling theory

Quantum critical theory emerged in a serious way as early as 1976, when J. A. Hertz extended recent work on ϕ-to-the-fourth theory to the case of a quantum critical point.[46] This forms the basis of our thinking about many of these problems today. However, the pure ϕ-to-the-fourth theory only has one component in it: the bosonic mode that is condensing at the critical point. This makes the theory appropriate for understanding quantum phase transitions in an insulator, where there are no other long-range modes in the system that one need keep track of. In a metal there is always a Fermi surface, which guarantees the presence of other low-energy modes, and these will couple to the critical bosons and modify their behavior all the way down to zero temperature. As we will see, it is the existence of these modes that creates problems.

The generic critical theory has the same starting point we saw above: ϕ^4 theory. We use the first two terms allowed by symmetry to parametrize the transition, but we will also allow the order parameter to vary in space and time as well, so that we may describe the

dynamics of the condensing mode (T_c has gone to zero):

$$F(T,\phi) = T\int dk \sum_m (ck^2 + \omega_m^2 + a)\phi^2 + \phi^4 \tag{2.4}$$

where ω_m are the Matsubara frequencies that arise in the quantum free energy ($\omega_m \equiv (2n+1)\pi/\beta$).

There are now two things to consider: the effect of the fermions on the bosons, and the effect of the bosons on the fermions. The first of these is reasonably benign. A simple Feynman diagram allows one to compute the effective free energy of the bosons:

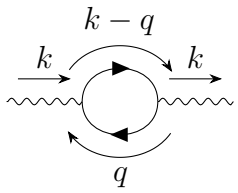

This results in an extra term in the propagator of the bosonic mode, and thus an extra term in the free energy.

$$F(T,\phi) = T\Sigma(ck^2 + \omega_m^2 + c\frac{|\omega_m|}{|k|} + a)\phi^2 + \phi^4 \tag{2.5}$$

This term will change the effective dimension of the theory because it adds another power of omega, but otherwise the theory will remain unchanged.[27]

The catastrophe emerges when we consider the other direction. To understand why this is, it is helpful to look first at the structure of ordinary Fermi liquid theory and to understand what makes it sound. A theory of completely free electrons has a Green's functions that look like:

$$G(\omega,k) = \frac{1}{\omega - \epsilon(k) + i\eta} \tag{2.6}$$

The infinitesimal quantity, η exists for mathematical consistency, and single-particle excitations of this system do not decay, as the free electron states satisfying $\omega = \epsilon(k)$ have infinite weight on the real axis. In a theory with interactions, however, these states are not pure eigenstates of the system. Interactions cause the overlap at finite time to be less than one, and the Green's function gains a finite imaginary term in its denominator:

$$G(\omega,k) = \frac{1}{\omega - \epsilon(k) + i\gamma(\omega,T)} \tag{2.7}$$

This γ term limits the lifetime of this state. The key requirement for a stable theory is that this term be small compared to the energy of the particle itself. This allows one to treat the single-particle excitations as being nearly the eigenstates of the system. In principle this is a hopeless criterion because the actual scattering of the electrons clearly grows with

temperature and and so can get arbitrarily large. The point is rather that there is some region of energies where $\gamma \ll \epsilon$, so that there is a reasonable starting point for understanding the system. This will inevitably be the region of low temperature, where scattering is minimized. The requirement for a sound theory is thus that γ disappears more rapidly than the average single-electron energy as zero temperature is approached.

Landau's major breakthrough was to realize that phase space restrictions on electron-electron scattering guaranteed that the scattering rate γ would disappear at low temperatures more quickly than T, which is the average energy of fermionic excitation.[69] In the simplest case this will go as $\sim T^2$, for reasons given in chapter 1. Therefore, the theory of interacting fermions at least has a controlled starting point. This sanctuary is denied to us, however, if critical bosons are introduced into the picture. The lowest order interaction which one can introduce between electrons and the critical fluctuations is of the Yukawa type, and introduces the following correction to the Fermion propagator.

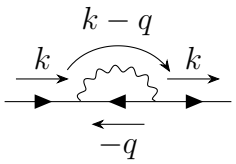

Let us consider the degree of scattering represented by this self-energy. If we are away from the quantum critical point, then the bosonic propagator has a gap. Therefore, at low enough temperatures, the contribution of this diagram will decay rapidly, more rapidly than the electron quasiparticle self-energy. Thus the basic structure of the excitation spectrum will be preserved. If, on the other hand, we are at the critical point, then the bosonic spectrum is gapless and this diagram will give a contribution proportional to the electron energy, ω. Thus scattering rate does not diminish any more rapidly than the quasiparticle energy and there is no limit in which the system has nearly free electron excitations.

2.4 T-linear resistivity and the phenomenology of the fan

Non-Fermi liquid physics can be identified via a violation of the Fermi liquid predictions for any of several physical properties. However, the violation of the $\sim T^2$ resistivity is especially problematic. The very stability of the theory hangs on the fact that scattering rate of the quasiparticles diminishes more rapidly than their energy on approach to zero temperature. Of course, this does not require that the resistivity have a T^2 power law, but T^2 will get you there. What it does require is that the scattering rate must have a temperature exponent larger than one. This makes $T-$linear resistivity in the zero temperature limit a deep problem for theory construction, from which no small patch will save you.

Therefore, the observation of $T-$linear resistivity at zero temperature seems to demand a new starting point for our theories. The claim has occasionally been made that $T-$linear

resistivity is actually natural in a scale invariant system. The argument goes roughly as follows. The scattering rate has dimensions of inverse time, or energy: $\gamma \sim E/\hbar$. In a system with scale invariant dynamics, there should be no intrinsic energy or time scale. Thus as the energy is varied, other quantities with the dimension energy must vary directly with the temperature, since there is no other quantity to provide another factor of energy. In contrast, in a Fermi liquid, the Fermi energy contributes the second factor of T to create a $\sim T^2$ scattering rate ($\gamma \sim T^2/E_F$). It is appropriate to have some level of skepticism towards this argument. Dimensional arguments are always suspect in a complex system, since it is always possible that there are background scales in the system that are canceling, and therefore not directly visible. Additionally, critical points generically generate "anomalous dimensions" that lead quantities to follow power laws different from what one would naïvely expect.[103] In any case, it should be clear that this argument is far from being a solid deduction from physical postulates.

Nonetheless, this argument is a decent demonstration of the fact that ideas of scaling are one way that we might understand the response functions of a system without resorting to a description of the system based on quasiparticles. These ideas have been rigorously and successfully applied to the many cases of classical critical systems. They therefore represent an oversimplified but nonetheless reasonable approach to representing the physics of certain non-Fermi liquid systems. In the spirit of Landau, it may be that all that is needed to make this argument correct is some mathematical formalism for understanding why all non-thermal parameters can be neglected in a certain limit.

Even though our theoretical understanding of a critical metal is limited, the idea of a diverging, dominant time scale also creates some genuine expectations for what the region around a critical point might look like. In particular it leads one to expect the "critical fan" observed in some of the systems described in chapter 1. Right at the critical point, the dynamics should "scale down" with temperature, according to some power law. If one now adds a small internal energy scale, effectively detuning the system from criticality, then this should lead to changes in the dynamics at temperatures where this energy scale is equal to or larger than the thermal energy scale. If the temperature is high enough that the thermal time scale in the system is much shorter than that imposed by the detuning energy, then the system will not notice the presence of that extra energy scale because all scattering events will complete before the detuning energy can influence them. This means that at high temperatures, the dynamics of the system will still be controlled by the critical physics. As the temperature is lowered however, the dominant thermal time scale will only increase until it reaches the detuning energy, which will then add some non-critical dynamics to the system. This means that the detuning energy acts as a kind of infrared cut-off for the critical dynamics. For this reason the temperature which bounds the high temperature critical regime is commonly called the "cut-off" temperature. As the detuning energy is increased, and the system moves further from criticality, the cut-off temperature will also increase. The result is a fan-shaped region that grows out of the critical point, within which critical physics dominates. A schematic illustration of this is given in Figure 2.1.[100]

This pattern of behavior is a very robust prediction, given that it just comes from com-

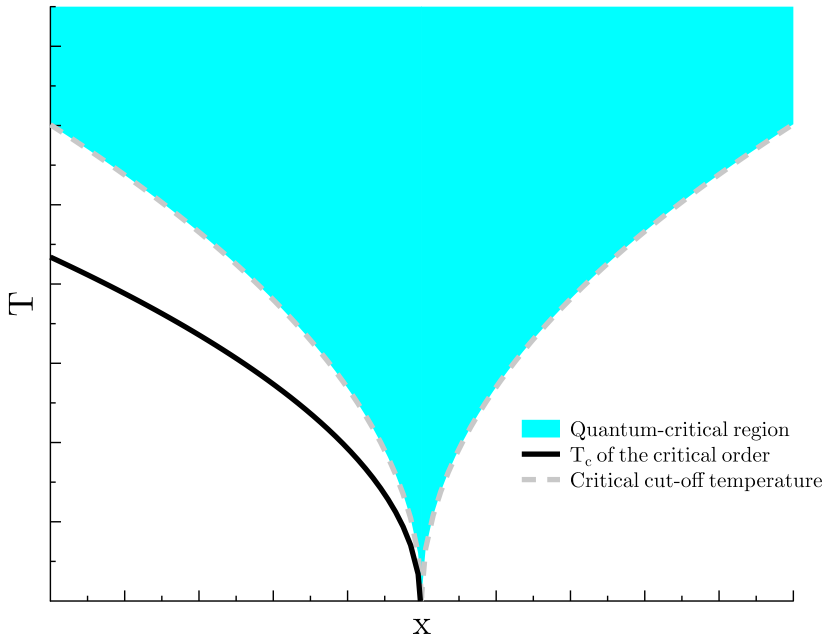

Figure 2.1: **Schematic phase diagram for a quantum critical point.** A quantum critical point occurs when a second order phase transition is suppressed to zero temperature as a function of some non-thermal parameter ("x" above). As long as the temperature is larger than the intrinsic energy scale in the system, which will increase as the system is moved away from the critical point on the x-axis, the response functions of the system will be dominated by fluctuations from critical point. This effect of the detuning energy on the critical fluctuations leads to the fan-like region in which the universal physics can be observed. This is one of the basic expectations for the physics of systems near a quantum critical point.

paring energy scales in a system near criticality. In particular, the observation of the critical behavior continuing to low temperatures is a direct way of observing how close the quantum phase transition is to being second order and continuous. In a first order phase transition, one would expect something similar, except that the correlation length may never get very long, and therefore the correlation time may never get very long, so that the response functions of the system never display anything like a fan. If the transition is weakly first order, then you would expect a moderately long correlation time, leading to a fan that comes close to, but never quite touches the zero temperature axis. Although it may be hard to determine the exact shape that response functions should take near criticality, if they are derived from the effects of a critical energy scale going to zero at the quantum phase transition, something like this fan phenomenology should be apparent. As emphasized above, this pattern is in

fact observed in the charge transport properties of some systems, and this is one of the signs of criticality that we will be looking for in $BaFe_2(As_{1-x}P_x)_2$.

2.5 Conclusion

The physics of non-Fermi liquid metals and of quantum critical metals in particular is a challenging subject. It remains an open question what the basic language is that one should use to describe these systems, as the quasiparticle concept seems to break down both empirically (because of the actual observation of $T-$linear resistivity down to low temperatures) and theoretically (because of the $T-$linear scattering rate predicted by analyses like that described in section 2.3). As was the case with the creation of Fermi liquid theory, it is likely that the correct theoretical framework will have to be inferred from the data, rather than guessed from general theoretical considerations. Ideas from the theory of critical systems are clearly relevant to many of these systems, but this has not been enough to establish a convincing theory for NFL metals. The data that will be presented in chapters 5 through 8 were taken with the partial aim of fleshing out the patterns that have so far been found to be consistent with this critical scenario. Such data are our best hope for seeing exactly what modifications need to be made to the naïve critical scenario in order to give us a handle on NFL behavior.

Chapter 3

Aspects of $BaFe_2(As_{1-x}P_x)_2$ Synthesis

3.1 Introduction

Every experiment in condensed matter physics begins, whether the experimenter realizes it or not, with the preparation of the system of interest from basic elements or compounds. Data obtained with the most sophisticated and expensive equipment are no better than the quality of the sample they are taken on. In order to obtain high quality transport data, one needs access to high quality single crystals. Since electrical transport measurements involve passing current through the entire sample over macroscopic distances, it is imperative that the sample not be contaminated with serious defects. It also needs to be large enough for the experimenter to attach contacts in a configuration that will allow him to back out intrinsic values for the transport coefficients. I have been privileged in my graduate work to synthesize and characterize my own samples. In addition to giving me confidence in and control over the subjects of my study, this provided me the opportunity to study as many doping levels of $BaFe_2(As_{1-x}P_x)_2$ as I wanted, and to abuse as many crystals as I needed to in the processes of ironing out the details of device design and pinning down the origin of apparently aberrant behavior. The significance of this latter point for this project will become clear in later chapters. This chapter will describe the methods used to synthesize single crystals of $BaFe_2(As_{1-x}P_x)_2$ and the characterization tools that were employed to locate individual samples on the doping phase diagram.

3.2 A tale of two methods: $Fe-As$ and $Ba-As$ fluxes.

There were two methods by which $BaFe_2(As_{1-x}P_x)_2$ was synthesized for this project. Both methods are examples of "flux growths" of intermetallic compounds. This means that the crystals were grown by creating a molten mixture containing the component elements of the target material, and then cooling it slowly, allowing the target compound to precipitate out of the mixture. To prevent the oxidation of the reactants, this process needs to be done in vacuum or an inert atmosphere. As long as the necessary molten mixture can be formed

at less than twelve hundred degrees celsius, the most efficient way to isolate the growth is to seal the reactants in an evacuated quartz ampoule, which is how it was done for this project. Since barium reacts with quartz, the reactants were kept inside an alumina crucible for the growth process. Several good reviews are available that describe the chemical principles behind the flux growth method.[19, 57, 41]

In most flux growths, the elements of the target compound are dissolved in another metal (the "flux") that has a low melting point. Both of the recipes used to grow $BaFe_2(As_{1-x}P_x)_2$ for this project are examples of "self-flux" growths, meaning that no extra element beyond the necessary barium, iron, arsenic, and phosphorous was introduced as a solvent. Growing a material by self-flux is usually preferable to dissolving the reactants in another metal, because it minimizes the possibilities for contamination. However, it greatly constrains the crystal grower's ability to create an efficient medium for the growth of the crystal. There must be a balance of the elements that make up the desired compound that will lead to a homogeneous liquid at accessible temperatures. For growths of $BaFe_2(As_{1-x}P_x)_2$ there are two ways to achieve this: use excess iron and arsenic in the growth (the $Fe-As$ flux method) or use excess barium and arsenic (the $Ba-As$ flux method).

The majority of the samples grown for this project were grown by the Ba_2As_3-flux method so I will discuss this method first. This method is based on the extensive work described in reference [82]. For these growths a liquid environment was created by maintaining a pnictogen-to-barium ratio in the mixture of nearly three-to-two. The doping level is controlled by combining different ratios of Ba_2As_3 and Ba_2P_3, thus maintaining the pnictogen to barium ratio at three-to-two. The importance of this ratio was observed empirically by Nakajima et al., but is easily understandable if one looks at the $Ba-P$ binary phase diagram.[118] The temperature at which the last solid phase melts has a sharp local minimum along the composition axis at around sixty percent phosphorous. There, the system is completely liquid by five hundred celsius. The $Ba-As$ binary phase diagram has not, to the author's knowledge, been carefully evaluated experimentally, but it seems reasonable to suppose that its broad features would be similar.

The very low melting point of the three-to-two mixture provides an especially favorable environment for two reasons. First, it makes it easier to separate crystals from the flux. This is done by removing the growth from the furnace at elevated temperatures and centrifuging the sealed ampoule. The flux then naturally flows away from the crystals. In order for this process to work, the growth needs to be removed from the furnace at a temperature considerably above the freezing point of the flux, so that it does not freeze before it separates from the crystals. Several hundred degrees is usually the minimum. Second, crystals grow better when the solution is well away from any freezing point.[57] By keeping the mixture several hundred degrees above the Ba_2P_3 freezing point, this recipe guarantees a high-mobility environment that is favorable for crystal growth.

To the barium-pnictogen mixture we add iron, which has been pre-reacted with arsenic or phosphorous to facilitate its mixture with the flux. Pre-reacting the pnictogens is essential because both of these elements sublime upon heating and so would not go easily into the melt if added to the mixture in elemental form. Instead, both Ba_2As_3 /Ba_2P_3 and $FeAs/FeP$ are

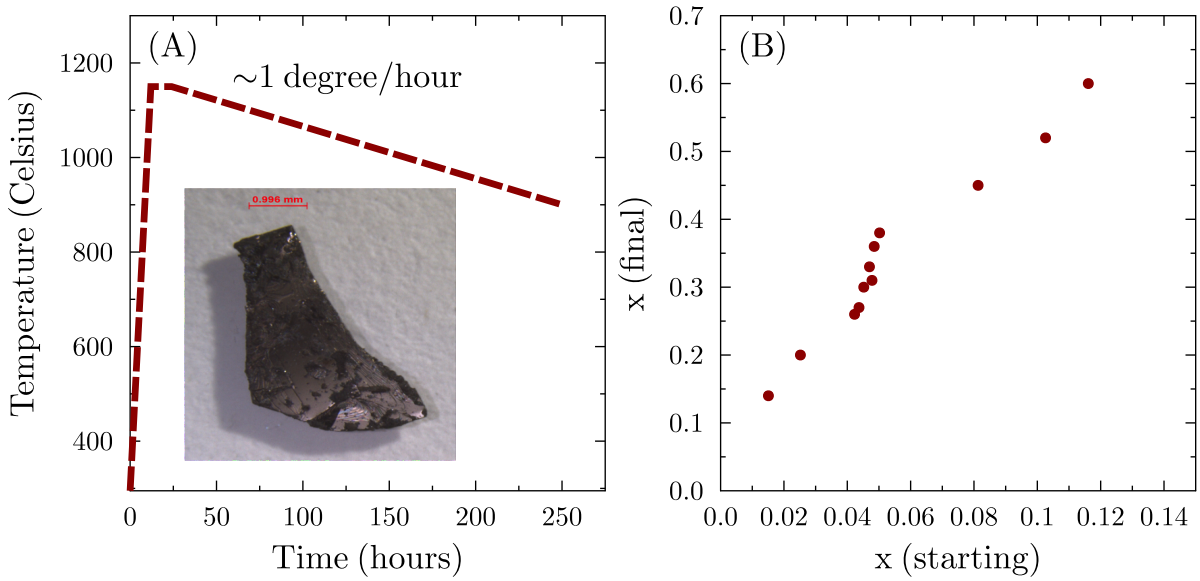

Figure 3.1: **The Ba-As flux method** (A) The thermal cycle used for growing $BaFe_2(As_{1-x}P_x)_2$ by the $Ba-As$ flux method. The inset show a typical crystal grown by this method. The scale bar is $\sim 1mm$. (B) Final phosphorous concentrations versus starting phosphorous concentrations for materials grown by the $Ba-As$ flux method.

made by slowly heating elemental arsenic or elemental phosphorous (for this work, in its "red" allotrope) with either elemental iron or elemental barium, sealing them in a quartz tube, and slowly heating the mixture to just below, and then eventually though, the pnictogen's sublimation point. This gives the gaseous atoms time to react and form the relevant binary compound. Once the pnictogens are bonded in compounds they will melt together with the barium and iron instead of subliming.

With these precursors in hand, one must chose a ratio in which to mix them to create the most favorable environment for the formation of $BaFe_2(As_{1-x}P_x)_2$ crystals. There are two important balancing acts here: one is between barium and iron, and the other between arsenic and phosphorous. First, there must be sufficient barium relative to iron to keep the whole system in a liquid state. Iron phosphide is a stable solid at twelve hundred degrees celsius, the highest temperature attainable for quartz-sealed growths. Therefore, sufficient barium must be present to dissolve that compound. The significance of this will be discussed below when I cover some of the challenges we had in growing phosphorous-rich crystals by this method. The second balance, between arsenic and phosphorous, controls the doping level of the crystals. Table 3.1 shows the compositions that were produced for various starting ratios of arsenic to phosphorous, in rough agreement with the nominal-actual doping level curve obtained by Nakajima et al.[82] One will notice immediately that phosphorous is included in the $BaFe_2(As_{1-x}P_x)_2$ crystals much more readily than arsenic. This is most likely because of a difference in the mobilities of the two atoms in the melt. Since the growth mixture

Table 3.1: Recipes for preparing various doping levels by Ba_2As_3 flux method. Masses are in milligrams and temperatures are in degrees Celsius.

Growth	Ba_2As_3	Ba_2P_3	$FeAS$	FeP	Ba	x_{nom}	x_{final}
AG184	814	9.1	71.1	1.1	0	0.0151	0.14
AG185	804	15.2	70.2	1.8	0	0.0252	0.20
AG186	805	27.9	70.3	3.3	0	0.0452	0.30
AG187	793	30.7	69.2	3.7	0	0.0502	0.38
AG263	802	30	70.7	2.7	0	0.0485	0.36
AG321	829	28	72.8	2.9	0	0.0441	0.25
AG502	804	29	70.6	2.6	0	0.0470	0.33
AG626	1195	43	70.5	3.4	0	0.0460	0.32
AG754	801	28	70.70	2.9	0	0.0478	0.31
AG777	808	27	70.9	2.9	0	0.0437	0.27
AG778	805	26	70.6	2.7	0	0.0423	0.26
AG1213	687.2	57.5	59.9	5.3	32.8	0.1026	0.53
AG1280	782.4	50.7	68.6	4.5	16.1	0.0813	0.45
AG1409	801	77	70.5	8.6	44	0.1161	0.60

is not stoichiometric, as the crystal grows it will locally deplete the pnictogens relative to the barium in the region immediately adjacent to the growth surface. For the growth to continue, pnictogens must diffuse into the growth region, and differences in the diffusion constants of the two species will cause them to be included in the crystal at levels different from that which exists in the melt. This is a well known phenomenon in crystal growth, were it is usually of concern for being one potential limit on the growth rate of the crystals.[57]

In any case, the essential fact is that one can tune the phosphorous content continuously and reproducibly by varying the composition of the original mixture. In principle, one can access any relative fraction of arsenic and phosphorous. In practice, it was difficult to grow crystals on the phosphorous-rich side of the phase diagram. The usual result for growths with more than $\sim 6\%$ starting phosphorous was almost pure iron-phosphide. This result stymied the author and his colleagues for over a year. In that time a great variety of tweaks were applied to the basic recipe given in Figure 3.1 and Table 3.1. The final insight came from a careful look at the $Ba - P$ binary phase diagram.[118] The actual region in which this binary forms a liquid to very low temperatures is fairly narrow, only covering a balance of 52% to 58% phosphorous. Any deviation from that balance would result in a poor environment for crystal growth. One day, while hurrying through the ampoule-sealing process to minimize exposure to air and oxidation of the Ba_2As_3, the author realized that the mild oxidation of the precursor compounds that he had thought were tolerable might not be. Barium oxide, in addition to being hazardous to the human body, is hazardous for crystal growth, since its melting point is around twenty-three hundred celsius and it is

Table 3.2: Recipes for preparing various doping levels by $FeAs$ flux method. Masses are in milligrams and temperatures are in degrees Celsius.

Growth	Ba	$FeAs$	FeP	x_{final}	Figures
AG064	817.5	998.2	535.2	0.46	
AG091	404.0	166.0	367.0	0.75	Figure 5.7, 5.8
AG1738	383.9	166.3	367.9	0.76	Figures 7.9 7.11
AG1802	359.5	178.2	393.5	0.73	Figures 7.9 7.11
AG1803	398.0	167.3	372.1	0.73	Figure 7.9
AG2001	353.0	138.1	307.8	0.84	Figures 7.9

not dissolved by any simple metal. Therefore, any quantity of barium that is allowed to oxidize before the growth is sealed will be taken out of solution. By adding a small amount of pure barium to the mixture, $BaFe_2(As_{1-x}P_x)_2$ crystals could be produced at the doping expected for the arsenic-phosphorous balance used. Table 3.1 includes several growths that utilized this extra barium. These values allowed reproducible production of phosphorous-rich $BaFe_2(As_{1-x}P_x)_2$ crystals. It is likely that the oxidation of barium is a self-limiting process, which would explain this reproducibility, but this still requires one to cut the barium pieces to a similar size for every growth. My recommendation to future researchers is to devise a method for sealing the growths that nearly eliminates the potential for oxidation, probably by loading the mixture in a glove box and attaching a sealing mechanism to the open end before removing and sealing. This would allow for a much more controlled growth process.

The Ba_2As_3/ Ba_2P_3 flux method produced the largest crystals of $BaFe_2(As_{1-x}P_x)_2$, especially especially near optimal doping, and so was the preferred method for synthesizing these materials. However, for overdoped samples and early on in the project, before the Ba_2P_3 flux method had been mastered, there was a useful alternative at hand. This method, which used an $Fe-As$ flux, was developed by my advisor, Professor Analytis, while he was a postdoc and later staff scientist at SLAC. An iron-arsenic mixture is a good choice for a flux, because $FeAs$ forms a liquid by eleven hundred celsius for most balances of the chemical species.[117] This should allow for a nice molten environment as the crystals grow. The challenge is introducing and controlling the phosphorous. As was mentioned before, iron-phosphide remains a solid to rather high temperatures. In one of those special insights that makes chemical synthesis seem like dark magic, Dr. Analytis noticed that it was the barium to iron-arsenide ratio that seemed to control the ultimate doping level of the crystals. The mechanism here is most likely that the solubility of phosphorous in the $Ba-Fe-As$ solution increases with an increasing barium fraction, so that with a reasonable phosphorous reserve, the $Ba/FeAs$ ratio fixes the phosphorous/arsenic ratio through the saturation of the melt with phosphorous.

For this reason, the recipe is not easily represented as a formula with a variable, x, that can tune the doping. Table 3.2 shows the recipes for the batches that were used in this

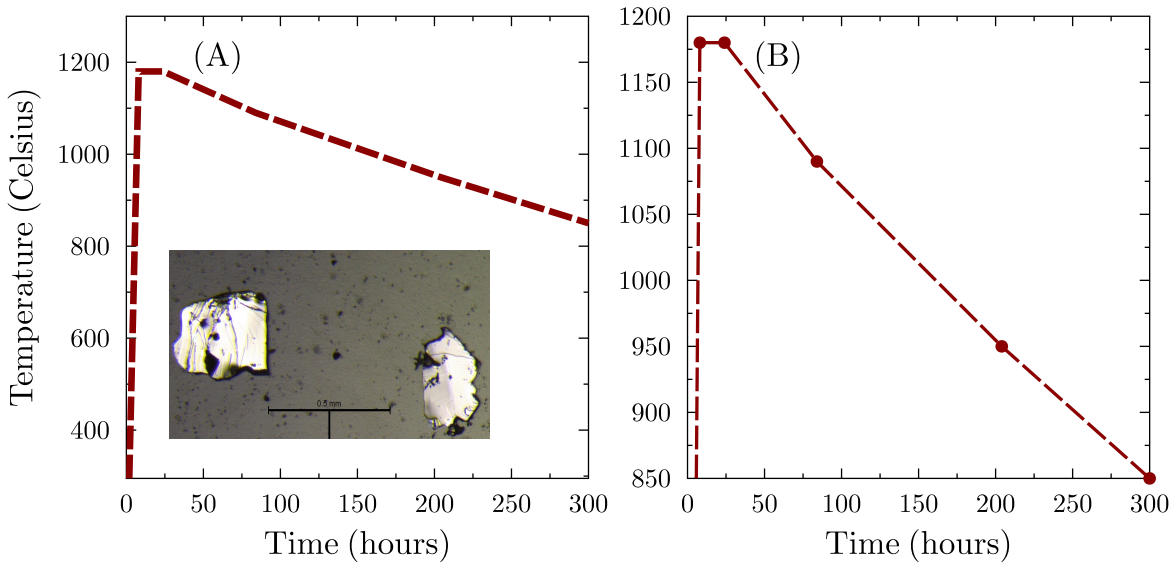

Figure 3.2: **The Fe-As flux method** A. The thermal cycle used for growing $BaFe_2(As_{1-x}P_x)_2$ by the $Fe-As$ flux method. Inset shows typical crystals grown by this method. The scale bar is $\sim 500\mu m$. B. A closer look at the slowly decreasing cooling rate for this growth method.

work. One can readily see that in each of the two broad parts of the phase diagram shown here (mildly overdoped and significantly overdoped) the ratio of $FeAs$ to FeP is constant, while the quantity of barium is varied. For the very overdoped sample where there was no superconducting phase transition, composition was determined by energy-dispersive x-ray measurements. The thermal cycle tor all of these starting compositions is the same and is given in Figure 3.2. As with the $Ba-As$ flux method, the arsenic and phosphorous were pre-reacted with iron to facilitate their absorption into the melt. These precursors were grown by the method described above. Looking at the ratios in Table 3.2, one notices that this method uses a much lower fraction of barium relative to phosphorus. Although the maximum temperature reached should be enough to melt the iron arsenide, the iron phosphide clearly is never fully melted. This likely means that the growth environment is not totally uniform, leading to many nucleation points, which possibly explains the smaller size of the crystals grown by this method ($\sim$ 100-300 μm instead of $\sim$ 1-2 mm, see Figures 3.1 and 3.2).

It is considerably more difficult to attach wires to a sample that is $100\mu m$ on a side than it is to do so to a sample that is $\sim 1mm$ on a side. Nevertheless, growing overdoped crystals by the $Fe-As$ flux method was much more consistent. As mentioned above, when trying to make a phosphorous-rich melt, it is essential to have just the right amount of barium to avoid the precipitation of iron phosphide. Since there is always excess iron-phosphide in the

iron-arsenic flux method, and one is only making use of the small amount dissolved by the barium, this is not an issue. As a result, all of the samples measured for this project with phosphorous fractions greater than sixty percent were grown by this method.

3.3 Sample properties

By the time the author started on this project, many doped versions of $BaFe_2As_2$ had been studied, including the phosphorous-substituted series, and the general features of the phase diagram were well known.[23, 55, 58] Characterization therefore consisted of first verifying that we had obtained the desired phosphorous fractions, and then evaluating the quality of the crystals. In practice, since the crystals showed the expected antiferromagnetic and superconducting transition temperatures, the measured transition temperatures together with phase diagrams taken from the literature were sufficient to determine the phosphorous content. This practice was vindicated on those occasions when we provided samples for experiments that had element-sensitive analysis. These included angle-resolved photoemission spectroscopy experiments (ARPES) and scanning transmission electron microscopy experiments (TEM) conducted on samples near optimal doping that confirmed the estimated phosphorous content, to within their experimental accuracy. For some samples, particularly on the overdoped side where no phase transitions are present, phosphorous content was verified by energy-dispersive x-ray spectroscopy (EDX).

Less direct evaluations of the phosphorous content could be made in-house by measuring the size of the unit cell in powder x-ray diffraction (PXRD) and using Vegard's law. This is the assumption that the unit cell of an alloy linearly interpolates between the sizes of the unit cell in the two stoichiometric compounds. This assumption is borne out in the literature on $BaFe_2(As_{1-x}P_x)_2$.[58, 111, 82] Figure 3.3 shows a sample PXRD spectrum. The results from PXRD agree with what has been measured in the literature, and with Professor Analytis' prior measurements of phosphorous content from x-ray photoelectron spectroscopy (XPS) measurements (unpublished). The phase diagram summarizing these relations is given in Figure 1.3, and it is both qualitatively and quantitatively consistent with those in the literature.[58, 55, 111]

In addition to PXRD, measuring the resistivity versus temperature and magnetization versus temperature where the two principle ways of characterizing the samples. Details of the resistivity measurements are discussed in the next chapter. Representative resistivity versus temperature data for a wide selection of dopings are shown in Figure 1.5. The qualitative features associated with the antiferromagnetic and superconducting transitions are readily apparent, allowing us to determine the transition temperatures, T_N and T_c respectively, of these phases. Beyond determining transition temperatures (and therefore phosphorous content), resistivity curves are useful for making a rough assessment of crystal quality. Two features are typically used: the residual resistivity ratio (RRR), meaning the ratio between the resistivity at three hundred kelvin and zero kelvin, and the width of phase transitions. The RRR is correlated with crystal quality because the only scattering that should be present

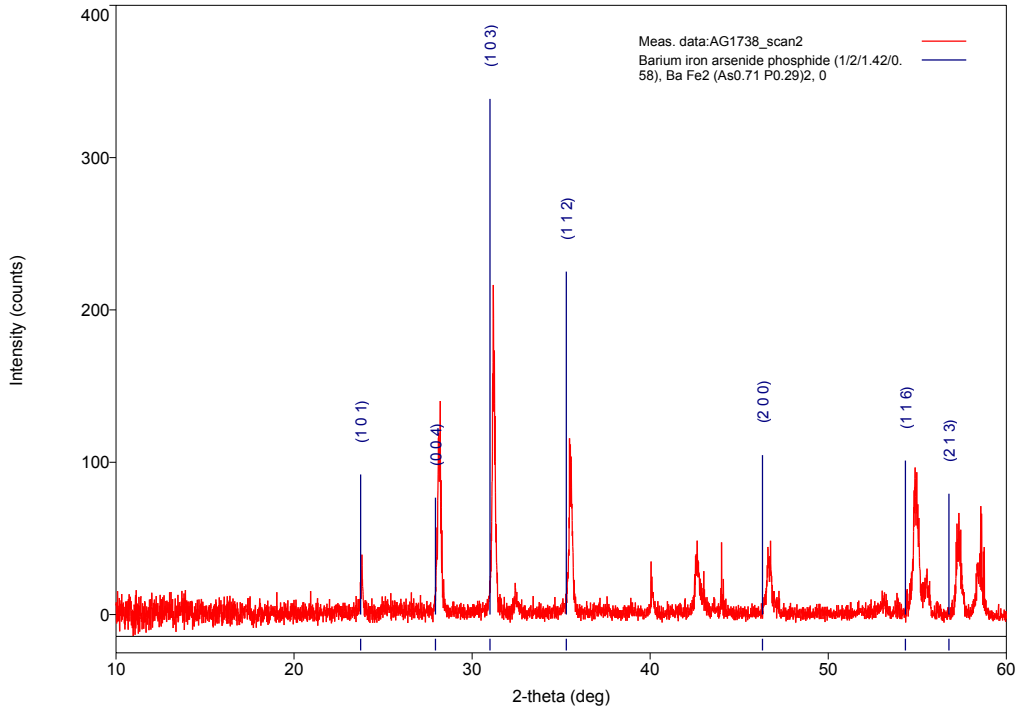

Figure 3.3: **A sample powder x-ray pattern for** $BaFe_2(As_{1-x}P_x)_2$**.** The diffraction peaks are shifted to higher angles because the sample is more overdoped than the reference pattern. This shift in the peak positions is one way of estimating the true phosphorous content of the samples.

at zero temperature is impurity scattering, while at high temperatures the resistivity should be dominated by intrinsic scattering (thermally excited phonons, etc.). Thus, the fewer impurities in the crystal the smaller the zero temperature resistivity should be relative to the intrinsic baseline measured at room temperature. It is worth stressing that this method of evaluating crystal quality is only useful for comparing samples within a single material class. Depending on the details of the electron dynamics, a given level of impurities could lead to quite a different residual resistivities. Furthermore, the high temperature resistivity obviously varies strongly between compounds. However, for making comparisons between different samples of one compound or even between different compounds in one material class, this is a reasonable way to decide which samples are cleanest.

Turning now to the resistivity data on $BaFe_2(As_{1-x}P_x)_2$, it is clear that the RRR for underdoped samples is significantly lower than for overdoped ones. This is even true of pure $BaFe_2As_2$. However, since the underdoped samples are antiferromagnetic, one cannot make a straightforward comparison between them and the overdoped samples. The antiferromagnetic ground state will host a different set of processes for relaxing momentum, especially

since those systems have significantly smaller Fermi surfaces.[58] The strong effects of annealing RRR for undoped $BaFe_2As_2$ (which can raise it from three to about fifty)[82] is good evidence that the resistivity in the AFM state is very sensitive to the presence of point defects.

Even restricting our attention to the optimally and overdoped samples, there remains the challenge of how to define RRR when superconductivity is present. I will follow the standard practice of using the value of the resistivity at the transition, even though this potentially short-changes samples with high transition temperatures. This gives us RRR values ranging from ~ 5 for optimal doping to ~ 15 near the edge of the superconducting dome. For a doped compound this is a fairly large RRR, and compares favorably to the RRRs found in other doped iron-pnictide superconductors, even other doped versions of $BaFe_2As_2$.[23, 38] This is perhaps to be expected, since $BaFe_2(As_{1-x}P_x)_2$ is an isovalently-substituted system. As described in section 1.3, this reduces disorder scattering from the doping sites because they have the same charge as the other ions, and is especially gentle when done on the arsenic site because these atoms contribute minimally to the orbital content at the Fermi surface.[63, 108] This last point makes sense of the fact that even the isovalently-substituted system $Ba(Fe_{2-x}Ru_x)As_2$ has significantly lower RRR than the phosphorous-substituted series.[38] Overall, this means that the resistivity measured in $BaFe_2(As_{1-x}P_x)_2$ shows the smallest contribution from disorder, giving us the best opportunity to study the intrinsic dynamics of the non-Fermi liquid state in doped iron-pnictide superconductors.

The distinctly high RRR value on the overdoped side of the phase diagram does prompt the question of why the RRR is so much lower near optimal doping. In fact, describing this difference in terms of RRR understates the difference in the residual resistivity because the resistivity at room temperature is much higher on the arsenic-rich side of the phase diagram (see Figure 1.5). This difference at high temperatures is easily understood on the basis of band structure changes that are expected and observed across the phase diagram.[106, 121] Both the electron and hole pockets in the system get larger as one moves to more phosphorus-rich samples, leading to a higher baseline conductivity, even without a change in the scattering rate. The difference in zero temperature resistivity between over- and optimally-doped samples is almost certainly not due to greater disorder in the later. The ineliminable disorder due to doping is going to be very similar across the entire superconducting dome, varying from one phosphorous atom per three pnictogen sites to two atoms per three sites. Given the very low RRRs observed for underdoped compounds, it seems natural to attribute it to the proximity to the antiferromagnetic phase. This attribution is supported by the fact that samples near optimal doping, whether they are magnetic or not, show a much smaller response to annealing than the undoped samples do.[82] Many questions remain about the exact interaction of disorder with the electron dynamics in $BaFe_2(As_{1-x}P_x)_2$, but it is intriguing to note that other systems thought to be near a quantum critical point show a local maximum in their low temperature resistivity near criticality.[18, 42] This question will be revisited in more detail in chapter 5.

There is a second part of resistivity versus temperature curves that can help diagnose crystal quality: the width of phase transitions. Disorder tends to broaden phase transitions

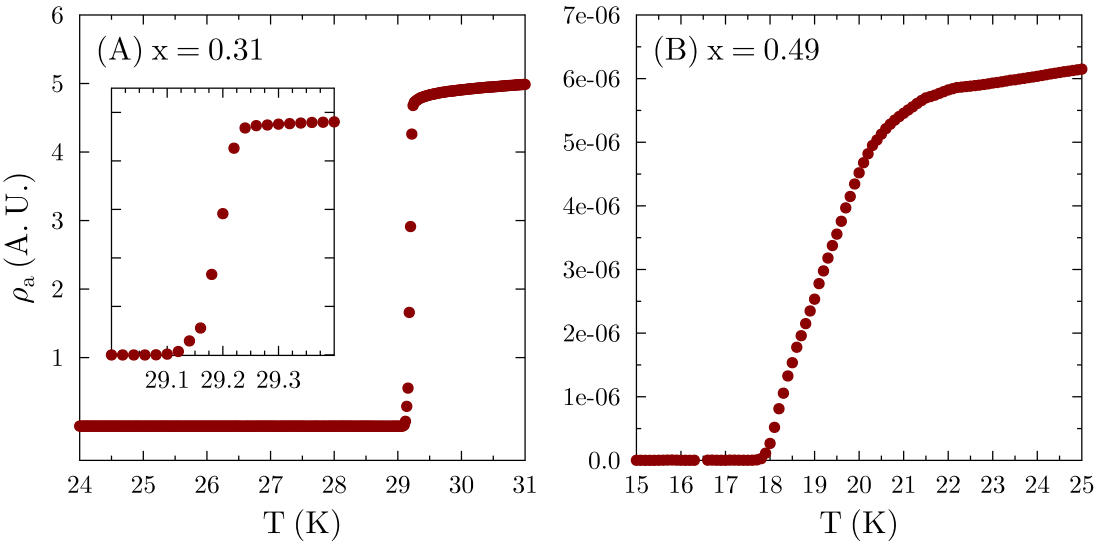

Figure 3.4: **The superconducting transition width in resistance versus temperature.** (A) Near optimal doping, the transition width is very sharp, $\sim 100mK$. (B) At much higher doping, the transition is much broader (about 20 times), but this is consistent with the samples having a similar variation in local phosphorous concentrations and a different slope of T_c versus x at higher dopings.

since it will vary the local thermodynamic potential in the crystal, effectively causing different parts of the sample to reach the ordered state at different temperatures. Once again things are simpler on the overdoped side, where there is only the superconducting phase transition to consider. Figure 3.4 shows close-ups of the superconducting transition for an optimally doped sample and an overdoped sample. It is obvious here that the samples near optimal doping have significantly sharper transitions than the overdoped samples. This suggests the opposite of the naïve conclusion implied by the RRR observations. This pattern in the transition widths can be explained by a close look at the phase diagram. We can see that the variation in T_c with doping has a larger gradient on the overdoped side (see the phase diagram in Figure 1.3). Therefore, a consistent level of disorder in the phosphorous distribution would lead to wider transitions in the overdoped samples. The gradient of T_c in x is approximately fifty millikelvin per one percent phosphorous while near fifty percent phosphorous substitution it is roughly one kelvin per one percent phosphorous. Thus a constant level of phosphorous inhomogeneity is consistent with the fact that the superconducting transitions are roughly twenty time broader on the overdoped side (see Figure 3.4).

Although it seems clear that local variations in the phosphorous content are responsible for much of the superconducting transition width, this measure still let's us put a ceiling of the level of disorder in the samples. On the basis of transition widths or RRR, these $BaFe_2(As_{1-x}P_x)_2$ crystals compare favorably with any other high$-T_c$ superconductors.[17]

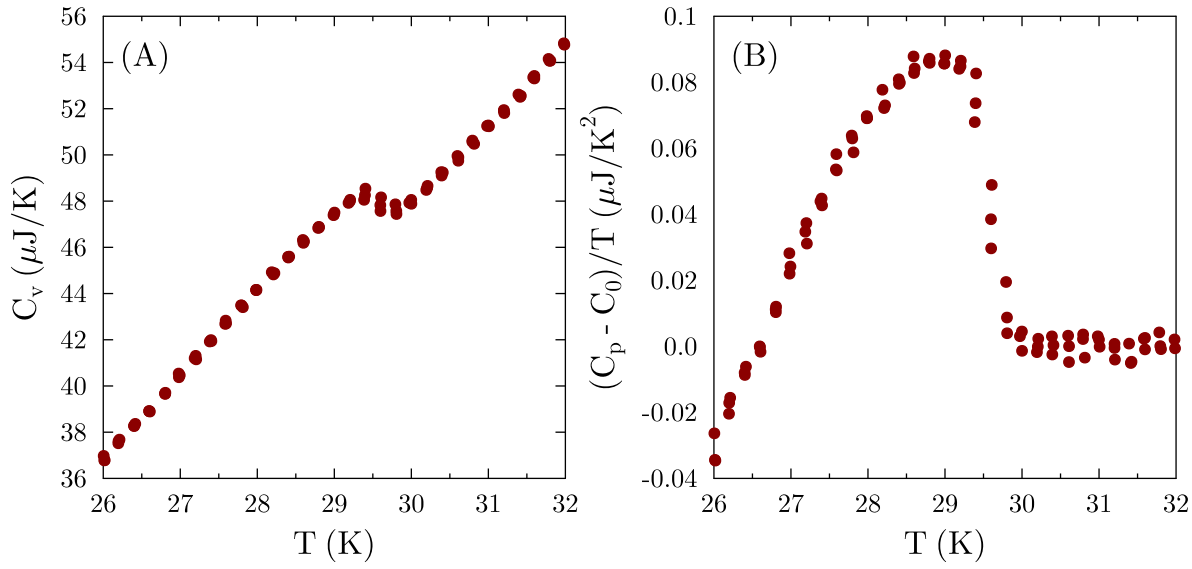

Figure 3.5: **The superconducting transition near optimal doping in the heat capacity.** (A) Raw C_p versus temperature data. A break in slope is clearly visible between 29 and 30 kelvin. Panel (B) shows the same data but with the background subtracted (found by fitting the high$-T$ part of the data to a low-order polynomial) and divided by the temperature. The critical temperature, determined by the center of the discontinuity is in good agreement with the resistive transition (see Figure 3.4), indicating that the samples are quite homogenous. The sample came from batch AG754.

However, a superconducting transition width measured in the resistivity can be misleading because the resistivity only need one small superconducting path to reach zero, which can obscure a broad thermodynamic transition. So it is worth examining the transition in proper thermodynamic quantities as well. Figure 3.5 shows heat capacity data on an optimally doped sample of $BaFe_2(As_{1-x}P_x)_2$, which shows the classic jump in C_p at the transition, also with a width of less than one kelvin. This can also be verified in measurements of the magnetic susceptibility. In addition to being perfect conductors, superconductors are perfect diamagnets, and measuring the magnetic susceptibility is a good way to check the that the superconducting transition is in fact a bulk transition. The diamagnetic transition seen in magnetization is both sharp and perfectly coincident with the resistive transition (see Figure 3.6).

Finally, it is worth mentioning that some of these crystals, particularly from batches AG186 and AG502 we the subject of transmission electron microscopy measurements done by Dr. Yun-Long Tang in the research group of Professor Ramesh here at UC Berkeley. Electron microscopy is a powerful microscopic probe that should easily diagnose any major quality issues in the samples. As mentioned above, electron energy loss spectroscopy done

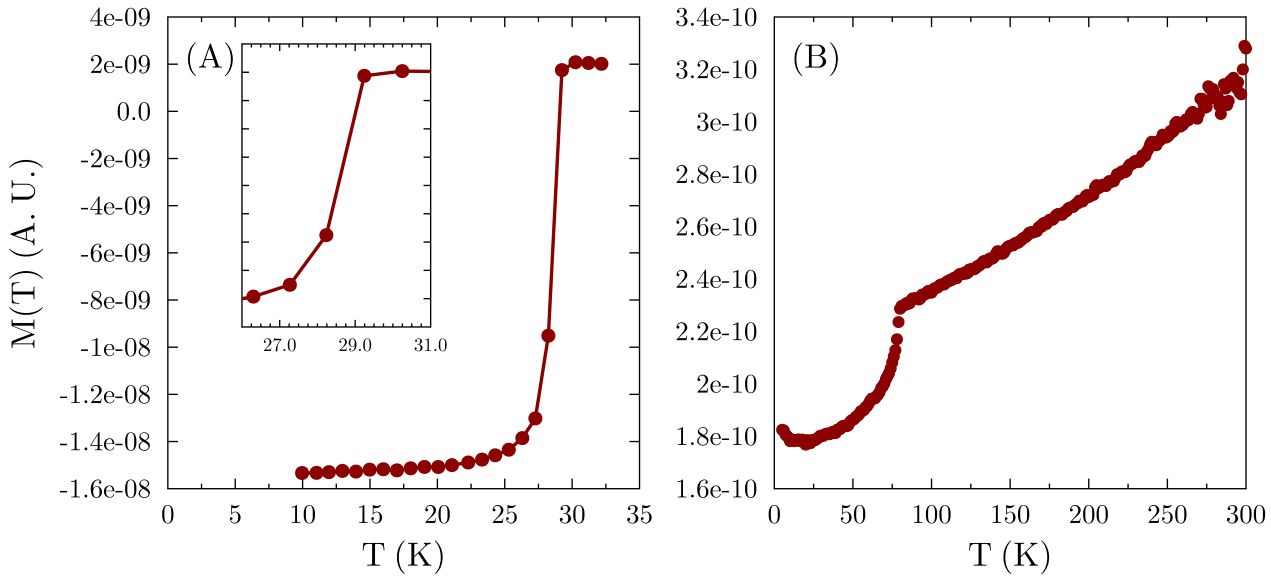

Figure 3.6: **Magnetization in $BaFe_2(As_{1-x}P_x)_2$ for optimally doped and underdoped samples.** (A) The diamagnetic transition at T_c, for sample AG186s1. Again the transition temperature agrees nicely with the transition temperature in the resistivity. (B) The antiferromagnetic/orthorhombic transition in an underdoped sample (AG185s1) also appears in the magnetization, as a kink at around eighty kelvin.

during these measurements confirmed the expected elemental composition. They also found the samples to be continuous single crystals. As they are layered materials, they inevitably had some planar defects, including inter-grown layers of iron-phosphide. Although this should make essentially no difference to the in-plane transport, it may well explain some of the challenges that we had in producing high quality devices for inter-layer transport measurements. These sort of planar defects can reroute a $c-$axis current dramatically. They can also act as little capacitors, which would add an extra phase between current and voltage in the resistivity measurement. Measurements on many of our $c-$axis in pulsed fields showed a variable phase as a function of field, which is readily understandable if the capacitance of these defects changed as a function of field, perhaps because of magnetostriction. This is currently our leading hypothesis for why those measurements were so challenging.

Chapter 4

Aspects of Device Design for Pulsed Magnetic Field Measurements

4.1 Introduction

Most of the data presented in this thesis were taken in pulsed, ultra-high magnetic fields. This environment poses a number of challenges for the researcher, starting with how to optimize signal-to-noise. In the sixty-five tesla, short-pulse magnets available at the National High Magnetic field Laboratory's pulsed field facility, the entire duration of the pulse is only about 25 milliseconds. This means that for a sixty-five tesla measurement, a data point has to be taken within about $50\mu s$ in order to get several data points per tesla. Furthermore, the discharge of energy in the magnet's coil is a violent process, leading to significant vibrations that can effect the measurement circuit. These facts make many devices that would be perfectly acceptable for resistivity measurements in a steady-field environment unusable in pulsed fields. This chapter will present the author's efforts to meet these challenges. First I will present the technical aspects of transport measurements in pulsed, ultra-high magnetic fields. Then, I will discuss the processes of crystal shaping and contacting that made these measurements possible. Finally I will survey the full set of devices used in this study.

4.2 Basic aspects of four point resistance measurements.

Measuring the low-frequency electrical resistivity of materials is an old art, if not an ancient one. A variety of methods exist, but if one wishes to extract something close to an absolute value, the four-point measurement on a sample in a favorable geometry is the method of choice. This method involves passing electrical current through your sample by the means of two terminals while the voltage difference is measured on another two. The value of using two pairs of terminals is that, because no current is passing through the voltage

terminals, there is no contribution to the measured voltage that comes from anything other than the resistivity of the sample. In particular no current flows through those contacts, so the resistance of the contacts will not contribute to the measured voltage signal. In principle, this completely eliminates systematic errors

Therefore, a four-point measurement reliably accesses the quantity of interest. However, there are several challenges associated with it. The first is that, although one is usually confidant that all of the current passed down to one terminal will go through the sample (because of the huge difference in resistivities between a typical insulator and a typical metal), the exact pathway of the current through the sample can be difficult to determine. This can pose a challenge for converting the value of the resistance one measures into a resistivity since one cannot simply divide by the length and multiply by a cross-sectional area. Cracks or other defects can cause major changes in the current path, but determining the current path can be a problem even in very well ordered systems if there is a large anisotropy in thekilohertz resistivity itself. Additionally, if one is trying to measure along the low resistivity axis, the current will only very slowly spread over the cross-section that one is using to compute the resistivity. Measuring the in-plane resistivity in the cuprates, where the anisotropy ρ_c/ρ_{ab} is typically several hundred, is tricky for this very reason.[49] Fortunately $BaFe_2(As_{1-x}P_x)_2$ has a relatively modest anisotropy: the interlayer resistivity, ρ_c, is only about five times the in-plane resistivity, ρ_{ab}. Furthermore, the crystals were large and could be easily cleaved. This allowed the contacts to be separated by a distance that was many times the $c-$axis width of the devices, making us confident that the

The second major challenge associated with a four-point measurement is achieving high quality contacts to the sample. Low quality contacts can add considerable noise to the measurement and, in the worst cases, lead to local heating or break off. The procedure that worked best for $BaFe_2(As_{1-x}P_x)_2$ involved two steps: sputtering gold on to the sample in the locations where contacts were desired, and then attaching wires to the sample with a commercial conductive epoxy, Epo-tek H20e. Without the gold sputtering step, samples had two-terminal resistances of 20-50 ohms. Contacting gold pads lead to two-point resistances of around 1-2 ohms for current contacts and 4-10 ohms for voltage contacts on Hall devices. Although these resistances are considerably larger than the roughly 50-500 milliohms sample signals that we could achieve given the constraints of sample geometry, they easily allow signal-to-noise ratios of 10^5 or 10^6 in our home systems. In fact these sensitivities were almost certainly limited by the electrical conditions in the measurement apparatus and not by the contacts.

Our sensitivity in pulsed fields was also limited by the electrical environment. To start, the field pulse lasts only about 25 milliseconds. This means that the lock-in frequency of the measurement must be at least 10 kilohertz in order to gather a satisfactory number of data points over 60 tesla. The lock-in processing is done on a digitized voltage reading with a fundamental frequency of around 20 megahertz. The front end of that digitizer has roughly one milliVolt of noise on it. On the highest gain settings, one can amplify the signal at the top of the probe by about a thousand, leading to a noise floor in the sample channel of around one microvolt. This creates a minimum sample signal size of around $50-100\mu V$. For

all channels except the in-plane resistivity, ρ_{ab}, this was the major consideration in sample design. Sections 4.3 and 4.4 cover the ways in which this challenge was met in detail.

Pulsed field experiments presented a few challenges beyond just achieving the highest possible signal size. The system is prone to strong vibrations during the pulse. This can cause the wires to move, which will induce voltages in the measurement circuit. As a result, it is essential to glue down even the wires used to make contact with the sample to avoid unnecessary noise. In addition to noise from vibrating wires, phase problems can be created when the wires are allowed to move freely in the magnetic field, creating variable capacitances in the measurement circuit. More then one experiment had to be abandoned because wires were not sufficiently immobilized for the device to produce a clean signal.

One final challenge with pulsed field measurements will be of interest to future pulsed field experimenters. In order to get the highest possible magnetic fields, the sample space in these systems is limited to about eight millimeters across. This leaves little room for cryogenics, which in turn limits the experimenter's ability to control the cool-down rate of his samples. If the sample contacts or any of the part of the device is made of a delicate materials like silver paste, it can easily crack if the system goes into an uncontrolled cool-down. Repairing contacts that are lost to thermal stress can consume days of precious experimental time. The author therefore strongly encourages the exclusive use of well-cured conductive epoxies to create contacts between wires and samples or other wires. In all of my many trips to Los Alamos, I have never had a solid glob of Epo-tek H20e break.

4.3 Material constraints: interlayer transport measurements in $BaFe_2(As_{1-x}P_x)_2$

As mentioned in the proceeding section, measuring the pure components of the resistivity tensor in a material with an anisotropic resistivity can be tricky. However, the anisotropy can also be helpful. If one wants to measure the larger component of the resistivity tensor, he can count on the current traveling outwards along the low resistivity directions quickly, so that the current is only traveling along the high resistivity axis by the time it reaches the voltage terminals. The interlayer resistivity is larger than the in-plane resistivity in $BaFe_2$-$(As_{1-x}P_x)_2$, but this advantage is swamped by the disadvantage imposed by the typical crystal dimensions. Their typical $c-$axis length is around 50 μm, while their typical cross-sectional area is quite large–about $150\mu m$ by $150\mu m$. This makes it basically impossibly to fit two voltage contacts next to each other on an $a-c$ plane by hand, and the device would provide a very small signal even if one could. In principle one could overcome these two limitations by a lithographic method like Focused Ion Beam lithography. Section 4.5 will explain why this was not pursued in this case. Furthermore, even if one could fit the wires, the contacts made to those faces turn out to be significantly worse than those made to $a-b$ surfaces. These considerations lead us to abandon the four-point measurement and adopt a two-point (or pseudo-four-point) method where the middle of a single wire was soldered

to each $a-b$ surface a cuboid crystal. One end of the wire can then be used as a current terminal for the measurement and the other for the voltage terminal.

This method is helpful for interlayer measurements in a number of ways. By placing the voltage contacts as far away from each other as possible, one makes use of as much of the interlayer dimension as possible, minimizing the impact of the unfavorable crystal geometry. By covering the entire surface with solder, one maintains a relatively even distribution of current across the $a-b$ plane of the sample, ensuring that the measured signal is due almost purely to the interlayer resistivity. Finally, making a broad contact with a solder joint minimizes the total contact resistance, ensuring that almost all of the signal comes from the sample. However, because the voltage contacts will have current flowing through them, the signal will contain a potentially unknown offset from the quantity in which we are interested. There are two things that minimize this disadvantage. First, we are primarily interest in the magnetoresistance in of these samples, and an amorphous material like the tin-lead solder used for making the contacts is likely to have very small magnetoresistance. Second, because $BaFe_2(As_{1-x}P_x)_2$ is a superconductor, there is a temperature region where we know that the resistivity of the sample is exactly zero. This allows us to find the contribution of the contacts by simply measuring the sample in its superconducting state. Any finite signal in this regime must be due to the contacts.

Although this sounds like a robust method of background subtraction, it has still has the shortcoming that we can only determine the the contact resistance in the superconducting state. If those resistances have any temperature dependence above T_c, we will not be able to tell. Fortunately, since we are primarily interested in the behavior below or around T_c, this is not too much of a limitation. In any case, it was essential to minimize the contact resistance as much as possible, both because of potential contamination of the signal and because the sample signal itself was likely to be small. For this reason contact to the sample needed to be made by soldering. This leads to lower contact resistances than making contacts with silver epoxy. However, solder contacts do have a rather large minimum footprint on the sample. This set a minimum $a-$axis dimension for the devices of about $150\mu m$. This minimum area means that soldering would not have helped much in making devices for in-plane resistivity measurements. In any case the $\sim 1\Omega$ contacts that could be achieved with silver epoxies were perfectly satisfactory for the in-plane devices.

Many attempts were made to produce samples by this method, and only a few produced samples with contact resistances low enough to be candidates for pulsed field measurements. In perfecting this process I was blessed to have the help of a dedicated undergraduate researcher, Zeyu Hao. Figure 4.1 shows pictures of two high-quality interlayer devices (AG263z1 and AG626z5) that were taken to the pulsed field lab, along with close-ups of their superconducting transitions. Important features of the overall resistance versus temperature curves will be discussed in chapter 6. For the purposes of understanding quality of these samples, the relevant part of the data is the vicinity of the superconducting transition and below. As discussed above, the resistance reading in the superconducting state must come entirely from the contacts. In fact, one can see that at around six kelvin the signal goes all the way to zero. This is because the solder is a tin-lead alloy which is itself a superconductor.

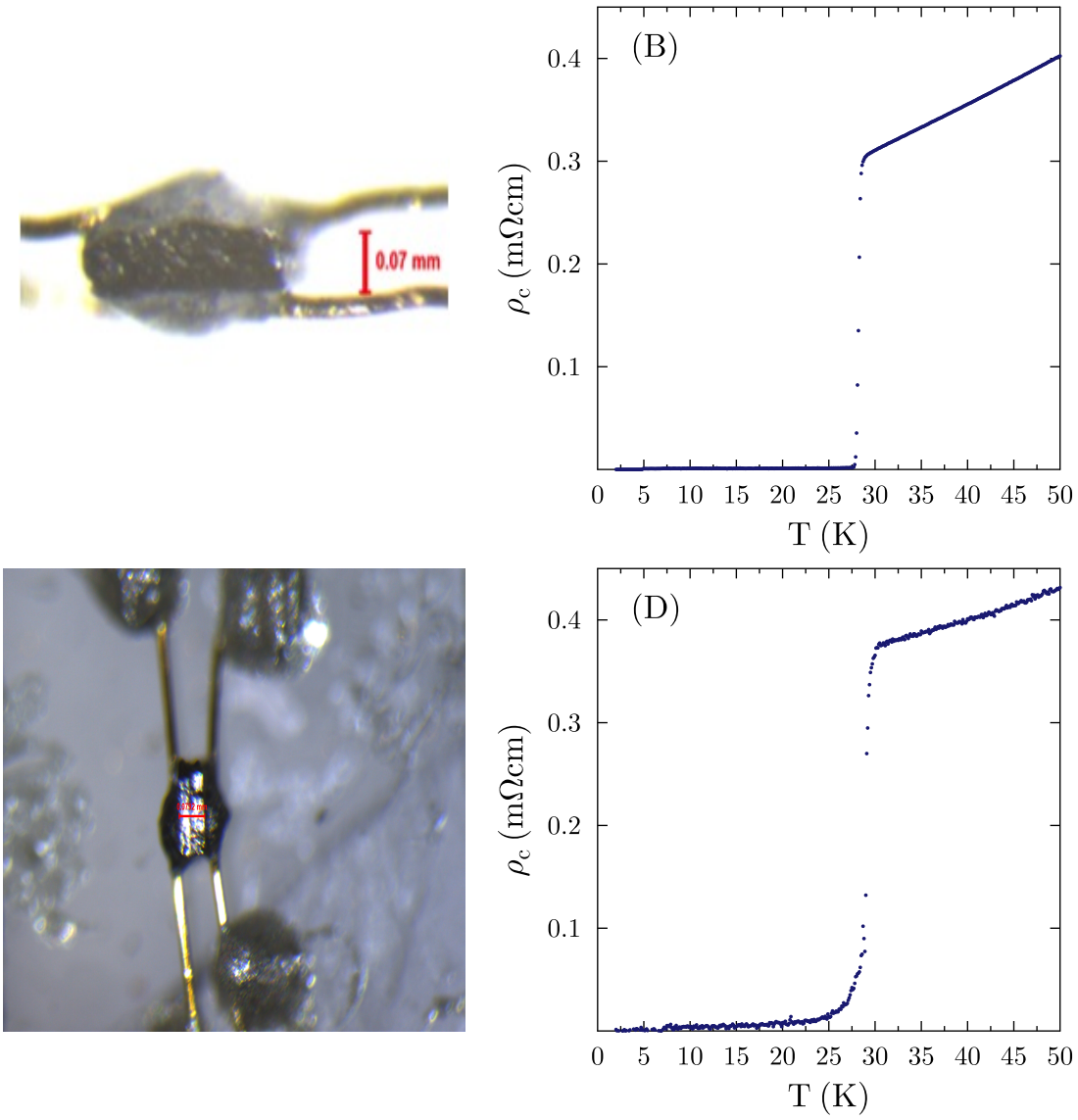

Figure 4.1: **Measurements of interlayer resistivity in** $BaFe_2(As_{1-x}P_x)_2$**.** Devices were made by soldering a pair of wires to opposing $a-b$ faces of a small cuboid crystal. Panel (A) shows device AG263z1 and Panel (C) device AG626z5. Panels (B) and (D) show the signals from these devices near the superconducting transitions. Fortunately, the solder contacts could be made negligible compared to the sample signal, as can be seen by looking at the fraction of the contact-sample-contact system that goes superconducting, especially on sample AG263z1.

The normal state resistance of the contacts can be evaluated just above this temperature. We see that sample AG263z1 has a total contact resistance of about $100n\Omega$, giving a sample-to-contact signal ratio of about 300-to-1. This turned out to be quite adequate for pulsed field measurements, and was large enough that we could totally neglect the contact resistance in the analysis.

4.4 Material constraints: Hall effect measurements in $BaFe_2(As_{1-x}P_x)_2$

Measuring the Hall resistivity, ρ_{xy}, of $BaFe_2(As_{1-x}P_x)_2$ in pulsed magnetic fields is a challenge primarily because the target signal is so small. Compensated metals like $BaFe_2(As_{1-x}P_x)_2$ have very small Hall signals in the low field regime ($\omega_c\tau << 1$, see chapter 7 for details) and have a very high threshold for reaching the high field regime.[93] The only way to boost the signal in the Hall channel is to make the sample thinner along the field axis, which in this case is the crystallographic $c-$axis. Near optimal doping, a $\sim 20\mu m$-thick sample of $BaFe_2(As_{1-x}P_x)_2$ has a Hall signal of around $100\mu\Omega$ per ten tesla. This means that to achieve the optimal signal size for measurements in Los Alamos (something around $100\mu V$, as discussed above) at fifty tesla, one would need to flow around $200mA$, which is not ideal. It was therefore essential to make the samples very thin to achieve respectable signals.

Fortunately, $BaFe_2(As_{1-x}P_x)_2$ is very forgiving in this regard. The material is very soft and cleaves nicely. A hard push of a standard number eleven surgical blade against an $a-c$ face usually creates a very even break in the crystal. The best results come from pressing against a corner, which ensures that the stress is applied to a point and does not distribute across a large distance in the $c-$direction. If the cleave does not run all the way to the edge of the sample, the upper layer can be cleanly pealed away. The challenging part of this process is holding the crystal in place while the cleave is being made with the scalpel. For thicker samples one can simply push them up against the end of a pair of tweezers or other barrier. However, crystals thinner than around ten microns will buckle under the pressure of the knife, leaving a deformed sample that is unusable for experiments.

In order to reach smaller dimensions, one has to glue the crystal down before cleaving it. He can either try to do this in such a way that the glue can be removed, leaving a freestanding sample, or he can plan on leaving the sample glued down. The freestanding geometry is preferable in that it leaves the sample in a strain-free environment, but the electrical contacts were sensitive to most solvents that might dissolve the adhesive, so the author elected to mostly just leave the samples glued to a substrate. It was possible to glue the corners of a crystal, cleave it, and then cut away those glued corners, but this simply deprived him of part of the sample in the best cases and frequently lead to the destruction of the sample as the crystal tended to rip in the unsecured area. For the central experiment on optimally doped $BaFe_2(As_{1-x}P_x)_2$ in high fields, two sample were measured. One was

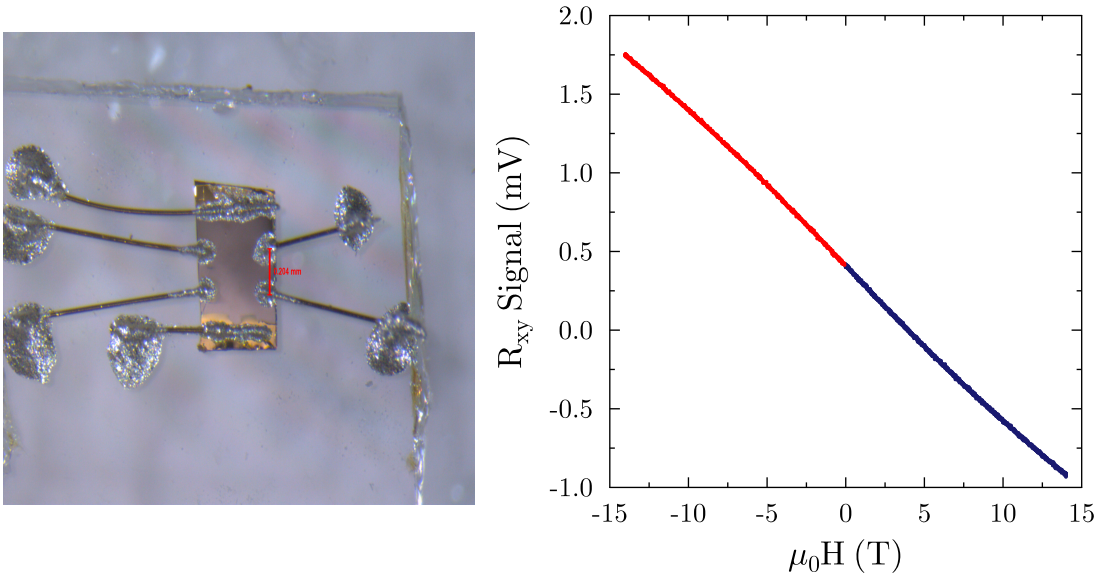

Figure 4.2: **Typical R_H measurements in $BaFe_2(As_{1-x}P_x)_2$.** A. A typical six point device with transverse and longitudinal contacts. The likely signal size of this device is not inferable from the picture, since it depends exclusively on the sample thickness. B. A typical Hall resistivity measurement requires sweeping positive and negative fields and taking their anti-symmetric combination. This anti-symmetrizing is necessary since even the most carefully placed contacts will result in a specious zero-field Hall resistance.

glued down while the other was not, and there was no discernible difference in their signals.

With a fully glued sample, very small $c-$axis dimensions could be achieved. First, a very even cleave must be made on a free crystal, so that the flat surface can serve as the back side of the sample. Obviously, if the first cleaved surface has height variations greater than or equal to the target thickness, it will not be possible to make a clean device. This flat surface then must be glued down. The author found that the best results were achieved by simply placing some conductive epoxy near the crystal and allowing the binding agent to run beneath it. This creates a very thin, very even layer of adhesive that does not conduct. Importantly, it also only adheres to the bottom face of the crystal. This allows any strain that forms on cooling to relax efficiently along the $c-$axis and it leaves the maximum amount of space for the experimenter to position a surgical blade and cleave the sample. It is also important to state here that adhesive part of the conductive epoxy does not conduct electricity, and therefore carries no risk of compromising the signal of the sample. Since the adhesive is extracted from a conducting epoxy, one might worry that it would be electrically conductive, even if no silver flakes were observable. This was checked both by the direct application of a multimeter to some bare adhesive, and by attempting to do a four-point measurement on the contacts of a glued sample that whose main body had been severed (so that the contact-crystal-glue pathway was tested). This is important for our interpretation

of the data presented in chapter 8.

Cleaving the crystals to below ten microns was not easy, even when they were glued in place. It is very hard to judge where to place the scalpel to obtain a $\sim 1\mu m$ cut, and many crystals were lost in attempts to reach the thinnest possible dimensions. However, sometimes the cleaves were successful, and these yielded samples with very high Hall resistances. There actual thickness could not be measured in an optical microscope and had to be measured by confocal microscopy. The thinnest devices obtained in this way were only about five hundred nanometers thick, which is a significant achievement for samples prepared from bulk single crystals.

4.5 Attempts at focused ion-beam lithography

Reducing the $c-$axis dimension of the samples is the only way to increase the signal in the Hall channel. For measurements of ρ_{xx} one has the options of reducing the thickness, reducing the width, or increasing the length. If one is making the devices by hand, then the maximum possible length is set by the size of the crystal, and the minimum width is set by the stability of one's hand. This leaves reducing the thickness of the samples as the one practical and effective means of significantly increasing signal size. However, in recent years, techniques that use focused ion beams (FIB) to pattern devices with micron-scale dimensions out of bulk single crystals have come to prominence. Modern FIBs have a resolution limit of less than one micron, which allows the experimenter to both radically reduce the cross-sectional area and, by creating a meandering path through the crystal, to significantly extend the length of his device. This can produce devices which have resistance signals a hundred times greater that what one can typically achieve in hand made devices.

This is a mouth-watering prospect for a user of pulsed magnetic fields. There is a fairly considerable noise floor in these experiments, which makes signal enhancement the only available route for improving the quality of data. Early on in the project, we began a collaboration with Dr. P. J. W. Moll, who is an expert in FIB lithography. He patterned a number of resistivity devices for us out of crystals with a number of different dopings. These produced variable results. Some of the devices made out of overdoped crystals provided beautiful data, fully consistent with that obtained on bulk samples but with much higher precision. Data on two of these samples (3747p1 and AG091p1) are presented in chapter 5. On the other hand, FIB devices made from optimally-doped crystals showed large discrepancies with their bulk counterparts. Figure 4.3 shows the resistance versus temperature curve of one of these devices, which may be compared with the data in Figure 1.4. Clearly there are significant differences between the two data sets. In particular, in the FIB device the $T-$linear resistivity is absent and the RRR is much reduced. This clearly makes the sample unusable in a study on $T-$linear resistivity. To this day we do not know the exact origin of this discrepancy. However, it seems reasonable to guess that it is due to the small dimensions to which the sample was cut. It was latter found that samples with small $c-$axis dimensions also deviate from the behavior shown by macroscopic samples in the Hall channel (see chap-

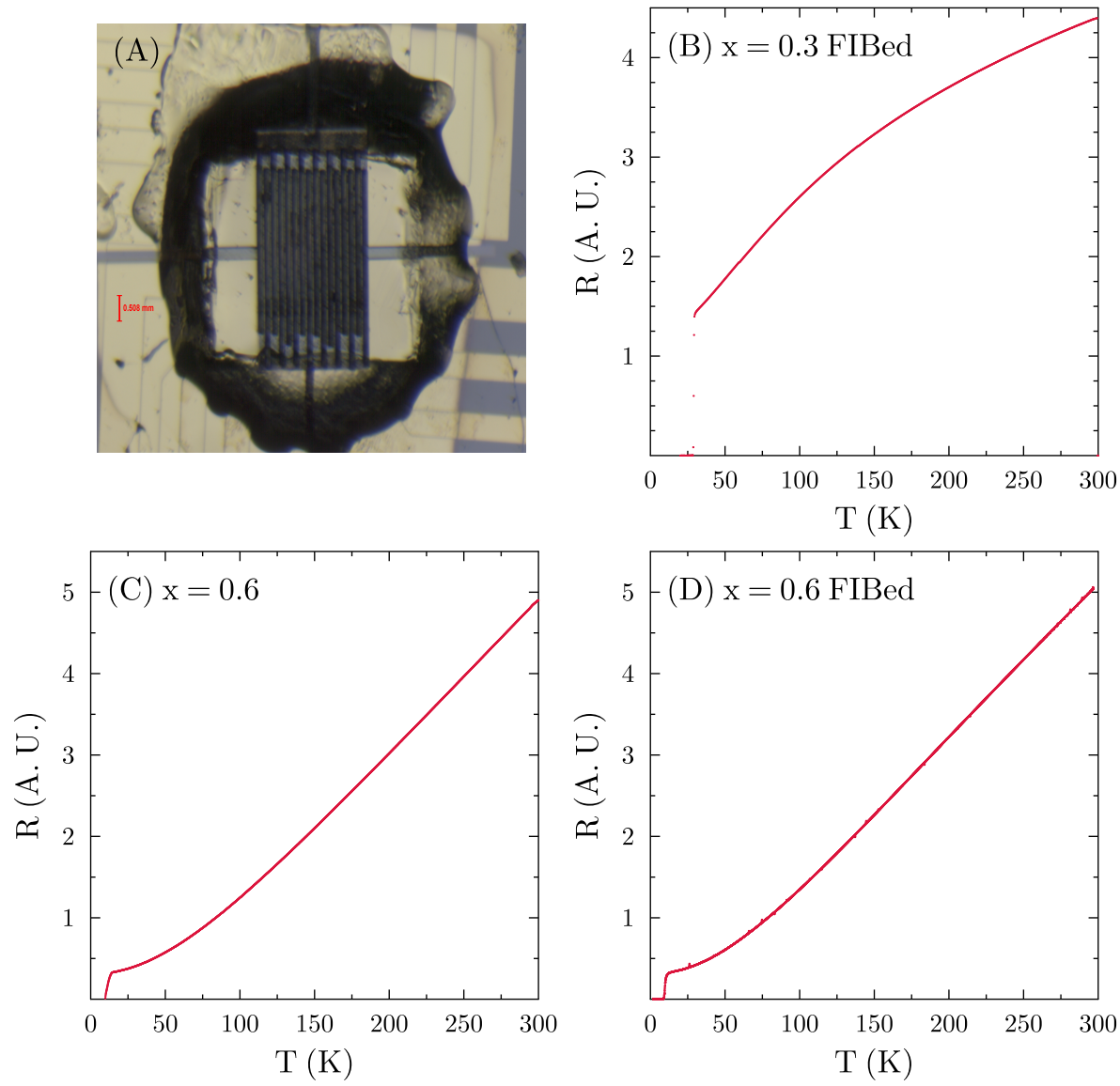

Figure 4.3: **Devices made by focused ion beam lithography.** (A) A picture of device AG186p4, showing the meandering path pattern. (B) The resistance of this device, showing clear deviations from the resistance of unFIBed samples. In contrast, overdoped samples which were micro-structured by FIB lithography (panel (D)) showed no meaningful deviations from bulk behavior (panel (C)).

ter 8). Since these discrepancies were confined to optimal doping (compare with panels (C) and (D) of Figure 4.3) there is a good chance that it has to do with long-wavelength physics in these systems.

The greatly enhanced signal of FIB devices would have been particularly valuable for the ninety tesla measurements, where, as the reader will see, signal-to-noise was an even bigger issue. Measurements of the interlayer resistivity would also have benefited greatly from this process. Unfortunately, in light of the changes in the sample's behavior, it would have been impossible to interpret the data from these devices. I hope, therefore, that the reader understands why the overdoped samples, for example in section 5.4, have significantly better signal-to-noise ratios than the supposedly more interesting optimally-doped samples.

4.6 Samples used in this study

In this and the last chapter I have reviewed the main facts about, and lessons from, the experience of synthesizing crystals of $BaFe_2(As_{1-x}P_x)_2$ and making devices out of them for high-field transport measurements. These lessons were hard earned, from dozens of growths and hundreds of destroyed crystals. In the coming chapters I will present data on a small subset of all the devices made. For measurements in pulsed magnetic fields, almost all of the data that were taken are presented here, but for low magnetic field measurements many more samples were measured than it makes sense to present here. Often, however, the conclusions to be drawn from them were reinforced by data taken on other devices. In an effort to be as transparent as possible about the origin of the data presented here, I will conclude this chapter with a list of all devices that provided that data. The samples are labeled by a growth batch number and a sample name. Batches labeled "AG###" were grown by the author. Those labeled simply with four numbers were grown by Professor Analytis and inherited by the author. The sample name is typically just "s#", although sometimes another letter was used, especially if the device was fabricated in conjunction with a collaborator. This may seem like a Byzantine system, but the author feels that renaming a sample after it has been measured is liable to create more confusion than it eliminates. I hope this will help the reader understand how the samples presented in the subsequent chapters relate to each other in terms of the batches they came from.

Table 4.1: Batches and samples appearing in this work

Growth	Sample	T_c	T_N	Flux	Figures
2767	i4	24.00 K	0 K	Ba_2As_3	Figure 5.7, 5.8
3747	p1	10.00 K	0 K	Ba_2As_3	Figure 5.7, 5.8
3947	s2	27.00 K	0 K	Ba_2As_3	Figure 5.6, 5.7, 5.8
3949	s3	29.50 K	0 K	Ba_2As_3	Figures 5.1, 5.2, 5.3, 5.5, 5.6, 5.9
AG091	s3	0 K	0 K	Ba_2As_3	Figure 5.7, 5.8
AG184	s3	0 K	100 K	Ba_2As_3	Figure 1.5
AG185	s1	0 K	80 K	Ba_2As_3	Figure 3.6
AG185	s4	2 K	80 K	Ba_2As_3	Figure 1.5
AG186	s1	29.25 K	0 K	Ba_2As_3	Figure 3.6
AG186	p4	29.25 K	0 K	Ba_2As_3	Figure 4.3
AG186	s10	29.25 K	0 K	Ba_2As_3	Figure 1.4
AG186	s15	29.25 K	0 K	Ba_2As_3	Figure 6.6, 6.7
AG186	s19	29.25 K	0 K	Ba_2As_3	Figure 1.4
AG263	s12	27.50 K	0 K	Ba_2As_3	Figures 7.4
AG263	s13	27.50 K	0 K	Ba_2As_3	Figures 7.8
AG263	z1	28.50 K	0 K	Ba_2As_3	Figures 4.1, 6.1, 6.2, 6.3, 6.4
AG263	s15	25.00 K	0 K	Ba_2As_3	Figures 7.12
AG321	s4	19.00 K	48 K	Ba_2As_3	Figures 1.5
AG502	s5	29.25 K	0 K	Ba_2As_3	Figures 5.1, 5.2, 5.3, 5.5, 6.5
AG626	z5	29.00 K	0 K	Ba_2As_3	Figures 4.1, 6.2
AG754	s14	29.00 K	0 K	Ba_2As_3	Figure 8.2 8.3
AG754	s20	29.00 K	0 K	Ba_2As_3	Figure 7.8, 1.5
AG754	s22	29.25 K	0 K	Ba_2As_3	Figure 7.1, 7.2
AG778	s4	24.00 K	35 K	Ba_2As_3	Figure 1.5
AG1213	s7	16.00 K	0 K	Ba_2As_3	Figures 7.8, 7.12
AG1280	s1	21.75 K	0 K	Ba_2As_3	Figures 7.8
AG1280	s6	21.50 K	0 K	Ba_2As_3	Figures 7.4, 7.12, 1.5
AG1409	s8	8.50 K	0 K	Ba_2As_3	Figures 7.9, 1.5
AG1803	s2	1.00 K	0 K	$FeAs$	Figures 7.11, 7.9, 1.5
AG1738	s1	0.00 K	0 K	$FeAs$	Figures 7.11, 7.9
AG2001	s1	0.00 K	0 K	$FeAs$	Figures 7.9

Chapter 5

Scaling in the Magnetoresistance of $BaFe_2(As_{1-x}P_x)_2$

5.1 Introduction

This chapter will cover the first round of high-field magnetoresistance measurements done on $BaFe_2(As_{1-x}P_x)_2$, focusing on the transverse magnetoresistance of the in-plane resistivity: ρ_{ab} with I//a, H//c. This configuration is the most convenient from the perspective of device design, as discussed in the previous chapter, and therefore provides the best opportunity for obtaining a good signal-to-noise ratio. This is a key consideration since pulsed field measurements have a significantly higher noise floor than measurements done in steady fields. Measurements were done on samples covering the entire overdoped side of the phase diagram, from $x = 0.3$ to$x = 0.75$. Two facts jump out from this extensive data set. Near optimal doping the low temperature magnetoresistance is linear in magnetic field, suggesting an analogy with the $T-$linear resistivity also present in these samples. Since this is only seen near the antiferromagnetic/orthorhombic quantum phase transition, it seems likely that it is connected to the physics of quantum criticality. Second, the magnetoresistance at optimal doping shows a scaling collapse in H/T, indicating that the electron dynamics is scale-invariant, as has been hypothesized to occur near a quantum critical point (see chapter 2). The scaling form that the data obey contains the $T-$linear resistivity and the $H-$linear resistivity as two limiting forms, confirming that the later is just the magnetic analogue of the former.

Most of the data discussed in this chapter and the conclusions reached herein were published, albeit in abbreviated form, as "Scaling between magnetic field and temperature in the high-temperature superconductor $BaFe_2(As_{1-x}P_x)_2$", *Nature Physics*, **12** 916-919 (2016).

5.2 H-linear resistivity

Data on the magneto-transport properties of $BaFe_2(As_{1-x}P_x)_2$ in high, pulsed magnetic fields were gathered over many trips to the National High Magnetic Field Laboratory's Pulsed Field Facility at Los Alamos National Laboratory (NHMFL-PFF). In this section I will present the data collected on two samples with composition near $x = 0.30$ (optimal doping). These were the samples for which a comprehensive data set of high enough quality could be obtained to analyze the full scope of MR phenomena. Both samples discussed here show the same magneto-transport behavior and no other sample was measured that gave data in tension with those shown in this chapter, even at a quantitive level. This gives us high confidence that the behavior presented here is intrinsic and reproducible, especially since these samples were grown by two different techniques, $Fe - As$ flux and $Ba - As$ flux. Although the data that they give is nearly identical, the author feels that it is appropriate to present both sets, given that the conclusions of this section are both strikingly novel and dependent on subtle features of the shapes of the curves taken in an intrinsically noisy environment. Indeed, a large fraction of the author's early days on this project were spent attempting various analyses of the data presented here, in order to find a robust and unambiguous way to confirm the existence of these phenomena.

The first important feature of the data is shown in Figure 5.1: the magnetoresistance of $BaFe_2(As_{1-x}P_x)_2$ at the lowest temperatures is linear in magnetic field above the superconducting transition. This can be seen in both samples (3949s3, AG502s5). Although the $H-$linearity is fairly clear from visual inspection, I have plotted their derivatives (evaluated as a linear fit to a five tesla field window) below each curve to make it clear that the only deviations from linearity are due to H_{c2} and that there is no upturn at high fields that would indicate the presence of a quadratic component in the field dependence. This is important to establish because a quadratic field dependence would be the natural behavior for a compensated metal like $BaFe_2(As_{1-x}P_x)_2$ (that is, one with equals numbers of electrons and holes). In the far overdoped region of the phase diagram, where we expect more conventional metallic behavior, the magnetoresistance of $BaFe_2(As_{1-x}P_x)_2$ does indeed display a quadratic dependence on field (see Figure 5.7).

A linear field dependence in the magnetoresistance is not easy to obtain in a conventional Fermi liquid picture. When it does appear, it is most commonly due either to strong disorder or to some extreme feature of the Fermi surface topology, such as a corner-like feature.[93] Neither of these is likely to exist in $BaFe_2(As_{1-x}P_x)_2$. As emphasized in chapter 1, this material is one of the cleanest of the doped iron-pnictide superconductors, even exhibiting magnetic quantum oscillations on the overdoped side, and its Fermi surfaces, as determined by both photoemission experiments and band structure calculations, are smooth.[106, 121, 63] Even if disorder were part of the story, there would still need to be an explanation for the fact that the $H-$linear resistivity is only seen at optimal doping, while the level of disorder in these samples should be similar throughout most of the doping phase diagram. This encourages us to consider a more exotic origin for this phenomenon. Given that the $H-$linear resistivity only exists near optimal doping, it seems natural to suppose that its

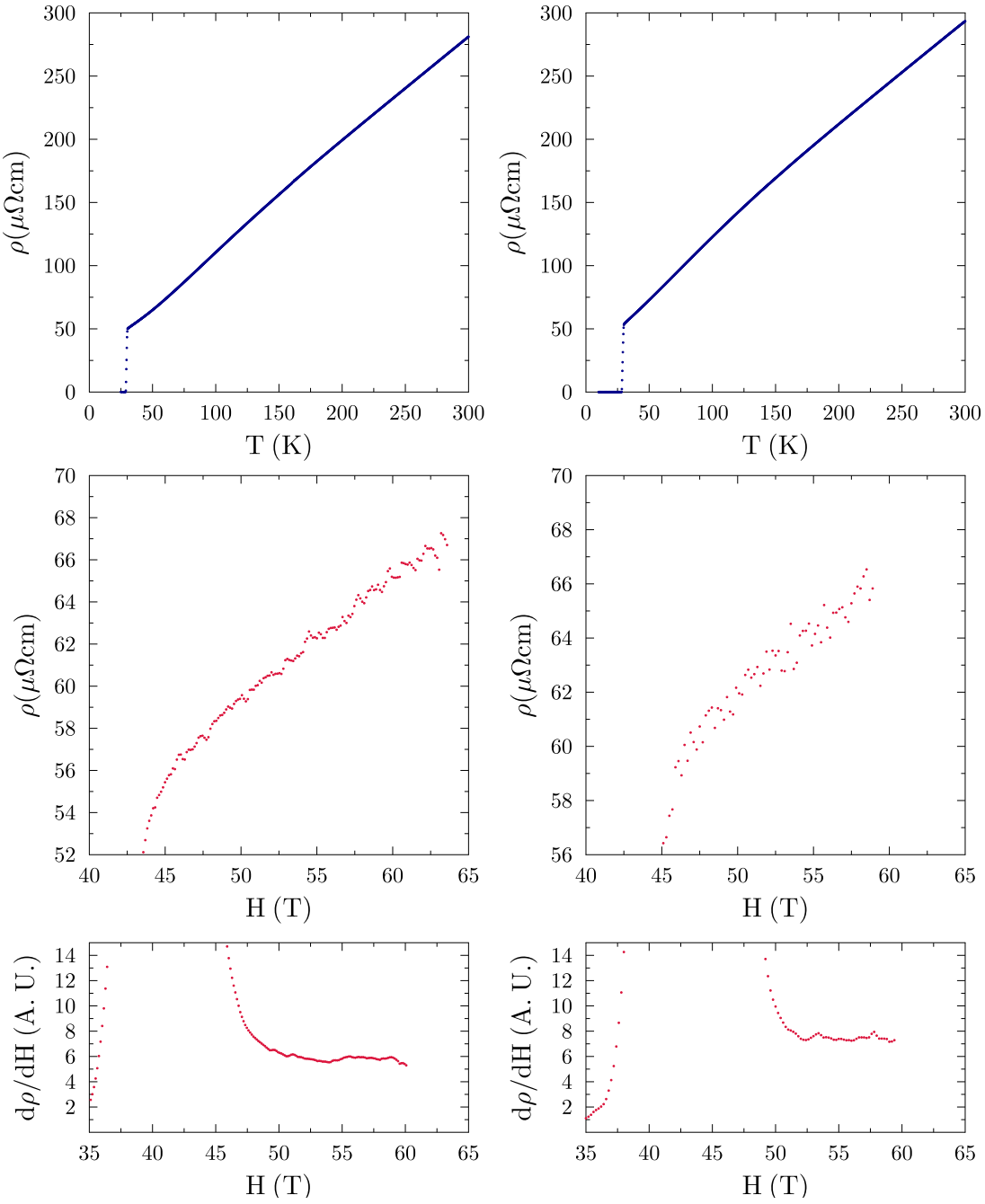

Figure 5.1: $H-$**linear resistivity near optimal doping in** $BaFe_2(As_{1-x}P_x)_2$**.** Panels (A) and (B) show the $T-$linear resistivity for two optimally doped samples of $BaFe_2(As_{1-x}P_x)_2$, x3949s3 and AG502s5. Panels (C) and (D) show the magnetoresistance of these two samples at four kelvin. Above the superconducting transition, the resistivity varies linearly with the magnetic field. The derivatives of these two curves (panels (E) and (F)) confirm this.

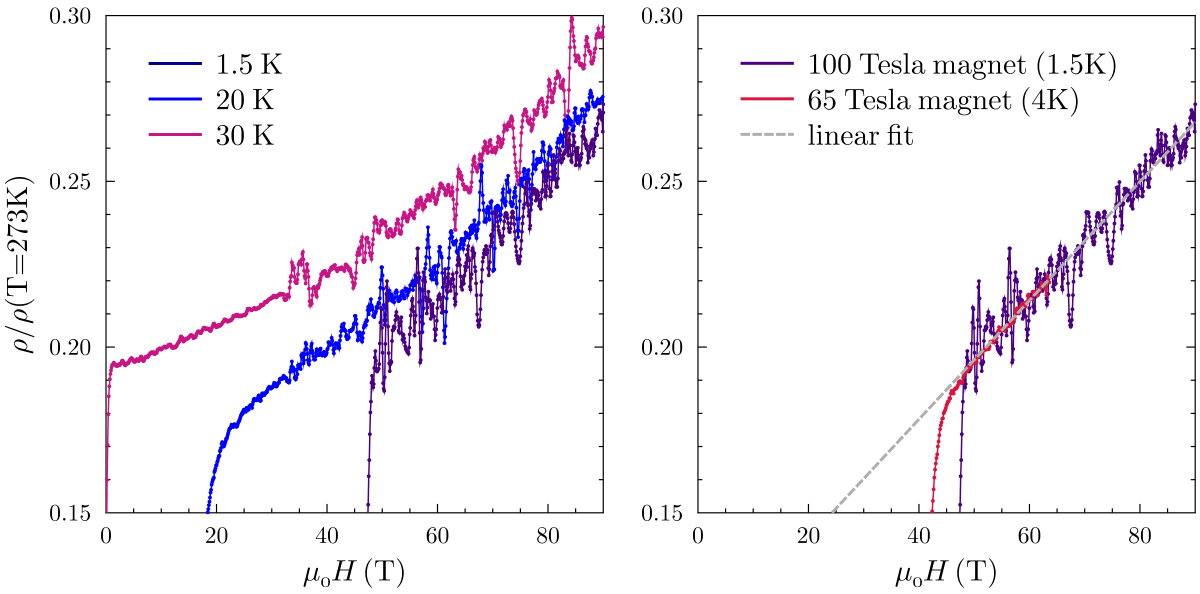

Figure 5.2: **Linear magnetoresistance up to ninety-two tesla in optimally-doped $BaFe_2(As_{1-x}P_x)_2$.** *A*. Magnetoresistance as a function of field for a few temperatures. The same basic pattern seen in the sixty-five tesla data are present in these data two, including linear magnetoresistance at the lowest temperatures and a convergence of the magnetoresistance curves at the highest fields for all temperatures. *B*. The data for 1.5 kelvin, shown with a linear fit and the data from the sixty-five tesla system where signal-to-noise is significantly better.

origin is in the dynamics associated with the antiferromagnetic and orthorhombic quantum phase transition. It also naturally prompts a comparison with the $T-$linear resistivity that is also seen at these doping levels (see figure 5.1). However, the field window that is available between the superconducting transition and the maximum field of this magnet is rather narrow. Before trying to reach too many conclusions based on this $H-$linearity, it behoves us to check whether the resistivity actually is $H-$linear by going to even higher fields. Unfortunately measurements in the 100 tesla magnet are considerably noisier that in the 65 tesla magnet. However, the signal-to-noise is still good enough to see that the curve is best fit by a line (see Figure 5.2). Furthermore, we can combine the 65 tesla and 92 tesla data to see that the line of best fit for the 92 tesla data is, in fact, a continuation of the linear MR observed below 65 tesla. This provides a more stringent test of the linearity of the resistivity than either data set alone.

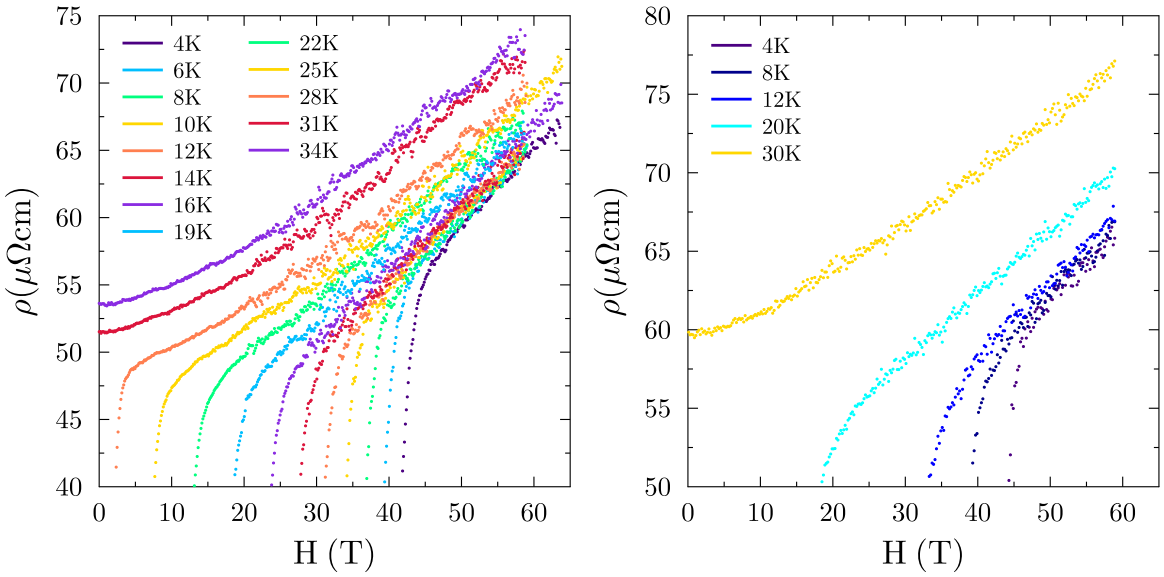

Figure 5.3: **Temperature dependent magnetoresistance of optimally doped $BaFe_2(As_{1-x}P_x)_2$.** The H-linear magnetoresistance exists only at the lowest temperatures. Above a few kelvin curvature begins to appear, first at lower fields, then gradually at higher fields as the temperature is raised. The resistance versus temperature at high fields is $\sim T^2$, creating an intriguing dichotomy between $T-$linear and $H-$squared resistivity, and $H-$linear and $T-$squared resistivity. The left panel shows data on sample 3949s3, and the right one shows data on sample AG502s5.

5.3 Field-temperature scaling in the resistivity

The suspicion that the $H-$linear resistivity might be connected to the $T-$linear resistivity in $BaFe_2(As_{1-x}P_x)_2$ and other compounds motivated us to look carefully at the T-dependence of the magnetoresistance as well. Figure 5.3 shows the magnetoresistance of these same two samples at several temperatures. Several important facts are apparent from the raw data. First, the $H-$linear resistivity is only present at low temperatures. As the temperature is raised the magnetoresistance gradually develops some curvature, especially at low fields. By about thirty kelvin there is no trace of an $H-$linear regime. Second, at sufficiently high fields, the resistivity is almost independent of temperature. As a result, the $T-$dependence of the resistivity is roughly quadratic for small temperatures at high fields. This yields a certain approximate symmetry between H and T, where $H-$linearity exists exclusively in the $T \sim 0$ regime and vice versa.

This apparent symmetry between field and temperature is intriguing. These two quantities are physically very different. One is a scalar, while the other is a vector. One is a field with a microscopic meaning and the other is measure of statistical behavior that is

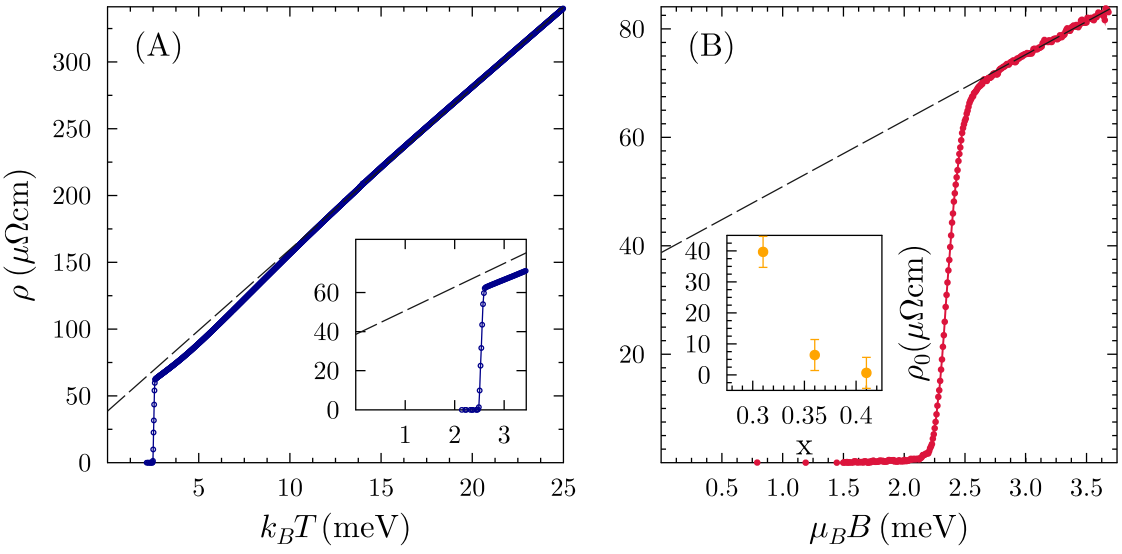

Figure 5.4: **$T-$linear versus $H-$linear and the residual resistivity of $BaFe_2(As_{1-x}P_x)_2$.** The two linear resistivities in $BaFe_2(As_{1-x}P_x)_2$ are plotted in common energy units. The extrapolated residual resistivity is the same for both curves. The inset to panel (B) shows the residual resistivities near optimal doping.

meaningful only in large systems considered over long times. The fact that they appear to enter the transport on equal footing strongly suggests that the magnetic field is playing the role of thermodynamic parameter. This leads us naturally to the realm of critical physics and phase transitions, where physical quantities often have singular dependencies on temperature and magnetic field. In the theory of a classical, second-order phase transition, the correlation length for the order parameter will diverge at the critical point, leading to a singularity int he free energy. This singularity will naturally dominate the derivatives of the free energy, which are exactly the thermodynamics observables. Thus, the dependencies of thermodynamic observables on external parameters like the magnetic field and the temperature will be exclusively determined by the influence of those parameters on the diverging correlation length. The complete dependence on multiple external parameters usually simplifies to a single expression, which is a scale-invariant function (i.e. a power law) in one of the parameters times a dimensionless function whose only variables are ratios of the other external parameters and the primary parameter. Each of the parameters in those ratios may carry different exponents if they "scale" differently, that is, if the correlation length diverges according to a different power laws in those two parameters.[103] As discussed in chapter 2, there are general reasons to expect this scaling behavior to extend to dynamic quantities like the resistivity when the critical point in question is a quantum critical point.[109]

Since we know the general form that an observable in a scaling regime should take, we can check for the presence of critical physics in an almost assumption-free way. We know the power law that the resistivity obeys as a function of temperature ($\rho \sim T^1$), so we can normalize all of the magnetoresistance curves to this power law and plot them versus the ratio of field and temperature. If there is a scaling form for the resistivity in H and T, the data will collapse onto a single curve. There is only one free parameter in this analysis: the relative exponent of field and temperature that appears in the scaling function. However, since we know that the resistivity is H-linear as well as $T-$linear, we are confidant that these two parameters have the same scaling exponent. Therefore we can use the simple ratio H/T on the $x-$axis. First, however, we have to remove the residual resistivity. Since $\rho \sim T + \rho_0$, ρ_0, the data will not collapse when normalized by the temperature unless this residual term is removed. Although optimally doped $BaFe_2(As_{1-x}P_x)_2$ is superconducting at zero kelvin, we can find the value of ρ_0 by extrapolating either the $T-$linear or $H-$linear magnetoresistance back to T or H equals zero. Fortunately, both methods give the same value for ρ_0, roughly $40\mu\Omega cm$. Figure 5.4 shows this extrapolation for sample 3949s3.

With this value in hand, we can perform the analysis described above on the data in Figure 5.3. The results are shown in Figure 5.5. The data from the normal state do in fact collapse on to a single curve as a function of H/T. This collapse strongly suggests that there is a single energy scale that controls the transport in these materials. The one limitation of a scaling analysis on these data is that the available field range is limited. We can improve this situation somewhat by including the ninety-two tesla data. However, those data are sufficiently noisy that the collapse plot one can obtain with them is not as convincing as it is for the sixty-five tesla data because the curves themselves simply occupy more space on the page. In any case, it is really the very low H/T region that would be most valuable from the perspective of identifying scaling physics, because in this region one can get the same value of H/T for the widest range of fields and temperatures. Unfortunately, this part will always be cut off by superconductivity. This makes finding quantum critical scaling in a superconductor a challenge, especially if the superconductor has a high transition temperature. Nonetheless, the collapse presented in Figure 5.5 is highly nontrivial and opens an important new window onto the electronic dynamics of the strange metal regime of the high$-T_c$ superconductors.

Before taking a closer look at the actual scaling form exhibited by the data, it is worth comparing this kind of scaling analysis to the most common kind of scaling analysis done on magnetoresistance data, Kohler scaling. Kohler's rule is a relationship between the field dependence of the resistivity and its zero field value.

$$\rho(H)/\rho(H=0) = f(H/\rho(H=0)), \tag{5.1}$$

The rule states that there should be one function, f, per material and it should hold across many values of the zero-field resistivity, which can be varied by disorder, or, to a limited degree, by changing the temperature. This result can be derived in the usual picture of a simple metal in a magnetic field, where the quasiparticles travel around the Fermi surface

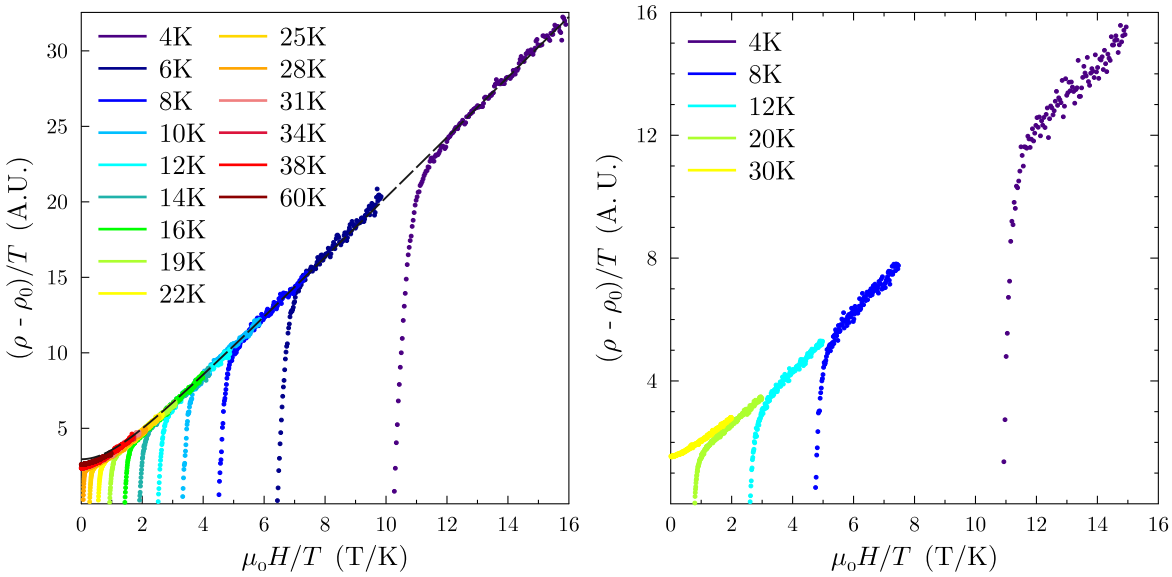

Figure 5.5: **Field-Temperature scaling in the resistivity of $BaFe_2(As_{1-x}P_x)_2$.** The magnetoresistance, with the residual resistivity subtracted (see Figure 5.4), is normalized to T and plotted versus H/T. The two panels show this analysis for the two data sets shown in Figure 5.3, on samples 3949s3 (left) and AG502s5 (right). All of the magnetoresistance data neatly collapse onto one curve, which is linear at high H/T and quadratic at low H/T. The curve approximately resembles a hyperbola, suggesting that the resistivity is set by a quadrature sum of these two parameters. A best-fit hyperbola is plotted as the gray dashed line. This shape of this curve motivates the ansatz in equation 5.2.

under the influence of the Lorentz force, and the magnetoresistance is caused by the lower average velocity that those quasiparticles will have as they are deflected around the Fermi surface. In this picture, the size of the magnetoresistance depends only on how far the quasiparticles are able to travel before they scatter. Assuming then, that ρ_0 is proportional to the scattering rate, doubling H and doubling ρ_0 simultaneously should have no effect on $\Delta\rho/\rho$, since the quasiparticles will orbit for half of the time but at twice the rate.[93]

However, all of this assumes that the scattering processes responsible for the resistivity are all of one type and can be captured in a single scattering rate. If the material has multiple Fermi surface sheets or if the scattering objects are changing as you change ρ_0, this argument breaks down. That second consideration in particular suggests that Kohler's rule will not hold on most systems when considering magnetoresistance curves taken at different temperatures. Phonons, which are principally responsible for the change in resistivity with temperature, will have a different average wavelength at different temperatures, and will therefore have a different scattering profile around the Fermi surface. So although it has

been known for decades that the magnetoresistance of the cuprates violates Kohler's rule, it is far from clear that this violation is the result of non-Fermi liquid physics.[44, 93]

On the other hand, it may appear that the scaling collapse in Figure 5.5 is actually just a variation of Kohler's rule. Since we know the resistivity is $T-$linear, then equation 5.1 should be obeyed given the collapse we see as a function of H/T, if $\rho \approx T$. However, the existence of a significant residual resistivity (roughly the same size as the variation in ρ between zero and sixty-five tesla), makes these two scaling phenomena distinct. In the argument leading to Kohler's rule, it is really essential to include the entirety of the resistance, because the scattering rate of the quasiparticles is proportional to the whole resistivity, not just the temperature-dependent part. Figure 5.6 shows the results of a Kohler analysis, in which it is clear that the data do not collapse at optimal doping. In the slightly overdoped samples, where the residual resistivity is smaller (see Figures 5.4 and 5.8) the Kohler scaling comes much closer to working (see Figure 5.6 panel (B)). However, the failure of Kohler's rule at optimal doping shows us that this is an accidental consequence of the small residual resistivity. Only the curves taken at temperatures above T_c are included, since a Kohler analysis requires one to know the resistivity at zero field. The failure of Kohler's rule in $BaFe_2(As_{1-x}P_x)_2$ has already been noted in the literature.[58] As emphasized above, the violation of Kohler's rule is not in itself strong evidence of a non-Fermi liquid magnetoresistance, but given the prevalence of this form of analysis in the literature, it is important to differentiate it from what is being done here, as well as to distinguish the kinds of phenomena that should lead to each.

This scaling curve in Figure 5.5 seems to be a hyperbola, with a limiting form at high H/T that is linear and a quadratic dependence at low H/T. Figure 5.5 shows a best fit hyperbola for the data. This leads us to the following ansatz for the scaling form:

$$\frac{\hbar}{\tau} = \sqrt{(\alpha k_B T)^2 + (\eta \mu_B B)^2} \equiv \Gamma, \tag{5.2}$$

where k_B (the Boltzmann constant) and μ_B (the Bohr magneton) have been used to convert temperature and magnetic field to units of energy. This expression is peculiar. It is calls to mind the picture of two energy scales adding in quadrature, such as the rest and kinetic energies in relativity theory. These expressions usually occur when the two terms in the quadrature sum represent different components of the same quantity. This idea meshes fairly well with the intuitive concepts of scaling, where we see either parameter as a way to tune the single relevant energy scale that is responsible for setting the electron momentum relaxation rate. This naturally raises the question of how the magnetic field is coupling to that energy scale. To approach that question it is essential to take a look at the size of the scale factor, η/α in equation 5.2. This number tells us how effectively the internal energy scale is tuned by field relative to temperature. The most robust way of extracting it from the data is to compare the slope of the zero tesla resistance versus temperature curve and the slope of the lowest temperature resistance versus field curve (getting to the very lowest temperature possible is not essential because already at four kelvin the temperature influence is negligible at fifty tesla because of the quadrature sum). This process yields a

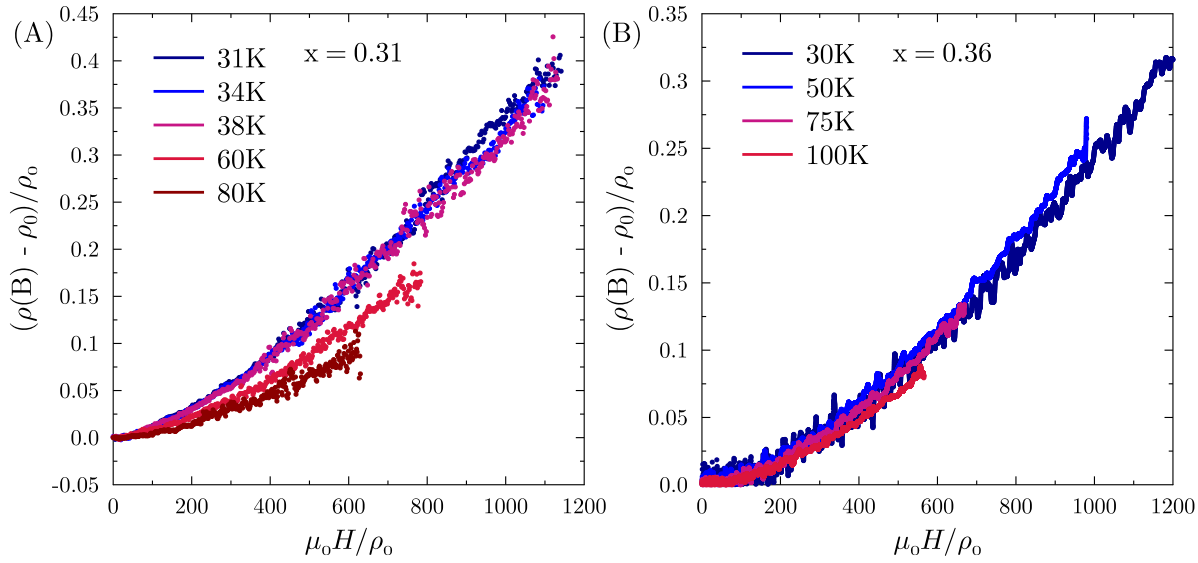

Figure 5.6: **The Failure of Koehler scaling in** $BaFe_2(As_{1-x}P_x)_2$**.** The fractional change in the resistivity is plotted versus $H/\rho(H = 0)$. If Koehler's rule held, all of the curves should lie on top of each other. This conclusion is supported by similar data and analysis in [58]. (B) The collapse is a bit better for the slightly overdoped samples above T_c, because they have smaller residual resistivities (see Figure 5.4)

value of 1.01 ± 0.07 in units of μ_B/k_B where the error has been determined by the worst fit within one standard deviation of the noise.

This value of the scale factor is intriguing because it seems to involve no material-dependent quantities. In reality, there are probably such quantities lurking in cancelations that are not evident in the final result. Nonetheless, looking at temperature in energy units, we can consider roughly what sorts of physical processes would lead to such an energy scale. There are two obvious candidates: spin and orbital energies. The Zeeman energy for a single free spin$-1/2$ with a g-factor of 2 would be exactly $\mu_B H$. The $g-$factor for electrons in the barium-122 system is believed to be around two, so this seems reasonable.[67] On the other hand, the energy between Landau levels would also be given by $\hbar\omega_c = 2\mu_B H$, which is also of the right order. However, in this second case, one expects the band mass to go into computation of ω_c. This is estimated to be between two and three bare electron masses, pushing the energy to nearly the right scale.[106] The appropriate way to distinguish between these mechanisms is to look at the dependence of the $H-$linear resistivity on the angle of the applied field, which will be done in the next chapter. For now, I wish to underline the fact that the energy scale seems to be roughly that of a single free electron in a magnetic field. It is somewhat surprising that this should be so, since we expect the dynamics of the critical point to governed by the collective dynamics of incipient antiferromagnetism (or

orthorhombicity/nematicity). It remains to be seen whether the value of the scale factor tell us anything significant about the origin of the scaling behavior, or whether it is simply a non-universal and essentially arbitrary property of $BaFe_2(As_{1-x}P_x)_2$.

One final point should be emphasized about the collapse of the data into a scaling form. The scaling analysis shown in Figure 5.5 was done on data that had a residual term subtracted. The neat collapse of the remaining data makes it look as though there really are two channels in resistivity, one of which involves scale-invariant physics and the other of which has no temperature or field dependence. It should be noted, however, that the total variation in the resistivity at low temperatures, from the estimated zero-field value to sixty tesla, is of the same order as the residual resistivity itself. In other words, even at sixty tesla, the system is not in a regime where the residual term is a small correction to the scaling resistivity. Therefore, we cannot simply neglect the residual term on the assumption that it is related to disorder scattering and can be treated a correction to the essential scaling physics. The idea that the size of the residual resistivity is simply a symptom of disorder is suspect anyway, for the reasons described in chapter 3. A strong enhancement of the resistivity, even at zero temperature, appears to be intimately connected to the physics of optimal doping. One major goal for further research into this problem would be to understand how and why such a significant enhancement in the residual resistivity arises and why this state supports two apparently serial resistivities, one with a strict scaling form and the other with no temperature or field dependence at all.

5.4 Overdoped and high temperature data

The striking $H-$linear magnetoresistance and scaling collapse that occur near optimal doping motivates a systematic investigation of the high field magnetoresistance of $BaFe_2(As_{1-x}P_x)_2$ across the phase diagram. These experiments required several further trips to the Pulsed Field Lab at Los Alamos, and resulted in relatively complete data sets on samples at four other dopings. These data are shown in Figure 5.7. These four new samples are 3947s2 ($x = 0.36$), 2767i4 ($x = 0.41$), x3474p1 ($x = 0.59$) and AG091p1 ($x = 0.75$). Of these four, the two closest to optimal doping were hand cut and contacted in a manner identical to that used for the optimally doped samples. The two more overdoped samples were cut and contacted by focused ion beam lithography (FIB). This is explains their significantly better signal-to-noise ratios (see Figure 5.7) despite their having lower resistivities. As discussed in chapter 4, this method, this technique lead to some significant changes in the resistivity when it was applied to optimally doped crystal, which is why the same technique was not used for any sample near $x = 0.3$. This difference in how the optimally and overdoped samples were prepared might lead one to question the validity of comparing data taken on those samples with the rest of the data set, especially in light of the strange behavior observed near optimal doping. However, as discussed in section 4.5, we know there are finite size effects in the optimally doped samples (see chapter 8 for details), which seems like the reasonable explanation for why we observed changes in the optimally-doped samples that

were contacted by FIB lithography. Additionally, the resistance versus temperature curves for the far overdoped samples were unaffected by the FIB process (see Figure 4.3). Both of these considerations give us confidence that the far overdoped data presented here are reflecting intrinsic behavior.

The magnetoresistance of these four samples shows clear differences from that of the optimally doped samples. For one thing, the low$-T$, $H-$linear magnetoresistance is absent for all samples not right at optimal doping. Therefore, it seems that at least this part of the phenomenology is restricted to the critical point. It is possible, however, that the magnetoresistance at higher temperatures is consistent with equation 5.2. In fact, this is what one would expect in a classic quantum critical scenario. As the system is tuned towards the antiferromagnetic phase transition from the overdoped side, there is some energy scale in the system that is going to zero. This scale defines the degree to which the system is "detuned" from the critical point. If the temperature is greater than this intrinsic energy scale, then the system is no longer aware that it isn't critical and its properties should be similar to what they are at the critical point. See section 2.4 for a fuller discussion of this point.

Doing a scaling analysis on the overdoped data is complicated by the need to remove the residual resistivity. Since there is no $H-$linear magnetoresistance at low temperature, we would not be able to corroborate any extrapolated value of the $T-$linear resistivity. However, using our knowledge of the scaling form obeyed at optimal doping, we can check whether the overdoped magnetoresistance has the right size and shape without worrying about the residual resistivity. One can view the right hand side of equation 5.2 as an energy scale that sets the electronic momentum relaxation rate. Since we have measured temperature and field at each data point, and we know the scale factor that converts one to the other, we can simply plot all of the data as a function of that energy scale (labeled "Γ" in the plot). If the resistivity is still controlled by the critical point, we expect all of the data to collapse as a function of Γ. The residual term will simply appear as an offset in this plot.

It is useful to include the zero-field resistivity in this analysis as well. Because Γ is a quadrature sum of H and T, at high temperatures the field sweeps populate energy space very sparsely and barely overlap. By including the zero field resistance we provide a point of comparison for every one of the magnetoresistance curves, since the zero field resistivity should represent the $H = 0$ limit of the scaling form. These plots are shown in Figure 5.8. Samples 3949s2 and 2767i4 do show a striking collapse even up to very high temperatures. As expected, the lowest temperature curves do not collapse. On the far overdoped side, however, there is nothing close to a collapse of the data, although sample looks like it might be trying. Note that the two near-optimally doped samples which show a collapse also have nearly $T-$linear resistivity, while the two more overdoped samples which show much more nearly quadratic dependence do not. This is about the correlation one would expect if he believed that the $T-$linear resistivity is connected to the scaling phenomenon.

In fact, on the far overdoped side the magnetoresistance has exactly the form that one would expect for a compensated multiband metal like $BaFe_2(As_{1-x}P_x)_2$. Systems with a single carrier type, especially if the have only one Fermi surface, tend to show relatively little

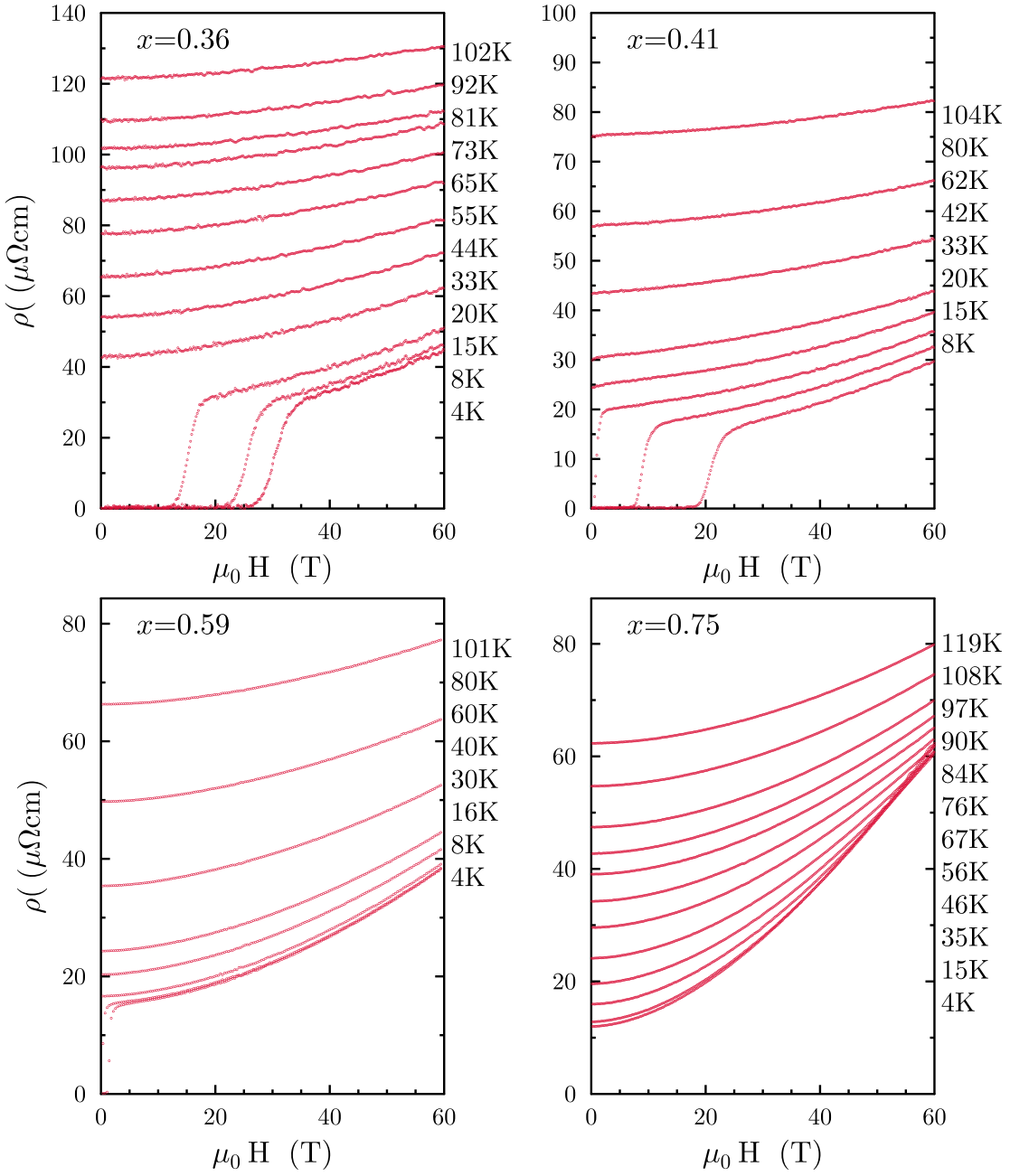

Figure 5.7: **The magnetoresistance of $BaFe_2(As_{1-x}P_x)_2$ across the phase diagram.** Comprehensive data sets for four doping levels ranging from optimal doping to the edge of the superconducting dome. Panels (A) through (D) show data for doping levels $x = 0.36, 0.41, 0.59, 0.75$.

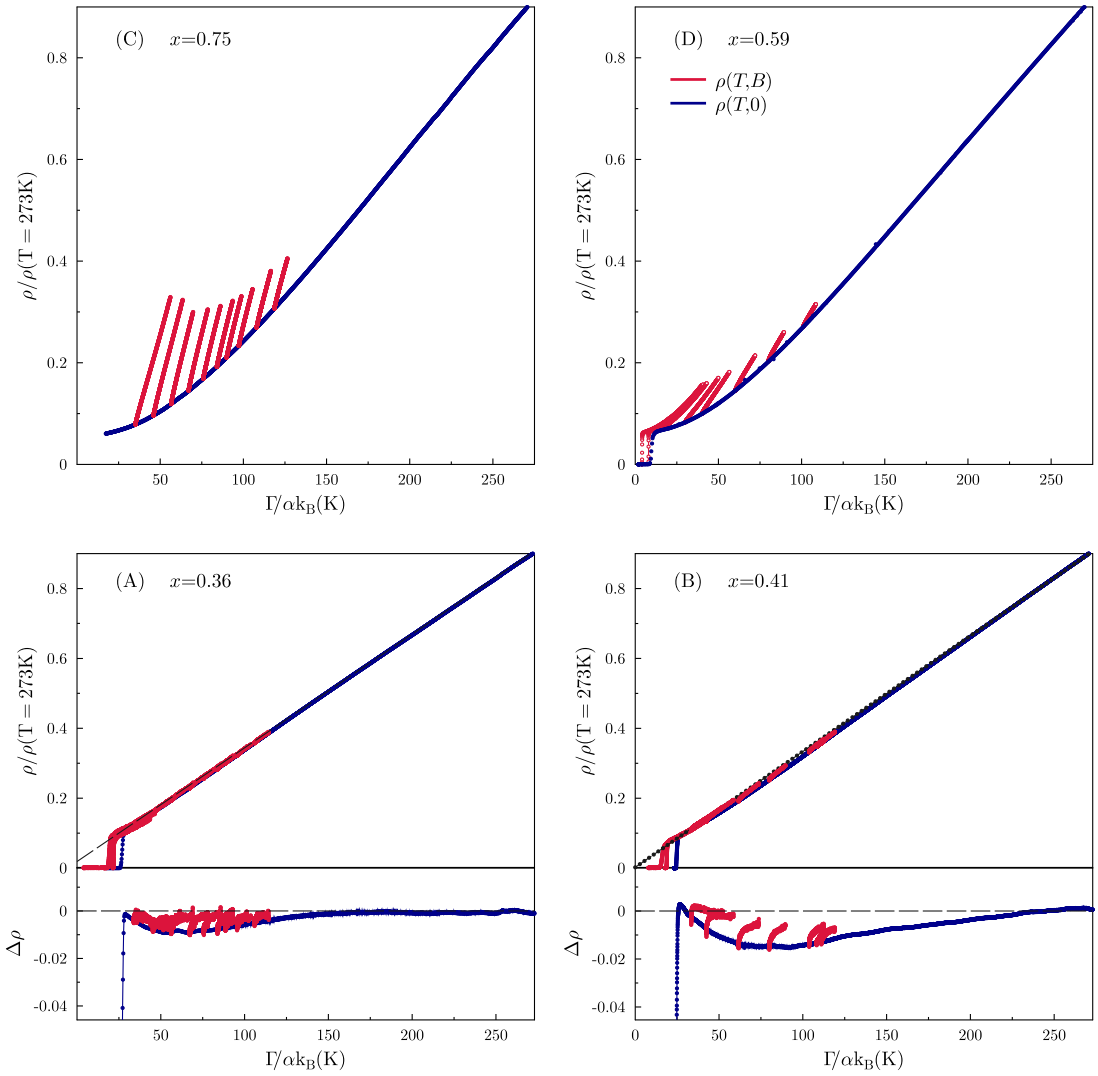

Figure 5.8: **The magnetoresistance of $BaFe_2(As_{1-x}P_x)_2$ across the phase diagram as a function of Γ.** The data from Figure 5.7 replotted as a function of Γ, showing the agreement between equation 5.2 and the data in the near-optimally doped samples at high temperature, but not in the far overdoped samples. Each data set is normalized the zero-field value at $273K$ to facilitate comparison between samples.

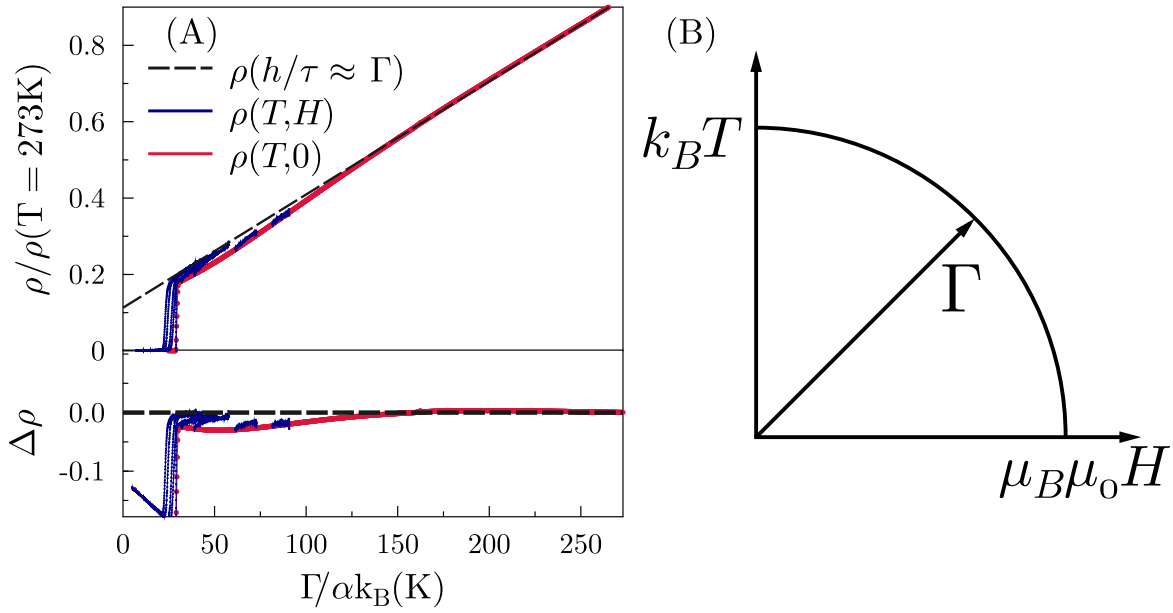

Figure 5.9: **The magnetoresistance of $BaFe_2(As_{1-x}P_x)_2$ at optimal doping as a function of Γ.** (A) These are the same data as are shown in Figure 5.3. In this sample the tendency for the MR to grow until it reaches the line defined by the high$-T$ extrapolation is particularly clear, as is the the agreement between the $H-$linear and $T-$linear extrapolations of the residual resistivity. (B) An illustration of the relationship between T, H, and Γ.

variation in their resistivities as a function of magnetic field. This is because of the Hall field that develops when electrons are deflected by the Lorentz force. To enforce the steady-state criterion that there be no transverse current, the Hall field has to exactly balance the average Lorentz force felt by the current carriers, leaving only the asymmetry between the most and least excited carriers to produce a net magnetoresistance. This situation is avoided if the system possesses similar numbers of electrons and holes. In this case the Hall fields from the two types of carriers cancel and the Lorentz force is able to efficiently reduce the velocities of all of the current carrying quasiparticles. This leads to a potentially large and non-saturating magnetoresistance that has a roughly $\sim H^2$ dependence. The field squared dependence comes from the approximately circular leading edge of the fermi surface.[93] Since this is exactly what the magnetoresistance looks like in the overdoped regime, it appears that all of the anomalous behavior occurs within a fairly narrow region around optimal doping.

Plotting all of the data (field sweeps and resistance versus temperature curves) together as a function of Γ reveals another interesting fact. The magnetoresistance curves are all very nearly linear as a function of Γ, but not all the way down to $H = 0$. Looking closely, we see that they rise quickly near zero field and then level off to a $\Gamma-$linear form. This appears to be connected to a feature of the zero-field resistivity versus temperature curve. Near optimal

doping these curves are all nearly linear but have a small deviation at low temperatures that is most pronounced near optimal doping. This indentation gives the overall curve the shape of a spoon, which gives this feature the name that it often goes by in the condensed matter community. The magnetoresistance curves in this region do not sit flush against the zero field resistance, but grow quickly as a function of Γ and then collapse on to the extrapolation from the $T-$linear region above the spoon. The difference between the $T-$linear extrapolation and the actual resistivity is not large, but it is large enough that this behavior is clearly visible in the data, especially in the background-subtracted plots of Figures 5.8 and 5.9.

This tendency for the magnetoresistance to grow and level off as a function of Γ is especially interesting because it mirrors the behavior of the resistivity in zero field. One way to interpret the spoon-like behavior seen in $BaFe_2(As_{1-x}P_x)_2$ and in the prototypical quantum critical materials is that the resistivity would naturally grow as the temperature squared, but it gets held back by some limit on the scattering rate. This idea has gained considerable currency with the recent observation of a semi-universal scattering rate per unit temperature in $T-$linear regimes.[18] One could then interpret the right hand side of equation 5.2 as the energy scale controlling this limit. In that case, we expect the resistivity in the spoon region to grow rapidly with field until it hits this limiting energy scale, defined by Γ, and then to just match the growth of Γ as the field is raised. That the resistivity wants to grow quickly is natural given how large the magnetoresistance is on the overdoped side of the phase diagram.

Another thing that is made apparent by the plots of resistivity versus Γ is that there is not a clear crossover point, as a function of temperature or of Γ, between the high$-T$ scaling regime and the low$-T$ non-universal regime. For both of the near-optimally doped samples, it seems that the transition happens somewhere around T_c, but there seems to be only a gradual approach to linearity and no consistent crossover point as a function of Γ; at very different values of Γ the system can apparently be an equal distance from the $\Gamma-$linear line. Furthermore, at a single value of Γ different curves can be different distances from it as well. Perhaps one only ever expects a gradual crossover between the critical and non-critical regimes, but the fact that the crossover temperature is not obviously rising as a function of doping is one limitation on our fitting this phenomenology neatly into a quantum critical picture. It is possible that with a much denser set of doping, one could identify a continuously rising cut-off temperature as a function of doping, but that would require much more time than a typical user can expect at the pulsed field lab.

5.5 Conclusion

The observation of scaling behavior in the resistivity of $BaFe_2(As_{1-x}P_x)_2$ near optimal doping has been of great interest for the field. It is consistent with some popular ideas about the nature of the electronic state near optimal doping, which has lead to significant attention.[84, 90, 124] Ideally, I would conclude this chapter with a discussion of the implications of the observations in this chapter for the various models that have been proposed

for the strange metal state of high$-T_c$ superconductors. However, that task will be greatly facilitated by further data on the angle-dependence of the scaling phenomenon, which will be presented in the next chapter. I will close this chapter instead with a general discussion of what it means that the resistivity of $BaFe_2(As_{1-x}P_x)_2$ scales as a function of H and T at the critical doping.

First, it is worth stating the obvious: the fact that the scaling appears only at the zero temperature endpoint of the antiferromagnetic/orthorhombic phase transition strongly suggests that it is the physics of quantum criticality that is responsible for the phenomenon. In fact, this almost counts as a confirmed prediction of the quantum critical theory. As discussed in the chapter 2, in quantum statistical mechanics the partition function includes a summation over an imaginary time variable that can be analytically continued to real time. This leads us to expect a diverging correlation time as well as a diverging correlation length at the critical point, which should lead to scale-invariant dynamics as well as scale-invariant thermodynamics.

However, it is possible to invert the logic here. Scaling is a hallmark of classical critical points precisely because those systems have a diverging length scale that dominates their thermodynamics. Hence, when you vary some external parameter of the system (assuming that you do not drive it too far from criticality) the only way that it can influence the observables of the system is by varying that one dominant length scale. This is why you can collapse all of the data on a single curve: there is only one number in the system that matters and all you are doing is walking back and forth along some function of that one number. Thus, we can look at the collapse seen in Figure 5.5 as evidence that there is just one time scale in the system that is controlling the momentum relaxation rate. In other words, the dynamics are approaching a scale-invariant regime at the quantum critical point. Apart from some observations of ω/T scaling in $Bi_{2.23}Sr_{1.9}Ca_{0.96}Cu_2O_{8+\delta}$, this would be the first direct evidence of this fact in a high$-T_c$ superconductor.[76]

The question then arises whether there is anything else that we can say directly from the data. One fact that was not emphasized above is that the scaling dimensions of magnetic field and temperature are the same in this system. In other words, the resistivity is $H-$linear as well as $T-$linear. This tells us that the time scale in question changes under the application of a magnetic field at the same rate that is changes under an increase of the temperature. Although the resistivity would have to be a power-law function of both H and T for the dynamics to be scale invariant, there is no general reason why the exponents in these two power laws would have to be the same. Typically, different external parameters have different scaling dimensions at a critical point.[103] This observation of $dim(H) = dim(T) = 1$ is helpful because it is often straightforward to compute the scaling dimensions of parameters in a particular model without solving the model completely. Indeed, some recent work has focused on explaining this fact in particular.[116]

Ultimately, the most significant fact about the data presented in this chapter is that it creates a new opportunities to study the problem of $T-$linear resistivity in the strange metal state. Work in this area has suffered over the years from the very limited experimental picture that has been obtained about the problem. The problem is defined by a very simple

temperature dependence, which doesn't on its own provide many clues about its mechanism. Now that the phenomenon has been linked to a certain behavior as a function of magnetic field, it is possible to probe the underlying physics more directly. Electrons have a known coupling to the magnetic field, so it is possible to restrict the class of relevant models for explaining $T-$linear resistivity. Additionally, the magnetic field is a vector, and so it is possible, for instance, to vary the direction at which it is applied and ask how the observed scaling changes. This allows the experimenter to probe the spatial symmetries of the underlying dynamics. Experiments of this type will be the subject of the next chapter. These data will thus provide inspiration for, as well as tests of, models for the strange electronic state out of which high$-T_c$ superconductivity emerges.

Chapter 6

Interlayer Magnetoresistance and Angle-Dependent Magnetoresistance

6.1 Introduction

The especially interesting properties of the transverse in-plane magnetoresistance in optimally doped $BaFe_2(As_{1-x}P_x)_2$ encourage us to investigate the rest of the resistivity tensor. As mentioned at the end of the last chapter, one wonderful consequence of identifying a magnetic analogue to the $T-$linear resistivity is that the magnetic field is a vector, which opens up the possibility of studying this phenomenon as a function of the relative orientations of field, current, and the crystallographic axes. This will provide a much richer phenomenology than has previously existed in this area. In this chapter I will present further high-field data obtained at the NHMFL's Pulsed Field Facility at Los Alamos National laboratory on both the interlayer and in-plane resistivities, ρ_c and ρ_{ab}, of optimally-doped $BaFe_2(As_{1-x}P_x)_2$ for a number of different field configurations. Magnetoresistance is a complex object and its interpretation is usually fraught unless it exhibits some acute phenomenon, like the $H-T$ scaling identified in the last chapter. Fortunately, $BaFe_2(As_{1-x}P_x)_2$ was generous in this regard. The scaling phenomenon is not restricted to the in-plane resistivity, but appears in the inter-layer resistivity as well. It is however, restricted to one particular configuration of the field: H parallel to the $c-$axis (or, perpendicular to the iron-pnictide planes). The significance of the $c-$axis is confirmed by the behavior of ρ_{ab} as a function of the angle of the applied field. The scaling is maintained for small deviations of the field from the $c-$axis, provided one uses the $c-$axis component of the field. Finally, the longitudinal in-plane resistivity shows significant negative longitudinal magnetoresistance, indicating that scattering off of magnetic fluctuations is a significant component of the scattering in these materials. Taken together, these observations paint of a consistent and startlingly simple picture of the scaling phenomenon, which should be a valuable guide to theory development.

Most of the data discussed in this chapter and the conclusions reached herein were published, albeit in abbreviated form, as "Magnetoresistance scaling reveals symmetries of the

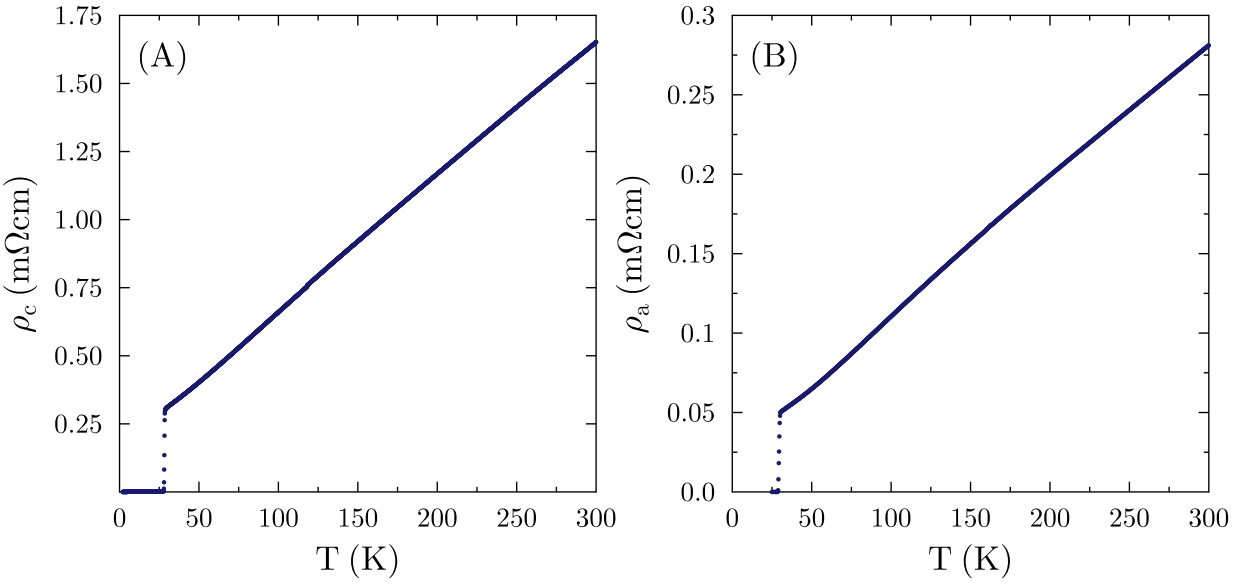

Figure 6.1: **Similarity of the resistance versus temperature in the interlayer and in-plane resistivity.** (A.) Resistance versus temperature of device AG263z1. This curve agrees with those found in reference [114]. The sample shows clear $T-$linear resistivity, qualitatively very similar to what is seen in the in-plane channel, for example in panel B. This is the same data shown in Figure 5.1. Note the factor of five difference in the absolute size of the resistivity

strongly correlated dynamics in $BaFe_2(As_{1-x}P_x)_2$", *Physical Review Letters*, **121** 197002 (2018).

6.2 Scaling in the longitudinal magnetoresistance of the interlayer resistivity

As discussed in section 4.3, creating devices to measure the interlayer resistivity, ρ_c, was a serious practical challenge. Of the six devices that were measured at the Pulsed Field Lab, only two had signals that were sensible, the others being marred by a phase that varied significantly as a function of field. For a relatively high frequency measurement, like those done at the Pulsed Field Lab, one must have a way of determining the phase at which current is moving through the sample. Because the current is traveling a long way from the generator to sample (to allow space for the magnet), the current running through the sample is not necessarily in phase with current being produced by the synthesizer. Typically, the largest component of the signal at the sample is the resistive signal. However, if the sample or contacts have significant capacitive or inductive components, this may not be true. Even

a large out-of-phase signal need not be fatal to the measurement if it is not changing as a function of field and one has a way of identifying the phase of the resistive signal. In a superconductor identifying that phase is straightforward because the resistive signal is known to be zero in the superconducting state. If this phase does not remain constant as a function of field, however, it is impossible to disentangle the resistive signal and therefore impossible to extract ρ as a function of field. Many interlayer resistivity devices had this problem, and it has a relatively straightforward explanation. Layer materials like $BaFe_2(As_{1-x}P_x)_2$ always have some amount of two-dimensional defects, such as cracks. This can lead to a capacitive signal within the sample itself. If the structure of these defects change at all as function of magnetic field, this capacitance will change as well, adding a variable phase to the sample signal. Since the problem arises from the effects of a rapidly-changing magnetic field, it was difficult to screen for this problem without going to the Pulsed Field Lab. As a result, several trips to Los Alamos were required to obtain the data shown in this section.

Of the two samples that did not have these phase problems, one had bizarre but reproducible fluctuations at low fields that seem unlikely to be due to the intrinsic physics of $BaFe_2(As_{1-x}P_x)_2$. They are likely due to small impurity inclusions in the sample. Crystals chosen for inter-layer measurements were typically cuboid (see section 4.3), which meant that it was easy for inclusions to hide. These fluctuations limited the field-temperature range from which reasonable conclusions could be drawn, but the very low temperature and high field part of the data seemed clean, so the data are included here because they offer support to the conclusions drawn from the most successful sample. Figure 6.2 shows these two data sets.

These were samples AG263z1 and AG626z5. An attentive reader will have noticed that these batches are actually slightly overdoped (see section 4.6). Although many crystals, especially from AG263, had superconducting transition temperatures as low as 27.5K, these two samples had T_cs of around 28.5K, indicating that they had only slightly higher phosphorous content than the most optimally doped crystals, probably $x = 0.33$ or 0.32 as opposed to $x = 0.31$. These samples were chosen for high field measurements because their resistance versus temperature curves were the most nearly linear of all of the samples considered (see Figure 6.1). The fact that it is at this doping, and not at $x = 0.31$, that the interlayer resistivity becomes most nearly $T-$linear was already noticed in the literature.[114] Since we are interested in the magnetoresistive correlates of the $T-$linear resistivity, we focused on $x = 0.33$ in creating interlayer resistance devices. Had the devices been easier to produce, a careful study of this doping region, and a comparison with the overdoped side would have been valuable additions to this study.

Before continuing on to a discussion of the data, I should say a few words about the mechanism responsible for the magnetoresistance of most metals. Fermi liquid theory maps the the low-lying excitations of a metallic system onto the the excitations of a non-interacting, degenerate Fermi gas. It therefore predicts that the carriers of electrical current will feel a Lorentz force in the presence of a magnetic field. If a net current is excited in the system, and the Fermi surface is shifted, the carriers on the leading edge of the Fermi surface will be deflected faster than those at the opposite face because the Lorentz force is proportional

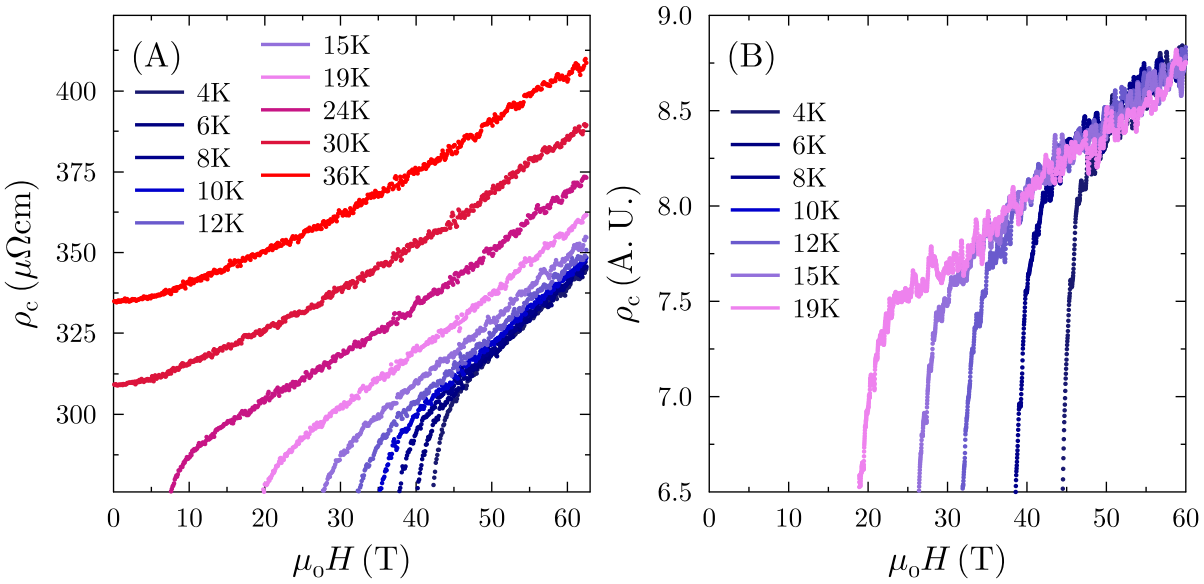

Figure 6.2: **Magnetic field dependence of the interlayer resistivity of $BaFe_2(As_{1-x}P_x)_2$ up to sixty-five tesla.** (A)The raw high field data on AG263z1. This sample showed excellent signal-to-noise and very pronounced $H-$linear magnetoresistance at low temperatures. B. The data for sample AG626z5. These data are clearly noisier and marred by the wiggles that appear at very low fields just above the superconducting transition.

to velocity. This will lead to a net reduction in the current. Because the excitations are those of degenerate Fermi gas and not of free electrons, the Lorentz force deflects particles along the Fermi surface and not along the trajectory of a free electron. This means that the magnitude of the magnetoresistance will depend on the local curvature on the leading edge of the Fermi surface in the direction perpendicular to the applied field. This makes the magnetoresistance a very sensitive probe of the shape of the Fermi surface, and it has historically been an essential tool for mapping the Fermi surface in most metals.[93] All of this means that, in $BaFe_2(As_{1-x}P_x)_2$, the magnetoresistance in the interlayer channel should not bear any particular resemblance to that in the in-plane channel. The Fermi surfaces are all quasi two dimensional, meaning that they cross the Brillouin zone boundary in the $c-$direction. As a result, a net current in the $c-$direction involves a completely different set of excitations and the size of the magnetoresistance will depend on the reduction of a different component of the Fermi velocity under the Lorentz force.

The arguments and discussions of chapter 5 suggest that the scaling seen in ρ_{ab} is not a simple result of the action of the Lorentz force on current-carrying quasiparticles, but a comparison of the magnetoresistance in ρ_c and ρ_{ab} allows us to settle the question. The central result is captured in Figure 6.2, which shows the interlayer resistivity as a function of magnetic field along the $c-$axis. The phenomenology here is the same as for the in-plane

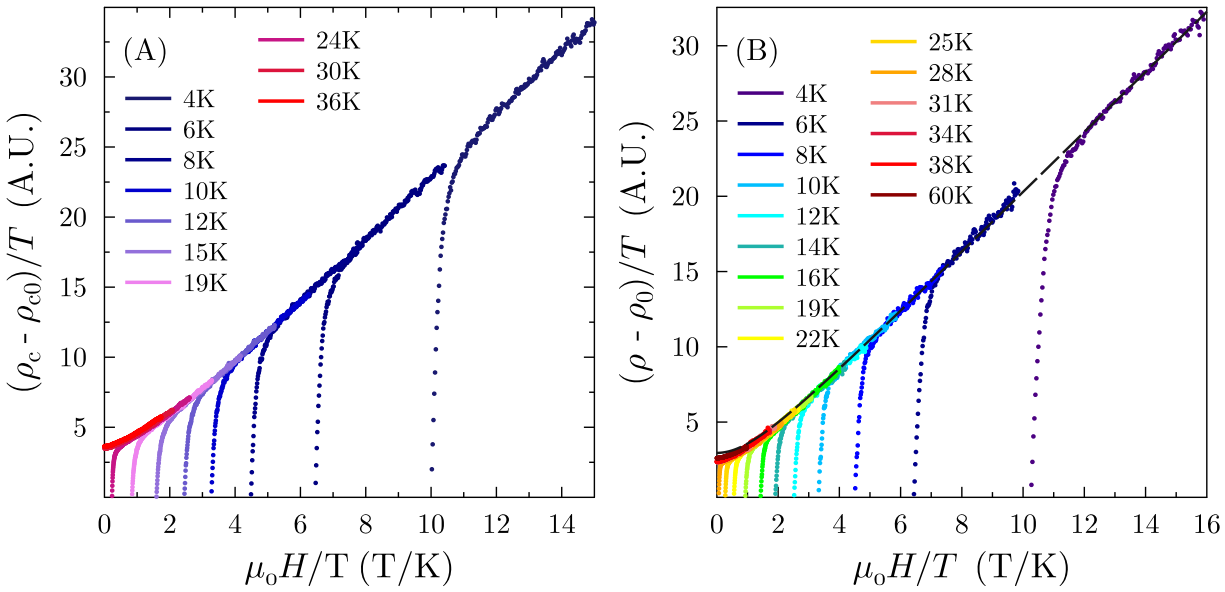

Figure 6.3: **Scaling in the interlayer resistivity of** $BaFe_2(As_{1-x}P_x)_2$**.** (A) The high field data on AG263z1 have been scaled by removing the residual resistivity (determined by extrapolating the $H-$linear resistivity to $H = 0$) and then normalizing both the remainder and the field to temperature. The result is a very clean hyperbole similar to that found for the in-plane resistivity. (B) The scaling plot for ρ_{ab}, reproduced for comparison.

channel in three important respects: the shape of the $\rho(H)$ curves, their size relative to each other as a function of temperature, and their magnitude relative the zero-field resistivity. First of all, the sample shows the same low$-T$, $H-$linear magnetoresistance as seen in ρ_{ab}. As the temperature is raised, curvature as a function of field appears, but with nearly no temperature dependence at high fields and moderate temperatures. These are the essential features of the scaling behavior in T and H and we can see in Figure 5.5 that the data collapse in an identical manner under the scaling analysis. The two channels even exhibit the same scale factor connecting H and T.

All of these features suggest that the same mechanism is at work in the two channels. In particular this rules out a mechanism based on the Lorentz force acting on quasiparticles. The third striking similarity between the two data sets is that the magnitude of the magnetoresistance represents the same percent change in the resistivity, despite there being a factor of five or so between the ρ_{ab} and ρ_c. This factor of five difference at zero field is reasonable given that $BaFe_2(As_{1-x}P_x)_2$ is a layered compound with cylindrical Fermi surfaces. This geometry means that the out-of-plane components of the Fermi velocity will be significantly smaller than the in-plane component. As a result, a similar excitation of the quasiparticles will lead to a much smaller current in the $c-$direction. For a pure cylinder with no warping,

there would be no $c-$axis conductivity at all. The pnictides are much farther from this limit than the cuprates and have correspondingly higher $c-axis$ conductivities ($\sim 10\%$ of the in-plane value rather than 1% or 0.1%), but the anisotropy is still in the direction that we expect for a layered system.[114, 49] The fact that the magnetoresistance has the same magnitude is the surprising fact. As discussed above, in the conventional picture of metallic magnetoresistance, the percent change in the resistivity should go as the correlation of the out-of-plane velocity under the average cyclotron orbit. For a Fermi surface with purely circular in-plane cross sections, there would actually be no variation of v_z at all when he field is parallel to c. The hole-like Fermi surfaces in $BaFe_2(As_{1-x}P_x)_2$ are of this form. The electron-like surfaces have a staggered ellipsoidal warping, so that v_z should undergo four sign changes over a complete orbit, while the in-plane velocity should only undergo two, which should still lead to a qualitatively different scale for the magnetoresistance in ρ_{ab} and ρ_c.[58, 45]

We can therefore conclude with some confidence that the scaling magnetoresistance in $BaFe_2(As_{1-x}P_x)_2$ does not have its origin in the deflection of quasiparticles by the Lorentz force. Although this is purely a negative conclusion, it is of immense value for our understanding of the strange metal state. Neither of the two canonical strange metal transport properties, a $T-$linear resistivity and a $T-$dependent Hall coefficient, is impossible to obtain from Fermi liquid theory in the temperature range that is accessible in high$-T_c$ superconductors. Thus far, the conclusion that these transport properties are due to a non-Fermi liquid state has only really been supported by analogies with systems where the low temperature limit is accessible. Only when the $T-$linear resistivity can be seen to continue down to the lowest temperatures, beyond the point were phonons should be frozen out, can a true tension with the T^2 resistivity of a pure Fermi liquid be demonstrated. By showing that optimally-doped $BaFe_2(As_{1-x}P_x)_2$ hosts a magnetotransport phenomenon that is inconsistent with the dynamics of ordinary quasiparticles, and that this phenomenon is intimately connected to the $T-$linear resistivity, we have demonstrated that these anomalous transport properties are, in fact, manifestations of physics beyond the standard model of metals.

From these data, this negative conclusion is the only one we can reach with high confidence. Creating a specific model that that would account for these observations is beyond the scope of this project and would, in any case, require many more experiments to verify. However, these data do provide important clues that will guide model builders in this area and it is worth stating one of these explicitly. The fact that the percentage change of the resistivity in field is so similar for the two different current directions seems to imply that the magnetic field is not coupling to the current, but to a more basic quantity in the electronic dynamics. This observation would be consistent with the idea that the field is somehow coupling directly to the scattering rate of the current carriers. It is not unreasonable to expect a magnetic field to do this in optimally doped $BaFe_2(As_{1-x}P_x)_2$. The self-energy of the single-particle Green's function will inevitably have contributions from the fluctuations of the nearby antiferromagnetic phase, and a magnetic field could certainly affect these fluctuations. The form that this coupling should take may be inferred from how different orientations of the magnetic field relative to the crystallographic axes affects the scaling

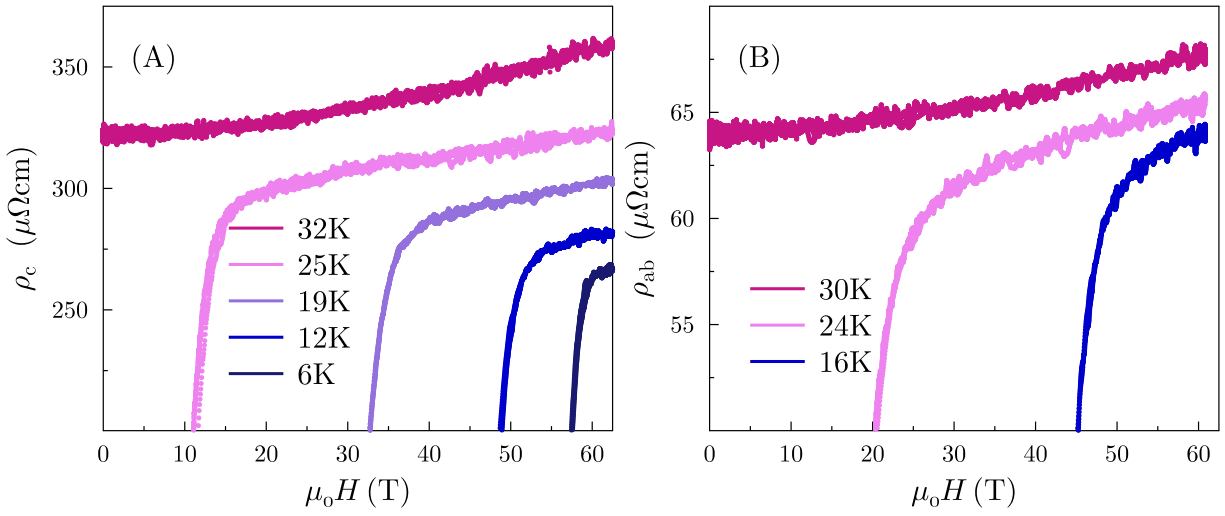

Figure 6.4: **Inter- and intra-layer resistivity of $BaFe_2(As_{1-x}P_x)_2$ with field in the iron-pnictide plane.** (A) The high field data on AG263z1 and (B) the high-field data on AG186s15 with with field in the plane and perpendicular to the current.

magnetoresistance. This will be the subject of the next three sections.

6.3 Magnetoresistance with field in the plane

The previous section showed data on the longitudinal interlayer resistivity. To round out our picture of the field-dependent resistivity tensor, we now consider the transverse magnetoresistance of ρ_c, as well as the transverse magnetoresistance of ρ_{ab} with field in the plane (instead of along the $c-$axis). The behavior of these quantities will allow us to determine if the scaling resistivity is truly an isotropic effect. The data for these two configurations are shown in Figure 6.4. Since only one sample gave high quality data on the interlayer resistivity (AG263z1), the experiment on $\rho_c(H//A)$ was done on that sample. The data on in-plane resistivity with field in plane were taken on sample AG502s5, which is one of those studied for the original in-plane scaling analysis (see chapter 5).

One important limitation of these experiments was the higher value of H_{c2} with the field in the plane. At four kelvin, the resistivity remains nearly zero up to about sixty tesla, instead of forty-five tesla. This is a relatively small degree of anisotropy when compared with the cuprates where the field-in-plane H_{c2} is unmeasurably high for some compounds.[96] However, a sixty tesla critical field is a meaningful limitation if one is working with a sixty-five tesla magnet. However, since we are looking for a pattern in field and temperature that continues up to several tens of kelvin, sixty-five tesla should be plenty to diagnose the presence or absence of an analogous scaling in the resistivity.

From the raw data it is immediately apparent that the magnetoresistance does not scale in the same way as it did for the configurations in which field was along the $c-$axis, in either the interlayer or in-plane resistivities. At four kelvin there is not enough of a field window to identify any $H-$linear resistivity that might exist, but if the same scaling form were obeyed, we should see the curves for six and ten kelvin taking on nearly the same value at high fields, since $6^2 \ll 60^2$. In fact, it seems as if one still has effectively $T-$linear resistivity at high fields and low temperatures, with the magnetoresistance representing only a small correction even at high fields. This means that the magnetoresistance is significantly smaller than it was when the field was along the the $c-$axis: $\sim 5\%$ instead of $\sim 30\%$ at thirty kelvin and sixty tesla.

One cannot, of course, say that the physical mechanism responsible for the scaling magnetoresistance is strictly irrelevant when the field is in the plane, but it certainly does not dominate the transport in this configuration. These data, together with those from the previous section and the previous chapter allow us to conclude that the $c-$axis is really a special axis for the scaling resistivity. This allows us to put valuable constraints on the possible origin of this scaling magnetoresistance. The mechanism cannot be completely isotropic in its coupling to the magnetic field, so the simplest spin models based on an isotropic spin-spin coupling are ruled out. This is significant as the energy scale implied by the scale factor between field and temperature suggested that a the coupling might be Zeeman-like. However, a single-particle Zeeman term is now extraordinarily unlikely because the the g-factor anisotropies in these materials is known to be small.[67] On the other hand, this behavior is being observed at the critical point of an in-plane magnetic order, which would naturally be more sensitive to fields oriented along the $c-$axis.[26] Thus, even without a clear model for this behavior, we can say at a qualitative level that it is still consistent with a scenario in which fluctuations of the nearby antiferromagnetic order dominate the electron dynamics. The next two sections will cover further experiments on the anisotropy of the magnetic response.

6.4 Negative longitudinal magnetoresistance in the in-plane resistivity

So far we have covered most configurations of field and current, but not yet longitudinal in-plane magnetoresistance (where the current is in the plane and the field is parallel to the current). From the apparent indifference of the magnetoresistance to the current direction when field is aligned along the $c-$axis we might guess that the the longitudinal, in-plane magnetoresistance would look just like the transverse in-plane magnetoresistance (with field in the plane). This does not turn out to be the case. Figure 6.5 shows high field data for this configuration. Right away one notices that the resistivity decreases with applied field, at least below about one hundred kelvin. This observation leads to two important conclusions, but before I discuss those I want to clarify why I believe this is not an experimental artifact.

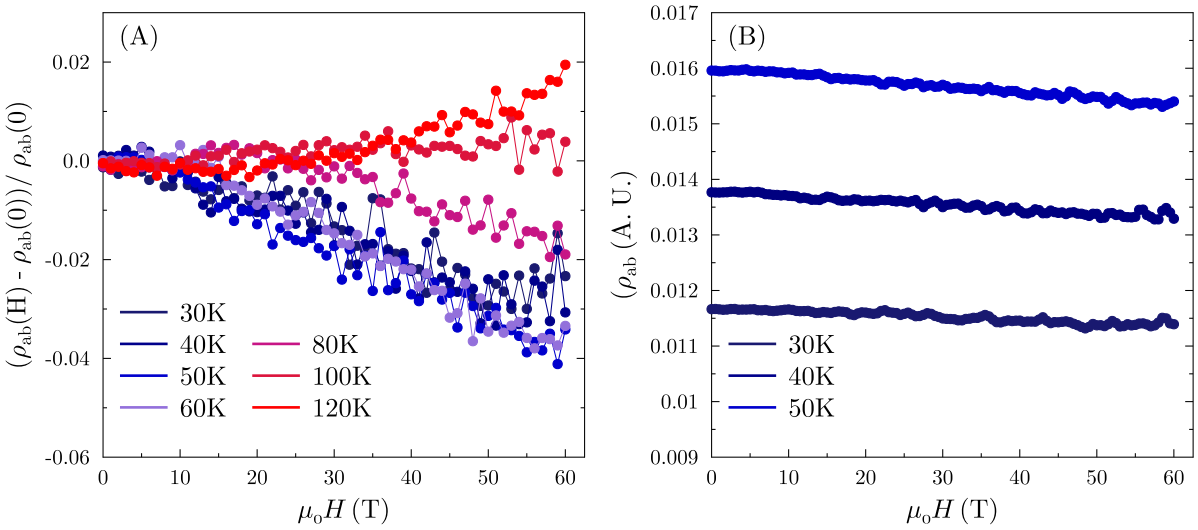

Figure 6.5: **Longitudinal magnetoresistance of the in-plane resistivity of $BaFe_2(As_{1-x}P_x)_2$.** (A.) The high field data on AG502s5 plotted as the fractional change in the resistivity as a function of field. Below one hundred and twenty kelvin there is a pronounced decrease in the resistivity with applied field. Intriguingly, below about sixty kelvin there seems to be a single functional form for $\Delta\rho/\rho_0$. (B) Low-field data on another device demonstrating that the phenomenon is not device-specific.

Apparent negative longitudinal magnetoresistance can arise from a phenomenon known a current jetting, where the magnetic field causes significant changes in the current paths within a sample. This has caused confusion in many instances, right up to the present day.[93] However, the conditions for current jetting are not present in our $BaFe_2(As_{1-x}P_x)_2$ devices. For one thing, as shown above, the magnetoresistance is not significantly anisotropic. In order to reorganize the current paths, the resistivities in the two transverse directions need to change appreciably, or else the current would simply follow the same path with an increased or decreased voltage. Second, the samples are not actually thick enough in the $c-$direction for current jetting to lead to much change in the current paths. As discussed in the chapter 4, by the time the current reaches the voltage terminals, it will have achieved a nearly uniform distribution across the sample. Therefore changes in ρ_c versus ρ_{ab} will not change the which path is most efficient for the current. For these reasons we believe that the data presented in Figure 6.5 reflect intrinsic changes in the conductivity of the material.

The fact that the resistivity cares about the relative orientation of field and current casts doubt on the idea that a magnetic field in the plane influences the resistivity through the same mechanism as a field oriented along the $c-$axis. The observation of scaling in both ρ_c and ρ_{ab} with the same magnitude strongly suggests that the effect does not arise from a direct interaction between field and current, but instead arises through a mechanism whereby the field, if it is oriented along the $c-$axis, tunes the dynamics of some other object which

then affects the quasiparticle lifetime (or the current-current correlation time). If a field in the plane also behaved in this manner, we would similarly expect the same effect on current traveling in all directions. So although the data in panels (A) and (B) of Figure 6.4 look very similar, this is more likely to be an accident than a reflection of come common underlying mechanism. This provides further support to the idea that the $c-$axis really is special as far as the scaling magnetoresistance is concerned.

The second interesting thing about these data is just the fact that the resistivity decreases with increasing field. The decrease is not insignificant; it reaches $\sim 4\%$ by sixty tesla at thirty kelvin. Negative magnetoresistance is uncommon in metals with a large Fermi surface. General arguments suggest that by scrambling the quasiparticle trajectories over the Fermi surface, an applied magnetic field should always lower the overall conductivity.[93] To increase the conductivity, one usually needs to reduce the scattering rate directly, rather than just rely on the deflection of the charge carriers. For an applied magnetic field to have this effect, the scattering must involve some magnetic objects. The canonical examples of this effect are in metals near a ferromagnetic transition, where the applied field polarizes the spins and leads to a reduction of the spin-flip scattering.[93]

This, of course, immediately suggests a mechanism for the negative magnetoresistance seen here. Since optimally doped $BaFe_2(As_{1-x}P_x)_2$ is near a magnetic phase, we know that there are magnetic fluctuations that are important for the electronic dynamics. However, the straightforward mechanism of polarizing fluctuations does not obviously apply in the case of incipient antiferromagnetism because there is no one direction that spins tend to align along. Instead, magnetic fields tend to suppress antiferromagnetic order, because spins tend to want to align with the field, which counteracts the tendency to AFM order. This is especially true if the field is applied along high-symmetry directions of that order.[25] For example, applied magnetic fields along the $c-$axis are known to decrease the magnetic transition temperature in $BaFe_2(As_{1-x}P_x)_2$.[23] If the scaling magnetoresistance in $BaFe_2(As_{1-x}P_x)_2$ is in fact driven by scattering off of magnetic fluctuations, it stands to reason that a suppression of those fluctuations would reduce the resistivity. If there is also some other effect (for example the conventional averaging-down of the current by the Lorentz force, which could easily still be applicable for the case of in-plane fields) and this effect is important in the transverse but not the longitudinal channel, that would explain why we only see negative magnetoresistance in the latter.

However, this story is not entirely satisfactory. The scaling magnetoresistance that we see when the field is applied along the $c-$axis is positive, and it seems overwhelmingly likely that the scaling behavior originates in some coupling to the magnetic degrees of freedom in $BaFe_2(As_{1-x}P_x)_2$. If the dominant effect on the magnetic fluctuations were merely to suppress them, then it is unclear how we would get a sizable positive magnetoresistance. The missing piece is probably the critical dynamics of the electrons (including their magnetic degrees of freedom) cannot be captured by this simple picture in which the current carriers see some external scattering potential that is being tuned by the magnetic field. Although this may be an attractive way to accommodate the two dimensional nature of the magnetic coupling with the three dimensional nature of the transport (see sections 6.5 and 6.6), it

is probably too simplistic a model given the theoretical complexities described in chapter 2. The primary conclusion we can draw from the existence of negative magnetoresistance is just that the transport is highly influenced by magnetic degrees of freedom. This is an unsurprising conclusion, but it is nice to be able to make it on the basis of data, rather than from theoretical expectations.

6.5 Angle dependence of the in-plane resistivity

Having determined that it is the field orientation ($H//c$) that is the crucial ingredient for the scaling magnetoresistance, it is natural to ask how the scaling disappears as we rotate the field away from the $c-$axis. In metals where the magnetoresistance is driven by the effects of the Lorentz force, the angle dependence of the magnetoresistance provides a lot of information about the shape of the Fermi surface. Historically this has been the primary way of determining the shapes of Fermi surfaces in metals, even more than through the observation of magnetic quantum oscillations.[93] This will not be our goal here since we do not believe that the Lorentz force is the primary driver of the magnetoresistance in $BaFe_2(As_{1-x}P_x)_2$, and its Fermi surface has anyway been determined via the de Haas-van Alphen effect and photoemission measurements.[3, 106, 121] Instead we hope to learn more about the coupling of the field to the peculiar electronic dynamics that are responsible for the scaling.

Measuring an angle dependence in pulsed magnetic fields is a delicate task. On a typical rotator probe wires are passed through the axel of a rotating stage to the sample platform so that the wires connecting to the sample can connect to the stage and remain fixed. For a rotator that must fit in the eight millimeter sample space, this means packing wires in a very small axle. Repeated rotations can lead to two wires being twisted together or even to abrasion of the insulation which can lead to relatively large capacitances in the measurement circuit. Since these wires carry current they will move around in field, which in turn can lead to large field-variable phase factors like those that prevented reasonable data from being taken on so many of the interlayer resistivity samples. This lead to a number of wasted cool-downs. My advice to future researchers is to simply let wires jump from the rotation stage to the fixed part of the probe.

Since we are interested in the evolution of the scaling behavior, it is simplest to just look at the evolution of the low temperature $H-$linear resistivity. Doing full rotations at many temperatures would require an extravagant investment of pulsed field time for little gain, since the $H-$linear magnetoresistance is the most prominent feature of this particular phenomenon. We want to know whether it exists for fields applied away from the $c-$axis, and if it does, whether the slopes and intercepts are constant. As with the field-in-plane measurements, the upper critical field of $BaFe_2(As_{1-x}P_x)_2$ can create problems since it reaches about sixty tesla when the field is aligned along the $a-$axis (as opposed to forty-five tesla when it is aligned along the $c-$axis). This can leave us without enough field range to characterize changes in the $H-$linear behavior in the sixty-five tesla magnets. To

compensate somewhat for this limitation we performed the primary rotation experiment at ten kelvin. At this temperature the resistivity is still dominated by the influence of the magnetic field ($10^2 = 100$ vs $60^2 = 3600$), so that we can evaluate the degree to which the scaling magnetoresistance is still present with confidence, and we are able to observe it to somewhat higher angles. A supplementary experiment at four kelvin was done that verifies the main conclusions of the ten kelvin experiment, albeit over a smaller field window (see Figure 6.7).

The data from the primary experiment are shown in Figure 6.6. In this experiment the field was always perpendicular to the current, even as it was rotated away from the $c-$axis. The first important observation is that for small deviations of the field from the $c-$axis, the linear magnetoresistance is still present, but the overall resistivity is smaller at high fields. The existence of $H-$linear resistivity for angles other than field along the $c-$axis shows that the effect is not limited to the pure field along c case. The quantitative details of the angle dependence can be revealed by fitting the linear part of the resistivity (above H_{c2}) and analyzing the angle dependence of the slope and the $H = 0$ intercept. Figure 6.6 shows these two quantities as a function of angle as well, in panels (C) and (D). The first thing to notice is that for some region near $\phi = 0$, the extrapolated intercept is constant as a function of angle, meaning that the magnetoresistance fits a form like $\rho = \rho_0 + A(\phi)H$, where ϕ is the angle between the field and the $c-$axis. This is already a nontrivial result, since it supports the idea that there really is a truly separate $H = T = 0$ term that exists in series with the scaling resistivity. The functional form of $A(\phi)$ is also striking. Since the slope is decreasing with increasing angle, the natural thing to check is whether it is tracking the component of the field along the $c-$axis. Panel (D) shows a $cos(\phi)$ curve along with the slopes of the linear fits, showing a fairly good agreement. However, rather than depend on a few data points, we can take advantage of the whole curves in a modified scaling analysis. Since it appears that the slope of the $H-$linear magnetoresistance is tracking the $c-$axis component of the field, we will plot all of these curves as a function of $\Gamma_c \equiv \sqrt{(k_B T)^2 + (\mu_B \mu_0 H)^2}$. This is done in panel (B). The curves collapse quite nicely, with some deviations appearing at the highest angles. Because this analysis does not even require an extended linear regime in which the data can be fit, it is possible to do this on data taken at lower temperatures as well. Figure 6.7 shows the data for a four kelvin rotation along with a scaling analysis in Γ_c. Again, the curves collapse quite nicely, especially at lower angles.

This seems to be the limit of the strict scaling regime. It is most intriguing, however, that there is a finite range of angles, below about sixty degrees, where the scaling seems to hold to very high accuracy. Since there is clearly some magnetoresistance at high angles (even $\phi = 90$ degrees), one might have expected this to mix with the scaling resistivity, so that every angle between zero and ninety involved some mixing of the two. This does not seem to happen at low angles. If the scaling magnetoresistance simply added to the magnetoresistance that we observe when field is in the plane, then at forty-five degrees we should see a roughly fifteen percent deviation from the scaling value ($\sim \frac{\Delta\rho(H||a)}{\Delta\rho(H||c)}$), which is clearly outside the error of the experiment.

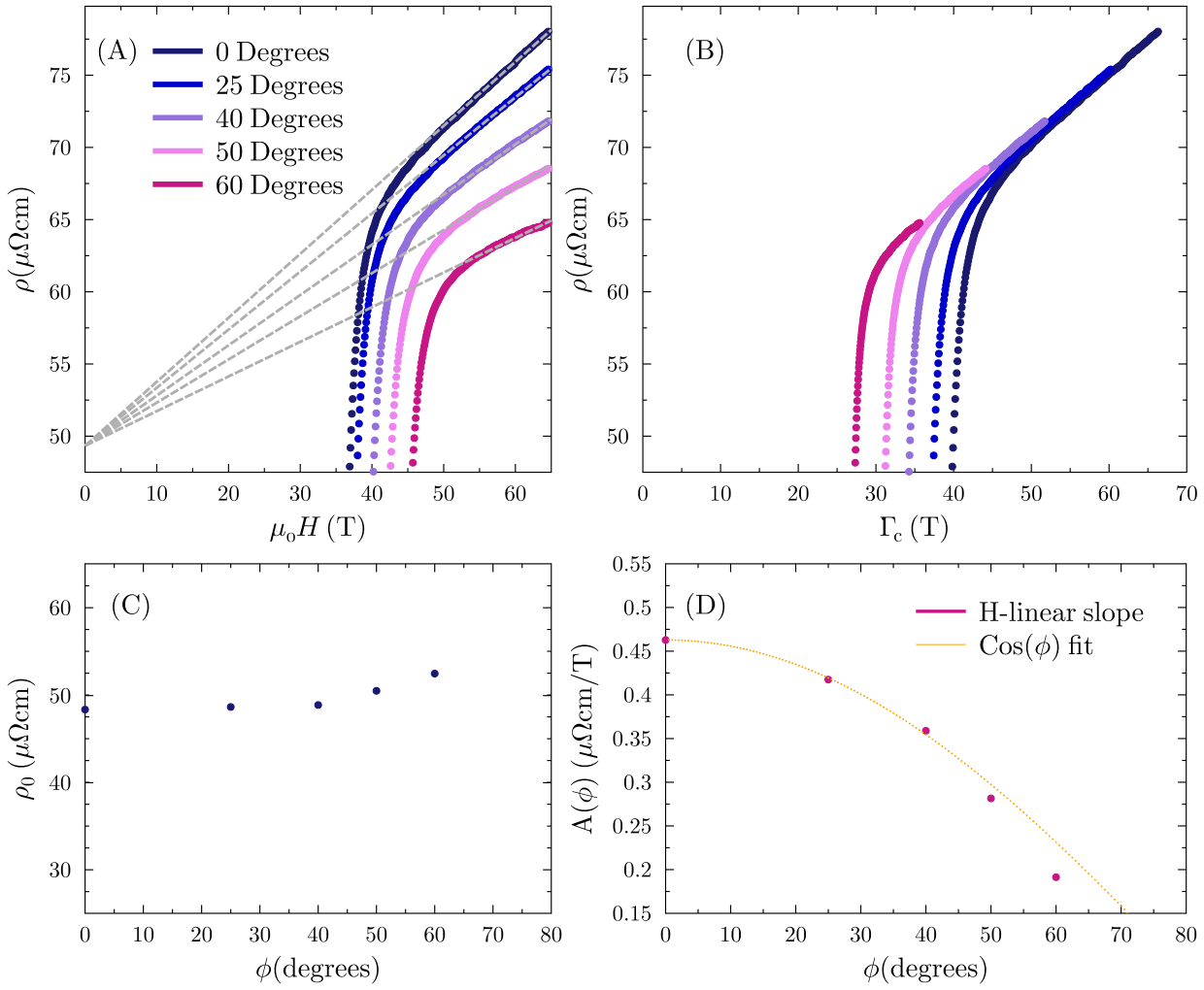

Figure 6.6: **Angle dependence of the in-plane magnetoresistivity of $BaFe_2(As_{1-x}P_x)_2$ at 10K.** (A) The high field data on AG186s15 at ten kelvin, taken with the field rotated away from the $c-$axis by the angle shown. The field was rotated in such a way that it is always perpendicular to the current. The $H-$linear resistivity is still clearly present but with a reduced slope. The dotted lines are guides for the eye. Significantly, the intercept is the same for all of these lines, at least at low angles. (B) A demonstration of the field-temperature scaling using only the $c-$axis component of the magnetic field. The $x-$axis is given by $\Gamma_c \equiv \sqrt{(k_b T)^2 + (\mu_0 \mu_B H_c)^2}$. Using this expression, the curves all collapse onto a single line. Panels (C) and (D) show the parameters from linear fits to the MR. The intercepts are nearly equal, especially at low angles, while the slopes decrease as $\sim cos(\theta)$, suggesting that the $H-$linear resistivity sees only the component of field along the $c-$axis.

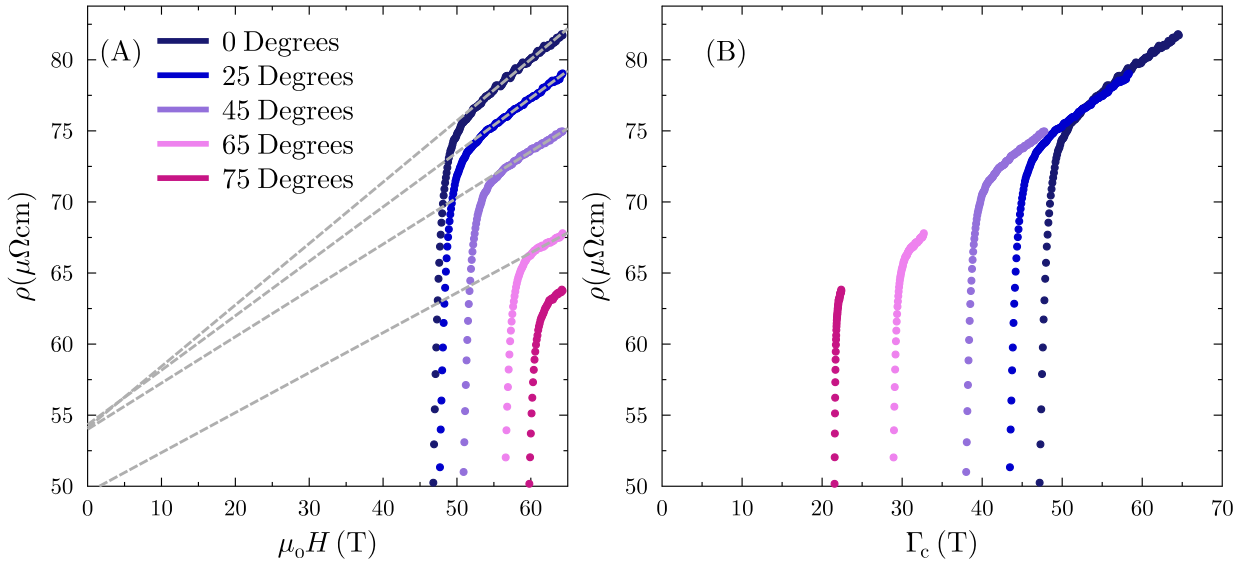

Figure 6.7: **Angle dependence of the in-plane magnetoresistivity of $BaFe_2(As_{1-x}P_x)_2$ at 4K.** (A) The high field data on AG186s15 at four kelvin. Angles are the rotation away from the $c-$axis. The field was rotated in such a way that it is always perpendicular to the current. The $H-$linear resistivity is still clearly present but with a reduced slope. The dotted lines are guides for the eye. (B) A demonstration of the field-temperature scaling using only the $c-$axis component of the magnetic field. The $x-$axis is given by $\Gamma_c \equiv \sqrt{((k_b T)^2 + (\mu_0 H_c)^2)}$. Using this expression, the curves all collapse onto a single line.

What sort of physics could account for this? Since the observed value of the resistivity is somewhat lower than the two-component model would suggest, we might say that the resistivity is subject to some limit on its growth. If the scaling form represented an upper bound on how fast momentum could be lost to the lattice, then the ordinary magnetoresistance we see in the field-in-plane configuration would appear to be absent once the scattering has reached this limit. This hypothesis is spiritually similar to various proposals that have existed in the literature for regarding $k_B T/\hbar$ as a fundamental limiting scale for scattering.[18, 122] These data on the angle dependence of the magnetoresistance suggest that this scale should be replaced by $\Gamma/\hbar$. From the perspective of this proposal, these data are valuable because they give us a chance to see that there is something that looks like a limit on scattering in the detailed behavior of a single system. Previously, this idea was motivated by the fact that this scale is seen in such a wide variety of compounds, so that something like a fundamental limit would be required to explain its universality. However, none of these proposals has been worked out in detail, and there seem to be very basic objections to the idea of the existence of a bound on scattering. Nonetheless, the data presented in this section and the detailed phenomenology of Γ and the spoon described in section 5.4 are striking enough that

the idea deserves renewed consideration.

Overall, then, the angle dependence of the magnetoresistance of $BaFe_2(As_{1-x}P_x)_2$ teaches us that the magnetic response that is responsible for the scaling must be very anisotropic. Because the dependence is very strictly $\sim Cos(\theta)$ for most angles, it looks like the relevant dynamics are somehow restricted to the iron-arsenic planes. This is quite a striking result because although the cuprates are very clearly effectively two-dimensional materials (the inter-plane coupling is small and seems to be incoherent) the same is not obviously true of the iron-based superconductors. Indeed, their Fermi surfaces have significant warping, signifying sizable out-of-plane coupling, and their resistive anisotropies are only about ten. It is also in strong tension with the observation that the scale-invariant dynamics seems to have an equal effect on currents in all directions. What this means for possible models of $T-$linear resistivity will be discussed in the next section.

6.6 Conclusion

The data presented in this chapter allow us to draw several important conclusions about the nature of the scaling resistivity identified in the preceding chapter. First, the microscopic mechanism responsible for it does not involve a direct coupling of the magnetic field to the current. If it did, it would not produce an identical phenomenology in the interlayer and the in-plane resistivities for the same orientation of the magnetic field. It does, however, seem to be a special consequence of the field orientation, as the resistivity shows no signs of scaling when the field is applied in the plane instead of along the $c-$axis. Furthermore, the scaling seems to specifically follow the component of field along the $c-$axis, such that the resistivity as a function of applied angle collapses as a function of $cos(\theta)H$ rather than as a function of H. Together, these two findings rule out most of the standard ways that one might hope to obtain the scaling from single-particle physics. Although the scale factor in the scaling relation suggests a Zeeman energy, thereby suggesting the coupling of individual spins to the magnetic field as a possible cause, there is no way to get an anisotropy in the Zeeman coupling that is large enough to reproduce the $\sim cos(\theta)$ angle dependence observed here. Indeed, measurements of the electron $g-$factor anisotropy via electron spin resonance measurements suggest a very isotropic magnetic environment.[67] On the other hand, any mechanism based on the trajectories of individual quasiparticles must respond differently when the current is aligned with the field and when it is orthogonal to the field. Because the scaling portion of the resistivity represents the major fraction of the overall resistivity (and if it is the root of the $T-$linear resistivity, almost all of the resistivity at high temperatures), the observations show that the charge transport in $BaFe_2(As_{1-x}P_x)_2$ is dominated by electron correlations and not by single particle physics. wave vector It is tempting to conclude that these measurements demonstrate that $BaFe_2(As_{1-x}P_x)_2$ is, in fact, a non-Fermi liquid metal. However, the only firm statement that can be made is that the dynamics responsible for momentum relaxation must take into account a significant amount of correlation between the individual quasiparticles. On some level, this is all that

one needs to say that the system is not Fermi-liquid-like, as the essence of FLT is that one can treat the system as a collection of weakly-interacting particles. However, one also needs to take account of the abundant evidence from quantum oscillations and photoemission experiments that a Fermi surface exists in $BaFe_2(As_{1-x}P_x)_2$ over most most of the phase diagram, including at optimal doping.[3, 106, 121] The most reasonable explanation of these phenomena is that they arise from the effects of critical fluctuations on reasonably well defined quasiparticles.

These findings do, however, produce certain acute challenges for candidate theories of the strange metal state in high$-T_c$ superconductors. This is easily seen in the very different symmetries of the magnetic response (roughly two dimensional, because of the $\sim Cos(\theta)$ dependence) and the current response (three dimensional because ρ_{ab} and ρ_c show identical scaling behavior) to the anomalous dynamics. It is generally difficult to get models that exhibit both two-dimensional and three-dimensional symmetry simultaneously, since the electrons are both the magnet objects in the system and the carriers of electrical current.

These observations cast significant doubt on approaches to these materials that depend on details of the Fermi surface. Much ink has been spilt on the relevance of Fermi surface "hot spots" for the charge transport. These are locations in momentum space where the antiferromagnetic wave vector connects two points on the Fermi surface, resulting in increased scattering.[47] It is plausible that the scattering in these areas could be dominated by antiferromagnetic fluctuations, which might have an anomalous temperature dependence. If one could then explain why the rest of the Fermi surface, which does not experience enhanced scattering, does not short-circuit the hot spots, this could conceivably explain $T-$linear resistivity. Some approaches exist for achieving this sort of averaging of the scattering rate, for instance by introducing significant disorder.[97] However, the $k-$dependent scattering in this picture only relaxes momentum in the plane, because that is where the antiferromagnetic wave vector lies, and so it could not explain why the $c-$axis transport is also dominated by this physics, as it appears to be in $BaFe_2(As_{1-x}P_x)_2$. Also suspect are approaches that make use of dynamic Fermi surface reconstruction to achieve areas of high Fermi surface curvature (which would naturally explain $H-$linear magnetoresistance, as mentioned in section 5.2) because, once again, these regions only have high curvature in the plane.[66]

Even models that begin from some sort of NFL starting point are challenged by the existence of the the $\sim cos(\theta)$ angular dependence. There are not many models that honestly achieve and maintain an NFL ground state. The most popular candidate these days is the Sachdev-Ye-Kiteav (SYK) model.[101] These are effectively zero-dimensional models where the coupling between any two sites, no matter how formally "distant" in the lattice, is a Gaussian random variable. Although they are physically unrealistic they have the virtue of realizing an NFL ground state. However, this NFL ground state sensitively depends on the randomness of all of the variables defining the interactions. If these terms acquire greater structure, then the system has a tendency to return to a Fermi liquid ground state. Some recent proposals have attempted to maintain the NFL characteristics while introducing some spatial structure by carefully segregating the degrees of freedom into SYK-type particles (which only have the random interactions) and more conventional quasiparticles which are

connected by regular hopping terms. One could then attribute the anisotropic magnetic response and the charge transport to the two different particle types. Presently this looks like the most promising avenue for these types of models.

Of course, the scaling behavior is naturally consistent with approaches to the strange metal state that are based on the fluctuations of an order parameter (either antiferromagnetism or its attendant nematic order). In these approaches, the fluctuations cut deeper into the quasiparticle picture than they do in the hot spot models. This need not lead to a wholesale destruction of the quasiparticles themselves, but the fluctuations should be of sufficient magnitude that the quasiparticle orbits are not highly relevant. The antiferromagnetism in this system at least has the right symmetry properties. It is planar, and therefore naturally more sensitive to out-of-plane fields. Indeed the observed magnetic response in the ordered state is highly anisotropic.[26] The question of whether the critical state that exists at the endpoint of this order would also lead to an isotropic current response is a question about the detailed nature of the quantum critical point, which there is currently no rigorous way to answer. Nevertheless, if we believe that transport in the critical regime is dominated by the lifetime of the current carriers, as is widely postulated to be the case, then changes in the particles' lifetime should affect transport in all directions. If the magnetic field is tuning the magnetic fluctuations, which in turn are effecting the quasiparticles' self-energy, this could lead to a magnetoresistance similar to what is seen. Of course, the difficulty with this approach is entirely in the theoretical challenges of handling this kind of coupling of fluctuations to free fermions, as was discussed in section 2.3.

Of the approaches that exist in the literature, the marginal Fermi liquid phenomenology comes the closest to meeting this challenge.[115, 116] This is the phenomenological approach pioneered by C. Varma and collaborators in the early days of high$-T_c$ research. In this picture the quasiparticle weight vanishes logarithmically at the Fermi surface, rather than being exactly zero. It is conceivable that contributions to the polarizability from antiferromagnetic fluctuation would be of the form required for this proposal. The fact that the quasiparticle weight vanishes logarithmically splits the difference between Fermi liquid and NFL physics, which potentially makes sense of the fact that many of the signs of quasiparticles are present. Whether or not this proposal actually meets the rigorous standards for an explanation of the strange metal state continues to be hotly debated.[7]

Finally I would like to mention again that subtle details of the angle dependence point in other directions. In the last chapter I pointed out how the $T-$linear resistivity of $BaFe_2(As_{1-x}P_x)_2$ is not actually of the form $\rho \sim T$, but involves a significant residual term. In other words, the resistivity is not proportional to temperature but has a constant gradient. This lends some support to ideas based on fundamental limits to the rate at which scattering can increase with temperature. In section 6.5 I pointed out that the $\sim cos(\theta)$ angle dependence is strict for angles close to zero. This makes it look as though the relevant scattering channel has reached some limit on how fast it can grow, given by $\Gamma = \sqrt{T^2 + H_c^2}$. Such a limit is not a natural consequence of the critical scenario, and may be another hint about how criticality actually manifests in metals.

Regardless of the tensions that exist in interpreting these data, they represent a significant positive development in the problem of $T-$linear resistivity. As discussed in chapter 1, the basic experimental picture that theories are attempting to explain has not evolved much in thirty years. In particular, because temperature is a scalar quantity that effects every aspect of the system, basic information like the symmetry of the underlying dynamics has been inaccessible. By connecting the magnetic field dependence to the $T-$ linear resistivity, the study of this scaling relation has revealed several additional concrete facts about the electronic dynamics in the strange metal state, including the symmetries of the magnetic coupling and the current carriers, and the fact that strong correlations dominate the charge transport. It now remains to be seen whether they can be worked into a quantitatively consistent picture that makes predictions with the clarity of Fermi liquid theory.

Chapter 7

The Strange Metal Hall Effect in $BaFe_2(As_{1-x}P_x)_2$

7.1 Introduction

On the basis of the extensive data set on longitudinal resistance that was presented in the last two chapters, we have reached the surprising conclusion that the magnetic field behaves much like a temperature in the way that it influences the electronic dynamics. This opens a new path for studying the physics of $T-$linear resistivity in the iron- and copper-based high-T_c superconductors. It also naturally motivates a study of the other anomalous feature of the charge transport physics in these materials, the $\sim 1/T$ enhancement of the Hall coefficient. This chapter will present data from a systematic study of the in-plane Hall Effect (I//a, H//c) in $BaFe_2(As_{1-x}P_x)_2$ up to sixty-five tesla, from optimal doping up to the non-superconducting overdoped side. The data indeed reveal that R_H has a strong dependence on the magnetic field that parallels its dependence on temperature. This field dependence allows us to track the strength of this $\sim 1/T$ enhancement across the phase diagram without having to do a complex multiband background subtraction. These data reveal two striking facts. First, within a fan-like region in the phase diagram that is centered around the quantum critical point, the enhancement in R_H is a function of temperature only, fitting the broad phenomenology of a quantum criticality surprisingly well. Second, this enhancement in R_H exists all the way until zero temperature throughout the superconducting dome, but not outside it. Although the non-superconducting samples also have an enhanced R_H at high temperatures, it decreases as a function of decreasing temperature and vanishes before the system reaches its ground state. This indicates that the phenomenon is intimately connected to the superconductivity in these materials, but in a way that is not anticipated in the theory of quantum critical metals. The chapter closes with a thorough comparison of these data with what exists in the literature on the cuprates and other quantum critical metals.

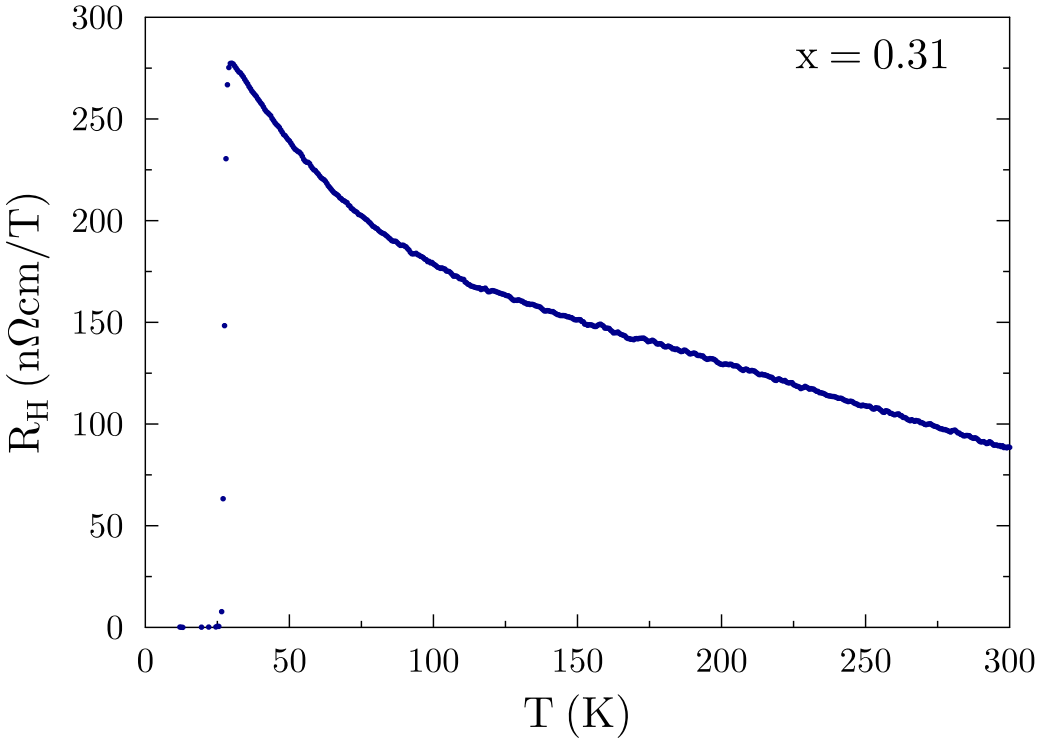

Figure 7.1: **The low-field Hall Coefficient in $BaFe_2(As_{1-x}P_x)_2$ near optimal doping.** Data on sample AG754s22, which is near thirty-one precent phosphorous substitution. The curve was taken by fixing field at plus or minus three tesla and then sweeping temperature and then anti-symmetrizing the data.

7.2 Prima facie phenomenology of R_H in $BaFe_2(As_{1-x}P_x)_2$

In the cuprates, the strongly temperature-dependent R_H is considered anomalous because those materials are single band metals. Unless the scattering rate varies significantly around the Fermi surface, the Hall coefficient of a single band material should not depend on temperature.[93] On the other hand, the iron-pnictides are multiband materials, which means that a temperature-dependent R_H is expected. It is therefore less straightforward to decide whether any given $T-$dependence in the Hall channel is a sign of similar physics. In the next section I will make a direct attack on the question of what a multiband model predicts in the case of $BaFe_2(As_{1-x}P_x)_2$. However, it is helpful to hear from the data first.

Figure 7.1 shows the Hall coefficient as a function of temperature for an optimally doped sample of $BaFe_2(As_{1-x}P_x)_2$ ($x = 0.31$). The Hall coefficient will be plotted as a positive number throughout this chapter for clarity, but the Hall effect is electron-like everywhere in

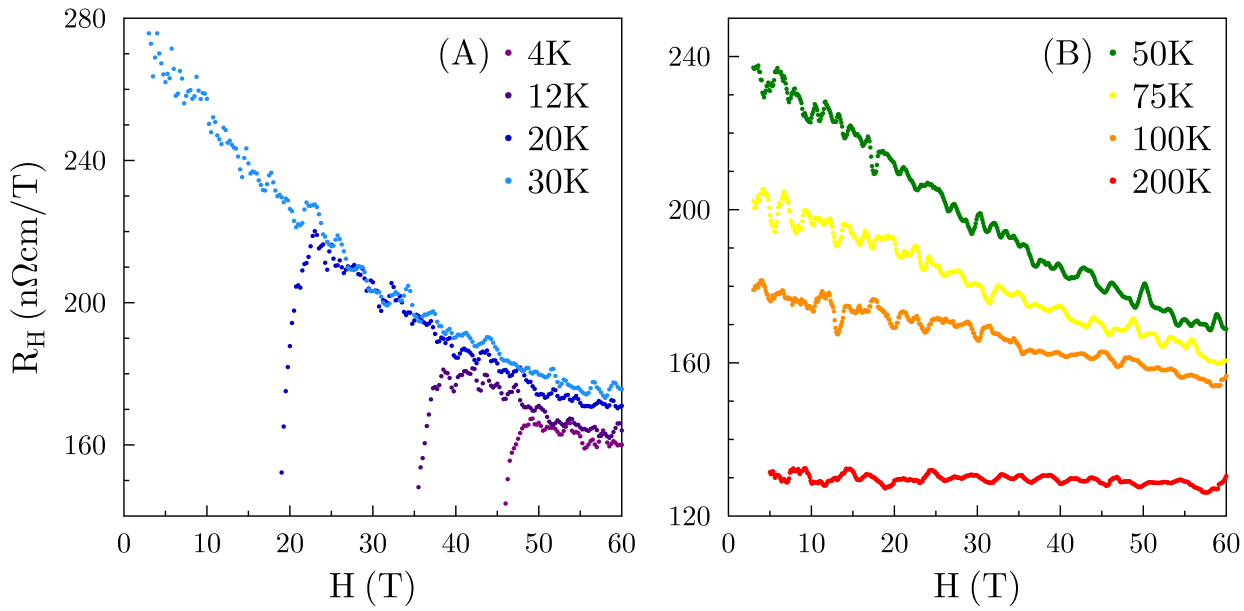

Figure 7.2: **The high-field Hall Coefficient in $BaFe_2(As_{1-x}P_x)_2$ near optimal doping.** Data on sample AG754s22, which is near thirty-one precent phosphorous substitution. There is a pronounced decrease in R_H with increasing field. This phenomenon is strongest in the temperature region where the low-field R_H shows a significant enhancement that is qualitatively similar to what has been reported in other high$-T_c$ superconductors, suggesting that it is also a feature of the strange metal physics.

the doping–temperature phase diagram. The data were taken by subtracting two temperature sweeps that were done in positive and negative magnetic field. The Hall coefficient is clearly not constant in temperature for any temperature region between T_c and 300K. However, there seems to be a qualitative change around about 175K. At higher temperatures, R_H has a weak and roughly linear temperature dependence, possibly transitioning to a nearly $T-$independent regime below about 200 kelvin. Well below 200K, R_H seems to increase with decreasing temperature, and does so at an increasing rate on approach to the superconducting transition. This low temperature behavior appears to be roughly $\sim 1/T$, similar to what is reported in the cuprates.[22, 49] If the Hall effect in $BaFe_2(As_{1-x}P_x)_2$ is displaying anything analogous to the cuprate behavior, it is doing so in this temperature regime. In light of the results obtained on H/T scaling in R_{xx}, the natural first question is whether there is any pronounced field dependence to R_H at these temperatures. Figure 7.2 shows high field Hall data for optimal doping ($x = 0.31$). These curves are obtained by taking the antisymmetric component of two traces of the voltage on the transverse contacts for up and down orientations of the magnetic field. The resulting R_{xy} versus field curve is then multiplied by the sample thickness and divided by the field to obtain a field-dependent $R_H \equiv \rho_{xy}/H$. The broad features of the field dependence are clear. The Hall coefficient decreases as a function

of increasing field, just as it decreases as a function of increasing temperature. Furthermore, this field dependence weakens as the temperature increases, effectively disappearing above 175K. The observed field dependence thus allows us to demarcate the two regimes in a second way: the regime of $R_H \sim 1/T$ is also a regime where R_H is reduced by a large magnetic field, and the high$-T$ regime is one where the Hall coefficient is constant in field.

This observation naturally inspires the thought that field and temperature are influencing R_H on the same footing, much as they appear to do in ρ_{xx}. In order to pursue this possibility with any rigor, it is necessary to understand the expected behavior of R_H in a multiband system in some detail. This will allow us to compare the observed field dependence to what is expected for single-particle physics, and will also allow us to judge the strength of the anomalous behavior relative to any multiband behavior that may still be in the system. Indeed, since there is a temperature dependence above 200 kelvin that seems to be unrelated to the strange metal physics (it shows no field dependence) it seems likely that the multiband nature of $BaFe_2(As_{1-x}P_x)_2$ is still influencing R_H. Ultimately, I will argue that various coincidences in the data, including the behavior near the antiferromagnetic and superconducting phase boundaries and some finite size dependencies (see chapter 8), make a convincing case that this low-temperature feature in particular is not the result of band structure and single particle physics. However, being aware of what we should expect purely on the basis of band theory will make this judgement easier to reach.

7.3 The Hall effect in multiband systems

The fact that $BaFe_2(As_{1-x}P_x)_2$ and the other iron-pnictide superconductors are multiband systems should be a liability for analyzing the field dependence of its Hall coefficient. There is a well known joke that the two-band model is wonderful because it can fit any data set. The equation for the low field Hall coefficient[93]

$$R_H = \frac{1}{en}\frac{\sigma_h - \sigma_e}{\sigma_h + \sigma_e} \tag{7.1}$$

may not seem that bad, but because there is often no good way of independently evaluating the mobilities of quasiparticles in different bands, it can be badly underdetermined experimentally. Things are even worse, however, in the case of $BaFe_2(As_{1-x}P_x)_2$ because it has four bands throughout most of its phase diagram: two electron-like bands and two hole-like bands. However, the situation is saved by the fact that $BaFe_2As_2$ is a compensated metal, meaning that it has exactly the same number of holes as electrons.[111] Because the phosphorous-for-arsenic substitution is isovalent, $BaFe_2(As_{1-x}P_x)_2$ is actually compensated throughout its phase diagram. Not only does the compensation condition eliminate a variable from the, multiband model ($n_e - n_h = 0$) but it actually directly fixes the behavior of R_H at high fields. At sufficiently high fields the Hall coefficient is always given by the net carrier density: $R_H(H \to \infty) = 1/(n_e - n_h)$ In a truly compensated system, this would give

an infinite Hall coefficient. In practice it means that systems that are nearly compensated end up with very large Hall coefficients at high fields.

To understand how R_H will approaches this limiting value, we have to take another look at the low-field regime. If $n_e = n_h$, then the sign of the numerator of equation 7.1 (and therefore the sign of R_H) will be determined by the sign of the more mobile carrier type. It should be clear that the low field Hall coefficient in a compensated system will be smaller than it would be for an analogous system with a single scattering rate and one carrier type, where R_H is always given by $1/en$. This makes sense physically. The magnitude of the Hall voltage is determined by the steady state criterion that there be no transverse current. Since electrons and holes are deflected in opposite directions by the Lorentz force, the transverse currents of the electrons and holes will partially cancel. In the limit of perfect compensation, meaning that the mobilities of electrons and holes are equal, there would be exactly zero transverse current, because the electrons and holes will carry equal amounts of current and therefore be deflected equally by the Lorentz force. Any real system will have a slight asymmetry in the mobilities of the two types of carriers. This will lead to a larger transverse current on the Fermi surface with the larger mobility, and the sign of the low-field Hall coefficient will reflect this fact.

Therefore, in a multiband system that is similar to $BaFe_2(As_{1-x}P_x)_2$, R_H will start out small and get large. The next step is to understand the transition from the low-field regime to the high-field regime. For the case of two bands it is simple enough to sum the conductivity tensors of the two sheets in parallel and invert the sum to get an analytic expression for the field dependence of $R_H \equiv \rho_{xy}/H$. The result can be found in several sources.[11, 93]

$$R_H = \frac{R_e\rho_h^2 + R_h\rho_e^2 + R_eR_h(R_e + R_h)H^2}{(\rho_e + \rho_h)^2 + (R_e + R_h)^2H^2} \tag{7.2}$$

One can see that R_H grows quadratically at low field and eventually saturates at a value given by the net carrier number. These are exactly the limits described above, and one can see directly from the equation that there is no combination of parameters that will lead to a second minimum as a function of field. Of course, there is one important difference between $BaFe_2(As_{1-x}P_x)_2$ and this model, and that is that $BaFe_2(As_{1-x}P_x)_2$ actually has two electron-like and two hole-like Fermi surface sheets, for four Fermi surfaces in total. This gives us several other parameters that we can tune to try to create the falling R_H that we observe in the experiments. In principle, if the mobilities on the two electron-like sheets are significantly different, then the system should exhibit a decreasing R_H at low fields. A decreasing R_H is actually the generic expectation for a system with one type of carriers existing on two different Fermi surfaces.[93] Although the analytic evaluation of a four band model is tedious and unilluminating, it is simple enough to evaluate this model numerically. These numerical simulations confirm that this effect could appear in $BaFe_2(As_{1-x}P_x)_2$ (see Figure 7.3). Normally this effect would be difficult to rule out because of the challenge of determining the mobilities on different Fermi surfaces. However, the observation of de Haas-van Alphen oscillations in $BaFe_2(As_{1-x}P_x)_2$ can help us evaluate at least the relative mobilities of the different electron sheets.[3, 106] Magnetic quantum oscillations appear when

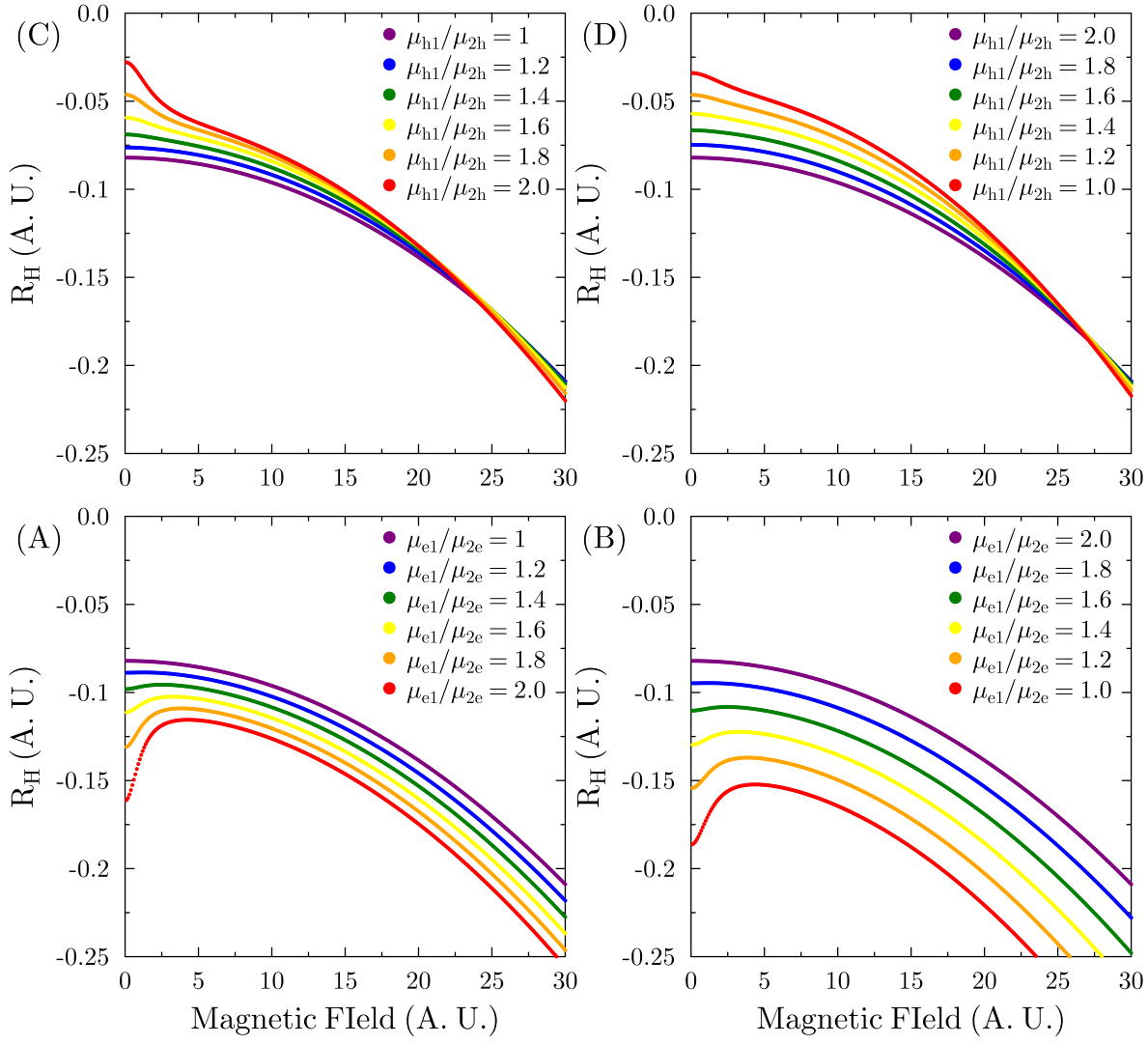

Figure 7.3: **Simulated R_H for a compensated four-band system.** Using the experimentally determined relative sizes of the Fermi surfaces, R_H has been computed in a simple four parallel channel model. The lower two panels show the results for differences on the two electron sheets (which have higher mobility overall) and the upper two panels for differences between the two hole sheets. In each case the results were computed for higher mobility on the large and on the smaller sheets. The only factor that can lead to a falling R_H is a difference (in either direction) of the mobilities on the electron sheets

$\omega_c\tau \approx 1$. In other words, the lowest field at which one can see them is roughly equal to the mobility. In all of these measurements, the oscillations from the two electron sheets appear at the same field. We can see from the plots in Figure 7.3 that the range of field over which R_H decrease is $\sim \Delta\mu$. Therefore, to obtain a falling R_H all the way out to sixty tesla (as wee see in Figure 7.2) would require a difference in mobilities of that order. This is implausible given that oscillations from both sheets appear around thirty tesla. The de Haas-van Alphen experiments do not give us information about the relative mobilities on the two hole-like sheets (because at most one of them is ever seen in a single experiment), but the simulations show us that a difference in mobilities on those sheets will only result in a stronger increase of R_H with field. This fact only depends on their being the sheets with lower mobilities, which we can safely infer from the sign of the low-field Hall coefficient (which is electron-like throughout the phase diagram) as well as from the quantum oscillation experiments.

Of course, this elementary phenomenon of the balancing of transverse currents on multiple Fermi surface sheets is only one of several effects that can lead to a field-dependent Hall effect. The Hall conductivity grows with the square of the scattering time, because an increase in the scattering time increases both the average velocities of the current carrier (and therefore the strength of the Lorentz force) and the time over which those carriers are deflected around the Fermi surface. The Hall coefficient, being related to the off diagonal *resistivity* therefore goes like

$$R_H = \frac{\langle \tau^2 \rangle}{\langle \tau \rangle^2}, \tag{7.3}$$

Generically then, anything that leads to a non-uniform scattering time in the system will make a contribution to the Hall coefficient.[30] In addition to the existence of multiple Fermi surfaces, this can be a variation of τ around a single Fermi-surface sheet, or the presence of a frequency-dependent scattering object. Clearly this opens up too many possibilities to be ruled out here. In fact, the existence of an unusual variation in the scattering time, either around the Fermi surface or between currents parallel and perpendicular to the Fermi surface, has been a popular proposal in the effort to understand high$-T_c$ superconductors.[4, 51] The conclusion of the this section should simply be that the lowest-order effects in multiband systems do not account for the field dependence of R_H that is actually observed. In fact, they tend to lead to strong increases of R_H with field, which any other mechanism would have to overcome to lead to the field dependence that we actually observe in optimally-doped $BaFe_2(As_{1-x}P_x)_2$. This field dependence is thus unnatural to some degree. However, it will ultimately be the peculiar patterns that this strange metal R_H displays in the $x - T$ phase diagram that weigh most heavily against its being a band-structure effect. If even more evidence for this were needed, we will see in chapter 8 that there are significant size effects in this system that appear only this part of the Hall coefficient, a fact that is utterly incompatible with its being caused by elementary multiband physics.

7.4 Analyzing the field dependence of R_H

Having concluded that the decrease of R_H that we observe near optimal doping does not arise from single-particle dynamics, we should try to understand how this anomalous behavior interacts with the ordinary band structure behavior that we see at high temperatures, high fields, and high dopings. The far overdoped side of the phase diagram shows a very nice $\sim H^2$ Hall coefficient at low fields (see Figure 7.11), which is exactly the prediction that comes out of equation 7.2. Figures 7.4, 7.8, and 7.9 show the main Hall data acquired for this project. One can see immediately that for dopings higher than optimal, there is an upturn in R_H at high fields. It is natural to suppose that this is a result of the underlying multiband physics, especially since the increase seems stronger the further one moves away from the anomalous regime near the antiferromagnetic and orthorhombic transition. It is worth trying to quantify this crossover, since it will allow us to see how the anomalous behavior changes as a function of temperature as well as as a function of doping. However, the main two conclusions mentioned in the introduction do not require this quantitive exercise. The can be made directly from the data on the basis of our understanding that a decrease in R_H with field is a sign of anomalous behavior. Nonetheless, I will cover the quantitative analysis first, as it helps bring the whole picture into focus quickly.

In order to quantify this anomalous field dependence we will have to determine its functional form, at least approximately. We will start by looking at the Hall data on an optimally doped sample at thirty or fifty kelvin up to sixty tesla. This is a useful spot in phase space to get one's bearings because it is at a high enough temperature that any field dependence due to multiband physics should be minimal, but since it is near optimal doping and not at too high a temperature, the size of the anomalous component should be significant. It is important to look at the largest field window possible to get the best perspective on functional form of $R_H(H)$.

Since the enhancement in R_H is thought to grow like $\sim 1/T$, we might expect that the high-field decay would go like $\sim 1/H$. However, this does not give a good fit to the data. This can best be seen by taking a derivative of the $R_H(H)$ curve. As Section 7.5 and chapter 8 will show, this strange metal behavior comes into the overall R_H as a second term that gets added to the background band structure behavior. Therefore, by looking at the derivative of the curve, we can remove the background R_H without needing to have already fit the curve and extracted the $H \to \infty$ limit. Figure 7.5 shows the derivative in field of R_H for optimal doing at thirty and fifty kelvin, evaluated by fitting a line to a ten tesla window. If the anomalous term decayed as $\sim 1/H$, the derivative would go as $\sim 1/H^2$. This means that between 30 and 45 tesla, the derivative should decay by a factor of $1.5^2 = 2.25$, but in the data it decays much more slowly than this. On the other hand, the ratios between successive values of the derivative are roughly constant. At thirty kelvin they are $0.79, 0.85, 0.83, 0.87$ for the points shown, and for fifty kelvin they are $0.90, 0.95, 0.91, 0.95$ for the points shown. The property of decaying by a constant fraction per unit length is the defining characteristic of an exponential function. Therefore, it seems reasonable to model the field dependence as a decaying exponential, at least at high fields.

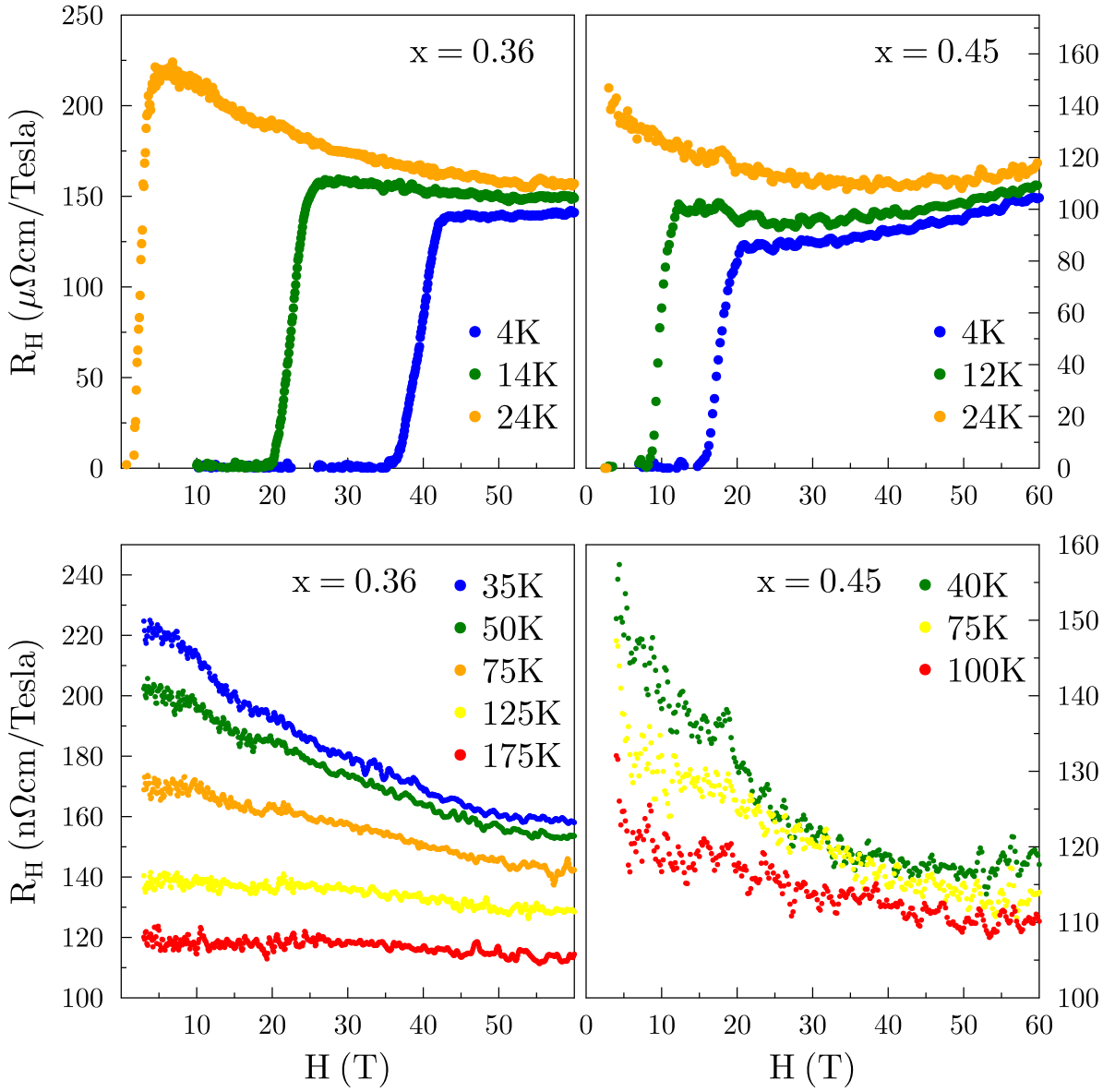

Figure 7.4: **The high-field Hall Coefficient in $BaFe_2(As_{1-x}P_x)_2$ near optimal doping.** High field R_H data on samples AG263s12, which is near thirty-six precent phosphorous substitution, and AG1280s6, which is near forty-five percent phosphorous substitution. Panels (A) and (B) show data below T_c and (C) and (D) show the data for above T_c.

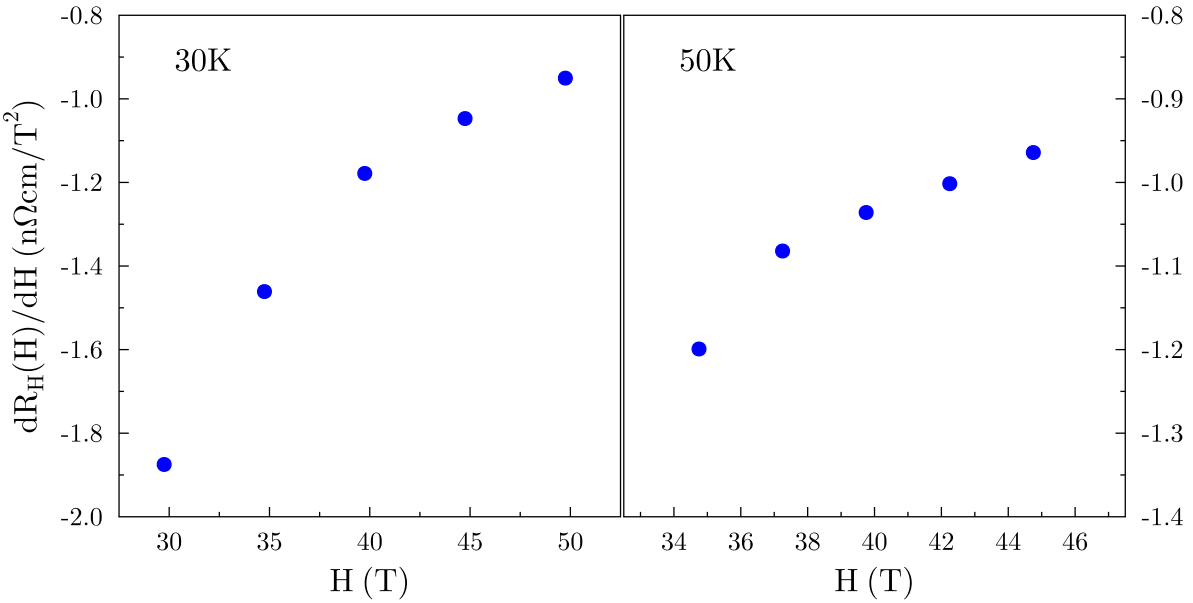

Figure 7.5: **The shape of the $R_H(H)$ curve.** The derivative in field of R_H for two temperatures above T_c.

However, since it is clear that there is some background multiband behavior in R_H, we should expect it to contribute some background field dependence as well, at least at low temperatures where the mobilities are highest. For this we will assume the form derived from pure multiband theory, since that does seem to account for the overdoped side quite well. This means that we will fit the high field regime to an expression like:

$$R_H(H) = R_{H0} + \frac{\beta}{2}H^2 + Ae^{-H/H_0} \tag{7.4}$$

This gives us four parameters to fit, which can be a little clunky given the signal-to-noise of pulsed field data. Since we are principally interested in the A and H_0 terms, it is slightly more efficient to fit to the field derivative in R_H, which eliminates the constant background term without any analysis. Figure 7.6 shows some sample fits of high field data.

This exponential decay is clearly not the whole story, however. At low fields we see that R_H actually has a very weak field dependence that gradually grows into the exponential-like term that is seen at higher fields. It is important to take account of this low-field behavior because it is often the only part of the $R_H(H)$ curve that is available to us, due simply to the fact that there is a finite amount of pulsed field time to be had on any given project. Several important questions are raised by this observation. Does the crossover from $\sim H^2$ to exponential decay happen at a fixed field? is the behavior at low fields correlate with the behavior at high fields? and how does this change the actual size of the enhancement in R_H from what we estimate using a pure exponential at high fields. Fortunately, it turns out

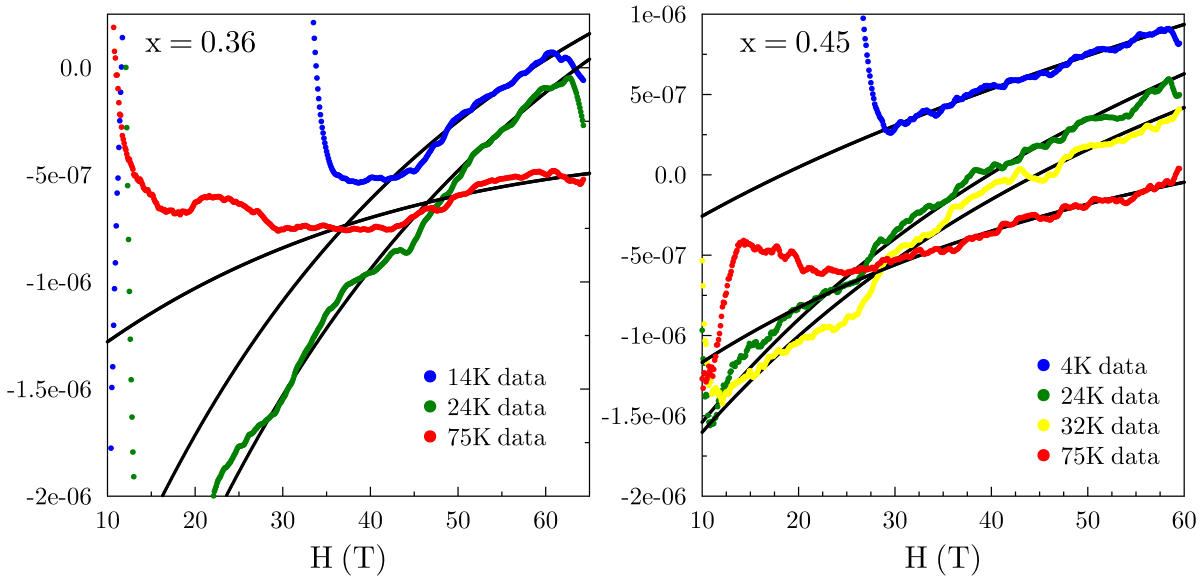

Figure 7.6: **Sample fits of the high field Hall coefficient.** High field R_H data on samples AG263s12, which is near thirty-six precent phosphorous substitution, and AG1280s6, which is near forty-five percent phosphorous substitution, have been fitted to equation 7.4, by first taking the derivative of the data. Quality fits are possible, especially at low temperatures and high fields.

that this low-field behavior is part of a single curve whose only evolution across the phase diagram is in its amplitude and field scale. In other words:

$$R_H(H) = Af(H/H_0) \tag{7.5}$$

This can be seen directly in Figure 7.7 where several curves from across the $x - T$ phase diagram have been collapsed on top of each other, just by rescaling their x and y axes. It is the fact that the high-field limiting form of $f(H)$ is exponential that allow us to estimate the overall size of A even though we do not completely suppress the strange metal enhancement, even at very high fields. However, once this has been evaluated for one curve, we can extract the values for A and H_0 by fitting even the low-field part of the curve and comparing it to the cleanest high-field curves available. This is done in Figure 7.7, panel (B) for an optimally doped sample at multiple temperatures. For samples on which we have both high field and low field data, we can cross-correlate these methods and see that they give very nearly the same values of A and H_0.

This is all we need to estimate the size of the strange metal contribution to R_H on the overdoped side of the phase diagram. My use of the word "estimate" is deliberate, as the precision of these procedures is severely limited. However, as will be discussed below, the main conclusions about the range of strange metal behavior in $BaFe_2(As_{1-x}P_x)_2$ can be

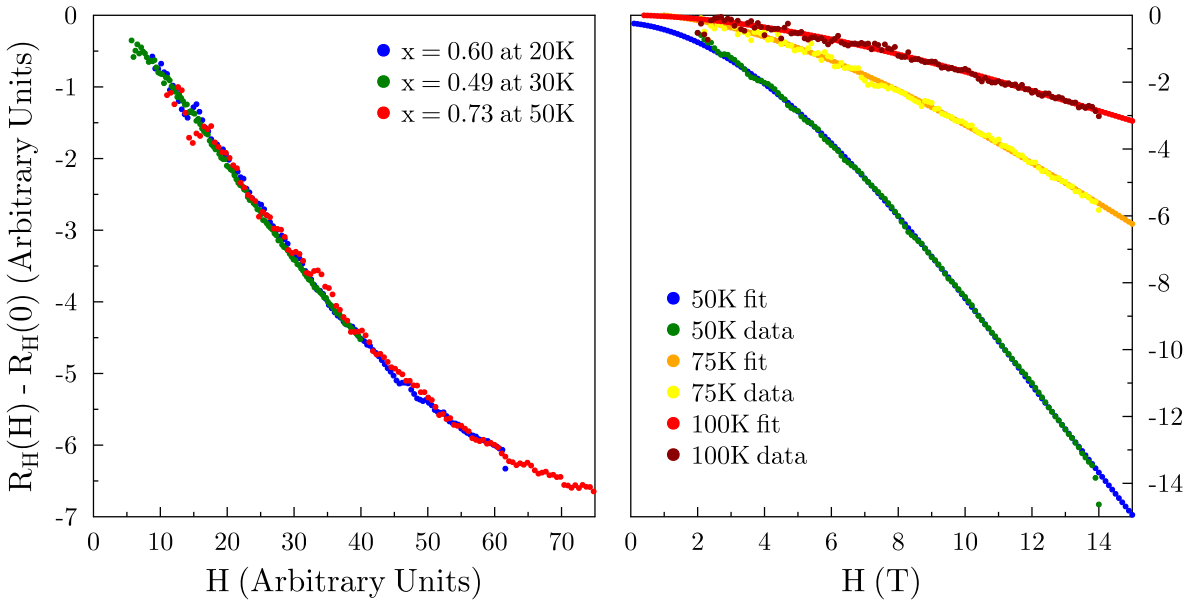

Figure 7.7: **The field dependence of R_H for several curves across the phase diagram.** The field-dependent part of $R_H = \Delta R_H(H)$ has been collapsed for two curves from opposite corners of the phase diagram, showing that they follow the same functional form up to a rescaling of field and amplitude. (B) The field-dependent part of R_H at 35 kelvin has been fit to the analogous curves at other temperatures, allowing an estimation of A and H_0.

made by a careful look at the unanalyzed data, once we have realized a decreasing R_H in field is a consequence of strange metal physics.

7.5 The anomalous component of R_H across the phase diagram

With the above analysis techniques in hand, we are ready to examine the anomalous behavior of R_H across the entire $x - T$ plane. It is worth emphasizing here that this is the first time that a high$-T_c$ superconductor has allowed a clean disentanglement of the single-particle dynamics from the strange metal physics in either transport coefficient. As a result, the trends and correlations reported below have not been identifiable previously. Indeed, before now it would seem highly unlikely that any such simple and clear trends existed in quantities as complicated as transport coefficients. Even the fact that strange metal behavior manifests as a simple additive enhancement to the Hall coefficient is a surprise that creates challenges for some of the leading proposals in the literature (see section 7.6). Like the identification of a magnetic analogue to the $T-$linear resistivity, these results will help focus theoretical efforts on a more precise phenomenology.

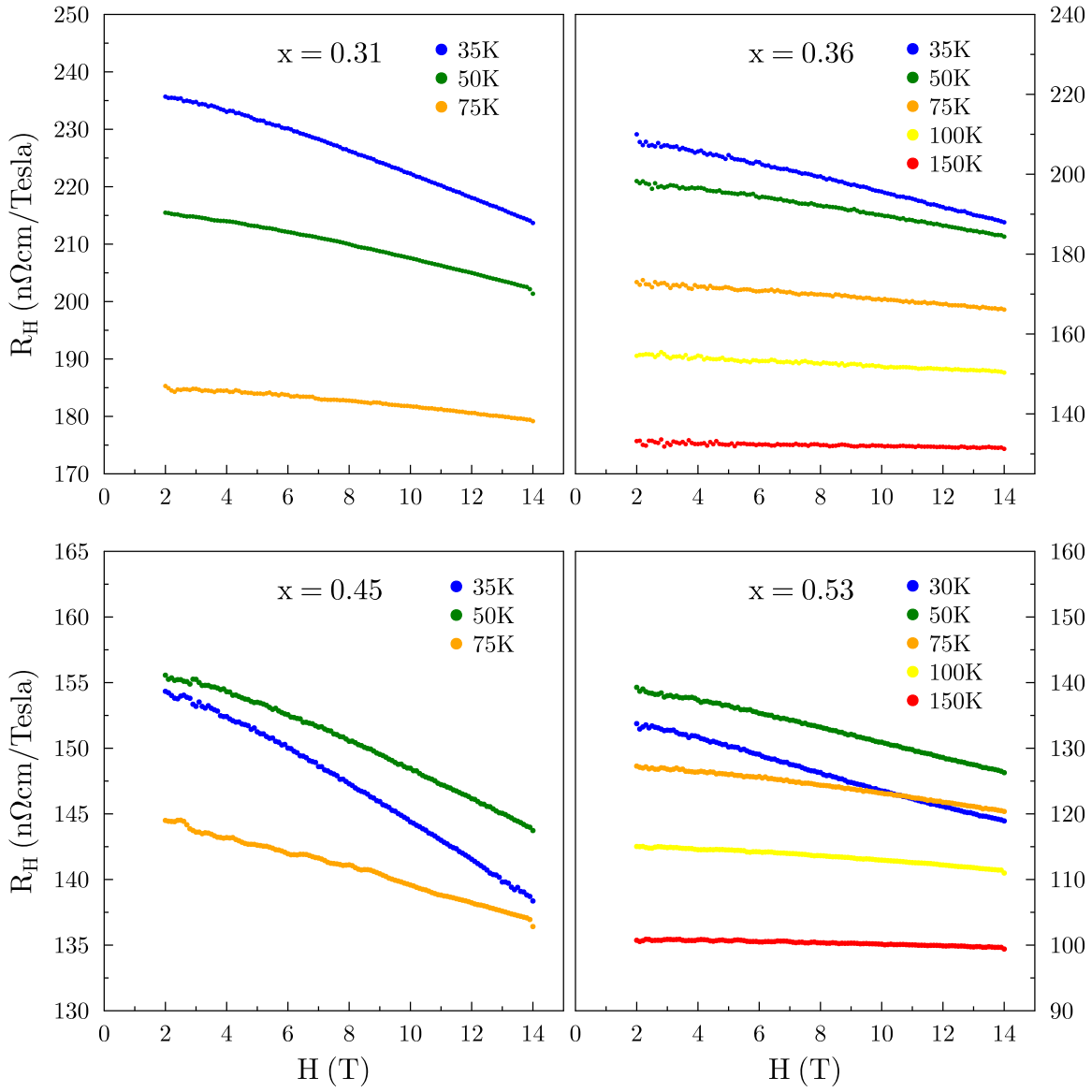

Figure 7.8: **The low-field Hall coefficient in $BaFe_2(As_{1-x}P_x)_2$ near optimal doping.** Low field R_H data on samples AG7545s20, AG263s13, AG1280s6, and AG1213s7, which have compositions $x = 0.31$, $x = 0.36$, $x = 0.45$, and $x = 0.53$.

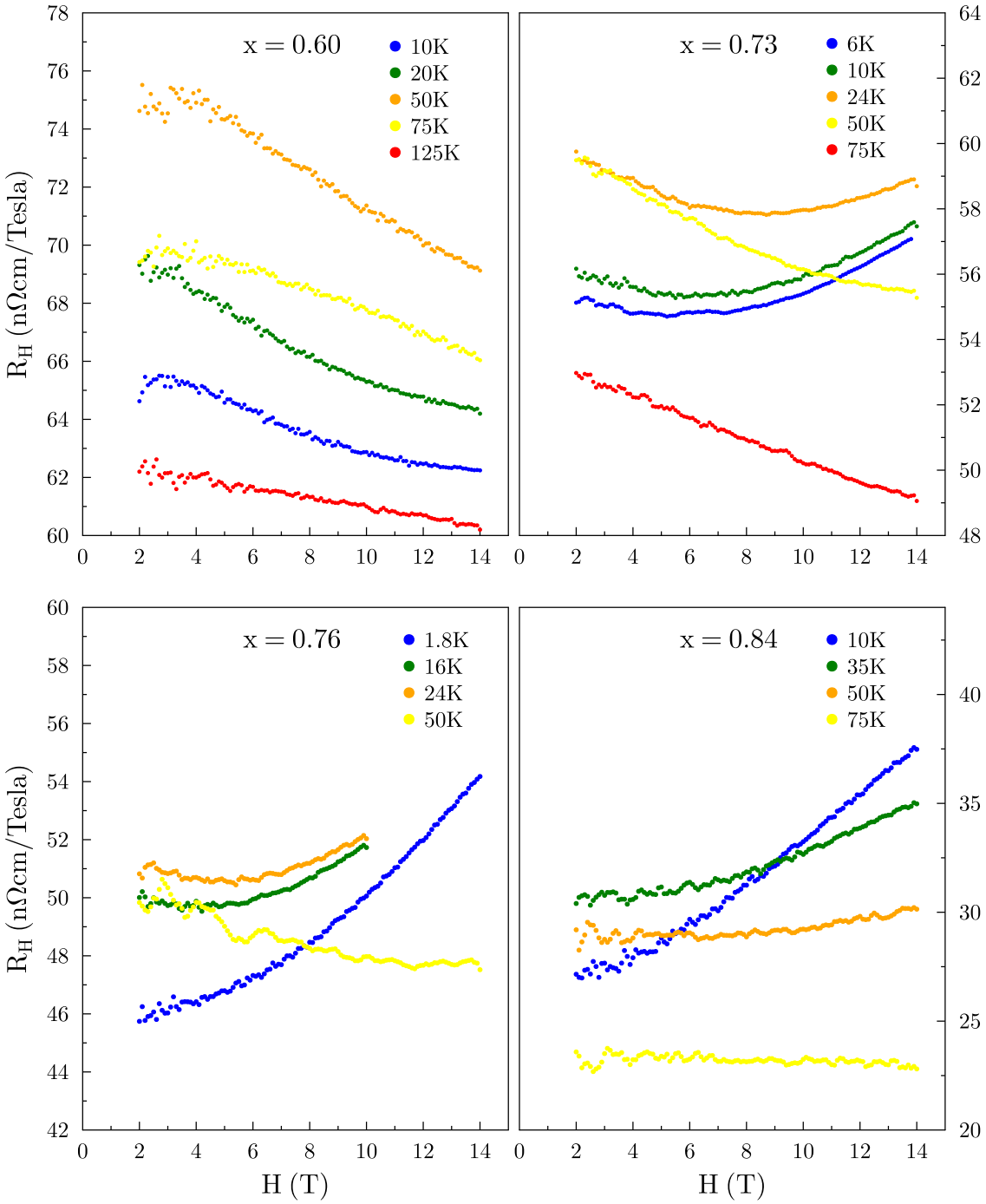

Figure 7.9: **The low-field Hall coefficient in $BaFe_2(As_{1-x}P_x)_2$ in the far overdoped regime.** Low field R_H data on samples AG1409s8, AG1802s3, AG1738s1, and AG2001s1, which have compositions $x = 0.60$, $x = 0.73$, $x = 0.76$, and $x = 0.84$.

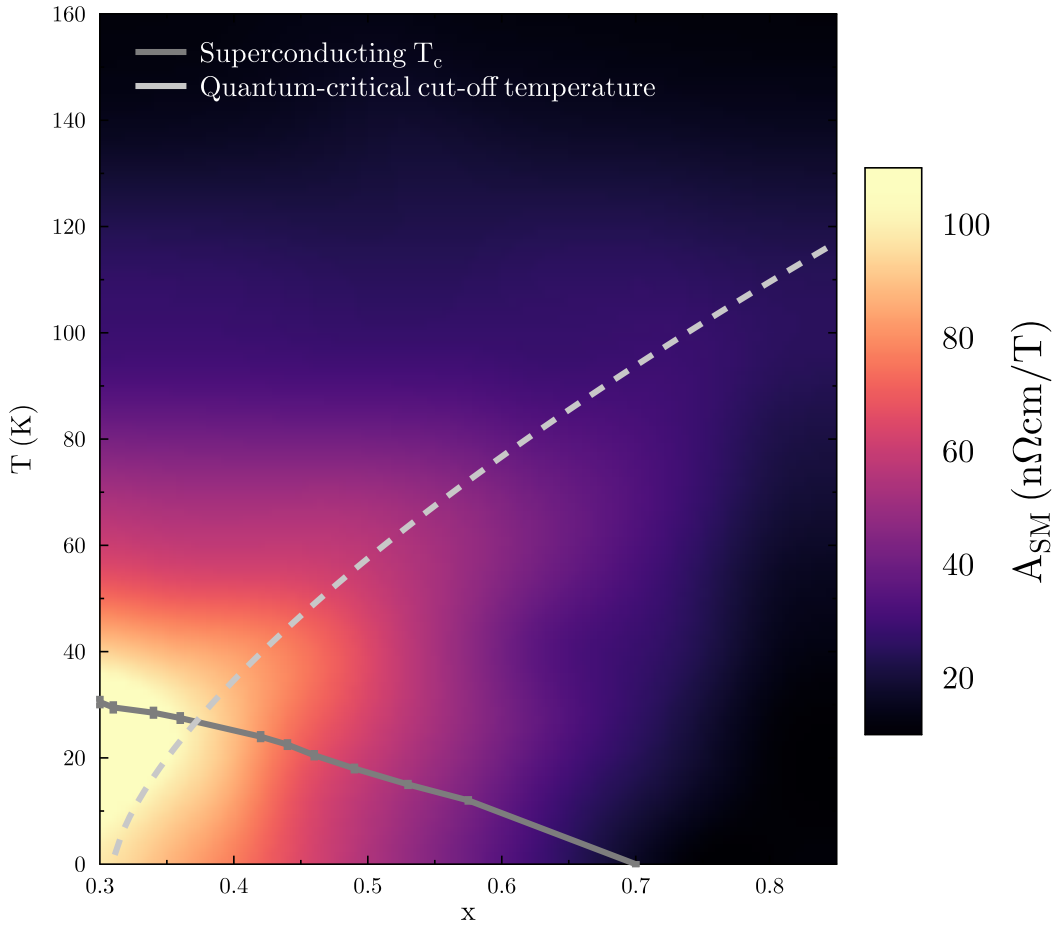

Figure 7.10: **The anomalous enhancement in R_H across the $x-T$ phase diagram.** An intensity plot of the strange metal component of R_H at zero field using the data shown in Figures 7.4, 7.8 and 7.9 and using the analysis techniques described in section 7.4.

The data used in this section were taken from a large set of samples with doping levels that span the antiferromagnetic/orthorhombic endpoint and the far overdoped, non-superconducting regime. They cover temperatures ranging from two to three hundred kelvin and fields from zero to sixty tesla. Using the relevant analysis technique for the particular region of field space that was available results in the set of values given in Table 7.1 for the size of the strange metal R_H in zero field. Figures 7.8 and 7.9 shows the raw data for most of these points in phase space. The built-in fitting function of the graphics software QGLE (quantitative graphics layout engine, available at http://glx.sourceforge.net) was used to produce the color plot shown in figure 7.10.

There are two striking features of figure 7.10. The first is that region of the phase diagram in which superconductivity exists perfectly matches the region in which there is a nonzero

Table 7.1: Samples used for the intensity plot of Figure 7.10

Sample			$A_{SM}(n\Omega cm/T)$							
Name	Doping	T_c	4K	25K	35K	50K	75K	100K	125K	150K
AG754s20	x = 0.31	29.25 K		119.6	107.3	68.8	47.2	23.6	18	7
AG263s12	x = 0.36	27.50 K	78	91.9	108.3	69.5	47.5			7.5
AG1280s6	x = 0.45	21.50 K	35	55.1	62.6	65.6	45	22.6	17	
AG1213s7	x = 0.53	16.00 K		30.0	41.3	46.7	45.0	23.0	15.5	10.7
AG1409s8	x = 0.60	8.50 K	8.3	15.7	20.1	29.5	36.0	20.4	17.4	8.6
AG1803s2	x = 0.73	1.00 K	4.8	16.2	17.2	18.6	24.6	21.5	17.0	8.5
AG1738s1	x = 0.76	0.00 K	0.0	8.8	13.8	15.8				
AG2001s1	x = 0.84	0.00 K	0.0	0.0	0.0	3	10	15.5	7.5	

strange metal signal at zero temperature. A number of studies have found correlations between strength of $T-$linear resistivity and T_c(see section 1.2 above for more details).[1, 37] However, to the author's knowledge no similar result exists for the Hall coefficient. Furthermore, most of the studies on the resistivity so not show an actual disappearance of an anomalous feature at the the edge of the superconducting dome. Rather, they identify a trend over part of the superconducting region that extrapolates to zero at the edge of the dome. This creates a novel and surprisingly direct link between strange metal physics and superconductivity.

This correlation is not an artifact of the fitting procedure and can be seen clearly in the raw data. Figure 7.11 shows data on samples just to either side of the edge of the superconducting dome at ~ 0.75. For the samples on the non-superconducting side, the lowest temperatures show a purely $\sim H^2$ field dependence (see Figures 7.11 and 7.9). This is the natural expectation from multiband physics, as described above. By contrast, the superconducting sample clearly has a very slightly derivative of R_H in field.

In addition to its striking behavior at low temperature, the strange metal behavior in R_H shows a familiar pattern at high temperatures. Directly above optimal doping we see that the strange metal enhancement is constant as a function of doping. Traveling towards the overdoped side, the strange metal enhancement eventually drops off at a cut-off doping which moves to higher values of x as the temperature is increased. The result is the fan-like shape that is expected on general grounds to appear near a quantum critical point (see section 2.4). This is a pleasing result as there had not previously been any quantity in a high$-T_c$ superconductor that showed a clear fan-like behavior on the overdoped side. This phenomenon can also be seen clearly in the raw data. Figure 7.12 shows the field-dependent part of the Hall coefficient at high temperatures for samples ranging from $x = 0.31$ to $x = 0.60$. By plotting the data in this way it is obvious that at high temperatures the samples all show the same decrease in R_H for the same applied field. Since the zero field value of R_H changes considerably across this doping range, the best account of these data

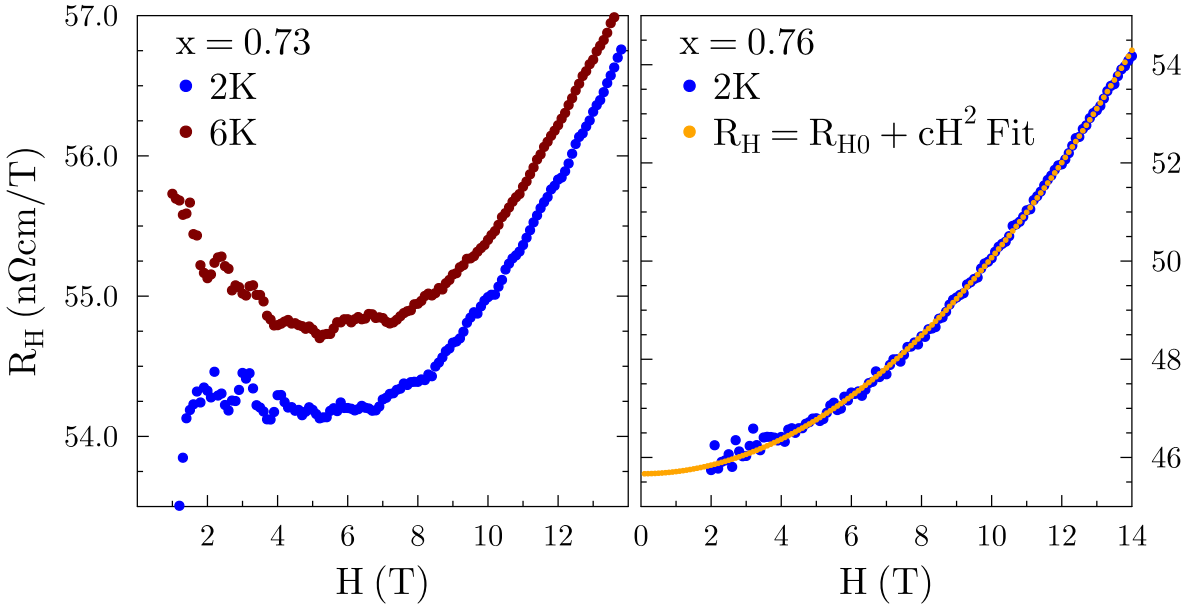

Figure 7.11: **The strange metal R_H and superconductivity in $BaFe_2(As_{1-x}P_x)_2$.** The low-field, low-temperature R_H curves for two dopings, on either side of the superconducting endpoint. The Hall coefficient is readily seen to decrease with field only for the superconducting sample. The first non-superconducting sample shows pure $\sim H^2$ behavior, which is exactly the prediction for a compensated metal at low fields (see equation 7.2).

is that there are two terms in the signal that add together: one that includes the strange metal field dependence and that doesn't change in magnitude across the phase diagram, and another which is set by the band structure. Any estimation of the size of the strange metal term will give the same value for all of these samples, since their field dependence is identical at these high temperatures.

At seventy-five kelvin, the most overdoped sample shows a weaker field dependence, while those close to optimal doping still have the same field dependence. As the temperature is lowered, this trend continues, with the region of strongest field dependence narrowing to just a few percent phosphorous by fifty kelvin. This is at once a remarkable confirmation of the relevance of critical physics, and a challenge to the conventional critical picture. The expectation for a critical metal is that as long as the system is at a temperature above the cut-off scale, observable quantities should be *dominated* by the critical physics. In the present case, the quantity that is universal above the cut-off is an addition to a background R_H, which seems to be present at all fields, dopings, and temperatures, and is well captured by the band structure of the system. The simple coexistence of two kinds of physics in the Hall channel is quite difficult to account for in any picture, and does seem to undermine the simplest picture of quantum criticality wherein fluctuations dominate the electronic dynamics

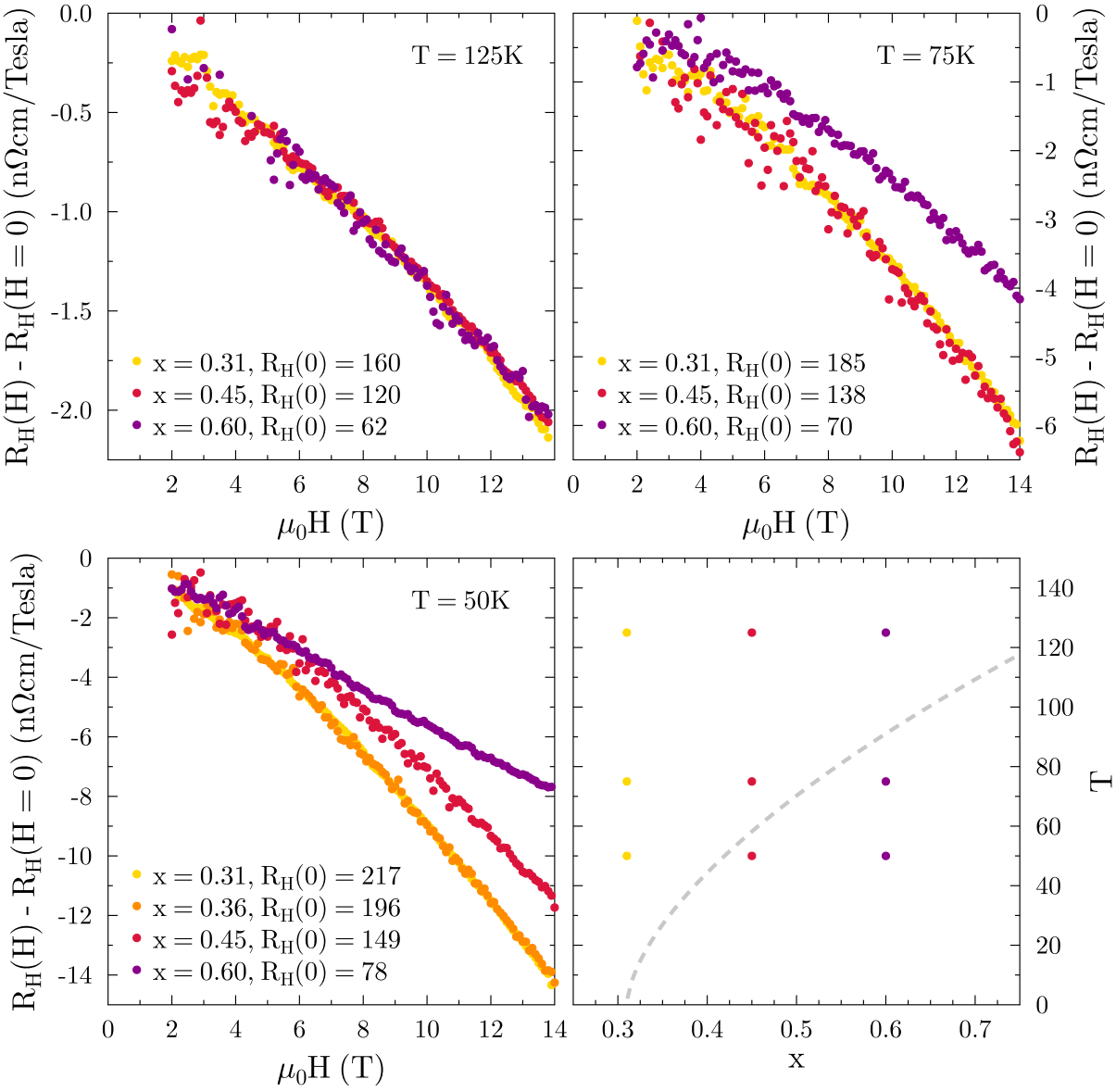

Figure 7.12: **Doping independent region of the anomalous R_H.** The low-field R_H curves for several dopings, illustrating the uniform temperature dependence of the strange metal R_H within the fan-like region that emanates from the putative critical point.

in the critical region, and quasiparticles are either irrelevant or gone. Nonetheless, it seems that there is feature of the dynamics that arises outside the simple quasiparticle picture, is universal within that fan region, and is clearly connected to the superconductivity in these materials.

It is especially interesting that these two observations are connected. In a naïve understanding of quantum criticality, the critical physics should only dominate within the fan-like region. On the disordered side, the effects of fluctuations should gradually diminish as the temperature is lowered, leading eventually to a ground state that only exhibits the physics of the disordered phase. However, zero-point fluctuations are expected in all quantum systems, and it is perhaps natural that near a critical point these would include fluctuations into the nearby ordered state. This paints a very different picture of how these fluctuations lead to superconductivity, as it is exclusively that part of the fluctuation spectrum that is protected by the uncertainty principle that contributes to the pairing interaction. This observation would not have been possible without a way to observe strange metal behavior separately at each temperature.

Finally, it is worth making some quantitative comments about the behavior of the strange metal R_H across the phase diagram. As I emphasized above, the methods developed in section 7.4 allow us to estimate the size of the amplitude and field scale of the anomalous enhancement in R_H, not to extract solid parameters in some well-defined model. Even including error bars is not quite theoretically sound, as there is no specific model parameter that is being extracted. Therefore, any quantitative relationship that is derived from them should be seen as suggestive and not definitive. Still, it is possible to make some meaningful statements about the existence or not of power laws.

Although the analysis described above is mostly aimed at extracting the zero-field "enhancement" in R_H, the intrinsic field scale (H_0 in Eq. 7.4) associated with this enhancement also shows interesting patterns across the phase diagram. First, it grows more or less directly with the temperature ($H_0 \sim T$). It is unlikely that this behavior continues down to zero temperature, as that would lead to a delta-function behavior at zero kelvin, while the actual data show R_H continues to decrease with increasing field as far out as sixty tesla. Nonetheless, the limiting high-temperature behavior of $H_0 \sim T$ is a potentially significant clue about the nature of the physics that leads to this enhancement. As we will see in the next chapter, this fact is what allows the field-dependent R_H to be scaled as a function of H/T at high temperatures.

This field-temperature equivalence only holds within the fan, however. As the doping is increased at a constant temperature within the fan, the value of H_0 remains constant. This should be clear from the fact that the field-dependence of R_H is identical for samples in that window (see Figure 7.12). As one crosses outside of the fan, the value of H_0 falls, as can be seen readily in Figure 7.12 panel (C). The most overdoped sample crosses over to the exponential regime sooner than the others because its intrinsic field scale has gotten smaller. Thus, nearly the entire strange metal component has vanished by fourteen tesla. Relatedly, as the temperature is decreased outside of the fan, the intrinsic field scale decreases more rapidly than it would within the fan. This is how one can obtain the difference in H_0 visible

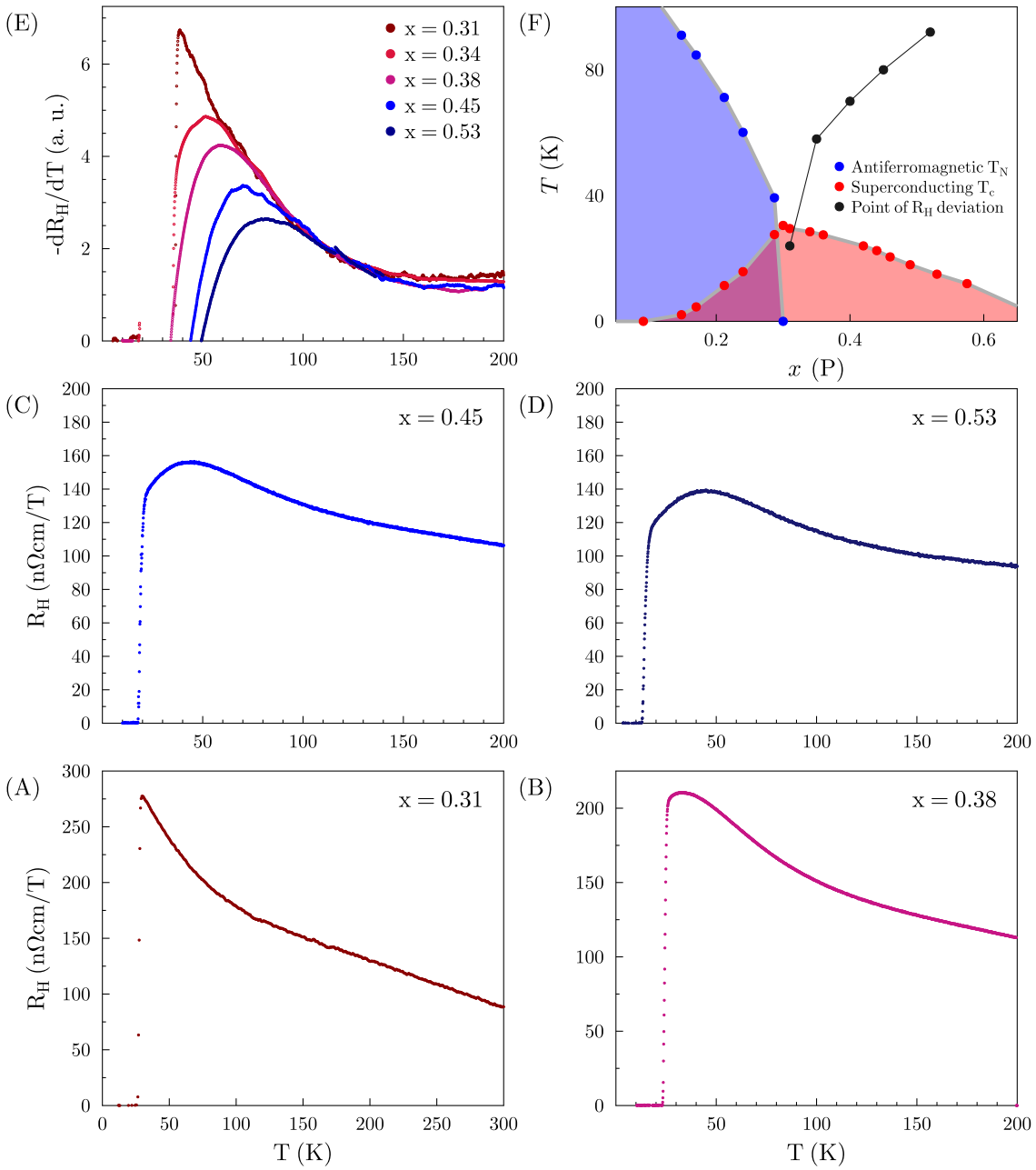

Figure 7.13: **The Hall coefficient versus temperature across the phase diagram of $BaFe_2(As_{1-x}P_x)_2$.** Panels (A) - (D) are taken from samples that have phosphorous concentrations $x = 0.31, 0.40, 0.45, 0.53$. The strange metal enhancement sets in below $150K$ in all samples, but ceases growing at higher temperatures as one moves to the overdoped side. This can be seen clearly by comparing the derivatives off all of these curves, which is done in panel (E). The fact that the curves are the same at higher temperatures is captured in the fan shape of the plot in Figure 7.10

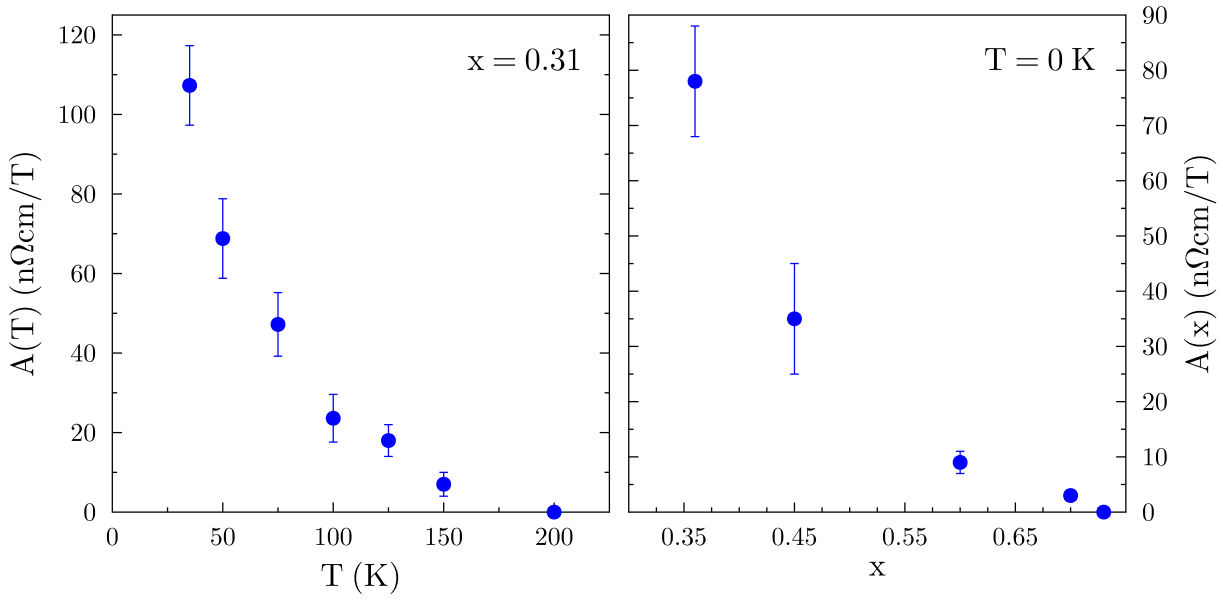

Figure 7.14: **The strange metal enhancement as a function of x and T.** Panel (A) shows the A coefficient at optimal doping as a function of temperature. Panel (B) shows the zero temperature anomalous term as a function of doping. Both curves a jump quickly to zero at their upper limits.

in figure 7.12 panel (C), while maintaining an equivalent field scale within the fan. In the limit of zero temperature, it should be readily apparent from Figure 7.4 that the field scale as well as the overall enhancement is decreasing continuously across the phase diagram.

Finally, the quantitative shape of the strange metal amplitude (A in equation 7.4) as a function of temperature does not fit any simple functional form. It is plotted in panel (A) of Figure 7.14 as a function of temperature for the optimally doped sample (so that no critical cut-off is present). Panel (B) shows the value of the strange metal amplitude as a function of x at zero temperature. No simple functional form could be found for either. In particular, $A(T)$ does not go as $\sim 1/T$ for the whole temperature range. This can be seen rather easily by noting that its value at two hundred kelvin is nearly zero, much less than half of what it is at one hundred kelvin. This is consistent with the findings in the cuprates, for example, in reference [53], where no simple functional form could be found for the temperature dependence of R_H. The absence of power law behavior may well create challenges for critical theories of the strange metal state, since criticality implies that observables should follow scale-invariant functions. Also notable is the fact that $A(x)$ does not simply follow T_c. Instead, there is a strong enhancement going towards optimal doping that is much stronger than the increase in the superconducting transition temperature. The author feels, however, that these results should be held at a slight discount, at least until

some convincing functional form is found for the field dependence of R_H that would allow a more robust determination of the size of the strange metal term in zero field.

7.6 Comparison with the Hall effect in the cuprates

Before moving on to an extended discussion of the implications of these observations, it is useful to review the known phenomenology of the Hall coefficient in other high$-T_c$ superconductors. My review of literature in chapter 1 did not cover the Hall phenomenology in the cuprates and quantum critical metals for reasons of space, but the anomalous temperature dependence in R_H is also an important part of the strange metal phenomenology in those compounds. Historically, discussions of the temperature dependence of R_H have played a major role in identifying the cuprates as "strange metals".[22, 4, 7] This comparison seems especially urgent given the close connection that exists in $BaFe_2(As_{1-x}P_x)_2$ between the Hall enhancement in the ground state and superconductivity.

First, I will summarize what we have seen in $BaFe_2(As_{1-x}P_x)_2$. There is a strong enhancement in R_H that grows strongly on approach to zero temperature at optimal doping, but gets cut off at successively higher temperatures as one moves to the overdoped side. This enhancement can be suppressed by the application of a magnetic field in much the same way that it is suppressed by increasing temperature, providing a striking parallel between field and temperature and supporting the observations we made about the field dependence of ρ_{xx}. Overall, the picture seems consistent with a quantum critical scenario similar to that that has been proposed for the cuprates, albeit one in which quasiparticles survive and play an important role in setting the value of the Hall coefficient.

The existence of qualitative similarities between the Hall effect in $BaFe_2(As_{1-x}P_x)_2$ and in cuprates was identified in some of the earliest papers on this compound.[58] Other doped versions of $BaFe_2As_2$ show qualitatively similar behavior in their Hall coefficients as a function of temperature, including a peak in R_H that moves as a function of doping.[59, 99, 87, 86] However, none of these studies extracts a truly systematic trend on the overdoped side of the phase diagram. Also, the distinctive patterns in the field dependence have not previously been reported, thanks in large part to the absence of any data above about fourteen tesla. Thus, the literature is consistent with the idea that the patterns uncovered here represent the universal behavior of the iron-based superconductors, but the existing data are not sufficient to demonstrate this.

Turning now to the cuprates, the strong temperature dependence of the Hall coefficient was noticed almost immediately after the cuprates were discovered.[22] From the beginning, the anomaly was usually discussed in the following way. The conductivity is proportional to the average lifetime of the quasiparticles, or, equivalently, the average timescale for momentum relaxation. The Hall conductivity goes as the square of that lifetime (as explained in section 7.3). Thus, there are two ways to extract the lifetime from the charge transport coefficients: σ_{xx} and $\sigma_{xy}/\sigma_{xx} \approx \rho_{xy}/\rho_{xx}$. This latter quantity is usually called the cotangent of the Hall angle because it represents the ratio of the voltages parallel and transverse to the

current, i.e. the cotangent of the angle between the actual electric field in the sample and the current. In an ordinary metal these two quantities are the same up to a constant, but in the cuprates they have different temperature dependencies. This way of viewing the problem was motivated by the observation that the cotangent of the Hall angle actually displays something very close to a strict $\sim T^2$ dependence in a number of compounds, and this might be reflecting another well-defined lifetime in the system.[22, 9] This lead to many discussions of "two lifetimes" models, were the Hall conductivity and longitudinal conductivity are set by different physics. The most prominent of these was Anderson's model where the the two relaxation times operated parallel and perpendicular to the Fermi surface, leading to the so-called 2D Luttinger liquid.[4, 30]

Of course, since the resistivity is roughly linear in temperature, this $\sim T^2$ behavior in the cotangent of the Hall angle implies a roughly $\sim 1/T$ dependence for the Hall effect, qualitatively similar to what we see in $BaFe_2(As_{1-x}P_x)_2$. However, it should be noted that neither the $\sim T^2$ behavior in the cotangent of the Hall angle or the $\sim 1/T$ behavior in R_H is obeyed over a very wide range of compounds or dopings. In the bismuth-based compounds, the T^2 power law is never really present, and in far overdoped samples of most cuprates a $T-$dependent R_H is observed only at low enough temperatures, violating the $\sim 1/T$ Hall coefficient and the $\sim T^2$ Hall angle. And then there is the very high temperature regime where R_H is flat and returns to its band value.[9, 49, 53]

All of these features reappear in $BaFe_2(As_{1-x}P_x)_2$, and here the cotangent of the Hall angle only goes as $\sim T^2$ for reasonably low temperatures near optimal doping (see Figure 7.15). The observation that the strange metal behavior arises from a second term in an otherwise normal Hall coefficient makes sense of the fact that the power law behavior in the Hall angle does not hold universally. After all, the cotangent of the Hall angle utilizes the whole ρ_{xy}, including whatever band component is present. However, there is one notable discrepancy between the Hall phenomenology in the cuprates and the data presented here. While the strange metal R_H in $BaFe_2(As_{1-x}P_x)_2$ is uniform at high temperatures, the R_H enhancement in the hole-doped cuprates clearly gets smaller as one moves to the overdoped side of the phase diagram. There appear to be two effects at play here: a reduction in the overall size of the enhancement, and a lowering of the temperature scale below which it sets in. The strange metal enhancement above the band value can be collapsed for different doping values if they are scaled to the band value (evaluated at high temperatures where R_H is constant) and scaled along the $T-$axis.[53] The key to understanding this difference between $BaFe_2(As_{1-x}P_x)_2$ and the hole-doped cuprates likely lies in the fact that the $x-$axis in the cuprate phase diagram represents an actual doping value. That is, doping in the cuprates actually changes the net carrier concentration. In contrast, the phosphorous-for-arsenic substitution that defines the $x-$axis of the phase diagram for $BaFe_2(As_{1-x}P_x)_2$ is isovalent. Although the sizes of the different Fermi surfaces change considerably across the phase diagram, the net number of electrons and holes $(n_e - n_h)$ does not.[121] In light of this, it seems reasonable to identify the "natural" quantum critical phenomenology that appears in $BaFe_2(As_{1-x}P_x)_2$ as a special case for transitions that do not change the net carrier concentration. Having identified one system to which the naïve picture applies, it should

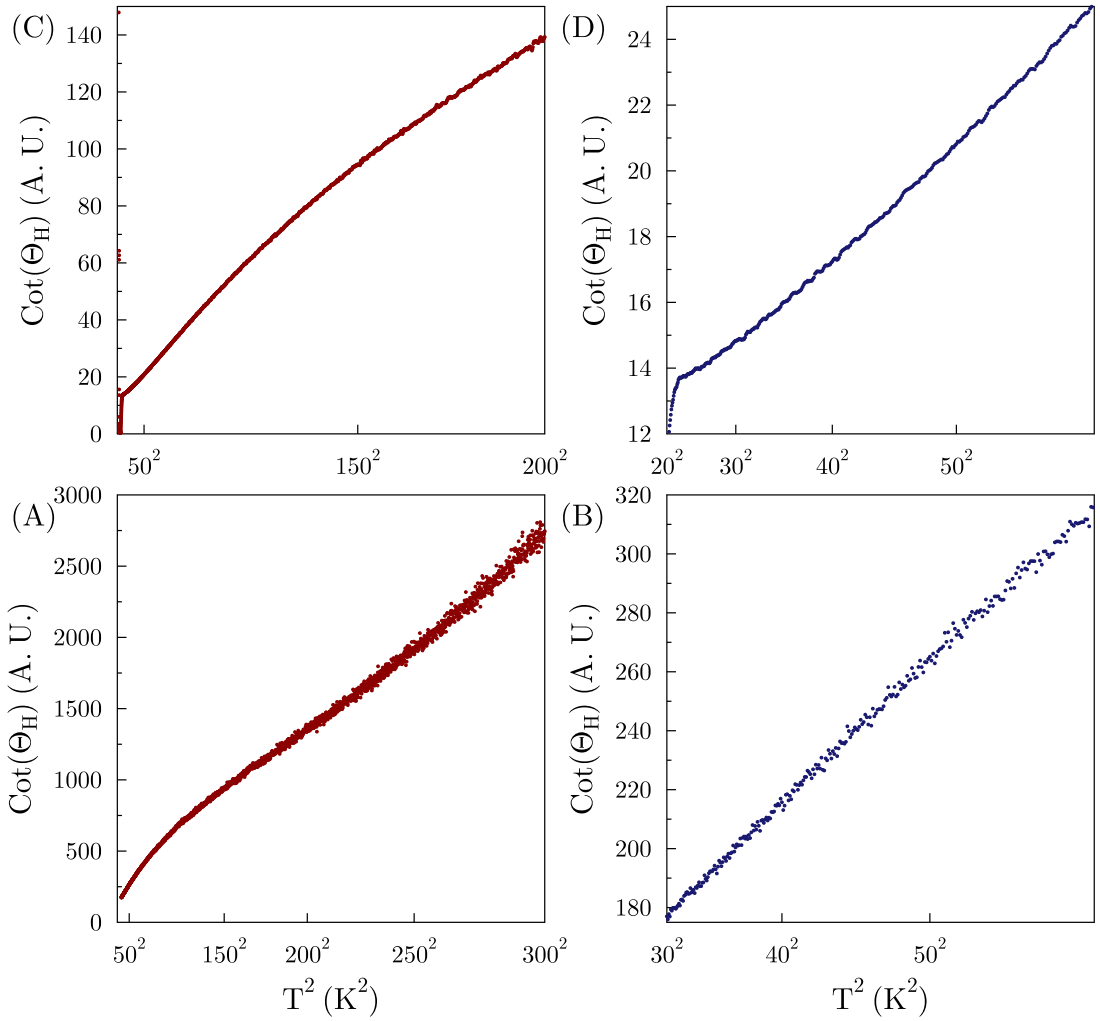

Figure 7.15: **The cotangent of the Hall angle near optimal doping in** $BaFe_2(As_{1-x}P_x)_2$ Panels (A) and (B) are taken from sample AG754s22, with $x = 0.31$, and panels (C) and (D) are taken from an overdoped sample with $T_c = 18K$, $x = 0.49$. The cotangent of the Hall angle $\equiv \rho_{xx}H/\rho_{xy}$, is plotted versus the square of the temperature. At low temperatures near optimal doping, $Cot(\Theta_H)$ follows a very nearly $\sim T^2$ form, similar to what is seen in the cuprates. However, this behavior does not persist even for the whole temperature range is which the strange metal Hall coefficient appears. Additionally, on the overdoped side it is not strictly T^2 even at low temperature. This is recognizable as a consequence of the downturn in R_H at low temperature, which breaks the $\sim 1/T$ form that makes up this phenomenology.

now be possible to back out the way in which the changing carrier number is modifying the critical dynamics in the cuprates. Unfortunately, such an effort is beyond the scope of this project.

Separating the strange metal contribution from a background band contribution also helps to make sense of what is seen in the electron-doped cuprates. In those systems there is also a strongly $T-$dependent R_H, but it does not appear strictly as a enhancement. Instead, R_H goes from small and positive at high temperatures, to large and negative at intermediate temperatures, and finally back to small and positive at low temperatures.[34] This looks much more like a second term of opposite sign that is being added to the band R_H than a multiplicative enhancement, which should maintain the sign of Hall coefficient. Also, the overall shape of the $R_H(T)$ curve is naturally consistent with the cut-off phenomenology being discussed here, where the additional term grows until some internal energy scale is crossed, and then is suppressed on approach to zero temperature. Although I have never seen a quantitative analysis of the data to support this, the cut-off scale does appear to move to higher temperatures on the overdoped side.[34]

Finally, it should be mentioned that strong variations in R_H as a function of temperature is a common feature of heavy fermion systems that are thought to be near a critical point.[110] In many cases, such as that of $CeCoIn_5$, the strongly $T-$dependent feature can be suppressed by applying a magnetic field.[83] This provides more evidence that the physics of criticality is in play in the high$-T_c$ materials. However, like the iron-pnictides, the heavy fermion systems often have many bands, and so separating out anomalous from conventional behavior is nontrivial. The author is not aware of any heavy fermion systems that are compensated metals, like $BaFe_2(As_{1-x}P_x)_2$, but the present results motivate a search for one.

7.7 Conclusion

Although there is a wide variety of experiments that show the relevance of some aspects of quantum critical physics (an enhancement of the effective mass, for instance) to the high$-T_c$ superconductors, one element of the conventional quantum critical picture has always been missing: a clear observation of a "cut-off" temperature that moves up and to the right from the putative critical point. One reasonable explanation for this is that it is very difficult to isolate the "critical component" of the resistivity at different temperatures. The best one can do in analyzing the temperature dependence of the resistivity is to use something like a logarithmic derivative to identify the local power law in T. However, it is far from obvious that the degree of critical behavior is measured by the nearness of this exponent from one. The phase diagrams obtained in this way usually show something more like a column of critical behavior with an extended region at low temperatures and an extreme slope at high temperatures on the overdoped side.[31, 58] Ultimately, it seems that the resistivity is simply too complicated of an object to reveal a sharp quantum critical phenomenology, except perhaps right at the critical point where the physics of criticality should dominate entirely.

By allowing us to clearly identify strange metal physics separately at various temperatures, the field dependence of R_H allows us to finally reveal this cut-off line. The existence of a clear fan that terminates at the zero temperature end point of the antiferromagnetic/orthorhombic transition provides much stronger evidence that the physics of quantum criticality is the basis of these common transport anomalies. Even if the exact phenomenology is not reproduced in the cuprates (as discussed in section 7.6), the existence of even one example system that shows the expected behavior will allow future researchers to probe the adequacy of the standard picture in a clear way.

As mentioned earlier, understanding criticality in metals is difficult because there is always a large energy scale in the system that should strongly influence the transport, namely the degeneracy pressure of the electrons (see chapter 2). Although many specific models of critical metals have been studied, our ability to make compelling general arguments about these systems has been limited. Against this background, the observation that the effect of the critical fluctuations in $BaFe_2(As_{1-x}P_x)_2$ is to simply add a second term to R_H is an unexpected and useful result. It is worth expanding on this fact in detail here. Since the size of the Hall coefficient expected from the band structure evolves across the phase diagram while the strange metal enhancement is fixed in magnitude, the critical fluctuations cannot be influencing R_H just by modifying the quasiparticle properties. In that case, the strange metal term would be modulated by the changes in the band structure and should change in magnitude across the phase diagram. In this respect the multiband nature of $BaFe_2(As_{1-x}P_x)_2$ is quite useful: by producing an change in the band structure R_H with doping that does not simply follow the change in net carrier number, it allows us to see that the strange metal effects in R_H decouple from the band structure effects. This casts doubt on approaches to the strange metal state that only make use of changes in the quasiparticle lifetime around the Fermi surface, changes in the effective carrier number with temperature, or other changes to the band structure.[47, 51] However, it also a poses a challenge for some approaches based on magnetic fluctuations. Standard treatments of antiferromagnetic fluctuations usually lead to anomalous prefactors in R_H, but not to a second term.[64] Indeed, it is very hard to imagine how to get a second term in to the Hall coefficient, as both strange metal dynamics and the band structure would have to see the entire current exciting the sample. It could not be, for example, that the fluctuations provide a second conduction channel in parallel to the ordinary quasiparticles, because the amount of current passing through that channel should depend on its conductivity relative to the conductivity of the quasiparticles, and the later changes considerably across the phase diagram. Thus, the observation of a uniform enhancement on R_H above the cut-off line provides a very specific and unexpected clue about how critical fluctuations actually manifest in metals near a quantum critical point.

Unveiling the temperature dependence of the strange metal physics also provides a very tight connection between criticality and superconductivity, and a clue about how they may be related physically. It opens up a variety of avenues for further study of the essential physics of high$-T_c$ superconductivity by observing the response of the field dependence in R_H to various perturbations, such as strain or increased pressure, that are reasonably

straightforward to model. A careful look the phase diagram of Figure 7.10 already holds an important theoretical clue: superconductivity appears exactly when the critical fluctuations are sustained by zero-point fluctuations alone. Whatever the threshold is for pairing in these materials, it is also the threshold for the existence of a strange metal term in the ground state of the Hall coefficient, but *not* the threshold for the appearance of a strange metal R_H at non-zero temperature. Importantly, the perfect correlation that seems to exist between strange metal or critical physics in the ground state and superconductivity implies that the critical physics is a sufficient as well as necessary cause of superconductivity in this system. A successful theory of high$-T_c$ superconductivity, then, should include some explanation for why fluctuations of the ordered phase do not get arbitrarily small on approach to zero energy. The results presented in this chapter should be a major stimulant for the field.

Chapter 8

Thickness Dependence in the Hall Resistivity of $BaFe_2(As_{1-x}P_x)_2$

8.1 Introduction

This chapter will present a serendipitous discovery that occurred during the course of the Hall effect measurements performed for chapter 7: that the strange metal behavior in the Hall coefficient is sensitive to length scales as long as $\sim 4\mu m$. Specifically, if a Hall device is thinner than this, the anomalous enhancement in R_H is larger than it would be in a macroscopic sample. This is an unusually large length scale to be relevant in a bad metal. The existence of such a long-range effect is intriguing because it is suggestive of the very long wavelengths that are expected to become relevant near criticality. Many measurements need to be done to flesh out the details of this effect, so I will not argue for a definitive interpretation here. However, even without knowing the physical origin of this effect, we can draw several important conclusions from its existence. First, since this effect is only seen bellow about one hundred and fifty kelvin, where the strange metal effect sets in, we can say that in this region the Hall effect is definitely influenced by some physics beyond just band structure. Second, based on the field dependence of R_H in this region, we can show that it is not the entire Hall coefficient that is seeing this extra enhancement, thereby demonstrating R_H must decompose into at least two terms. This result was strongly suspected on the basis of the data presented in chapter 7, but the data below make the conclusion truly solid. Finally, thinner samples simply provide much larger signals and therefore cleaner data in pulsed fields. This allows more a clearer look at the field dependence of R_H up to sixty-five tesla, which will support the general conclusion that critical physics is at play in the strange metal regime of $BaFe_2(As_{1-x}P_x)_2$. Much more work remains to be done on this subject, which promises to provide a valuable new avenue for manipulating critical behavior.

8.2 The Hall coefficient in ultra-thin $BaFe_2(As_{1-x}P_x)_2$

Details of the process by which Hall samples were made for this project were given in section 4.4. To review very briefly, the key steps for making very thin samples were gluing a very flat crystal down such that it could still be cleaved from the side, and then peeling the top layers off with a scalpel. By this process, dimensions as small as small as $\sim 500nm$ could be achieved. The original motivation for making these very thin samples was not to search for effects of the finite size on the transport properties–that would have seemed all but impossible prior to these measurements. It was to improve signal-to-noise in the pulsed field measurements of R_H. In this respect these efforts succeeded dramatically. Figure 8.3 shows some high field data for a device who's thickness is roughly $400nm$. Clearly these data compare favorably to those from the macroscopic sample presented in chapter 7.

However, this triumph was tempered by a lack of consistency between these thinner samples and the original ones. Measurements of R_H at high and low temperatures did not yield a consistent thickness for the thinner sample. In other words, the curve of R_{xy} versus temperature for the two samples were not simply proportional to each other, so no single value of the thickness could explain the size of the signal. This means that the thinning of the sample must be affecting the Hall resistance in some way other than the usual geometric effect whereby $R_{xy} \propto 1/d$, where d is the thickness of the sample. To be able to identify which part of the $R_H(T)$ curve is being tuned by the thinning, we need to be able to evaluate the absolute value of R_H and therefore we need to know the thickness of these very thin samples. This was accomplished by confocal microscopy, which is a very efficient way for measuring depth at the micron scale. This process uses a pinhole filter to restrict an image to light that is in-focus, and therefore was reflected at a set distance from the objective. This allows for very fine spatial resolution in the out-of-plane direction.

With the thickness of the samples in hand, we can plot their Hall signals in absolute units. The results are shown in Figure 8.1. These samples are all of the same doping (in fact they are from the same batch, AG754) and have nearly the maximum T_c for $BaFe_2(As_{1-x}P_x)_2$. From these data it is clear that the thinner samples are showing a change in R_H below around two hundred kelvin. This is the region in which the strange metal behavior in R_H turns on, strongly suggesting that it is exactly this part of the Hall signal that is responding to the very small $c-$axis dimension. Above two hundred kelvin, it is clear that R_{xy} scales directly with the thickness of the sample, even into the sub-micron regime. This is reassuring, since we had previously attributed all behavior in that temperature regime to single-particle physics, which should definitely not exhibit any sensitivity to a length scale that is hundreds of crystal unit cells long.

On the other hand, something essentially different has to be going on at lower temperatures. This is the first important conclusion that these data provide, and, usefully, it does not depend at all on the specific origin of this effect. Although the field dependence of R_H made it seem unlikely that the Hall coefficient in this temperature regime is due simply to multiband physics, and the pattern of that unusual field dependence across the phase diagram made it seem exceptionally unlikely, the fact that the Hall coefficient at these tem-

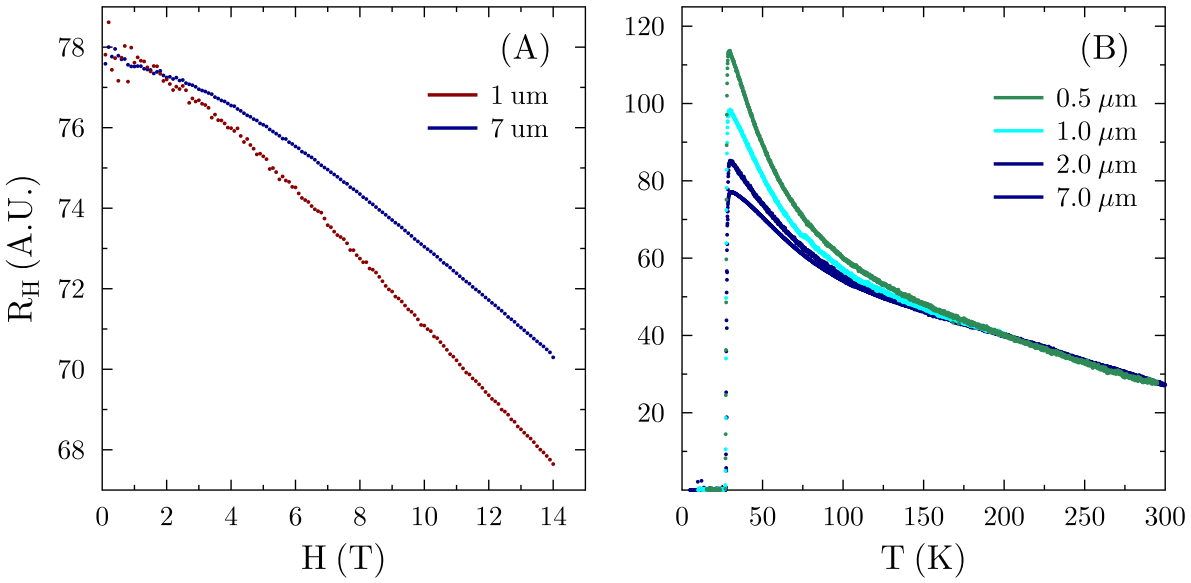

Figure 8.1: **Changes in the strange metal R_H with sample thickness** Panel (A) shows a comparison of R_H versus field for two samples of optimally-doped $BaFe_2(As_{1-x}P_x)_2$ with different thicknesses. The data have been scaled so that the zero field value of R_H is the same in the two cases. The fact that the two curves do not line up at nonzero magnetic fields demonstrates that the strange metal R_H is not the result of the entire band value of R_H being modified, but must result from the addition of a second term. Panel (B) shows low field R_H (evaluated at three tesla) for samples of different thicknesses. The thinnest samples show a marked increase in R_H in the region where strange metal behavior is manifest. At higher temperatures, R_H follows the expected geometric scaling, $R_H \propto 1/d$, where d is the thickness of the sample.

peratures can be tuned independently of the Hall coefficient at higher temperatures makes the conclusion inescapable.

By examining the field dependence at low temperatures we can verify another conclusion that was reached in the previous chapter: the the strange metal component enters the Hall signal as a second term that adds to the background multiband behavior and not as a prefactor that multiplies it. Figure 8.1 shows the field dependence of two samples in the low-thickness regime, normalized to the their zero-field values. Clearly the two curves are not the same. If the strange metal contribution were a prefactor to the single-particle R_H, then we would expect these two curves to be the same. Even thought the strange metal enhancement would be different in these two samples, we should expect it to carry the same field dependence. These curves do not show the same absolute change in R_H either.

Using the techniques described in section 7.4, we can estimate the size of the strange metal term for these two samples. The difference between the size of the strange metal amplitude

evaluated in this way neatly matches the difference between the zero field values of R_H in the two samples. In other words, it appears that the change in zero field R_H is entirely caused by the a change in the size of the strange metal term. Thus, these observations provide strong support for the idea that the Hall coefficient is composed of two terms, one of which is set by the band structure and is insensitive to the finite size of the sample, and one which is the result of strange metal physics and is entirely responsible for the negative derivative of R_H in field. Considering all the phenomena that we observed in chapter 7, there was already strong support for this interpretation. Now, however, it seems inescapable.

8.3 A closer look at the high-field R_H: scaling and cut-offs

In addition to providing clear confirmation of the fact that the strange metal behavior in R_H originates in a second term, the cleaner pulsed field data obtained on this ultra-thin sample allow us to make two other important observations, one based on the behavior above T_c and the other based on the data at low temperatures. First, the high temperature data give us the best possible chance of answering a question that naturally arises given the scaling we observed in ρ_{xx}: does R_H or R_{xy} also show scaling? This question is slightly trickier in the case of the Hall resistivity than it was for ρ_{xx} because of the presence of the background R_H. When analyzing the resistivity there was also a background that we had to subtract: the residual term at $T = H = 0$. That background subtraction was easy, however, because it was a single number that we could evaluate by using either the $T-$linear or the $H-$linear extrapolation. Furthermore, those two methods gave the same value. It was assumed that all of the field and temperature dependence was contained in the scaling term.

Simply subtracting a number from R_H is not an option in this case because the background has both a field dependence and a temperature dependence of its own. This is why we had to model the shape of the curve with equation 7.4 in chapter 7. However, the great strength of the scaling analysis done in chapter 5 was that it was model independent, and if we want to make an affirmative statement to the effect that the Hall response is scale-invariant, we need to be able to do a similar analysis. This is possible for the high temperature data because the multiband field dependence of R_H should disappear at sufficiently high temperatures. For data above about fifty kelvin, the field dependence of R_H coming from the band structure should be minimal. This can be easily checked by looking at the data on the far overdoped samples (since these have the smallest strange metal influence) in Figure 7.9

To analyze only the strange metal part, we will use only the field-dependent part of the data, $\Delta R_H \equiv R_H(H) - R_H(H = 0)$. Since we believe that only the strange metal part of the Hall coefficient carries any field dependence at these temperatures, this should restrict our analysis to the strange metal behavior without any need to evaluate the "background" Hall coefficient. The only other ingredient we need for the scaling analysis is some guess for

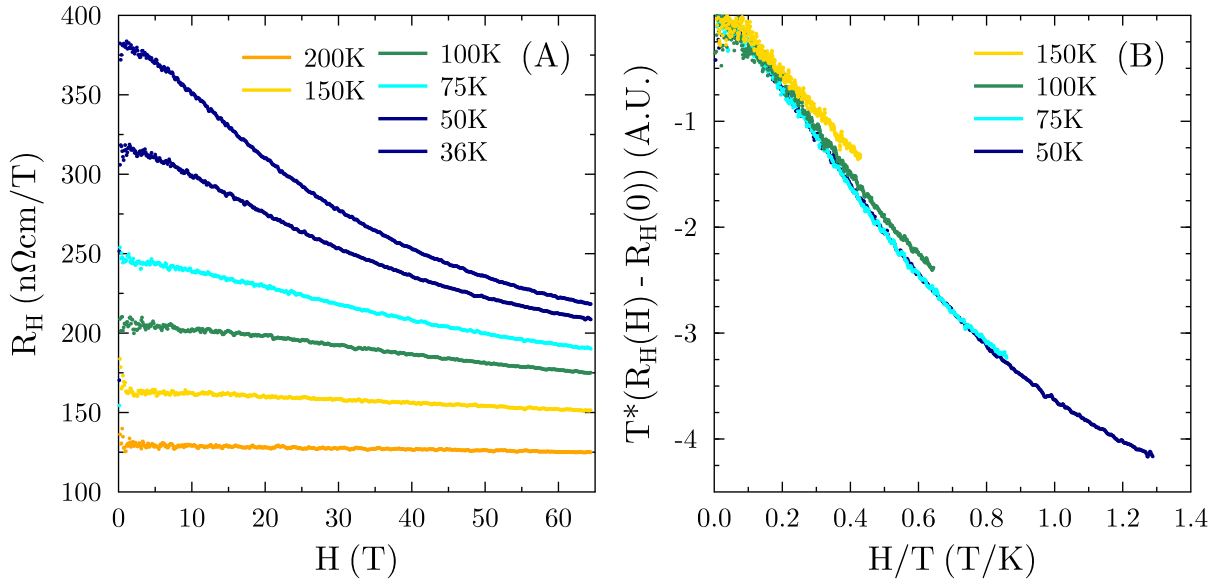

Figure 8.2: **The high field Hall effect in optimally doped $BaFe_2(As_{1-x}P_x)_2$, measured on sample AG754s14.** The field dependence is qualitatively identical to that shown in chapter 7, but exaggerated as a fraction of the total R_HB. A scaling plot of the data in panel (A), assuming a $\sim 1/T$ dependence to the strange metal Hall effect. There is good collapse bellow about 150 K, where the strange metal behavior turns on.

the power law of the $T-$dependence of the strange metal R_H. Figure 8.2 shows the raw data at high fields from sample AG754s14, along with a scaling analysis of that data. There is clearly fairly good agreement for temperature below about one hundred kelvin. However, one hundred kelvin curve clearly shows some deviations. This is consistent with our observations in chapter 7 that a $\sim 1/T$ power law could not possibly describe the strange metal term over the entire temperature range. However, it is significant that the scaling seems to be good at lower temperatures.

Ideally we would try scaling the low-temperature data as well, but the presence of a large H_{c2}—which prevents us from just using ΔR_H—and of a significant background field dependence—which would require some fitting to remove—makes this impractical. For example, schemes like taking three derivatives of the data to remove the background still result in a ton of noise, even given the amazing signal-to-noise achieved with this sample. Nonetheless, the collapse observed in Figure 8.2 strongly suggests that the strange metal behavior in the Hall channel is consistent with the conclusion, made in chapter 5, that the dynamics are scale-invariant. There could well be only one important time scale in the system, such that the size of the strange metal term is tuned exclusively through the effect of field and temperature on that one scale.

The markedly improved signal-to-noise in these high field data also allows us to examine

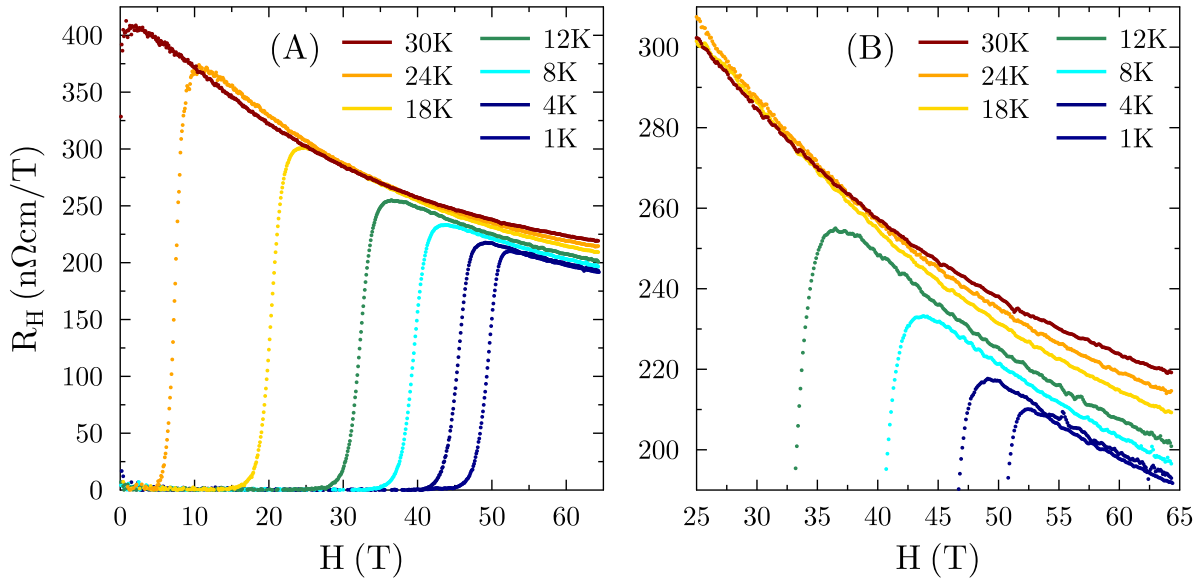

Figure 8.3: **The monotonic increase of the strange metal R_H below T_c.** The two panels show the full field range and a close-up of the very high field part. It is clear that the slope of R_H in field is monotonically increasing on approach to zero temperature.

the behavior of R_H below T_c with much greater confidence. The noise in the thicker samples is an even larger issue below T_c because there is a much more limited field range to work with as well as a much smaller change in R_H over that field window. In this data set we can see that the slope of R_H at sixty tesla grows continuously as the temperature is lowered. This is significant because we have already determined that the shape of the $R_H(H)$ curve at high fields is an exponential, and that the field scale of that exponential is decreasing with temperature. Both this decreasing field scale and the increase in the background field dependence at low temperatures would tend to decrease the slope of R_H at high fields. In order for it to grow, the size of the strange metal amplitude has to be growing all the way down to $1.5K$. This supports the idea that there is no internal energy scale in this sample that will cut off the growth of the strange metal R_H. Although we do not have a predicted form for $R_H(T)$, all of the overdoped samples eventually show a decrease in R_H below some temperature. It would be easy to imagine that this internal energy scale gets close to zero but still hits some minimum before reaching the antiferromagnetic phase boundary. This would happen if the quantum phase transition were first order. It is striking therefore that no cut-off is observable in $R_H(T)$, at least not above $1.5K$, and this fact provides further support for the idea that the electronic dynamics of $BaFe_2(As_{1-x}P_x)_2$ are in some important sense critical.

There is a second important fact about these low-temperature data; although the approximate relationship $H_0 \sim T$ suggests that the strange metal term would approach something

like a delta function at zero temperature, there is clearly a finite field scale. Therefore, strange metal R_H is not just sensitive to the thermal time scale, but ultimately runs into a scale that is set by quantum fluctuations near zero temperature. This is especially important in light of the fact that there seems to be a residual strange metal R_H at zero temperature beyond the critical point. These observations strongly suggest that there are important facts to be learned about the limit that these materials reach at zero kelvin, which will be essential for understanding the nature of criticality in metals and high$-T_c$ superconductivity.

8.4 Conclusion

The finite size dependence observed in $BaFe_2(As_{1-x}P_x)_2$ is mysterious. There is no obvious phenomenon that could explain the sensitivity of a transport coefficient to dimensions of one micron or more. Although quantum criticality is supposed to involve a diverging length scale, this scale is also supposed to be truncated at finite temperatures. Direct measurements of the magnetic correlation length from neutron scattering give values below one hundred nanometers even at the lowest temperatures.[48] It is possible that nematic fluctuations reach larger dimensions, but this seems unlikely due to their close association with magnetism in this compound. Finding the right explanation for this phenomenon will take time. I included these data here because they allow us to say two things about the Hall coefficient in this compound with much greater confidence than we could in light of the data presented in the previous chapter.

First, the strange metal behavior in R_H is definitively not a band structure effect. The band structure should easily be well-defined at a hundred lattice spacings, which would lead to a Hall coefficient that scales directly with the thickness above that dimension. Indeed, the high temperature R_H (above two hundred kelvin), which I identified as being determined solely to the underlying band structure, does scale inversely with thickness. The fact that the low temperature region responds differently to a one micron cut-off shows definitively that it can be tuned separately from effects on the band structure. This conclusion is unchanged whatever the final mechanism for the thickness dependence turns out to be.

Second, these data strongly support the claim that the strange metal behavior in the Hall coefficient enters as a second term. As described in section 8.3, estimates for the size of strange metal term based on the field dependence yield a difference in the size of the zero field component that exactly matches the measured difference in the zero-field values of R_H. For reasons described in chapter 7, it is very odd that R_H should have two terms that act in series like this. This makes it extremely valuable to be able to demonstrate conclusively that this is the right way to understand the strange metal Hall effect.

Having access to very high signal-to-noise data up to sixty-five tesla also allows us to make two more broad observations that support the quantum critical picture: there is scaling in R_H, and there is no observable intrinsic cut-off scale in R_H at optimal doping. Both of these observations confirm key parts of the critical picture and suggest that the assumptions of zero internal energy scale and one dominant time scale are indeed good starting points

for understanding this anomalous metallic state. Much more work remains to be done on this subject. The most obvious question that needs answering is whether or not a similar pattern of behavior appears as a function of reduced thickness in the plane (instead of along the $c-$axis). That experiment will require focused ion beam lithography, since cutting a one micron wide sample by hand is not feasible. A careful examination of the influence of strain on these devices would also be useful, as $BaFe_2(As_{1-x}P_x)_2$ and other doped iron-pnictides are known to be very sensitive to strain, and that may a contributing factor to the difference between the ultra-thin and the macroscopic devices.[24] These data leave open many promising avenues for the further investigation of the strange metal properties of this system.

Chapter 9

Conclusion: How Strange is the Strange metal?

Why are we so keen to find a theory of strongly correlated electrons? Because without such a theory, it is impossible to know what we are missing. The history of research on superconductivity offers a useful example of this. Once the Bardeen-Cooper-Schreiffer theory arrived, the path to finding materials with the highest possible superconducting critical temperatures seemed to be clear. Cogent arguments, due primarily to McMillan, Cohen, and Anderson, showed that the energy scales in real materials, which are limited by the physical nature of electrons and nucleons, would never lead to critical temperatures much above thirty kelvin.[77, 28] This estimate is probably correct; the record for highest temperature of a conventional superconductor at ambient pressure is held by MgB_2, which has a T_c of a little under forty kelvin.[80] Nature, of course, had other ideas. The Bardeen-Cooper-Schreiffer theory is based on a specific mechanism in a specific model of metals (Fermi liquid theory) and therefore was not capable of predicting the extremely high transition temperatures seen in the cuprates. Today we do not even have a good guess as to whether the current record for T_c at ambient pressure (135 K) is close to any fundamental limit, because we do not know which parameters are involved in determining T_c.[60] It's possible to not know what you are missing. It's also possible to know that you do not know what you are missing.

As inspiring as this may be, we are still in the challenging position of having to feel our way through the dark towards a theory that does not yet exist. The project of understanding ordinary metals was greatly aided by the fact that the theory of truly noninteracting Fermions is both essentially exact and easy to visualize and work with. The broad phenomenology of the strange metal—including $T-$linear resistivity and a $\sim 1/T$ Hall coefficient—that appears in many high$-T_c$ superconductors and quantum critical systems points to the existence of some new picture for metallic behavior. In this dissertation I have shown that both of these anomalous temperature dependencies have magnetic analogues, and I have shown that this extended phenomenology agrees surprisingly well with certain pieces of the paradigm of quantum criticality. This agreement is based on two general predictions of from the theory of quantum criticality: the existence of scale-invariant dynamics, and the existence of a clear

critical-cut-off temperature that collapses to zero at the quantum phase transition. The first of these we saw via the direct observation of a scaling collapse of the magnetoresistance of $BaFe_2(As_{1-x}P_x)_2$ at the zero temperature endpoint of the antiferromagnetic phase transition. Just as it does in classical critical systems, the existence of this collapse is a sign that there is a single scale in the problem that is solely responsible for changes in the electronic dynamics. The fact that this scaling is only observed near the critical point lends strong support to the idea that this controlling length scale is related to the strong fluctuations of either the antiferromagnetic or nematic order.

This scale-invariance leads to a magnetoresistance that is also linear in H at low temperatures. The the possibility that this might be a universal feature of metallic quantum critical points motivates the search for $H-$linear resistivity in other materials. Already there exist examples in the literature. Both the hole- and electron-doped cuprates have now shown $H-$linear resistivity, indicating that the phenomenon may be a part of the universal physics of high$-T_c$ superconductivity. In each of these cases, however, interpreting the phenomenon in terms of the simplest models of criticality is challenging. On the electron-doped side, the $H-$linear resistivity is observed over a broad doping range, rather than at a single point that could be identified with a critical phase transition.[56] In the hole-doped case, the $H-$linearity is localized near the pseudogap endpoint,[43] however, the status of the pseudo-gap is still a hotly debated topic. In contrast, the critical phenomenology is in $BaFe_2(As_{1-x}P_x)_2$ is exceptionally clear, which should make it a very useful testbed for elucidating the true nature of quantum criticality in metals.

The prediction of a critical cut-off temperature is also satisfied in a surprisingly clear manner in $BaFe_2(As_{1-x}P_x)_2$. This is the second main finding of this dissertation. For reasons given in chapter 2, the influence of the a quantum critical point is expected to be uniform throughout a fan-like region emanating from the critical point. Such a fan-like region is clearly visible in the Hall coefficient of $BaFe_2(As_{1-x}P_x)_2$. The key step in seeing this is to identify strange metal physics by its field dependence instead of its temperature dependence. This was inspired by the observation that in the resistivity a magnetic field essentially behaves as an effective temperature. Thus we expect that the the Hall coefficient, which has a $\sim 1/T$ dependence, should also decrease with field. This allows us to readily separate the Hall signal into two components, one of which comes from the band structure and the other of which comes from strange metal physics. From there, the critical fan can be seen with essentially no further data analysis. The strange metal field dependence is perfectly uniform at a given temperature with that region.

This is a remarkably faithful fulfillment of the naïve picture given to us from our picture of quantum critical metals, so much so that it allows us to say with high confidence that the critical picture is an at least approximately accurate representation of the physics of these materials, even without a detailed prediction to compare it to. Nonetheless, it is still surprising in a certain way. Most of the theoretical attempts on the problem of metallic quantum criticality indicate that we should expect the quasiparticle to breakdown as faithful representation of the excitations of the system. However, the neat separation of the Hall resistivity into a strange metal component and band structure component suggests that

quasiparticles are still a strong influence on the system. Somehow the system manages to retain knowledge of its weakly-interacting electronic structure, even as strong correlations set in near the critical point.

This two-faced nature of the critical dynamics is apparent in the resistivity as well. The angle dependence of the scaling phenomenon and its manifestation in the interlayer resistivity suggest that the fluctuations responsible for the scaling are strongly two-dimensional, even as those fluctuations couple equally to currents in all directions. It is hard to imagine how these two symmetries can be reconciled in a single model. The easiest way forward would be to posit the coexistence of two different types of degrees of freedom, one of which was principally responsible for the transport and was fully three dimensional, and another that dominated the coupling to the magnetic field. This is in fact how many magnetic systems are treated theoretically, but it certainly seems rather artificial.[93] However, if we focus instead on correlations, as we are encouraged to do by the apparent dominance of critical physics in this system, we could make the more reasonable-sounding statement that the spin and charge correlations in $BaFe_2(As_{1-x}P_x)_2$ decouple. Amusingly, this would lead us back to some of the earliest ideas about high$-T_c$ superconductivity.[4] In any case, the observations presented in chapter 6 create a concrete challenge for future theories of the strange metal state in high$-T_c$s.

The tight connection between this strange metallic behavior and superconductivity gives us hope that we don't have far to go before reaping the rewards of this new physics, whatever it might be. Considering all of the data presented here, some picture based on quantum criticality seems like the best bet. Of course, as it is conventionally formulated, quantum critical physics seems inconsistent with the dynamics of fermions, for all of the reasons given in chapter 2. Following the example of Landau, we may hope that the only major theoretical step remaining is to explain why these apparent divergences aren't really a problem. But that still does not lead to any clear, consistent way to describe these systems microscopically. Until we have that, our best hope for progress lies in identifying consistent patterns across material systems that suggest a universal picture. Determining whether the field-dependent extensions of the standard strange metal phenomenology, described here for the case of $BaFe_2(As_{1-x}P_x)_2$, apply more broadly is the next step in this program.

Bibliography

[1] M. Abdel-Jawad et al. "Correlation between the Superconducting Transition Temperature and Anisotropic Quasiparticle Scattering in $Tl_2Ba_2CuO_{4+\delta}$." In: *Phys. Rev. Lett.* 99 (10 Sept. 2007), p. 107002. DOI: 10.1103/PhysRevLett.99.107002. URL: https://link.aps.org/doi/10.1103/PhysRevLett.99.107002.

[2] Elihu Abrahams and Qimiao Si. "Quantum criticality in the iron pnictides and chalcogenides." In: *Journal of Physics: Condensed Matter* 23.22 (2011), p. 223201. URL: http://stacks.iop.org/0953-8984/23/i=22/a=223201.

[3] J. G. Analytis et al. "Enhanced Fermi-Surface Nesting in Superconducting $BaFe_2(As_{1-x}P_x)_2$ Revealed by the de Haas–van Alphen Effect." In: *Phys. Rev. Lett.* 105 (20 Nov. 2010), p. 207004. DOI: 10.1103/PhysRevLett.105.207004. URL: https://link.aps.org/doi/10.1103/PhysRevLett.105.207004.

[4] P. W. Anderson. "Hall effect in the two-dimensional Luttinger liquid." In: *Phys. Rev. Lett.* 67 (15 Oct. 1991), pp. 2092–2094. DOI: 10.1103/PhysRevLett.67.2092. URL: https://link.aps.org/doi/10.1103/PhysRevLett.67.2092.

[5] P. W. Anderson. "The Resonating Valence Bond State in La2CuO4 and Superconductivity." In: *Science* 235.4793 (1987), pp. 1196–1198. ISSN: 0036-8075. DOI: 10.1126/science.235.4793.1196. eprint: http://science.sciencemag.org/content/235/4793/1196.full.pdf. URL: http://science.sciencemag.org/content/235/4793/1196.

[6] P. W. (Philip W.) Anderson. *Basic notions of condensed matter physics*. English. "The Advanced book program.". Reading, Mass. : Addison-Wesley, 1997. ISBN: 0201328305.

[7] Philip W. Anderson. "Four Last Conjectures." In: *arXiv* (2018), p. 1804.11186. URL: https://arxiv.org/abs/1804.11186.

[8] Yoichi Ando et al. "Electronic Phase Diagram of High-T_c Cuprate Superconductors from a Mapping of the In-Plane Resistivity Curvature." In: *Phys. Rev. Lett.* 93 (26 Dec. 2004), p. 267001. DOI: 10.1103/PhysRevLett.93.267001. URL: https://link.aps.org/doi/10.1103/PhysRevLett.93.267001.

[9] Yoichi Ando et al. "Evolution of the Hall Coefficient and the Peculiar Electronic Structure of the Cuprate Superconductors." In: *Phys. Rev. Lett.* 92 (19 May 2004), p. 197001. DOI: 10.1103/PhysRevLett.92.197001. URL: https://link.aps.org/doi/10.1103/PhysRevLett.92.197001.

[10] N. P. Armitage, P. Fournier, and R. L. Greene. "Progress and perspectives on electron-doped cuprates." In: *Rev. Mod. Phys.* 82 (3 Sept. 2010), pp. 2421–2487. DOI: 10.1103/RevModPhys.82.2421. URL: https://link.aps.org/doi/10.1103/RevModPhys.82.2421.

[11] N. W. Ashcroft and N. D. Mermin. *Solid State Physics*. Brooks/Cole, 1976.

[12] P. L. Bach et al. "High-temperature resistivity in the iron pnictides and the electron-doped cuprates." In: *Phys. Rev. B* 83 (21 June 2011), p. 212506. DOI: 10.1103/PhysRevB.83.212506. URL: https://link.aps.org/doi/10.1103/PhysRevB.83.212506.

[13] G. Baskaran and P. W. Anderson. "Gauge theory of high-temperature superconductors and strongly correlated Fermi systems." In: *Phys. Rev. B* 37 (1 Jan. 1988), pp. 580–583. DOI: 10.1103/PhysRevB.37.580. URL: https://link.aps.org/doi/10.1103/PhysRevB.37.580.

[14] J. G. Bednorz and K. A. Müller. "Possible high Tc superconductivity in the Ba-La-Cu-O system." In: *Zeitschrift fur Physik B Condensed Matter* 64 (1986), pp. 189–193. DOI: DOI:10.1007/BF01303701. URL: http://adsabs.harvard.edu/abs/1986ZPhyB..64..189B.

[15] N. Bohr. *Atomic Physics and Human Knowledge*. Dover Books on Physics. Dover Publications, 2010. ISBN: 9780486479286. URL: https://books.google.com/books?id=tPEuDQAAQBAJ.

[16] R. A. Borzi et al. "Formation of a Nematic Fluid at High Fields in $Sr_3Ru_2O_7$." In: *Science* 315.5809 (2007), pp. 214–217. ISSN: 0036-8075. DOI: 10.1126/science.1134796. eprint: http://science.sciencemag.org/content/315/5809/214.full.pdf. URL: http://science.sciencemag.org/content/315/5809/214.

[17] I. Božović et al. "Dependence of the critical temperature in overdoped copper oxides on superfluid density." In: *Nature* 536 (Aug. 17, 2016), URL: https://doi.org/10.1038/nature19061.

[18] J. A. N. Bruin et al. "Similarity of Scattering Rates in Metals Showing T-Linear Resistivity." In: *Science* 339.6121 (2013), pp. 804–807. ISSN: 0036-8075. DOI: 10.1126/science.1227612. eprint: http://science.sciencemag.org/content/339/6121/804.full.pdf. URL: http://science.sciencemag.org/content/339/6121/804.

[19] P. C. Canfield and Z. Fisk. "Growth of single crystals from metallic fluxes." In: *Philosophical Magazine B* 65.6 (1992), pp. 1117–1123. DOI: 10.1080/13642819208215073. eprint: https://doi.org/10.1080/13642819208215073. URL: https://doi.org/10.1080/13642819208215073.

[20] A Carrington. "Quantum oscillation studies of the Fermi surface of iron-pnictide superconductors." In: *Reports on Progress in Physics* 74.12 (2011), p. 124507. URL: http://stacks.iop.org/0034-4885/74/i=12/a=124507.

[21] M. K. Chan et al. "In-Plane Magnetoresistance Obeys Kohler's Rule in the Pseudogap Phase of Cuprate Superconductors." In: *Phys. Rev. Lett.* 113 (17 Oct. 2014), p. 177005. DOI: 10.1103/PhysRevLett.113.177005. URL: https://link.aps.org/doi/10.1103/PhysRevLett.113.177005.

[22] T. R. Chien, Z. Z. Wang, and N. P. Ong. "Effect of Zn impurities on the normal-state Hall angle in single-crystal $YBa_2Cu_{3-x}0_{7-\delta}$." In: *Phys. Rev. Lett.* 67 (15 Oct. 1991), pp. 2088–2091. DOI: 10.1103/PhysRevLett.67.2088. URL: https://link.aps.org/doi/10.1103/PhysRevLett.67.2088.

[23] Jiun-Haw Chu et al. "Determination of the phase diagram of the electron-doped superconductor $Ba(Fe_{1-x}Co_x)_2As_2$." In: *Phys. Rev. B* 79 (1 Jan. 2009), p. 014506. DOI: 10.1103/PhysRevB.79.014506. URL: https://link.aps.org/doi/10.1103/PhysRevB.79.014506.

[24] Jiun-Haw Chu et al. "Divergent Nematic Susceptibility in an Iron Arsenide Superconductor." In: *Science* 337.6095 (2012), pp. 710–712. ISSN: 0036-8075. DOI: 10.1126/science.1221713. eprint: http://science.sciencemag.org/content/337/6095/710.full.pdf. URL: http://science.sciencemag.org/content/337/6095/710.

[25] Jiun-Haw Chu et al. "In-plane electronic anisotropy in underdoped $Ba(Fe_{1-x}Co_x)_2As_2$ revealed by partial detwinning in a magnetic field." In: *Phys. Rev. B* 81 (21 June 2010), p. 214502. DOI: 10.1103/PhysRevB.81.214502. URL: https://link.aps.org/doi/10.1103/PhysRevB.81.214502.

[26] Jiun-Haw Chu et al. "In-Plane Resistivity Anisotropy in an Underdoped Iron Arsenide Superconductor." In: *Science* 329.5993 (Aug. 2010), pp. 824–826. ISSN: 0036-8075, 1095-9203. DOI: 10.1126/science.1190482. URL: http://www.sciencemag.org/content/329/5993/824.

[27] A. Chubukov. *Quantum-critical Phenomena*. A Tutorial at the March Meeting of the American Physical Society. 2018.

[28] M. L. Cohen and P. W. Anderson. *Comments on the maximum superconducting transition temperature*. United States: American Inst of Physics, 1972. URL: http://inis.iaea.org/search/search.aspx?orig_q=RN:03030038.

[29] R. Coldea et al. "Quantum Criticality in an Ising Chain: Experimental Evidence for Emergent E8 Symmetry." In: *Science* 327.5962 (2010), pp. 177–180. ISSN: 0036-8075. DOI: 10.1126/science.1180085. eprint: http://science.sciencemag.org/content/327/5962/177.full.pdf. URL: http://science.sciencemag.org/content/327/5962/177.

[30] P Coleman, A J Schofield, and A M Tsvelik. "How should we interpret the two transport relaxation times in the cuprates?" In: *Journal of Physics: Condensed Matter* 8.48 (1996), p. 9985. URL: http://stacks.iop.org/0953-8984/8/i=48/a=020.

[31] R. A. Cooper et al. "Anomalous Criticality in the Electrical Resistivity of $La_{2-x}Sr_xCuO_4$." In: *Science* 323.5914 (2009), pp. 603–607. ISSN: 0036-8075. DOI: 10.1126/science.1165015. eprint: http://science.sciencemag.org/content/323/5914/603.full.pdf. URL: http://science.sciencemag.org/content/323/5914/603.

[32] J. Custers et al. "Evidence for a Non-Fermi-Liquid Phase in Ge-Substituted $YbRh_2Si_2$." In: *Phys. Rev. Lett.* 104 (18 May 2010), p. 186402. DOI: 10.1103/PhysRevLett.104.186402. URL: https://link.aps.org/doi/10.1103/PhysRevLett.104.186402.

[33] J. Custers et al. "The break-up of heavy electrons at a quantum critical point." In: *Nature* 424 (July 31, 2003), URL: http://dx.doi.org/10.1038/nature01774.

[34] Y. Dagan and R. L. Greene. "Hole superconductivity in the electron-doped superconductor $Pr_{2-x}Ce_xCuO_4$." In: *Phys. Rev. B* 76 (2 July 2007), p. 024506. DOI: 10.1103/PhysRevB.76.024506. URL: https://link.aps.org/doi/10.1103/PhysRevB.76.024506.

[35] Jianhui Dai et al. "Iron pnictides as a new setting for quantum criticality." In: *Proceedings of the National Academy of Sciences* 106 (11 2009), pp. 4118–4121.

[36] Andrea Damascelli, Zahid Hussain, and Zhi-Xun Shen. "Angle-resolved photoemission studies of the cuprate superconductors." In: *Rev. Mod. Phys.* 75 (2 Apr. 2003), pp. 473–541. DOI: 10.1103/RevModPhys.75.473. URL: https://link.aps.org/doi/10.1103/RevModPhys.75.473.

[37] Nicolas Doiron-Leyraud et al. "Correlation between linear resistivity and T_c in the Bechgaard salts and the pnictide superconductor $Ba(Fe_{1-x}Co_x)_2As_2$." In: *Phys. Rev. B* 80 (21 Dec. 2009), p. 214531. DOI: 10.1103/PhysRevB.80.214531. URL: https://link.aps.org/doi/10.1103/PhysRevB.80.214531.

[38] M. J. Eom et al. "Evolution of transport properties of $BaFe_{2-x}Ru_xAs_2$ in a wide range of isovalent Ru substitution." In: *Phys. Rev. B* 85 (2 Jan. 2012), p. 024536. DOI: 10.1103/PhysRevB.85.024536. URL: https://link.aps.org/doi/10.1103/PhysRevB.85.024536.

[39] B. Fauqué et al. "Magnetic Order in the Pseudogap Phase of High-T_C Superconductors." In: *Phys. Rev. Lett.* 96 (19 May 2006), p. 197001. DOI: 10.1103/PhysRevLett.96.197001. URL: https://link.aps.org/doi/10.1103/PhysRevLett.96.197001.

[40] Julia Ferstl et al. "Tuning YbRh2Si2 to a non-magnetic state by La-doping." In: *Physica B: Condensed Matter* 359-361 (2005). Proceedings of the International Conference on Strongly Correlated Electron Systems, pp. 26–28. ISSN: 0921-4526. DOI: https://doi.org/10.1016/j.physb.2004.12.045. URL: http://www.sciencedirect.com/science/article/pii/S0921452604013018.

[41] I.R. Fisher, M.C. Shapiro, and J.G. Analytis. "Principles of crystal growth of intermetallic and oxide compounds from molten solutions." In: *Philosophical Magazine* 92.19-21 (2012), pp. 2401–2435. DOI: 10.1080/14786435.2012.685192. eprint: https://doi.org/10.1080/14786435.2012.685192. URL: https://doi.org/10.1080/14786435.2012.685192.

[42] P. Gegenwart et al. "Magnetic-Field Induced Quantum Critical Point in $YbRh_2Si_2$." In: *Phys. Rev. Lett.* 89 (5 July 2002), p. 056402. DOI: 10.1103/PhysRevLett.89.056402. URL: https://link.aps.org/doi/10.1103/PhysRevLett.89.056402.

[43] P. Giraldo-Gallo et al. "Scale-invariant magnetoresistance in a cuprate superconductor." In: *Science* 361.6401 (2018), pp. 479–481. ISSN: 0036-8075. DOI: 10.1126/science.aan3178. eprint: http://science.sciencemag.org/content/361/6401/479.full.pdf. URL: http://science.sciencemag.org/content/361/6401/479.

[44] J. M. Harris et al. "Violation of Kohler's Rule in the Normal-State Magnetoresistance of $YBa_2Cu_3O_{7-\delta}$ and $La_{2-x}Sr_xCuO_4$." In: *Phys. Rev. Lett.* 75 (7 Aug. 1995), pp. 1391–1394. DOI: 10.1103/PhysRevLett.75.1391. URL: https://link.aps.org/doi/10.1103/PhysRevLett.75.1391.

[45] K. Hashimoto et al. "A Sharp Peak of the Zero-Temperature Penetration Depth at Optimal Composition in $BaFe2(As_{1-x}P_x)_2$." In: *Science* 336.6088 (June 2012), pp. 1554–1557. ISSN: 0036-8075, 1095-9203. DOI: 10.1126/science.1219821. URL: http://www.sciencemag.org/content/336/6088/1554.

[46] John A. Hertz. "Quantum critical phenomena." In: *Phys. Rev. B* 14 (3 Aug. 1976), pp. 1165–1184. DOI: 10.1103/PhysRevB.14.1165. URL: https://link.aps.org/doi/10.1103/PhysRevB.14.1165.

[47] R. Hlubina and T. M. Rice. "Resistivity as a function of temperature for models with hot spots on the Fermi surface." In: *Phys. Rev. B* 51 (14 Apr. 1995), pp. 9253–9260. DOI: 10.1103/PhysRevB.51.9253. URL: https://link.aps.org/doi/10.1103/PhysRevB.51.9253.

[48] Ding Hu et al. "Structural and Magnetic Phase Transitions near Optimal Superconductivity in $BaFe_2(As_{1-x}P_x)_2$." In: *Phys. Rev. Lett.* 114 (15 Apr. 2015), p. 157002. DOI: 10.1103/PhysRevLett.114.157002. URL: https://link.aps.org/doi/10.1103/PhysRevLett.114.157002.

[49] N E Hussey. "Phenomenology of the normal state in-plane transport properties of high$-T_c$ cuprates." In: *Journal of Physics: Condensed Matter* 20.12 (2008), p. 123201. URL: http://stacks.iop.org/0953-8984/20/i=12/a=123201.

[50] N E Hussey, J Buhot, and S Licciardello. "A tale of two metals: contrasting criticalities in the pnictides and hole-doped cuprates." In: *Reports on Progress in Physics* 81.5 (2018), p. 052501. URL: http://stacks.iop.org/0034-4885/81/i=5/a=052501.

[51] N. E. Hussey et al. "Angular Dependence of the c-axis Normal State Magnetoresistance in Single Crystal $Tl_2Ba_2CuO_6$." In: *Phys. Rev. Lett.* 76 (1 Jan. 1996), pp. 122–125. DOI: 10.1103/PhysRevLett.76.122. URL: https://link.aps.org/doi/10.1103/PhysRevLett.76.122.

[52] N. E. Hussey et al. "Dichotomy in the T-linear resistivity in hole-doped cuprates." In: *Philosophical Transactions: Mathematical, Physical and Engineering Sciences* 369.1941 (2011), pp. 1626–1639. ISSN: 1364503X. URL: http://www.jstor.org/stable/41148883.

[53] H. Y. Hwang et al. "Scaling of the temperature dependent Hall effect in $La_{2-x}Sr_x$-CuO_4." In: *Phys. Rev. Lett.* 72 (16 Apr. 1994), pp. 2636–2639. DOI: 10.1103/PhysRevLett.72.2636. URL: https://link.aps.org/doi/10.1103/PhysRevLett.72.2636.

[54] K. Ishida et al. "Spin-triplet superconductivity in Sr2RuO4 identified by 17O Knight shift." In: *Nature* 396 (Dec. 17, 1998), URL: https://doi.org/10.1038/25315.

[55] Shuai Jiang et al. "Superconductivity up to 30 K in the vicinity of the quantum critical point in $BaFe2(As_{1-x}P_x)_2$." en. In: *Journal of Physics: Condensed Matter* 21.38 (2009), p. 382203. ISSN: 0953-8984. DOI: 10.1088/0953-8984/21/38/382203. URL: http://stacks.iop.org/0953-8984/21/i=38/a=382203 (visited on 01/21/2016).

[56] K. Jin et al. "Link between spin fluctuations and electron pairing in copper oxide superconductors." In: *Nature* 476 (Aug. 3, 2011), URL: http://dx.doi.org/10.1038/nature10308.

[57] Mercouri G. Kanatzidis, Rainer Pöttgen, and Wolfgang Jeitschko. "The Metal Flux: A Preparative Tool for the Exploration of Intermetallic Compounds." In: *Angewandte Chemie International Edition* 44.43 (2005), pp. 6996–7023. DOI: 10.1002/anie.200462170. eprint: https://onlinelibrary.wiley.com/doi/pdf/10.1002/anie.200462170. URL: https://onlinelibrary.wiley.com/doi/abs/10.1002/anie.200462170.

[58] S. Kasahara et al. "Evolution from non-Fermi- to Fermi-liquid transport via isovalent doping in $BaFe_2(As_{1-x}P_x)_2$ superconductors." In: *Physical Review B* 81.18 (May 2010), p. 184519. DOI: 10.1103/PhysRevB.81.184519.

[59] Naoyuki Katayama et al. "Variation in Electronic State of $Ba(Fe_{1-x}Co_x)_2As_2$ Alloy as Investigated in Terms of Transport Properties." In: *Journal of the Physical Society of Japan* 78.12 (2009), p. 123702. DOI: 10.1143/JPSJ.78.123702. eprint: https://doi.org/10.1143/JPSJ.78.123702. URL: https://doi.org/10.1143/JPSJ.78.123702.

[60] B. Keimer et al. "From quantum matter to high-temperature superconductivity in copper oxides." In: *Nature* 518 (Feb. 11, 2015), URL: https://doi.org/10.1038/nature14165.

[61] M. G. Kim et al. "Spin dynamics near a putative antiferromagnetic quantum critical point in Cu-substituted $BaFe_2As_2$ and its relation to high-temperature superconductivity." In: *Phys. Rev. B* 92 (21 Dec. 2015), p. 214404. DOI: 10.1103/PhysRevB.92.214404. URL: https://link.aps.org/doi/10.1103/PhysRevB.92.214404.

[62] Steven A. Kivelson, Daniel S. Rokhsar, and James P. Sethna. "Topology of the resonating valence-bond state: Solitons and high-T_c superconductivity." In: *Phys. Rev. B* 35 (16 June 1987), pp. 8865–8868. DOI: 10.1103/PhysRevB.35.8865. URL: https://link.aps.org/doi/10.1103/PhysRevB.35.8865.

[63] A. Koitzsch et al. "Valence-band and core-level photoemission spectroscopy of $LaFeAsO_{1-x}F_x$." In: *Phys. Rev. B* 78 (18 Nov. 2008), p. 180506. DOI: 10.1103/PhysRevB.78.180506. URL: https://link.aps.org/doi/10.1103/PhysRevB.78.180506.

[64] Hiroshi Kontani. "Anomalous transport phenomena in Fermi liquids with strong magnetic fluctuations." In: *Reports on Progress in Physics* 71.2 (2008), p. 026501. URL: http://stacks.iop.org/0034-4885/71/i=2/a=026501.

[65] J. Korringa. "Nuclear magnetic relaxation and resonance line shift in metals." In: *Physica* 16 (7-8 1950), p. 601. DOI: 10.1016/0031-8914(50)90105-4. URL: https://www.sciencedirect.com/science/article/pii/0031891450901054.

[66] A. E. Koshelev. "Magnetotransport of multiple-band nearly antiferromagnetic metals due to hot-spot scattering." In: *Phys. Rev. B* 94 (12 Sept. 2016), p. 125154. DOI: 10.1103/PhysRevB.94.125154. URL: https://link.aps.org/doi/10.1103/PhysRevB.94.125154.

[67] H.-A. Krug von Nidda et al. "Electron spin resonance in Eu-based iron pnictides." In: *Phys. Rev. B* 86 (9 Sept. 2012), p. 094411. DOI: 10.1103/PhysRevB.86.094411. URL: https://link.aps.org/doi/10.1103/PhysRevB.86.094411.

[68] Hsueh-Hui Kuo et al. "Ubiquitous signatures of nematic quantum criticality in optimally doped Fe-based superconductors." In: *Science* 352.6288 (2016), pp. 958–962. ISSN: 0036-8075. DOI: 10.1126/science.aab0103. eprint: http://science.sciencemag.org/content/352/6288/958.full.pdf. URL: http://science.sciencemag.org/content/352/6288/958.

[69] L. Landau. "The Theory of a Fermi Liquid." In: *Sov. Phys. JETP* 3 (Jan. 1957), p. 920. DOI: 10.1016/B978-0-08-010586-4.50095-X. URL: https://doi.org/10.1016/B978-0-08-010586-4.50095-X.

[70] L. D. Landau. "On the theory of phase transitions." In: *Zh. Eksp. Teor. Fiz.* 7 (1937). Ukr. J. Phys.53,25(2008), pp. 19–32.

[71] Hilbert v. Löhneysen et al. "Fermi-liquid instabilities at magnetic quantum phase transitions." In: *Rev. Mod. Phys.* 79 (3 Aug. 2007), pp. 1015–1075. DOI: 10.1103/RevModPhys.79.1015. URL: https://link.aps.org/doi/10.1103/RevModPhys.79.1015.

[72] Xingye Lu et al. "Avoided Quantum Criticality and Magnetoelastic Coupling in $Ba(Fe_{1-x}Ni_x)_2As_2$." In: *Phys. Rev. Lett.* 110 (25 June 2013), p. 257001. DOI: 10.1103/PhysRevLett.110.257001. URL: https://link.aps.org/doi/10.1103/PhysRevLett.110.257001.

[73] Xingye Lu et al. "Short-range cluster spin glass near optimal superconductivity in $Ba(Fe_{1-x}Ni_x)_2As_2$." In: *Phys. Rev. B* 90 (2 July 2014), p. 024509. DOI: 10.1103/PhysRevB.90.024509. URL: https://link.aps.org/doi/10.1103/PhysRevB.90.024509.

[74] Huiqian Luo et al. "Coexistence and Competition of the Short-Range Incommensurate Antiferromagnetic Order with the Superconducting State of $Ba(Fe_{1-x}Ni_x)_2As_2$." In: *Phys. Rev. Lett.* 108 (24 June 2012), p. 247002. DOI: 10.1103/PhysRevLett.108.247002. URL: https://link.aps.org/doi/10.1103/PhysRevLett.108.247002.

[75] A.P. Mackenzie et al. "Quantum criticality and the formation of a putative electronic liquid crystal in $Sr_3Ru_2O_7$." In: *Physica C: Superconductivity* 481 (2012). Stripes and Electronic Liquid Crystals in Strongly Correlated Materials, pp. 207–214. ISSN: 0921-4534. DOI: https://doi.org/10.1016/j.physc.2012.04.018. URL: http://www.sciencedirect.com/science/article/pii/S0921453412002067.

[76] D. van der Marel et al. "Quantum critical behaviour in a high$-T_c$ superconductor." In: *Nature* 425 (Sept. 18, 2003), URL: http://dx.doi.org/10.1038/nature01978.

[77] W. L. McMillan. "Transition Temperature of Strong-Coupled Superconductors." In: *Phys. Rev.* 167 (2 Mar. 1968), pp. 331–344. DOI: 10.1103/PhysRev.167.331. URL: https://link.aps.org/doi/10.1103/PhysRev.167.331.

[78] P. Monthoux and D. Pines. "$YBa_2Cu_3O_7$: A nearly antiferromagnetic Fermi liquid." In: *Phys. Rev. B* 47 (10 Mar. 1993), pp. 6069–6081. DOI: 10.1103/PhysRevB.47.6069. URL: https://link.aps.org/doi/10.1103/PhysRevB.47.6069.

[79] E. M. Motoyama et al. "Spin correlations in the electron-doped high-transition-temperature superconductor Nd2-xCexCuO4$\pm\delta$." In: *Nature* 445 (Jan. 11, 2007), URL: https://doi.org/10.1038/nature05437.

[80] Jun Nagamatsu et al. "Superconductivity at 39 K in magnesium diboride." In: *Nature* 410 (Mar. 1, 2001), URL: https://doi.org/10.1038/35065039.

[81] Y. Nakai et al. "Unconventional Superconductivity and Antiferromagnetic Quantum Critical Behavior in the Isovalent-Doped $BaFe_2(As_{1-x}P_x)_2$." In: *Phys. Rev. Lett.* 105 (10 Sept. 2010), p. 107003. DOI: 10.1103/PhysRevLett.105.107003. URL: https://link.aps.org/doi/10.1103/PhysRevLett.105.107003.

[82] Masamichi Nakajima et al. "Growth of BaFe2(As1-xPx)2 Single Crystals ($0 \leq x \leq 1$) by Ba2As3/Ba2P3-Flux Method." In: *Journal of the Physical Society of Japan* 81.10 (2012), p. 104710. DOI: 10.1143/JPSJ.81.104710.

[83] Y. Nakajima et al. "Non-Fermi Liquid Behavior in the Magnetotransport of CeMIn5 (M: Co and Rh): Striking Similarity between Quasi Two-Dimensional Heavy Fermion and High-Tc Cuprates." In: *Journal of the Physical Society of Japan* 76.2 (2007), p. 024703. DOI: 10.1143/JPSJ.76.024703. URL: https://doi.org/10.1143/JPSJ.76.024703.

[84] Q. Niu et al. "Quasilinear quantum magnetoresistance in pressure-induced nonsymmorphic superconductor chromium arsenide." In: *Nature Communications* 8 (June 5, 2017), URL: https://doi.org/10.1038/ncomms15358.

[85] B. Odom et al. "New Measurement of the Electron Magnetic Moment Using a One-Electron Quantum Cyclotron." In: *Phys. Rev. Lett.* 97 (3 July 2006), p. 030801. DOI: 10.1103/PhysRevLett.97.030801. URL: https://link.aps.org/doi/10.1103/PhysRevLett.97.030801.

[86] Kenya Ohgushi and Yoko Kiuchi. "Doping dependence of Hall coefficient and evolution of coherent electronic state in the normal state of the Fe-based superconductor $Ba_{1-x}K_xFe_2As_2$." In: *Phys. Rev. B* 85 (6 Feb. 2012), p. 064522. DOI: 10.1103/PhysRevB.85.064522. URL: https://link.aps.org/doi/10.1103/PhysRevB.85.064522.

[87] A. Olariu et al. "Different effects of Ni and Co substitution on the transport properties of $BaFe_2As_2$." In: *Phys. Rev. B* 83 (5 Feb. 2011), p. 054518. DOI: 10.1103/PhysRevB.83.054518. URL: https://link.aps.org/doi/10.1103/PhysRevB.83.054518.

[88] Johnpierre Paglione and Richard L. Greene. "High-temperature superconductivity in iron-based materials." In: *Nature Physics* 6 (Aug. 29, 2010), URL: http://dx.doi.org/10.1038/nphys1759.

[89] A. Pal et al. "Quasistatic internal magnetic field detected in the pseudogap phase of $Bi_{2+x}Sr_{2-x}CaCu_2O_{8+\delta}$ by muon spin relaxation." In: *Phys. Rev. B* 97 (6 Feb. 2018), p. 060502. DOI: 10.1103/PhysRevB.97.060502. URL: https://link.aps.org/doi/10.1103/PhysRevB.97.060502.

[90] Aavishkar A. Patel et al. "Magnetotransport in a Model of a Disordered Strange Metal." In: *Phys. Rev. X* 8 (2 May 2018), p. 021049. DOI: 10.1103/PhysRevX.8.021049. URL: https://link.aps.org/doi/10.1103/PhysRevX.8.021049.

[91] R. S. Perry et al. "Metamagnetism and Critical Fluctuations in High Quality Single Crystals of the Bilayer Ruthenate Sr_3Ru2O_7." In: *Phys. Rev. Lett.* 86 (12 Mar. 2001), pp. 2661–2664. DOI: 10.1103/PhysRevLett.86.2661. URL: https://link.aps.org/doi/10.1103/PhysRevLett.86.2661.

[92] D. Pines and P. Nozières. *The Theory of Quantum Liquids: Normal Fermi liquids*. The Theory of Quantum Liquids. W.A. Benjamin, 1966. URL: https://books.google.com/books?id=GP1QAAAAMAAJ.

[93] A.B. Pippard. *Magnetoresistance in Metals*. Cambridge Studies in Low Temperature Physics. Cambridge University Press, 2009. ISBN: 9780521118804. URL: https://books.google.com/books?id=JYSfMgEACAAJ.

[94] D. K. Pratt et al. "Incommensurate Spin-Density Wave Order in Electron-Doped $BaFe_2As_2$ Superconductors." In: *Phys. Rev. Lett.* 106 (25 June 2011), p. 257001. DOI: 10.1103/PhysRevLett.106.257001. URL: https://link.aps.org/doi/10.1103/PhysRevLett.106.257001.

[95] A V Puchkov, D N Basov, and T Timusk. "The pseudogap state in high$-T_c$ superconductors: an infrared study." In: *Journal of Physics: Condensed Matter* 8.48 (1996), p. 10049. URL: http://stacks.iop.org/0953-8984/8/i=48/a=023.

[96] B. J. Ramshaw et al. "Quasiparticle mass enhancement approaching optimal doping in a high-Tc superconductor." In: *Science* 348.6232 (2015), pp. 317–320. ISSN: 0036-8075. DOI: 10.1126/science.aaa4990. eprint: http://science.sciencemag.org/content/348/6232/317.full.pdf. URL: http://science.sciencemag.org/content/348/6232/317.

[97] A. Rosch. "Magnetotransport in nearly antiferromagnetic metals." In: *Phys. Rev. B* 62 (8 Aug. 2000), pp. 4945–4962. DOI: 10.1103/PhysRevB.62.4945. URL: https://link.aps.org/doi/10.1103/PhysRevB.62.4945.

[98] A. W. Rost et al. "Thermodynamics of phase formation in the quantum critical metal Sr3Ru2O7." In: *Proceedings of the National Academy of Sciences* 108.40 (2011), pp. 16549–16553. ISSN: 0027-8424. DOI: 10.1073/pnas.1112775108. eprint: http://www.pnas.org/content/108/40/16549.full.pdf. URL: http://www.pnas.org/content/108/40/16549.

[99] F. Rullier-Albenque et al. "Hole and electron contributions to the transport properties of $Ba(Fe_{1-x}Ru_x)_2As_2$ single crystals." In: *Phys. Rev. B* 81 (22 June 2010), p. 224503. DOI: 10.1103/PhysRevB.81.224503. URL: https://link.aps.org/doi/10.1103/PhysRevB.81.224503.

[100] Subir Sachdev. *Quantum Phase Transitions*. 2nd ed. Cambridge University Press, 2011. DOI: 10.1017/CBO9780511973765.

[101] Subir Sachdev and Jinwu Ye. "Gapless spin-fluid ground state in a random quantum Heisenberg magnet." In: *Phys. Rev. Lett.* 70 (21 May 1993), pp. 3339–3342. DOI: 10.1103/PhysRevLett.70.3339. URL: https://link.aps.org/doi/10.1103/PhysRevLett.70.3339.

[102] D. J. Scalapino, E. Loh, and J. E. Hirsch. "Fermi-surface instabilities and superconducting d-wave pairing." In: *Phys. Rev. B* 35 (13 May 1987), pp. 6694–6698. DOI: 10.1103/PhysRevB.35.6694. URL: https://link.aps.org/doi/10.1103/PhysRevB.35.6694.

[103] J. P. Setna. *Statistical Mechanics: Entropy, Order Parameters and Chaos*. Oxford Master Series in Condensed Matter Physics. Oxford University Press, 2005.

[104] Arkady Shekhter et al. "Bounding the pseudogap with a line of phase transitions in YBa2Cu3O6+δ." In: *Nature* 498 (June 5, 2013), URL: http://dx.doi.org/10.1038/nature12165.

[105] T. Shibauchi, A. Carrington, and Y. Matsuda. "A Quantum Critical Point Lying Beneath the Superconducting Dome in Iron Pnictides." In: *Annual Review of Condensed Matter Physics* 5.1 (2014), pp. 113–135. DOI: 10.1146/annurev-conmatphys-031113-133921. URL: https://doi.org/10.1146/annurev-conmatphys-031113-133921.

[106] H. Shishido et al. "Evolution of the Fermi Surface of $BaFe_2(As_{1-x}P_x)_2$ on Entering the Superconducting Dome." In: *Physical Review Letters* 104.5 (Feb. 2010), p. 057008.

[107] D. Shoenberg. *Magnetic Oscillations in Metals*. Cambridge Monographs on Physics. Cambridge University Press, 1984. DOI: 10.1017/CBO9780511897870.

[108] D.J. Singh. "Electronic structure of Fe-based superconductors." In: *Physica C: Superconductivity* 469.9 (2009). Superconductivity in Iron-Pnictides, pp. 418–424. ISSN: 0921-4534. DOI: https://doi.org/10.1016/j.physc.2009.03.035. URL: http://www.sciencedirect.com/science/article/pii/S0921453409000768.

[109] S. L. Sondhi et al. "Continuous quantum phase transitions." In: *Rev. Mod. Phys.* 69 (1 Jan. 1997), pp. 315–333. DOI: 10.1103/RevModPhys.69.315. URL: https://link.aps.org/doi/10.1103/RevModPhys.69.315.

[110] G. R. Stewart. "Non-Fermi-liquid behavior in d- and f-electron metals." In: *Rev. Mod. Phys.* 73 (4 Oct. 2001), pp. 797–855. DOI: 10.1103/RevModPhys.73.797. URL: https://link.aps.org/doi/10.1103/RevModPhys.73.797.

[111] G. R. Stewart. "Superconductivity in iron compounds." In: *Rev. Mod. Phys.* 83 (4 Dec. 2011), pp. 1589–1652. DOI: 10.1103/RevModPhys.83.1589. URL: https://link.aps.org/doi/10.1103/RevModPhys.83.1589.

[112] H. Takagi et al. "Systematic evolution of temperature-dependent resistivity in $La_{2-x}Sr_xCuO_4$." In: *Phys. Rev. Lett.* 69 (20 Nov. 1992), pp. 2975–2978. DOI: 10.1103/PhysRevLett.69.2975. URL: https://link.aps.org/doi/10.1103/PhysRevLett.69.2975.

[113] G. N. Tam et al. "Resistivity of $Ba(Fe_{1-x}Co_x)_2As_2$: Evidence for a broad composition range of non-Fermi-liquid behavior." In: *Phys. Rev. B* 88 (13 Oct. 2013), p. 134503. DOI: 10.1103/PhysRevB.88.134503. URL: https://link.aps.org/doi/10.1103/PhysRevB.88.134503.

[114] M. A. Tanatar et al. "Interplane resistivity of isovalent doped $BaFe_2(As_{1-x}P_x)_2$." In: *Phys. Rev. B* 87 (10 Mar. 2013), p. 104506. DOI: 10.1103/PhysRevB.87.104506. URL: https://link.aps.org/doi/10.1103/PhysRevB.87.104506.

[115] C. M. Varma et al. "Phenomenology of the normal state of Cu-O high-temperature superconductors." In: *Phys. Rev. Lett.* 63 (18 Oct. 1989), pp. 1996–1999. DOI: 10.1103/PhysRevLett.63.1996. URL: https://link.aps.org/doi/10.1103/PhysRevLett.63.1996.

[116] Chandra M Varma. "Quantum-critical fluctuations in 2D metals: strange metals and superconductivity in antiferromagnets and in cuprates." In: *Reports on Progress in Physics* 79.8 (2016), p. 082501. URL: http://stacks.iop.org/0034-4885/79/i=8/a=082501.

[117] Pierre Villars and Hiroaki Okamoto, eds. *As-Fe Binary Phase Diagram 0-100 at.% Fe: Datasheet from "PAULING FILE Multinaries Edition – 2012" in SpringerMaterials (https://materials.springer.com/isp/phase-diagram/docs/c_0904752)*. accessed 2018-11-19. URL: https://materials.springer.com/isp/phase-diagram/docs/c_0904752.

[118] Pierre Villars and Hiroaki Okamoto, eds. *Ba-P Binary Phase Diagram 0-100 at.% P: Datasheet from "PAULING FILE Multinaries Edition – 2012" in SpringerMaterials (https://materials.springer.com/isp/phase-diagram/docs/c_0900364)*. accessed 2018-11-19. URL: https://materials.springer.com/isp/phase-diagram/docs/c_0900364.

[119] P. Walmsley et al. "Quasiparticle Mass Enhancement Close to the Quantum Critical Point in $BaFe_2(As_{1-x}P_x)_2$." In: *Phys. Rev. Lett.* 110 (25 June 2013), p. 257002. DOI: 10.1103/PhysRevLett.110.257002. URL: https://link.aps.org/doi/10.1103/PhysRevLett.110.257002.

[120] W. W. Warren et al. "Cu spin dynamics and superconducting precursor effects in planes above T_c in $YBa_2Cu_3O_{6.7}$." In: *Phys. Rev. Lett.* 62 (10 Mar. 1989), pp. 1193–1196. DOI: 10.1103/PhysRevLett.62.1193. URL: https://link.aps.org/doi/10.1103/PhysRevLett.62.1193.

[121] T. Yoshida et al. "Two-Dimensional and Three-Dimensional Fermi Surfaces of Superconducting $BaFe_2(As_{1-x}P_x)_2$ and Their Nesting Properties Revealed by Angle-Resolved Photoemission Spectroscopy." In: *Phys. Rev. Lett.* 106 (11 Mar. 2011), p. 117001. DOI: 10.1103/PhysRevLett.106.117001. URL: https://link.aps.org/doi/10.1103/PhysRevLett.106.117001.

[122] Jan Zaanen. "Why the temperature is high." In: *Nature* 430 (July 28, 2004), URL: https://doi.org/10.1038/430512a.

[123] L. Zhao et al. "A global inversion-symmetry-broken phase inside the pseudogap region of YBa2Cu3Oy." In: *Nature Physics* 13 (Nov. 21, 2016), URL: http://dx.doi.org/10.1038/nphys3962.

[124] Liujun Zou, Samuel Lederer, and T. Senthil. "Theory of anomalous magnetotransport from mass anisotropy." In: *Phys. Rev. B* 95 (24 June 2017), p. 245135. DOI: 10.1103/PhysRevB.95.245135. URL: https://link.aps.org/doi/10.1103/PhysRevB.95.245135.